Thermodynamic and kinetic effects of static magnetic field on phase transformations in low-alloy steels

Thomas Garcin

▶ To cite this version:

HAL Id: tel-00519996

https://theses.hal.science/tel-00519996

Submitted on 22 Sep 2010

Université de Grenoble - Ecole doctorale IMEP2

Ingénieries-Matériaux Mécanique Energétique Environnement procédées Production

THÈSE

présentée pour obtenir le grade de

DOCTEUR EN SCIENCES

DE L'UNIVERSITE JOSEPH FOURIER - GRENOBLE

Spécialité Matériaux et Génie des Procédés

par

Thomas Garcin

Thermodynamic and kinetic effects of static magnetic field on phase transformations in low-alloy steels

soutenue publiquement le 02 Décembre 2009 devant le jury composé de

Eric Beaugnon	*Directeur*
Yves Brechet	*Examinateur*
Hélène Réglé	*Examinatrice*
Sophie Rivoirard	*Co-Directrice*
Ivan Skorvanek	*Rapporteur*
Thierry Waeckerle	*Rapporteur*

Abstract

This work is devoted to the quantification of the magnetic field effect on phase transformations in iron based alloys and steels. Pure iron, Fe-xNi substitutional alloys, Fe-xC-Mn steels and Fe-C-Mn-xSi steels are used to explore a wide range of transformations and microstructures. A high temperature dilatometer and a magnetic balance for magnetic susceptibility measurements are used for the in situ characterisation of diffusional phase transformation in magnetic field up to 16T. A third device has been developed for the treatment of materials in magnetic field and includes, for the first time, a quenching step using water, oil or pulsed gas. Non-equilibrium transformation temperatures measured up to 16T in a large set of materials are found to be increased by the application of a magnetic field. In a similar approach as the model used to estimate the effect of hydrostatic pressure on the phase equilibrium, the shift induced by the magnetic field is calculated. Microstructure characterisation of rapidly cooled plain carbon steels has shown large structural modifications induced by the magnetic field. From a mixture of bainite and martensite in the sample treated without any magnetic field, the austenite transforms into allotriomorphic ferrite and Widmanstätten ferrite in a matrix of bainite and martensite in the presence of magnetic field. This work brings solid evidence that magnetic field can be used as a new degree of freedom in physical metallurgy. Combined with existing techniques, it could lead to the successful processing of improved materials.

Résumé

Ce travail est dédié à la quantification de l'effet du champ magnétique sur les transformations de phases dans les alliages à base de fer et en particulier dans les aciers. Le Fer pur, les alliages Fe-xNi, et les aciers au carbone faiblement alliés Fe-xC-Mn et Fe-C-Mn-xSi sont étudiés afin d'explorer une large gamme de transformations et de microstructures. Un dilatomètre haute-température et une balance magnétique pour la mesure de susceptibilité magnétique sont utilisés pour la caractérisation des transformations diffusive dans un champ magnétique allant jusqu'à 16T. Un troisième outil d'élaboration sous champ magnétique a été entièrement développé au cours de ce travail et permet pour la première fois une étape de trempe des matériaux à l'eau, à l'huile ou par gaz pulsé. Les températures de transformation hors-équilibre mesurées jusqu'à 16T dans une large gamme d'alliages sont augmentées par l'application d'un champ magnétique. Ces variations dans la température de transformation sont modélisées par un calcul thermodynamique basée sur une analogie avec l'effet d'une pression hydrostatique sur les équilibres de phases. Les microstructures d'aciers faiblement alliées obtenue par trempe sont largement modifiées par l'application du champ magnétique : d'une structure composée de martensite et de bainite sans l'application d'un champ magnétique, l'austénite se décompose en un mélange de ferrite allotriomorphe et de ferrite de Widmanstätten dans une matrice de bainite et de martensite en présence d'un champ magnétique. Ce travail apporte la preuve que le champ magnétique est devenu un paramètre prometteur en métallurgie physique. Associé aux techniques existantes, son utilisation peut conduire à l'obtention de matériaux aux propriétés innovantes.

Remerciements

J'exprime mes profonds remerciements à mon directeur de thèse, le Professeur Eric Beaugnon, pour la confiance et la liberté qu'il m'a accordées au cours de ces trois années au Laboratoire CRETA. En m'impliquant directement dans l'encadrement de stagiaires (non francophones pour la plupart), en me laissant présenter mes travaux dans des réunions de projet ou au cours de conférences internationales, il a su me montrer ce dont j'étais vraiment capable. Je suis en cette fin de thèse intimement persuadé que cette indépendance de travail qu'il m'a accordée est en partie à l'origine de la réussite de cette thèse et je le remercie pour cela.

Je souhaite à présent adresser mes très sincères et chaleureux remerciements au Dr Sophie Rivoirard qui a été ma co-directrice de thèse. Je la remercie tout d'abord de m'avoir proposé de m'inscrire au DEA Science et Génie des Matériaux, ce qui m'a permis de débuter une thèse au Laboratoire. Par ses grandes connaissances scientifiques dans le domaine de la métallurgie et du magnétisme, elle a su m'orienter judicieusement dans les voies intéressantes à explorer. Par son enthousiasme sans limite, elle a su me redonner à chaque instant la force de continuer. La relation que nous avons développée au cours de ce travail dépasse largement le cadre d'un groupe de travail. Une réelle amitié s'est construite à travers les nombreux moments passés ensemble. Je tiens à lui exprimer mon infinie gratitude et je lui souhaite énormément de bonheur autant dans sa vie professionnelle que personnelle.

Je remercie ensuite les différents membres de mon Jury de thèse pour avoir accepté de juger mon travail. J'adresse au Professeur Yves Brechet de plus particuliers remerciements pour avoir été un de mes pères dans le domaine de la métallurgie physique. Par l'intermédiaire de ses enseignements et travaux scientifiques, il a su me faire découvrir le monde complexe et fantastique des aciers. Je remercie ensuite le Professeur Ivan Skorvanek et le Dr Thierry Waeckerle pour avoir rapporté mon manuscrit de thèse. Leurs conseils et suggestions ont été d'une très grande importance pour la crédibilisation des idées proposées et me seront d'une immense aide pour concrétiser ce travail par l'écriture de publications scientifiques. Enfin, je remercie le Dr Helene Réglé qui m'a suivi au cours de la thèse dans le cadre d'une collaboration entre le Laboratoire et ArcelorResearch. Je tiens à lui exprimer mes

sincères remerciements pour avoir su m'indiquer avec beaucoup de clarté les problématiques du monde industriel afin que je puisse en appréhender le fonctionnement ainsi que pour avoir examiné ma thèse.

Je souhaite continuer en exprimant mes remerciements aux différents membres du projet Européens MAGPRO que je n'ai pas eu l'occasion de remercier jusque là. Je pense au Dr Ilaria Salvatori, au Dr Catherine Elghoyen et au Dr Philippe Pouteau avec qui nous avons échangé des discutions toujours enrichissantes pour l'avancement de ce travail. Je les remercie pour la confiance et le respect qu'ils m'ont apporté. Cela a contribué grandement à me construire de solides bases nécessaires à la présentation de travaux scientifiques et à l'échange au cours de réunions de travail. Je n'oublie pas les différents assistants ingénieurs et techniciens comme Marco Gazzini, Etienne Potier de Courcy que je remercie pour avoir participé activement à l'exploitation des données et aux travaux de recherche que nous avons menés.

Je souhaite ensuite remercier deux personnes qui ont travaillé à mes cotés quelques mois au cours de ces trois ans. J'adresse tout d'abord mes sincères remerciements au Professeur Roman Mogunov, éminent chercheur originaire de Russie, qui m'a donné de nombreux conseils et astuces pour devenir un scientifique respecté. J'espère ne jamais oublier tous ces moments passés en France à proximité du trou de champ d'une bobine résistive de 16 T ou au Japon perdu dans un magnifique Ryokan dans une petite rue de Tokyo. La seconde personne avec qui j'ai eu la chance de travailler est le Dr Vivian Nassif. Je la remercie pour être devenue, là encore, bien plus qu'une collègue de travail mais une vraie amie. Son investissement, son dévouement, sa gentillesse et son humour resteront à jamais un magnifique souvenir. Je lui souhaite énormément de bonheur et je lui promets de revenir la voir régulièrement, peut être, qui sait, dans une nouvelle collaboration pour la construction d'un grand appareil scientifique.

Je ne saurais à ce stade manquer de citer les personnes dont la disponibilité et la rigueur m'ont apporté des moments de fierté, de persévérance dans l'ardeur au travail et de me sentir fortement impliqué dans la recherche scientifique. Je pense tout d'abord à Pierre-Fréderic Sibeud, qui pour moi est une des pierres de voutes du Laboratoire sans qui peu d'appareils et d'expériences scientifiques ne pourraient fonctionner. Je lui exprime mon profond respect pour son investissement sans limite dans la bonne marche des équipements mais également

Content

Preface

This dissertation describes work carried out in the Research Consortium for the Emergence of Advanced Technologies, which is a Laboratory of the National Centre of Scientific Research in Grenoble (France) between October 2006 and October 2009 under the supervision of Pr E.Beaugnon and Dr S.Rivoirard. This work was supported by the European project "*MAGPRO*" (TGS6, RFSR-CT-2006-00019).

Thomas GARCIN

September 2009

General introduction

- 4 -

The purpose of the work presented in this thesis is a continuation of studies investigated on the use of strong magnetic field in the processing of materials. This recent "Magneto-Science" research topic is an emerging field of material science and technology, which has expanded rapidly during the last ten years in the materials science community and among others in the CNRS/CRETA laboratory together with Dr Robert Tournier and his research group.

We are particularly interested in this present work in the modifications induced by magnetic field in the processing of steels. The goal of such magnetic processing is to achieve superior materials properties that cannot be obtained through the more conventional thermo-mechanical treatments. This is possible because magnetic field can significantly change the phase stability, phase transformation kinetics and resulting microstructures in alloys in which the phases involved exhibit different magnetisation responses.

In the first chapter, a general overview of Electromagnetic Processing of Materials (EPM) is given. More particularly, the most important results obtained in previous works on the effect of static magnetic field in the processing of iron-based alloys are described. This part points out the essential metallurgical and magnetism concepts relative to the processing of steels in magnetic field.

The second chapter concerns the description of apparatus used in this present work for the processing of steel and in situ analyses of phases transformations in magnetic field. They are mainly composed of high temperature furnaces inserted in the bore of high field magnets. Various techniques are used for the in-situ real time control of phase transformations such as thermometry, magnetometry and dilatometry. One of these apparatus has been completely developed during the thesis and represents the first and unique experiment in the magneto-science community that allows the rapid cooling of a material by water quenching in a static and strong magnetic field. This unique device paves the way of the study of martensitic and bainitic transformation in steel in high magnetic field. Brief description of the various external characterisation techniques is given in the end of this part.

The third chapter is devoted to the presentation of the different studies that have been investigated on the diffusional decomposition of austenite in pure iron, iron substitutional alloys, and plain carbon steels. The aim is to present a reasonably complete set of experimental data on the stability of ferrite and austenite in magnetic field in iron based alloys. In situ dilatometry measurements are done for the determination of the transformation

temperatures in magnetic field. Magnetic measurements are done to test for the Molecular Field model which is actually the adopted theory for the prediction of the magnetisation of a ferromagnetic material around its Curie point and under the application of an external magnetic field. These measurements are used for the experimental evaluation of the magnetic Gibbs free energy term added in the system. Thermodynamic analysis is proposed for the prediction of the non-equilibrium transformation temperature in magnetic field.

The fourth chapter is focused on the martensitic and bainitic transformation in magnetic field in plain carbon steels. Fist, the effect of magnetic field on T_0 line in the Fe-C system is theoretically calculated. This line defines the thermodynamic limit for displacive transformation. Then, the impact of magnetic field on the microstructures obtained after rapid cooling is observed in detail in two sets of plain carbon steels: the one with increasing carbon content and the second with increasing silicon content. The experiments are done in the new furnace in which alloys are water cooled in magnetic field from the austenite state. This chapter brings promising results on the effect of static magnetic field on the martensitic and bainitic transformation that are of capital importance in the majority of high strength steels widely used in industrial processes.

In order to explore a wide range of compositions and microstructures, various alloys are casted for experiments. They are Fe-Ni alloys and plain carbon steels containing C, Mn, Si with a total amount of alloying element always lower than 4 wt%.

The objective of this experimental work is to bring evidences that the magnetic field is now become a promising parameter in physical metallurgy and especially in the processing of steels. Combined with existing alloy design techniques, it could lead to the successful exploitation of new ultra high strength steels.

Chapter 1

State of the art

No substance has been as important as metal in the history of Man's control of his environment. Advances in agriculture, warfare, transport, even cookery would have been impossible without the technology of metals and their practical use. Therefore metallurgy has always been an important research topic in materials science in exploring a wide range of composition and in combining various manufacturing processes such as shaping (casting, forging, flow forming, rolling, extrusion, sintering, metalworking, machining), surface treatments and heat treatments (of many kinds).

Nevertheless, major innovations are increasingly difficult to find because of decades of research, development and global competition. As a result, one of the major routes of progress remains the differentiation through innovation, aiming both at a significant increase in performances of existing products as well as at the reduction of elaboration costs. This differentiation through innovation has pushed forward the use of new technologies becoming gradually mature on an industrial scale. Magnetic fields processing is one of them.

With the availability of intense varying (AC) or static (DC) magnetic fields, the potential use of magnetic field as an additional external parameter in material processing has become attractive. As an introduction to this work, this chapter gives the main results and applications in electromagnetic field processing of materials. The first part is devoted to the presentation of general implications of magnetic fields in the elaboration of materials. The second part is focused on the results obtained recently on the processing of Fe-based alloys and more specifically steels in high magnetic field.

1.1. General Review of Electromagnetic Processing of Materials

Electromagnetic processing of materials (EPM) is a unique technology that utilizes various kinds of interactions between material and electromagnetic field for materials processing. Such interactions originate from the nature of material, generate particular functions and applications. Induction heating and melting, electromagnetic stirring or structure control by use of mid- or high-frequency alternating magnetic fields are well-known functions based on the use of Joule effect and electromagnetic forces. Control convection in liquid metals, materials texturing or magnetic levitation are other applications based on the use of magnetisation forces and Lorentz forces obtained by static magnetic fields.

This part is a non-exhaustive list of applications of the use of magnetic fields in the processing of materials. If some are already directly involved in industrials processes, others are still subjected to fundamental studies. Last but not least, EPM activities are devoted to the economical aspect relating to mass productions and should be devoted also to solving environment problems. The new concept of Nature-Guided Materials Processing is expected to be introduced into EPM.

1.1.1. Varying magnetic field in the processing of materials

Induction heating of materials

The high frequency induction heating is one of the first applications of electromagnetic fields [ASMH91]. It is a method of heating electrically conductive materials by the application of a varying magnetic field. In this process, the varying magnetic field induces an electric potential, which can then create an electric current depending on the shape and on the electrical characteristics of the workpiece. These so-called eddy currents dissipate energy and produce heat by flowing against the resistance of the imperfect conductor. Because all metals are fair electrical conductors, induction heating is applicable to several types of metal processing operations such as melting, welding, brazing, heat treating, stress inducement, zone refining, or also heating prior to hot working [RUDN03].

The basic components of an induction heating system are an induction coil, an alternating-current power supply, and the workpiece itself. The coil, which may take different

shapes depending on the required heating pattern, is connected to the power supply so that a magnetic field is generated from the current flow (Figure 1.1).
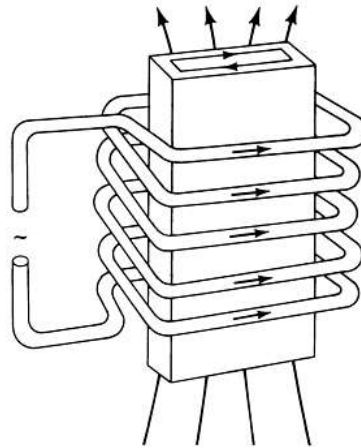
Figure 1.1   Pattern of currents and the magnetic field in a solenoid coil and workpiece. Note that the induced eddy current in the specimen is opposite to that in the coil [ASMH91].

The magnitude of the field depends upon the strength of the current and the number of turns in the coil. For an electrically conductive object, placed inside a coil with a varying current, eddy currents are generated from the varying magnetic field within the object. These eddy currents are induced as a result of Faraday's law of electromagnetic induction [SOMM66]:

$$e = -N_C \frac{d\Phi}{dt}$$ (1)

which relates an induced voltage (e) to the time rate of change of the magnetic flux (Φ) and the number of turns (N_C) in the coil.

The induced currents generate their own magnetic fields, which are in opposition to the field generated by the coil and thereby prevent the field from penetrating the centre of the object. Therefore, the eddy currents are more concentrated at the surface and decrease in strength toward the centre of the object. This phenomenon of the eddy currents travelling closer to the surface of a conductor is called "skin effect". A definition of an "effective" depth of eddy currents is usually adopted where the current density has dropped by $1/e$ of its surface value and is given by:

$$d = \sqrt{\frac{\varrho}{\pi \mu_0 \mu_r f}} \qquad (2)$$

where d is the reference depth, ϱ is the resistivity of the workpiece, μ_0 is the magnetic permeability of the vacuum, μ_r is the relative magnetic permeability of the workpiece (dimensionless), and f is the frequency of the alternating magnetic field of the work coil.

Alternating magnetic fields are thus now widespread in metallurgical processes. Initially used for heating and melting electrically conducting materials, it has been discovered that the magnetic field was able to induce many other effects such as bulk stirring, free surface control or also defect structure reduction.

The stirring of liquid metal and control of solidification by AC magnetic field

In recent years, most steelmakers have recognized that control of fluid flow and mixing phenomena in a liquid metal is necessary to improve the overall quality of cast billets. More specifically, in addition to reducing solute segregation during solidification, the flow may play a key role in eliminating inclusions, blowholes and centre porosity. As a result, electromagnetic stirring has become an integral component of the continuous casting process [MOSH63, BIRA83]. More in details, the function of fluid driving is induced by imposing an electric current and a magnetic field, $F_{mag} = J \wedge B$, or by imposing a travelling magnetic field [GELF03].

Thanks to the flexibility of the high frequency electric power sources, it is now possible to generate complex alternating magnetic fields [GALI07]. As an illustration, such types of magnetic fields are able to provide better chemical homogeneity of the cast alloy composition [TZAV74], control temperature gradient in separate zones of the furnace [LANT07] or also control the instabilities on the surface of a melt [PRIE06].

In the same way, it is possible to control the solidification of a metallic alloy by the use of alternating magnetic fields. Travelling or rotating magnetic fields are actually used to generate forced convection [GAIN75]. With the development of numerical modelling coupled to experiments, it is now possible to have a deeper understanding of the subtle effects of forced convection. As an example, it has been recently shown that the homogeneity of the deposit thickness of gold on electrical connectors could be optimized by the use of a strong

alternating magnetic field of low frequency [OLIV04]. Another example is the use of electromagnetic forces to change the flow structure in the bulk liquid. In this way, they modify the pressure differences at the solidification front, changing the channel segregation pattern and partly preventing the unsteadiness of buoyancy effects [MEDI07].

1.1.2. Processing of materials in static magnetic field

The control of convection in liquid metal with static magnetic field

As previously introduced, the convection in a liquid metal is important for problems involving heat transfer and crystal growth from a melt. When an electrically conducting fluid moves in a DC magnetic field, Lorentz forces dampen the fluid motion with respect to $F_{mag} = \sigma(v \wedge B) \wedge B$. The application of magnetic fields has thus been used in various industrial fields such as magnetic suppression of convection in molten semiconductor material [SERI91] or magnetic control of molten iron flows in steel industry [IDOG93].

Lorentz forces do not apply to electrically non-conducting materials. Nevertheless, magnetisation forces, which act on almost every material, can be used to control convection [BRAI91, QIWA01, WANG02, FILA05]. Regarding magnetisation force given as $F_{mag} = (\chi/\mu_0)(B \cdot \nabla)B$, there are two kinds of forces that are available in materials processing. One is the force pulling ferromagnetic and paramagnetic materials to a magnet and repulsing diamagnetic ones, and the other is force rotating a materials in the magnetic field direction as for example, a compass rotates to the north direction.

The driving force for convection is usually the density difference between the hot and cold regions of the fluid. If the fluid has a magnetic susceptibility that varies with temperature, magnetic forces can drive convective motion. Not only in liquid metal, it has been shown recently that the magnetic force is acting on oxygen gas, which is paramagnetic, and that it affects air convection and promotes combustion through magnetoaerodynamics [WAKA96].

Texturing materials in static magnetic field

The ability to impose a preferred orientation, or texture, on a crystalline material is important in many fields of materials science, because texture has significant implications on

material functional properties. Texturing allows the most favourable direction to be used in applications.

Magnetic forces and torques are used for texturing, by solidification, materials that have a residual anisotropy in their magnetic susceptibility at high temperature [DERA91, CHAU97]. More recently, it has been recognized that the magnetisation forces can be effective even in non-magnetic materials when those are placed under a high magnetic field. Several results have thus been obtained in the control of crystal orientation in materials processing such as electrodeposition, vaperdeposition, solidification, baking, slip-casting and precipitation. Review of these applications can be found elsewhere [ASAI03].

Magnetic levitation of diamagnetic material

Moreover, magnetic levitation of diamagnetic materials has received much attention as a new method for materials processing in high magnetic fields [BEAU91]. In the magnetic levitation state, the magnetic force acting on materials balances with the gravitational force $F_{mag} = mg$. As a recent illustration of this phenomenon, Figure 1.2 shows an experiment carried out in the Nijmegen High Field Magnet Laboratory where a frog (alive) was put in a strong magnetic field and levitated.

Figure 1.2   Magnetic field levitation of a frog

Since such a balance holds for each molecule or atom constituting the materials, the magnetic levitation is considered to be almost equivalent to microgravity condition. Its application to materials synthesis enables many novel techniques such as containerless crystal

growth. A containerless technique provides clean environment that is free from contamination from a container. Suppressing uncontrollable heterogeneous nucleation, the liquid easily undergoes a supercooled or supersaturated state [TAKA06].

1.1.3. Future prospect for Electromagnetic Processing of Materials

A variety of problems and applications has been shown in this part concerning the use of alternating or static magnetic fields. Heating and stirring of molten metal, convection control in liquid metal and separation of non-conductive materials in a conducting medium are based on the Lorentz force. Levitating diamagnetic materials, crystal orientation and matter transportation are based on the magnetisation force and torques. The recent introduction of high magnetic fields into EPM has provided several new applications in electro-deposition, crystal orientation, phase transformation, self-assembling and particles patterning. These new functions have been explained using the magnetisation energy or polarization effect. Up to now, industrial applications have been mainly concentrated on applications related to the Lorentz force. The use of magnetisation force induced by high magnetic fields has scarcely been seen in practical applications.

In conclusion, it is found that Lorentz force, magnetisation force and magnetic energy play different roles on the solidified structures, whose dominancy depends on different physical properties of metals, alloying elements or phases involved. These results indicate that it is possible to control solidified structures so as to improve the performances of inorganic and even organic materials using Electromagnetic fields in the Processing of Materials.

1.2. Processing of Steel in High Magnetic Field

In the previous part, the most important effects of AC and DC magnetic fields observed in materials science have been described from a general point of view. This second part is more specifically focused on the results obtained on the processing of iron-based alloys and more particularly on steels.

In ferrous alloys, magnetic field effects were first noticed in texture formation more than half a century ago [SMOL49], when the available field intensity was an order of magnitude or less than one Tesla. Then, the effects on spinodal decomposition were studied with a magnetic field of similar intensity [CAHN63]. In the 1960's it became known that

magnetic fields promote martensitic transformation in ferrous alloys [SATY68]. Otherwise, much stronger magnetic field are needed to study precipitation and phase transformation whose chemical driving force is large compared to the energy of interaction with external fields. Owing to the development of superconducting technology, new instruments producing magnetic fields as high as 10 T or more have appeared. Thereby, experimental setups have been developed in high field environments and allow heat treatment in a static magnetic field for a substantial amount of time.

In this paragraph, the effect of magnetic fields on the kinetics and microstructures of steels during various phase transformations (i.e. ferrite, martensite and bainite) is reviewed. As an introduction, a general overview of phase transformations in steels (without any magnetic field) is given.

1.2.1. Overview of transformation in steels

Before discussing the effect of magnetic fields, a short description of the solid state phase transformations involved in iron alloys is made. Basic concepts concerning lattice structure, mass transfer, reaction at the interface and phases involved in steels are reviewed.

<u>Polymorphic transformation in iron</u>

At atmospheric pressure and at temperatures between 1183 K and 1673 K, iron exists as a face-centred cubic (FCC) arrangement of iron atoms called austenite (γ). Unlike other FCC metals, lowering the temperature leads to the formation of a less dense, body-centred cubic (BCC) allotrope of iron called ferrite (α). Figure 1.3 shows the variation of the lattice parameter usually adopted for pure iron [PHIL98]. Above 1673 K, a (BCC) structure called δ-ferrite transforms from austenite with increasing temperature. In Figure 1.3, we can notice the good agreement between the expansion coefficient of the two phases α and δ.

The change in crystal structure between austenite and ferrite can occur at least in two different ways. Given sufficient atomic mobility, the FCC lattice can undergo a complete reconstruction into the BCC ferrite structure, with diffusive rearrangement of atoms at the transformation interface. On the other hand, if the FCC phase is rapidly cooled down to a very low temperature, well below 1183 K, there may not be enough time or atomic mobility to enable diffusional transformation. Nevertheless, the driving force for transformation increases

with undercooling, and the diffusionless formation of martensite occurs, by a displacive mechanism involving the systematic and co-ordinated transfer of atoms across the interface.
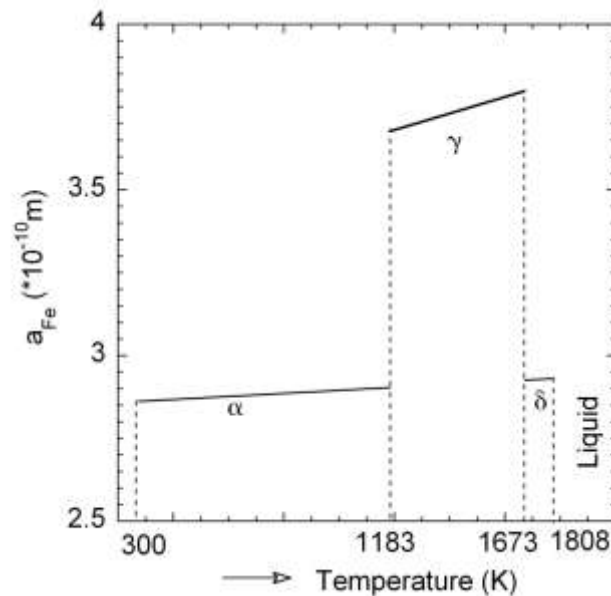
Figure 1.3   Variation of the lattice parameter of iron as a function of temperature under atmospheric pressure.

Interstitial and substitutional alloying of iron

When interstitial and substitutional alloying additions are made to pure iron, many subtle variations of the displacive and diffusional mechanisms arise, together with the possibility of other phases and morphological variations. The versatility of steels depends to a large extent on this wide variety of microstructures that can be obtained by transformation from austenite. The microstructure varies not just in morphology, but in phase composition, defect structure, stored energy and thermodynamic stability.

Indeed, addition of elements to a pure material induces an increase or a decrease of its transformation temperature. Moreover, the transition is spread over a wider range of temperatures below or above the transformation temperature of the pure material. The alloying elements of iron are generally classified into two classes according to their effect on the stability domain of austenite [BAIN39]. The first class of alloying elements widens the temperature range for stable austenite by depressing the austenite-ferrite transformation temperature. This is the case of carbon or nitrogen which formed interstitial solution with iron. This is also the case of nickel, cobalt, or manganese which formed substitutional solution

with iron. The second class of alloying elements reduces the stability domain of austenite. They are for example metallic elements such as vanadium, niobium, chromium or aluminium but also non-metallic elements such as silicon, phosphorus or sulphur.

Iron-Carbon Equilibrium Phase Diagram

Figure 1.4 shows the schematic illustration of the iron rich part of the iron-carbon phase diagram in which the stable phases which appears in steels are marked. The vast majority of steels are in the austenitic condition at temperatures above 1200 K. Austenite tends to decompose into ferrite and cementite (Fe_3C). Steels with a carbon concentration less than about 0.8 wt% are hypoeutectoid; those with greater concentrations are hypereutectoid. Steel with exactly 0.8 wt% carbon will tend to decompose into an intimate mixture of cementite and ferrite, called pearlite by a eutectoid reaction as $\gamma \rightarrow \alpha + Fe_3C$. Hypoeutectoid steel will first decompose during cooling to ferrite at the austenite grain boundaries; the austenite is consequently enriched in carbon and will eventually form pearlite giving a mixed microstructure of ferrite and pearlite.
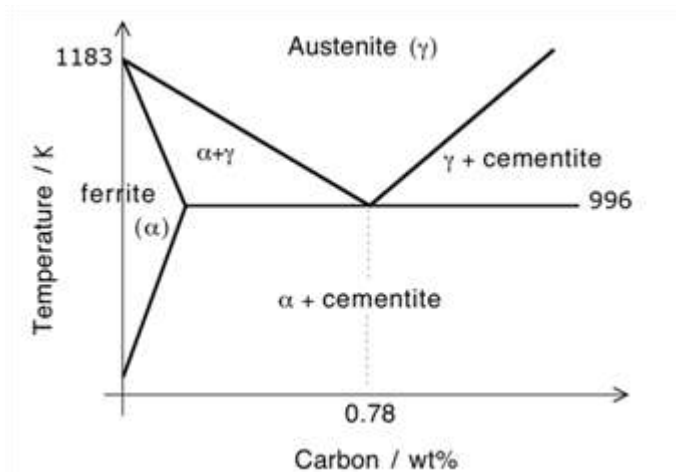
Figure 1.4   Iron-Carbon phase diagram

Figure 1.5 shows a schematic illustration of the position of a carbon atom (in black) in the lattice of FCC austenite (left) and BCC ferrite (right). The carbon atom in the FCC austenite lattice is in a regular octahedron and causes a uniform expansion of the lattice. This isotropic volume change does not interact with shear strength of dislocation and thus, carbon atoms in austenite only weakly interact with the dislocation strength field [KITT98]. As a consequence, the amount of strengthening caused by carbon atom in austenite is weak.

However, the carbon atom in the BCC ferrite lattice is in an irregular octahedron that has two long axes and one short axis. This asymmetry induces a tetragonal distortion of the lattice. Thus, the carbon atom in BCC ferrite will interact with strength fields of dislocation and will cause a huge amount of hardening. Because carbon atom causes a very large strength in ferritic iron, the solubility of carbon in ferritic iron is very small (0.02 wt%), and on the contrary the solubility in austenite is much higher because the distortion caused by carbon is smaller.
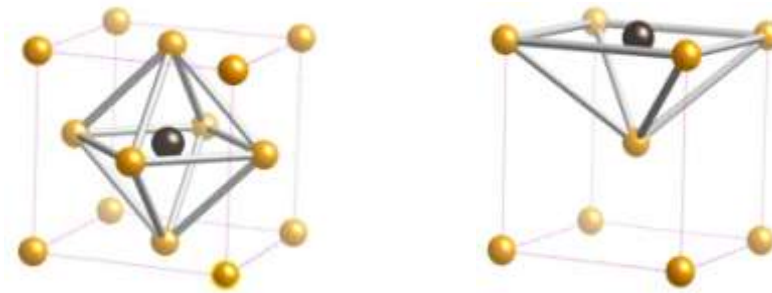
Figure 1.5   Carbon atom in (left) FCC austenite lattice and (right) BCC ferrite lattice

Classification of steel microstructures

Ferrite which grows by a diffusional mechanism can be classified into two main forms [BHAD85]: allotriomorphic ferrite and idiomorphic ferrite. The term 'allotriomorphic' means that the phase nucleates at prior austenite grain boundaries and tends to grow along the boundaries at a rate faster than in the direction normal to the boundary plane. Its shape is thus strongly influenced by the presence of the boundary and hence does not necessarily reflect its internal symmetry. The term idiomorphic implies that the phase concerned has faces belonging to its crystalline form. Idiomorphic ferrite usually forms intragranularly, presumably at inclusions or other heterogeneous nucleation sites. Nevertheless, the extent of penetration into particular austenite grains may vary since interface mobility can change with the α/γ crystallographic orientation relationship, mass transfer or also internal stresses.

Pearlite is another common constituent in low-alloyed steels and consists of two phases: ferrite and cementite. The formation of pearlite involves the co-operative, diffusional growth of ferrite and cementite from austenite. In two-dimensional sections, this eutectoid mixture appears to consist of alternate lamellae of ferrite and cementite, which together form a pearlite colony. Actually, the cementite and ferrite within a given colony are single crystals,

the lamellae of each phase being connected in three dimensions [HILL62]. Examples of pearlite in hypoeutectoid steels are given in the optical micrograph shown in Figure 1.6. Many colonies of pearlite are shown in this micrograph. A colony represents a single orientation of the pearlite lamella.
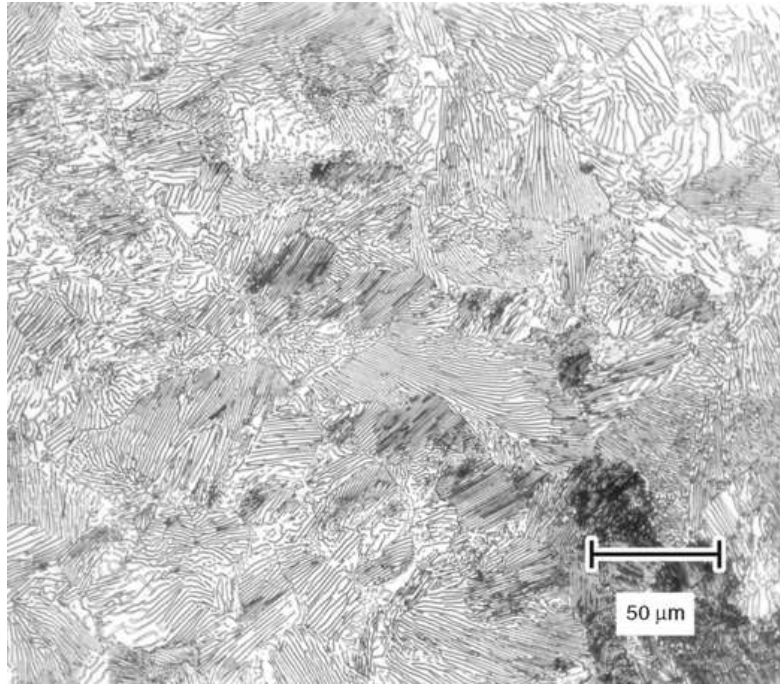
Figure 1.6   Microstructure of a Fe-0.8C-0.7Mn (wt%) steel showing colonies of pearlite. 4 % picral etch. Original magnification 200× [ASMH04]

Figure 1.7 and Figure 1.8 show optical micrograph of hypoeutectoid steels illustrating the various morphologies of ferrite grains. This microstructure consists of ferrite grains (the light-appearing constituent) and pearlite (the dark-appearing constituent). The interesting feature of the microstructure shows in Figure 1.7 is the ferrite formed on the original or prior-austenite grain boundaries during cooling from austenite. Ferrite in this form is called allotriomorphic ferrite. Figure 1.8 shows the microstructure of another hypoeutectoid steel. The microstructure also consists of ferrite and pearlite but is mostly ferrite with a small volume fraction of pearlite. The ferrite in this form is called equiaxed ferrite. The lower volume fraction of pearlite indicates that this steel has much lower carbon content than the steel shown in Figure 1.7.
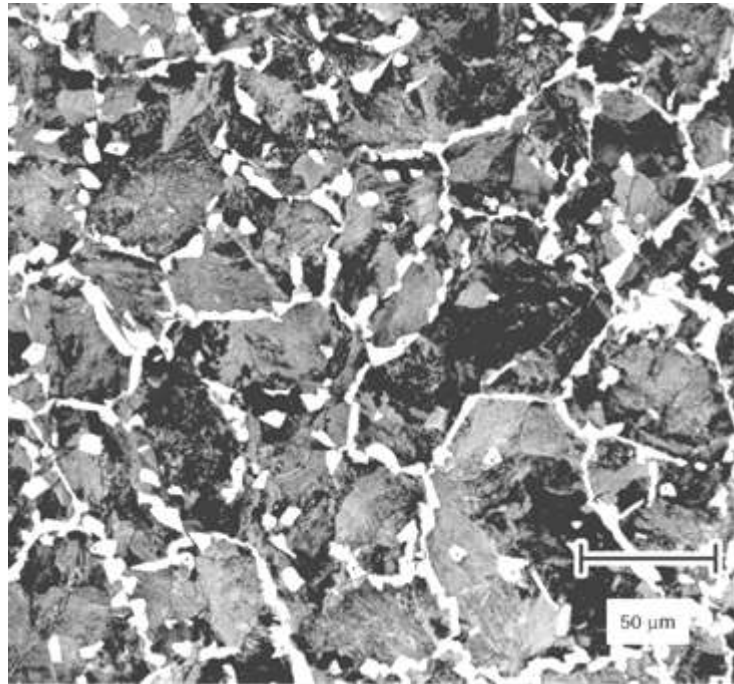
Figure 1.7   Microstructure of a Fe-0.4C-0.7Mn (wt%) steel showing equiaxed proeutectoid ferrite grains (in white) outlining the prior-austenite grain boundaries. The matrix is pearlite (dark etching constituent). 4 % picral etch. Original magnification 200×[ASMH04]
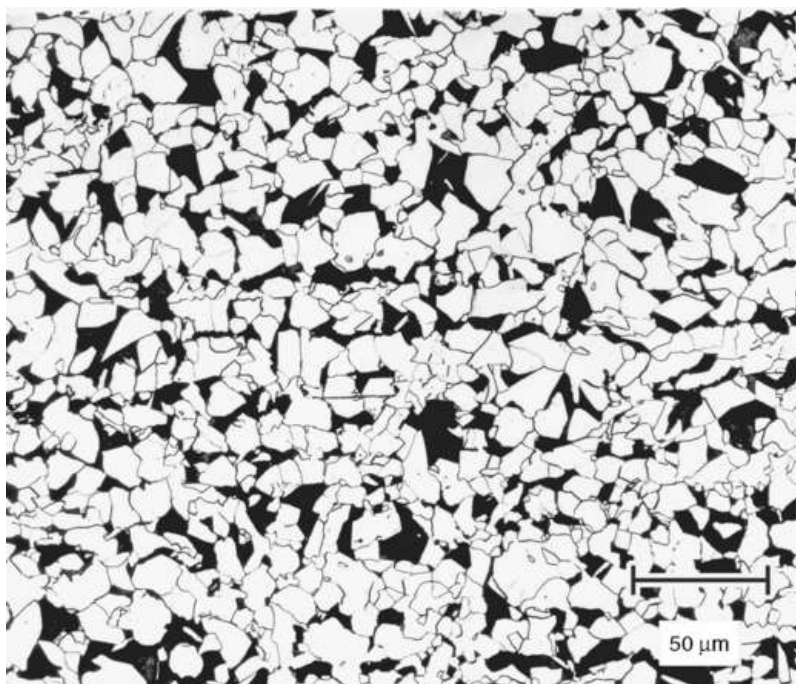
Figure 1.8   Microstructure of a Fe-0.14C-0.7Mn (wt%) steel showing equiaxed ferrite grains with pearlite islands. 4 % picral + 2 % nital etch. Original magnification 200×[ASMH04]

Martensite is a product of diffusionless transformation and can occur in the form of thin, lenticular plates which often extend right across the parent γ grains, or as packets of approximately parallel, fine laths whose size is generally smaller than that of the γ grains. Example of martensitic microstructure is given in Figure 1.9. In both cases, the parent and product crystals are related by an atomic correspondence and the formation of martensite causes the shape of the transformed region to change. Martensite can occur at very low temperatures and its interface with the parent phase necessarily has to be glissile. The thermodynamic of this transformation has been often regarded since the works of Hillert in 1958 [HILL58].
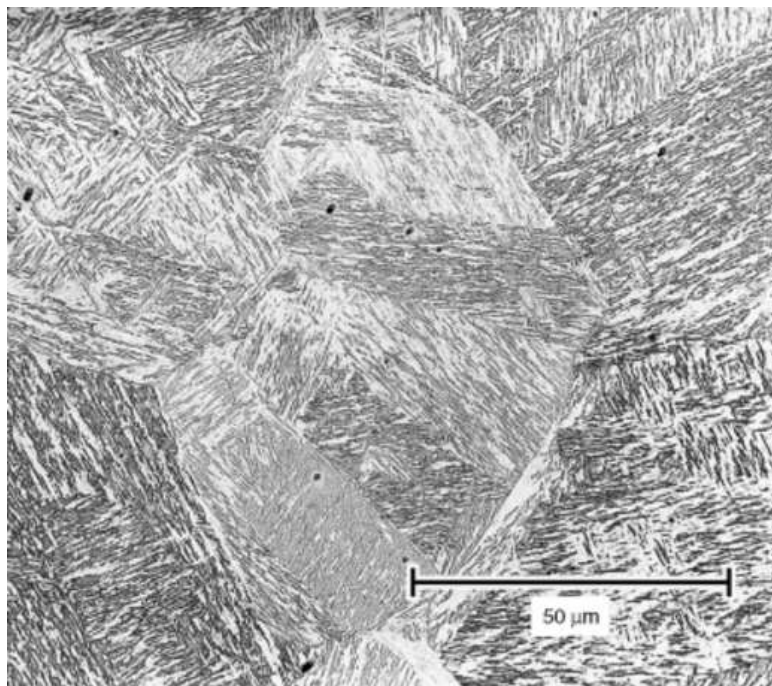
Figure 1.9   Microstructure of water-quenched low-alloy steel showing lath martensite. 2% nital etch. Original magnification 500×[ASMH04]

Widmanstätten ferrite or acicular ferrite can form at low undercooling below the equilibrium transformation line between austenite and ferrite where the driving force for transformation is small, so that the partitioning of carbon during transformation is a thermodynamic necessity. On an optical scale, Widmanstätten ferrite has the shape of a thin wedge, the actual shape being somewhere between that of a plate and a lath as shown in Figure 1.10 [WATS73]. The shape change accompanying Widmanstätten ferrite growth implies the existence of a glissile interface between parent austenite and growing ferrite plate. The rate of growth is expected to be controlled by the diffusion of carbon in the austenite

ahead of the moving interface, even when the reaction occurs at a low temperature. Nevertheless, Widmanstätten ferrite cannot be regarded as a product of diffusional transformation since iron and substitutional atoms do not diffuse during growth and there is no reconstructive diffusion during transformation.
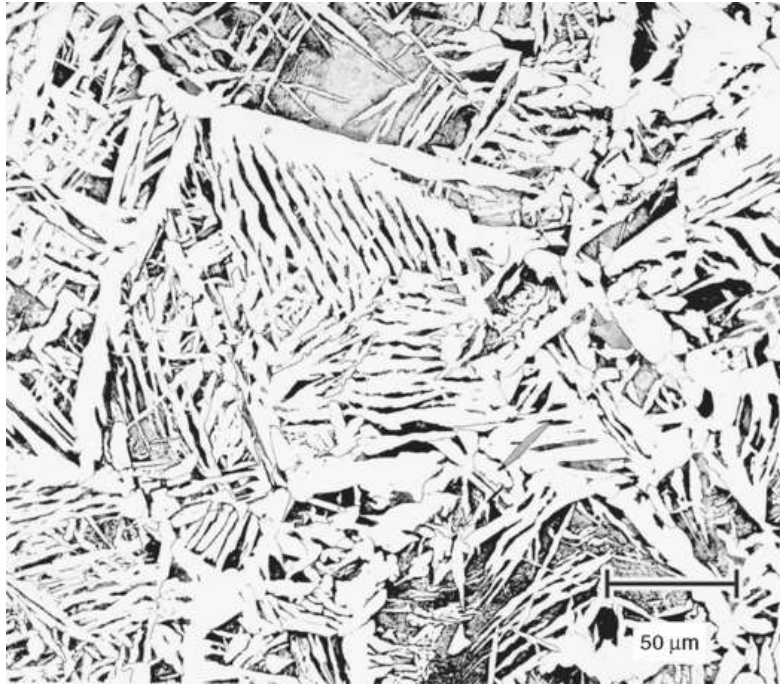
Figure 1.10   Microstructure of a Fe-0.14C-0.4Mn (wt%) steel showing acicular ferrite with some pearlite (dark etching constituent). This type of acicular appearance is called Widmanstätten structure. 4 % picral etch. Original magnification 500×[ASMH04]

Bainite occurs at a higher undercooling relative to Widmanstätten ferrite and grows in the form of sheaves originating from γ grain boundaries. The sheaves consist of much smaller platelets of ferrite. Bainite structure is often divided into two classes that are upper and lower bainite depending on the mechanism of carbide precipitation. Cementite precipitation occurs from the austenite between the sub-units in the case of upper bainite, in lower-bainite, the cementite can also precipitate from within the ferrite [BHAD80]. Lower bainite occurs at a lower temperature compared with upper bainite. Bainite transformation is likely to be the most complex austenite transformation because it exhibits features of both diffusive and displacive transformations [QUID01]. Figure 1.11 shows an optical micrograph of low-carbon steel with a bainitic microstructure.
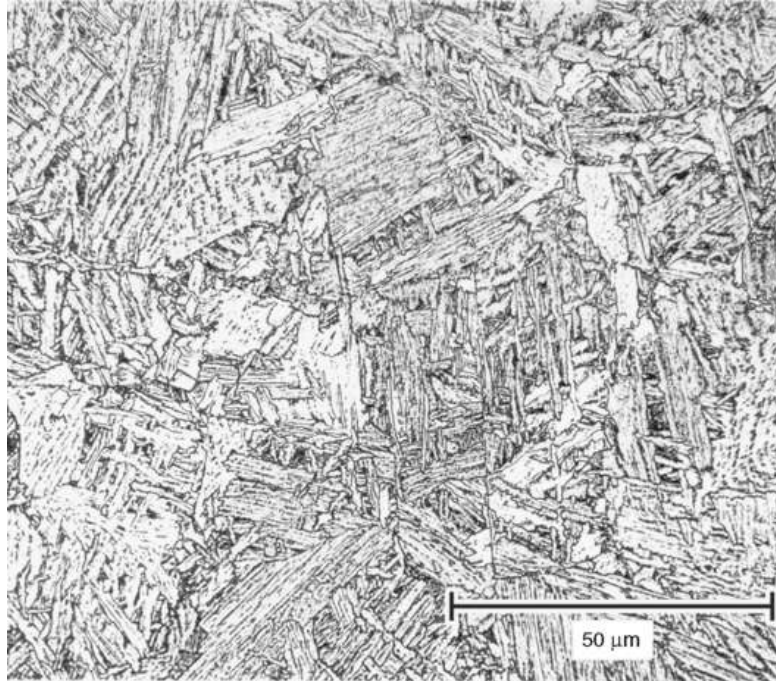
Figure 1.11   Microstructure of heat treated low-alloy steel showing bainite. 4% picral + 2% nital etch. Original magnification 500×

In effect, the formation of Widmanstätten ferrite, upper bainite, lower bainite and lath martensite should be regarded as a continuous series even though there are significant distinctions between neighbouring products. It was proposed by Purdy and Hillert in [PURD84] that important changes occur in the properties of the interface with decreasing temperature and result in changes from one product to the next.

Interfacial conditions and origin of the driving force for ferrite transformation

Upon cooling from the austenite temperature region, the ferrite to austenite transformation is usually the first to occur in most steels of industrial importance. Description of ferrite formation in steel is summarized rapidly in this part in order to point out important concepts of driving force, mass transfer and interface motion [BRAD77, BRAD81].

In the Fe-C binary system, the α and γ phases are in equilibrium when they have equal Gibbs free energy (Figure 1.12) [GUST85]:

$$G^{\alpha} = G^{\gamma} \tag{3}$$
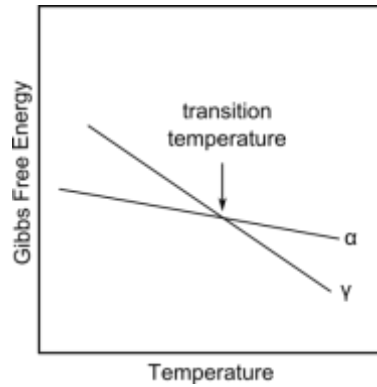
Figure 1.12   The transition temperature for an allotropic transformation.

The Gibbs free energy is in general a function of the mole fraction of Fe and C in the respective phases and is simply the weighted mean of the free energies of its component atoms:

$$G^\alpha = (1-x)\mu_{Fe}^\alpha - x\mu_C^\alpha \tag{4}$$

$$G^\gamma = (1-x)\mu_{Fe}^\gamma - x\mu_C^\gamma \tag{5}$$

where x is the mole fraction of C, μ_i^α and μ_i^γ represent the partial free energies of element i for the α and γ phase respectively and μ is called the chemical potential of i in J/mol. The expressions for the chemical potential are available in literature [DINS91, GUST85] and are usually introduced in the databases of thermodynamics software. The chemical potentials are changing with compositions according to the slope of the tangent of the free energy curve as shown in Figure 1.13(a).

The coexistence of the two α and γ phases in equilibrium conditions is only possible if the iron atoms in γ have the same free energy than that of the iron atoms in α and if the same is true for the carbon atoms.

$$\mu_{Fe}^\gamma = \mu_{Fe}^\alpha \tag{6}$$

$$\mu_C^\gamma = \mu_C^\alpha \tag{7}$$

The equilibrium compositions are identified as x_C^α and x_C^γ and are used to build the equilibrium phase boundaries of phase diagram as illustrated in Figure 1.13(b). When the chemical potentials of the two components in the ferrite and austenite phase are equal, no driving force exists for the interface migration. However, in real case, a driving force is

required for the transformation and there must be some free energy dissipated by the structural rearrangement from FCC to BCC structure. Since it is the iron atoms that facilitate the structural change, the required driving force is naturally defined in term of chemical potential differences of iron across the interface. Besides, it is expected that the carbon atoms may diffuse quickly enough in the vicinity of the interface to avoid any gradients in carbon concentration across the interface. This case is schematically illustrated in Figure 1.13(a) with the dashed lines construction.
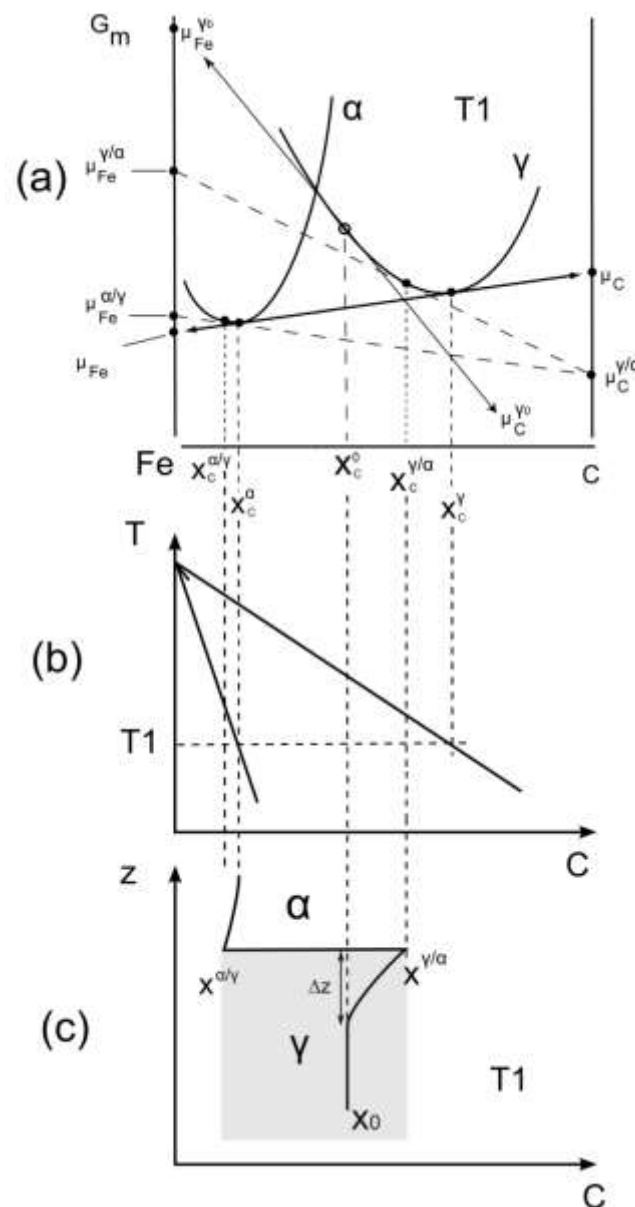
Figure 1.13   (a) Gibbs free energy –composition diagram for the α and γ phase in Fe-C system [INDE03], (b) Equilibrium phase boundaries for the α and γ phase in Fe-C system. (c) Carbon concentration profile at the ferrite austenite interface

The carbon concentration in both sides of the interface is given by $x_C^{\gamma/\alpha}$ in austenite and $x_C^{\alpha/\gamma}$ in ferrite. Through this construction, a difference in chemical potential of Fe atoms exists and the resulting force is used to drive the interfacial process. As ferrite is growing, its diffusion field extends so that the solute (carbon atoms) has to diffuse over a larger distance. Assuming that the carbon concentration gradient in the matrix is constant and that the far-field concentration x_C^0 never changes, the concentrations at the interface for an isothermal concentration are given by the tie-line of the phase diagram as shown in Figure 1.13(b) at temperature T1. Across the interface, the diffusion flux of solute, i.e. carbon atoms, from the interface must equal the rate at which the solute is incorporated in the parent phase so that:

$$(x_C^{\gamma/\alpha} - x_C^{\alpha/\gamma}) \; \frac{\partial z^*}{\partial t} = D \frac{\partial x_C}{\partial z} \approx D \frac{x_C^0 - x_C^{\gamma/\alpha}}{\Delta z} \tag{8}$$

where z is a coordinate normal to the interface with a value z^* at the interface position and D is the diffusivity of C in the γ phase in $m^2.s^{-1}$. Figure 1.14 shows the diffusion coefficient of carbon in both ferrite and austenite [JACO97]. The second equation that can be derived from these conditions is obtained by considering the overall conservation of mass as illustrated on Figure 1.13(c):

$$(x_C^{\alpha/\gamma} - x_C^0)z^* = \frac{1}{2}(x_C^0 - x_C^{\gamma/\alpha})\Delta z \tag{9}$$

Finally the interface velocity can be derived in combining equations (8) and (9) to eliminate Δz as:

$$\frac{\partial z^*}{\partial t} = \frac{D_C(x_C^0 - x_C^{\gamma/\alpha})^2}{2z^*(x_C^{\gamma/\alpha} - x^{\alpha/\gamma})(x_C^{\alpha/\gamma} - x_C^0)} \tag{10}$$

It follows that the thickness of ferrite increases with the square root of time and that the growth rate is slowing down as time is increased:

$$z^* \propto \sqrt{D_C t} \tag{11}$$
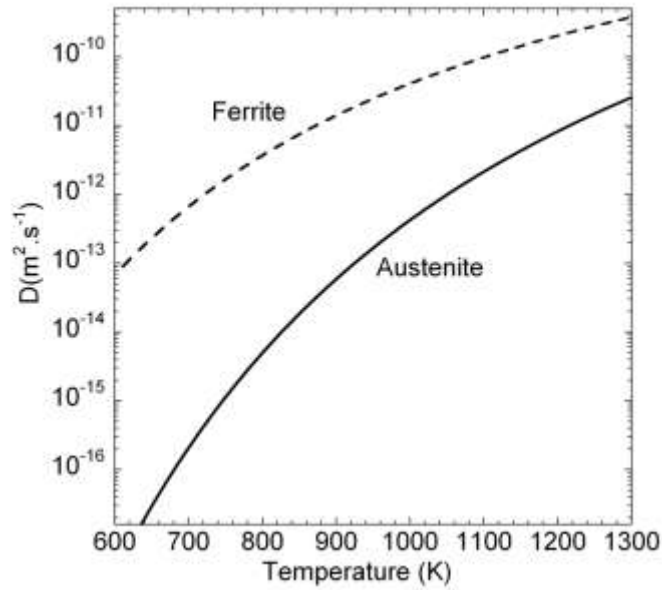
Figure 1.14   Diffusivity of carbon D_C in the bulk of ferrite and austenite [JACO97]

In the case of an interface controlled reaction, the interface velocity can be evaluated either from the interface reaction or from the mass balance and the interfacial conditions must be such that they give the same velocity [HILL75]:

$$v = Mob \cdot \Delta G^{FCC \rightarrow BCC}/V_m \approx Mob \cdot (\mu_{Fe}^{\gamma/\alpha} - \mu_{Fe}^{\alpha/\gamma})/V_m \qquad (12)$$

$$v = \frac{D_C}{x^{\gamma/\alpha} - x^{\alpha/\gamma}} \cdot \frac{\partial x^{\gamma/\alpha}}{\partial z} \qquad (13)$$

where *Mob*, the interface mobility in m.m^4.J^{-1}.s^{-1} is a kinetics parameter which relates to the free energy dissipated at the interface and to the interface velocity [HILL75]. V_m is the volume of one mole of iron ($V_m \approx 7.10^{-6}$ m^3.mol^{-1}). A commonly adopted expression given by Hillert [HILL06] for the grain boundaries mobility in the $\gamma \rightarrow \alpha$ transformation at very low carbon contents as a function of temperature *T* is:

$$Mob = Mob_0 e^{-\frac{Q}{RT}} \qquad (14)$$

R is the ideal gas constant, Mob_0 is the intrinsic mobility ($Mob_0 = 0.0035$ m^4.J^{-1}.s^{-1} [HILL75]) and Q is the activation energy of the interface mobility ($Q = 147000$ J.mol^{-1} [HILL75]).

Most of industrial steels contain many other substitutional elements (named X) beside carbon and the growth of ferrite has to be described in a system based on Fe-C-X. Two different models have been proposed to describe growth in these higher order systems. These are the local equilibrium (LE) conditions and the paraequilibrium (PE) conditions.

In the case of ternary steels, equations based on equations (6) and (7) have to be satisfied simultaneously, i.e. one for each Fe, C and X element. The diffusivity of carbon is, in general, much higher than that of the X element and this system cannot be simultaneously satisfied with a tie-line passing through both far-field compositions x_C^0 and x_C^0. Other tie-lines are thus to be chosen such as, for example, $x_C^{\gamma/\alpha} = x_C^0$ as illustrated in Figure 1.15(a) (line AB). In this case, the gradient of carbon concentration across the interface is small and the diffusivity of carbon is reduced so that the flux of carbon atoms is forced to slow down to a rate consistent with the diffusion of the substitutional element X. In this circumstance, ferrite is said to grow in Local Equilibrium with Partition of the substitutional element (LE-P).
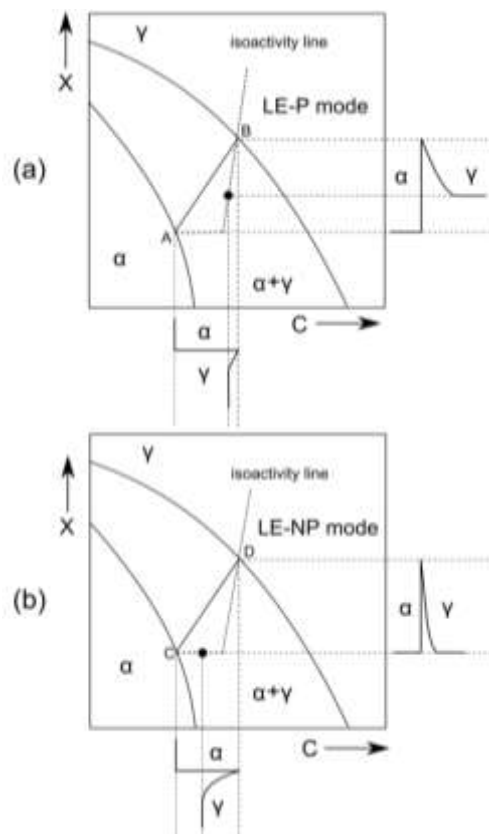
Figure 1.15   Schematic isothermal section of the Fe-C-X system, illustrating ferrite growth occurring with Local Equilibrium at the interface (a) with partition and (b) without partition of the substitutional element during transformation. The bulk alloy composition is marked with a black circle.

In a second example, the chosen tie line allows $x_X^{\gamma/\alpha} = x_X^0$ as illustrated with line CD in Figure 1.15(b). In this case, the concentration gradient of the element X is drastically increased since a very small amount of X is partitioned into the austenite [REED92]. This corresponds to the Non-Partitioned Local Equilibrium (LE-NP) growth mode of ferrite in recognition to the fact that the X content of the ferrite is approximately equal to that in austenite.

Beside the LE conditions, another growth mode, where the tie-lines are all virtually parallel to the carbon axis, is usually defined as the paraequilibrium which is a constrained equilibrium. The paraequilibrium is based on the idea that the substitutional element X becomes virtually immobile and cannot redistribute during the transformation. The ratio of X to Fe concentration is thus identical in the two phases [HILL53]. In this model, carbon atoms are in local equilibrium [HILL53]. These conditions can occur when one of the components can diffuse much faster than the others. The α/γ paraequilibrium boundary conditions are reduced to:

$$
\begin{aligned}
\mu_{Fe}^\alpha + \kappa\, \mu_X^\alpha &= \mu_{Fe}^\gamma + \kappa\, \mu_X^\gamma \\
\mu_C^\alpha &= \mu_C^\gamma
\end{aligned}
\tag{15}
$$

where $\kappa = x_X^0/x_{Fe}^0$ is the ratio of X to Fe concentration. Under these conditions it is possible to have a partially partitionless transformation where a new phase can form with different contents of the mobile component but with the same composition of the slow diffusing components. Paraequilibrium can be calculated both in single equilibrium calculations and also in step-by-step calculations. Such calculations are useful e.g. when studying phase transformations in systems with large differences in the diffusivities of different elements.

Information on steel microstructure are given in more details in [ASMH04]. More consideration relative to thermodynamics, diffusion, recristallisation but also heat treatments and materials characterisation in steels will not be introduced in this section because this subject is too wide. Large set of information can be found in the following literature [ASMH93, PHIL98, BUDD03, INMA65]. The above-mentioned topics will be discussed more specifically regarding the effect of magnetic field on transformations in steels in the following parts of this manuscript.

1.2.2. Magnetic field influence on phase transformations in iron-based alloys

In this part and in the rest of the manuscript, the term magnetic field is used for two different vector fields such as B and H. The B-field, usually called magnetic induction is expressed in Tesla and is usually defined as a fundamental quantity. The H-field, in A/m, is a derived field which is defined as a modification due to magnetic fields produced by magnetic media as :

$$H = \frac{B}{\mu_0} - M \tag{16}$$

where M is the magnetisation of the materials in $A.m^{-1}$. Outside a magnetic material H-field lines are identical to B-field lines, but inside, they point in opposite directions.

Thermodynamics analysis: Partial molar "magnetic" free energies

Definition of the "magnetic" free energies

Magnetisation and magnetic field can be incorporated in the free energy function in an analogous manner to pressure and volume. The interaction energy per one mole of magnetic phase with external field is written as,

$$\mu_i^B = -\frac{M^{mol}}{\rho_i \mu_0} \int_0^B M^P dB \tag{17}$$

where M^P is the magnetisation of the phase P (austenite or ferrite) per volume unit in $A.m^{-1}$, B is the magnetic field in T. M^{mol} is the molar mass in $kg.mol^{-1}$ and ρ_i is the specific mass in $kg.m^{-3}$ of the species i.

Magnetisation in the paramagnetic state

The magnetisation of a paramagnetic phase P such as austenite and ferrite well above the Curie point of iron is given by the linear relationship:

$$M^P = \frac{1}{\mu_0}\chi^P B \tag{18}$$

where χ^P is the paramagnetic susceptibility of the phase P per unit of volume. The magnetic susceptibility in paramagnetic materials is always positive and obeys the Curie-Weiss law as [JILE91]:

$$\chi^P = \frac{C^P}{T - \theta_c^P} \tag{19}$$

where C^P is the Curie-Weiss constant, θ_c^P is the paramagnetic Curie temperature and T is the absolute temperature in K. Both C^p and θ_c^P are functions of the alloy composition.

The magnetic susceptibility of iron at high temperatures has been measured under low magnetic field by Arajs and Miller [ARAJ60] and Briane [BRIA72] (Figure 1.16) and the corresponding equations for the susceptibility of ferrite and austenite as a function of temperature (above 1100 K) are given respectively by:

$$\chi^\alpha = 4\pi \, 10^{-3}\rho \, \frac{2.33 \, 10^{-2}}{T - 1078} \, [SI] \tag{20}$$

$$\chi^\gamma = 4\pi \, 10^{-3}\rho \, \frac{1.33 \, 10^{-1}}{T + 3451}[SI] \tag{21}$$

Because of the lack of susceptibility measurements at higher field strengths, these susceptibility data are generally used in the prediction of Fe-C phase diagram in magnetic field well above the Curie point of iron. From Figure 1.16, we observe that the paramagnetic susceptibility of austenite is one order of magnitude lower than the paramagnetic susceptibility of ferrite.

Near the Curie point of iron and below, the magnetic susceptibility of ferrite deviates from the Curie-Weiss law due to the magnetic transition. In this case it is commonly adopted to estimate the magnetisation of ferrite with the Molecular Field model [BOZO78, CHOI00, GUOE00, ENOM01, ZAHE05, ZHAN07].
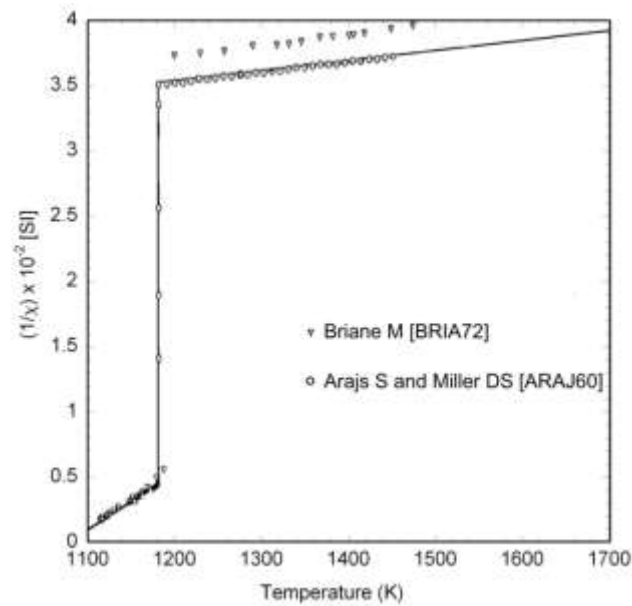
Figure 1.16   The inverse paramagnetic susceptibilities of ferrite and austenite in pure iron. The solid lines represent the regression line evaluated by Arajs and Miller and corresponding to eq. (20) and (21). The triangles correspond to Briane's data.

Magnetisation from the Molecular Field model

The Molecular Field theory is an extension to the classical theory of Langevin Paramagnetism in which the collective magnetic behaviour of elementary magnets submitted to an external magnetic field is calculated by supposing that each elementary magnet does not have any influence on its neighbours ("atoms or molecules" were assumed to be far enough one from the others so that their mutual forces could be neglected). In the Molecular Field theory, Weiss introduced two new quantities: the Molecular Field Constant w and the Molecular Field wM^P which account for the interactions between neighbouring magnets (atoms). The temperature and field dependence of magnetisation is calculated from the orientations of magnetic moments. The magnetic field causes alignment, whereas thermal agitation destroys this alignment.

In the Molecular Field Model, applied to pure iron, a magnetic field is applied to a collection of N_V^α iron–atoms (per volume unit) of the alpha-iron phase. Each atom has a magnetic moment m_{Fe}. Due to the internal magnetic interactions, the magnetic moments are aligned in the direction of the external field. The magnetisation M^α of the whole set is expressed as [BOZO78]:

$$M_{Fe} = N_V^\alpha m_{Fe} B_j(\eta) \qquad (22)$$

where $B_j(\eta)$ is the Brillouin function defined by,

$$B_j(\eta) = \frac{2J+1}{2J} coth \frac{2J+1}{2J}\eta - \frac{1}{2J} coth \frac{1}{2J}\eta \qquad (23)$$

J is the quantum number associated with the total angular momentum. It characterise the total angular momentum of a particle in combining the orbital angular momentum L and the spin angular momentum S. The orbital angular momentum characterise the interaction between the electronic orbital nodes and the nucleus and thus localised electrons are mainly concerned. The total spin angular momentum corresponds to the interaction of the spin of each electron in each orbital to that of its immediate neighbours. Both itinerant and localised electrons are associated to this interaction. J can take different values between *L-S* and *L+S* depending on whether the magnetic carriers are localized or itinerant in the media [BOZO78]. For iron, it is found in [KUBL07] that a better description is given by a local moment approximation. In [BOZO78], it is shown that $J = 0.5$ give slightly better fit than $J = 1$ to the observed dependence of the spontaneous magnetisation of iron.

The magnetic moment of each atom interacts with its neighbours with a magnitude proportional to the magnetisation and temperature and the η function is expressed as a ratio between magnetic and thermal energy by:

$$\eta = \frac{m_{Fe}(B + wM_{Fe})}{k_B T} \qquad (24)$$

where k_B is the Boltzmann constant. At very low temperature and high magnetic field, the magnetisation of iron approaches the saturation magnetisation M_{Fe}^0 given by:

$$M_{Fe}^0 = N_V^\alpha m_{Fe} = N_V^\alpha J g \mu_B \qquad (25)$$

where g is the g-factor or Lande factor. It is a dimensionless quantity which characterizes the magnetic moment and gyromagnetic ratio of a particle. It is essentially a proportionality constant that relates the observed magnetic moment of a particle to the appropriate angular

momentum quantum number J and the Bohr magnetron μ_B. It has been experimentally determined to be close to 2 for iron [SCOT55]. The Curie temperature, that can be experimentally determined [TANA97], is related to the molecular field constant by the following relation:

$$T_c = \frac{(j+1)N_V^\alpha m_{Fe}{}^2 w}{3jk_B} \qquad (26)$$

In practice, the variation of the saturation magnetisation of the ferromagnetic phase as a function of temperature and magnetic field is numerically determined as shown on Figure 1.17. The molecular field constant is first determined with eq. (26) and normalized magnetisation is derived from (24) as:

$$\frac{M_{Fe}}{M_{Fe}^0} = \frac{k_B T\eta - m_{Fe}B}{m_{Fe}wM_{Fe}^0} \qquad (27)$$
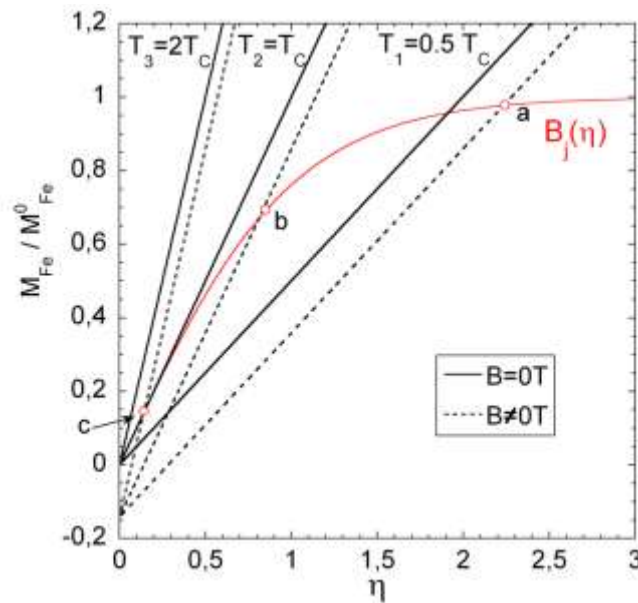
Figure 1.17   Schematic illustration of the determination of magnetisation from Weiss molecular field theory. The magnetisation at field intensity B ≠ 0 is given by points a, b and c for $T = 0.5T_c$, $T = T_c$ and $T = 2T_c$ respectively.

The intersection of equation (23) and (27) gives the variation of the magnetisation with temperature and magnetic field (points a, b and c). At zero field (solid line), the straight line of eq. (27) is tangential to the curve of eq. (23) at $\eta = 0$ and at the Curie temperature. When

an external magnetic field is applied, the straight lines are shifted to the right (dotted lines) and a non-zero magnetisation is observed even above the Curie temperature. Figure 1.18 shows the variation of the saturation magnetisation of iron with temperature calculated from the Molecular Field theory for two different values of J and for 0, 10 and 50 T.

In the absence of applied field (B = 0 T) a non-zero magnetisation is obtained only at temperatures below T_C. On the contrary, at non-zero field, a finite magnetisation is obtained not only below but also above T_C.

In the above description, the magnetisation of α and γ phases in pure iron is calculated. However, we will use the same magnetisation calculation in the case of ferrite and austenite in steels because the effect of carbon on the magnetisation of these two phases can be neglected. Magnetic measurements presented in part will corroborate this assumption. The respective magnetisations of the two phases alpha and gamma being known, the interaction energy per one mole of the respective austenite and ferrite phases with external field can then be calculated, from equ. (17).
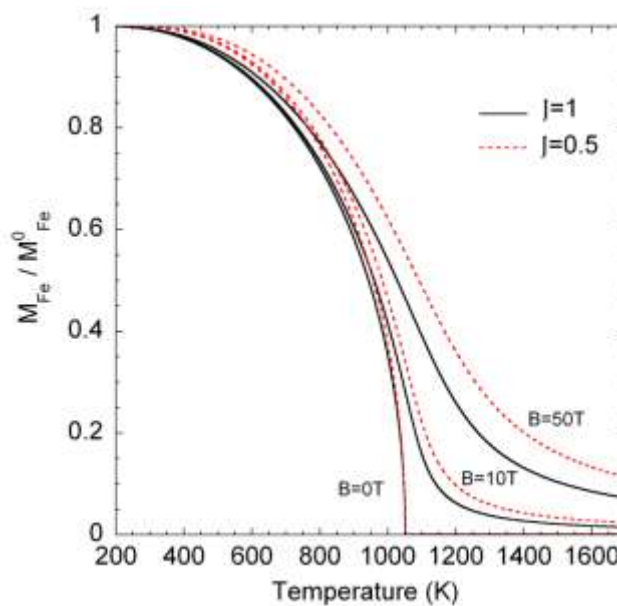
Figure 1.18   Magnetisation of iron vs temperature calculated at B=0, 10 and 50T with J =1 (solid curves) and J =0.5 (dotted curves).

Equilibrium condition in the presence of a magnetic field

As previously introduced, the equilibrium condition between ferrite and austenite, are obtained in equalling the chemical potential of all elements in α and γ by the common tangent

construction. Under the influence of an external magnetic field, the equilibrium conditions are defined similarly. The magnetic energy is simply added in the system as:

$$\mu_{Fe}^{\alpha} + \mu_{Fe}^{\alpha B} = \mu_{Fe}^{\gamma} + \mu_{Fe}^{\gamma B} \tag{28}$$

$$\mu_{C}^{\alpha} + \mu_{C}^{\alpha B} = \mu_{C}^{\gamma} + \mu_{C}^{\gamma B} \tag{29}$$

$$\mu_{X}^{\alpha} + \mu_{X}^{\alpha B} = \mu_{X}^{\gamma} + \mu_{X}^{\gamma B} \tag{30}$$

$\mu_{i}^{\alpha B}$ and $\mu_{i}^{\gamma B}$ are the partial molar "magnetic" free energies respectively for ferrite and austenite of the corresponding element i due to the interaction with the magnetic field.

The magnetic free energy term of equ.(17) for iron is now well defined for austenite and for ferrite in both sides of the Curie point of ferrite. To complete the equilibrium calculation, chemical terms μ_{Fe}^{α} and μ_{Fe}^{γ} are found as a function of temperature in [DINS91]. As an illustration of the use of such a model and for future prospection detailed in this work, FORTRAN® code is written to calculate numerically the equilibrium condition for iron under the influence of magnetic field. In Figure 1.19(a) is plotted the variation of the total Gibbs free energy between ferrite and austenite $\Delta \mu_{Fe}^{tot}$ as:

$$\Delta \mu_{Fe}^{tot} = (\mu_{Fe}^{\alpha} + \mu_{Fe}^{\alpha B}) - (\mu_{Fe}^{\gamma} + \mu_{Fe}^{\gamma B}) \tag{31}$$

At the equilibrium condition, $\Delta \mu_{Fe}^{tot} = 0$. The temperature range where austenite phase is stable becomes narrower as the magnetic field strength increases. It is interesting to note that, under the magnetic field strength over about 70T (not shown in this figure) the austenite phase cannot be stable in the whole temperature range of pure iron. In addition are compared in Figure 1.19(b) the shift of the equilibrium temperature between austenite and ferrite calculated with MF model and with the Curie Weiss law (eq. 20 and 21). These two different approaches give a similar estimation of the equilibrium boundaries under magnetic field up to about 30T.

In the Fe-C system, it is usually assumed that the change in the magnetisation between ferrite and austenite due to the presence of carbon atoms is vanishingly small so that there is no magnetic contribution from C to the free energy: $\mu_{C}^{\alpha B} = \mu_{C}^{\gamma B}$
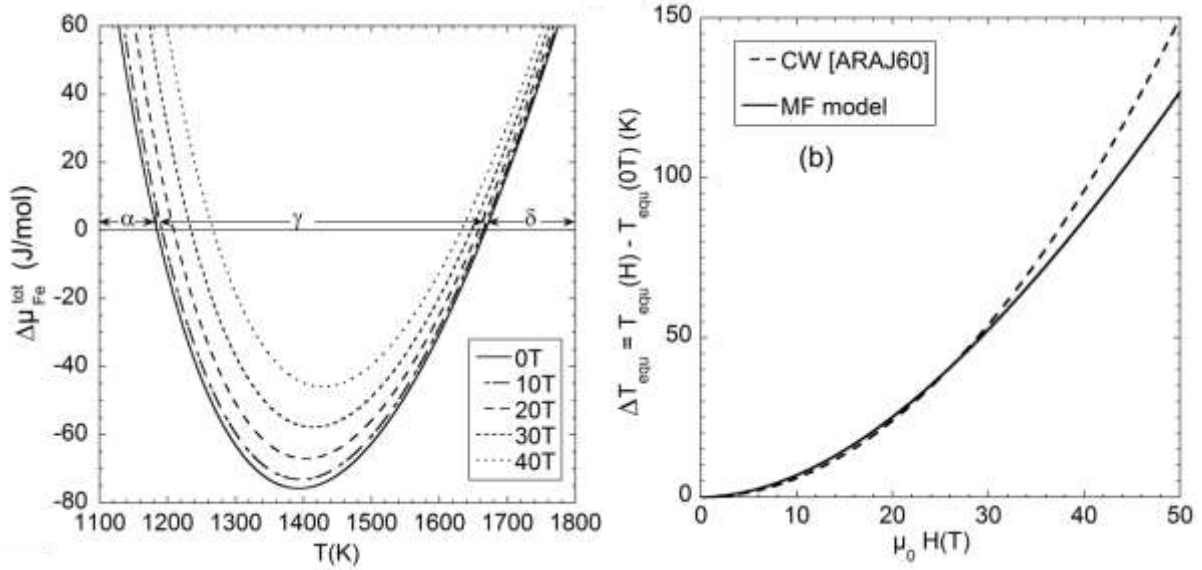
Figure 1.19   (a) Variation of Gibbs free energy difference between ferrite and austenite of pure iron with magnetic field strength calculated with the MF model, (b) Relative change in the austenite ferrite equilibrium temperature of pure iron calculated with the CW law of equ. (20), (21) (dotted line) and calculated with the MF model (plain line)

However, substitutional alloying elements may influence the magnetic properties of the two phases (ferrite and austenite) via their influence on the magnetic moment and on the Curie temperature of the iron solid solution. In a first approximation and if the X concentration is less than several percents, the alloying element is assumed to only modify the average Fe magnetic moment of the solid solution as a dissolution effect. The effect of X in the magnetic properties of Fe-X alloys can be found in [ISHI75] and is reported in Table 1.1 for several alloying elements. The Curie temperature and the magnetic moment of the atom in ferrite are expressed as:

$$T_C = T_C^0(1 + ac_X) \tag{32}$$

$$m = m_{Fe}^0(1 + bc_X) \tag{33}$$

where T_C^0 and m_{Fe}^0 are the respective Curie temperature and magnetic moment of pure iron. In Table 1 the values of coefficient a and b for some elements are shown.

In Table 1.1, the positive b implies that the magnetic moment per one atom in the solid solution and thus the interaction energy with external magnetic field increases by alloying. If a is positive, the Curie temperature is increased so that the range of temperature between Tc and a given transformation temperature below the Curie point is increased and thus the

magnetisation is larger at the transformation point. As a result, the addition of Cobalt stabilizes ferrite most efficiently in a magnetic field. Nickel raises the magnetic moment but reduces the Curie point so that the effect of Nickel on the stability of ferrite in an external field is not much different from that of iron. Manganese reduces both the magnetic moment and the Curie temperature. As a result, it has a considerable destabilizing effect on ferrite phase in addition to the well-known thermodynamic effect in the absence of magnetic field.

Alloying element	dT_c/dc_x (K/at%)	$a = 100(\frac{dT_c}{dc_x})/T_C^0$	dm/dc_x (μ_B)	$b = 100(\frac{dm}{dc_x})/m_{Fe}$
V	7.5	0.72	-2.68	-1.22
Cr	-1.5	-0.14	-2.29	-1.04
Mn	-15	-1.44	-2.11	-0.96
Co	12	1.15	1.11	0.5
Ni	-3.6	-0.34	1.30	0.59
Mo	0.0	0.0	-2.11	-0.96
Si	-3.5	-0.34	-2.29	-1.04

Table 1.1: Influence of some substitutional alloying elements on the Curie temperature and on the magnetic moment of iron in iron solid solutions [ISHI75, GUOE00]

Several equilibrium phase diagrams in magnetic field, such as the Fe-C [CHOI00, ZAHE05], Fe-Si [GAOB06], Fe-Ni [NICH04], Fe-C-Mn, Fe-C-Si [GUOE00] and Fe-C-Ni [ENOM01] have been calculated with this model and can be found in literature.

Experimental evidence of the change in the phase stability in Fe-C-X alloys

Experimental measurements of phase transformation temperatures in presence of magnetic field are highly needed to check the validity of calculated phase diagram in magnetic fields. However, very few experiments have been performed and a direct comparison between the magnetic contribution calculated from the Weiss Molecular Field model and experimental data is unfortunately rare. In order to check for the validity of predicted phase diagrams under the influence of magnetic field, experimental facilities installed in superconducting magnet are often coupled with in situ measurement such as

resistivity [FUKU06] measurement, thermometry [HAOO04] or dilatometry (this work). Up to now, the γ/α transformation temperature at equilibrium was mainly considered. In order to compare the calculated shift of the equilibrium temperature by the field with experimental transformation temperature data, the average temperature for austenite to ferrite and its reverse transformation temperatures were usually taken as the equilibrium temperature.

It was found that the average γ/α transformation temperature for pure iron [FUKU06, HAOO04] and Fe–0.8wt%C (eutectoid composition) [HAOO04] was increased with increasing magnetic field strength. The change in transformation temperature was almost proportional to the magnetic field when the ferrite phase is ferromagnetic at the transformation temperature (as it is the Fe–0.8wt%C), whereas it was proportional to the square of the magnetic field when the ferrite phase was paramagnetic (as it is the case in pure iron). In both cases, the average γ/α transformation temperature measured experimentally could be easily compared to the calculated γ/α equilibrium temperature because the hysteresis of the transformation temperature was very narrow. Thus the experimental data were in very good agreement with the calculated ones, based on the Molecular Field Theory. However, few intermediate proeutectoid steel compositions were studied up to now. In this composition range, the $(\alpha + \gamma)$ region is large and it would have been meaningless to define an average γ/α transformation temperature in order to compare it with a calculated γ/α equilibrium temperature.

Experimental results on Fe-xCo samples (with x = 0, 10, 20, 25, 30 wt%) [FUKU06, KAKE06, HAOO04] gave a similar dependence of the average γ/α transformation temperature against the magnetic field intensity but relatively far from the calculated data, probably because of the large hysteresis of the transformations (Figure 1.20). The ferrite-phase was paramagnetic for x = 0 and 10 wt%Co in the transformation temperature range, while it was ferromagnetic for x = 20 and 30 wt%Co. It was found that the transformation temperature increases almost proportionally to magnetic field for the Fe-20Co and Fe-30Co alloys, while it is almost proportional to the square of the magnetic field for pure Fe and the Fe-10Co alloy. The increase by applying magnetic field of 10 T was about 7 K for pure Fe, 18 K for the Fe- 10Co alloy, 24 K for the Fe-20Co alloy and 20 K for the Fe-30Co alloy.
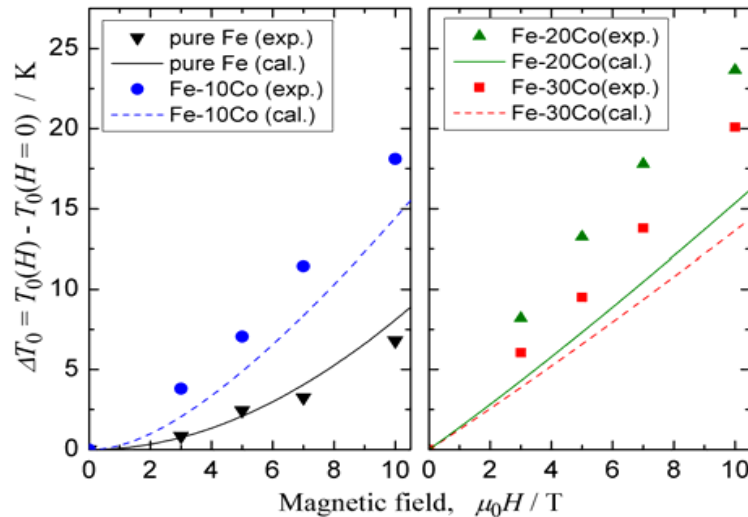
Figure 1.20   Change in the austenite/ferrite equilibrium transformation temperature $\Delta T_0 = T_0(H) - T_0(0)$ by application of magnetic field where $T_0(0)$ is the equilibrium temperature under zero magnetic field. Marks are obtained experimentally by resistivity measurement, and lines are calculated from Molecular Field theory.

Recently, another approach was proposed to discuss the magnetic field dependence of diffusional phase transformation temperatures taking into account the existence of temperature hysteresis due to the large driving force required for transformation. It was successfully applied to Fe-xRh alloys (with x=2, 5, 10 wt%) [KAKE09]. A shift of the austenite to ferrite transformation of about 2 K/T was measured by resistivity measurement. Still in this study, the change in transformation temperature was almost proportional to magnetic field when the ferrite phase was ferromagnetic at the transformation temperature whereas it was proportional to the square of the magnetic field when the ferrite phase was paramagnetic.

Phase transformation kinetics in a high magnetic field

During the γ/α phase transformation, a large driving force is provided because magnetostatic energy is supplied by the magnetic field. Therefore, diffusional transformations are expected to be accelerated by applying a magnetic field. The experimental studies of magnetic field effects on transformation kinetics that involves solute diffusion and grain boundary mobility are quite rare. The effect of magnetic field on carbon diffusivity has been reported by [NAKA05] and [OHTS06b]. They both found that it is retarded in magnetic field but they did not find any anisotropy of diffusivity. Up to now, the focus has been made on the

effect of magnetic field on proeutectoid ferrite transformation whether under isothermal holding or during continuous cooling.

Acceleration of the austenite decomposition around 1000 K in a field of 1.9 T was reported in [PETE73]. More recently, it was shown that a 10 T magnetic field can significantly stimulate the ferrite transformation during isothermal holding of a Fe-C-Mn-Nb steel [XUOH99]. The number of ferrite nuclei together with the nucleation rate was found to increase with the presence of magnetic field. However, the growth rate was decreased to 70 percent of that without magnetic field under certain conditions [OHTS01]. In the case of the pearlite transformation for Fe-13Mn-1C (in wt%), the growth rate was found to either increase (at grain boundaries) or decrease (inside austenite grains). In another work, the kinetics of pro-eutectoid ferrite transformation in Fe-C, Fe-C-B and Fe-C-Ni alloys was studied in a magnetic field of 7.5 T [ENOM01]. The fraction transformed and the number of ferrite particles after isothermal holding was evaluated. A systematic acceleration of the transformation kinetics not only below but also above the Curie temperature was found.

The effect of a high magnetic field on the isothermal growth of ferrite from austenite was investigated in a Fe-1.42Mn-0.15C (in wt%) steel [RIVO05]. A strong effect of the magnetic field on the ferrite content was evidenced, for different dwell temperatures and dwell durations (Figure 1.21).
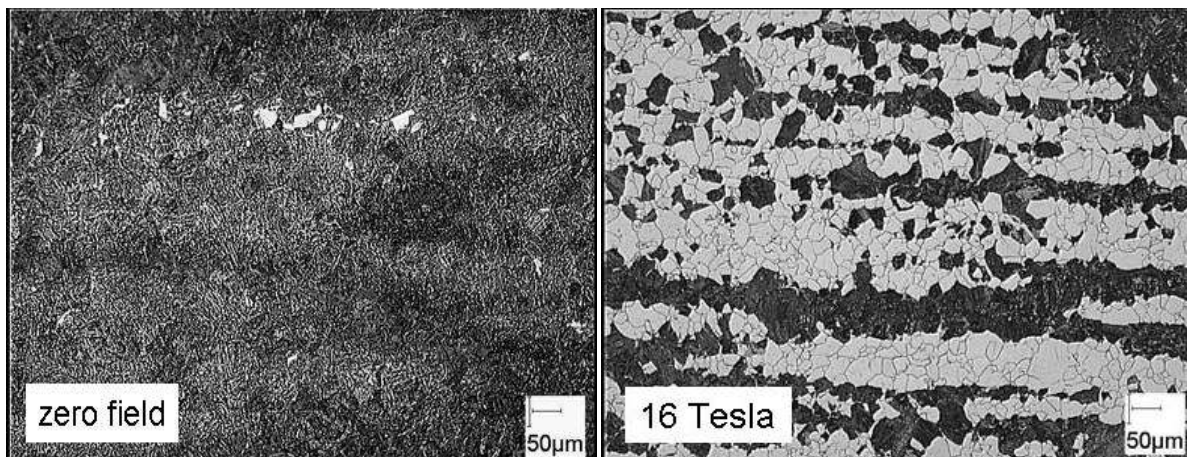
Figure 1.21   Microstructure of a Fe-0.15C alloy. Samples were austenitised at 1000 °C, for 10 minutes and then cooled down to the 973 K dwell and maintained for 16 hours without magnetic field and under 16 T [RIVO06].

From image analysis, it was found that the nucleation rate was strongly increased in high fields (The number of nuclei was doubled in a field of 16 T compared to 0 T). This result is consistent with the theoretical observation made in Figure 1.19a. Indeed, at a given temperature in the ferrite temperature range, an increase in the free energy change due to an external magnetic field leads to a decrease in the critical nucleation radius for ferrite, which is inversely proportional to the free energy change between ferrite and austenite [PHIL98]. The decrease in the critical radius may explain the sharp increase in the nucleation rate.

However, the effect of the magnetic field on the growth rate still remains unclear: a contradictory result was observed, since a very large increase of the growth rate was observed for short dwell durations, together with an apparent grain size limitation in high magnetic fields. Later on, the isothermal transformation of ferrite following two regimes was confirmed by in-situ magnetic measurements [RIVO06]. It was shown that the magnetic field has an effect during the first stage of the ferrite transformation, suggesting a larger effect on nucleation rather than on growth.

In a Fe-C-Mn-Si steel, quantitative analysis of microstructure showed that without magnetic field, the isothermal transformation did not lead to any pearlite transformation whereas on application of a 30T magnetic field, the austenite transformed into pearlite [JARA05b]. In another work of the same group, in situ temperature measurements associated with the recalescence of latent heat during the ferrite formation on continuous cooling showed an increase of about 70-90 K for the sample treated in a magnetic field of 30T together with an increase in the ferrite content (Figure 1.22) [LUDT04]. An acceleration of the austenite decomposition kinetics was suggested by these various results.
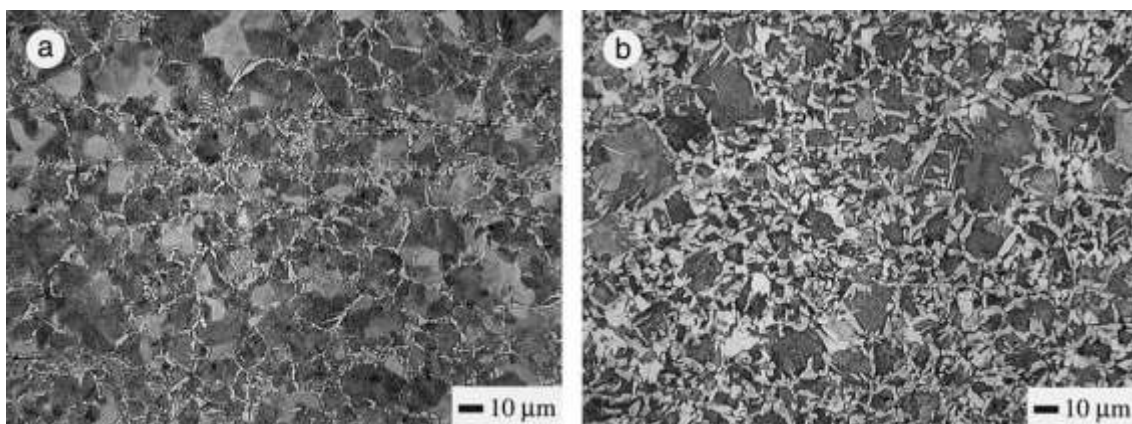
Figure 1.22   Optical micrograph of a Fe-0.45wt%C-0.8wt%Mn cooled (a) without and (b) with a 30T magnetic field (2% Nital) [LUDT04].

In conclusion, the magnetic field effect on kinetics of the austenite to ferrite/pearlite transformation has been confirmed experimentally and is thought to be due to an increase in the nucleation rate together with a possible decrease in the austenite grain size. However, the effect on growth kinetics is not clarified yet.

Magnetic field-control of microstructure in steels

Another unique feature of the transformed structures in an external magnetic field is the alignment and elongation of ferrite grains. The first observation of aligned and elongated microstructures in steels was done on Fe-0.1C and Fe-0.6C (in wt%) [SHIM00]. The application of magnetic fields during the $\alpha \rightarrow \gamma$ inverse transformation developed a two-phase microstructure with the paramagnetic γ phase aligned as chains or columns in the matrix of the ferromagnetic α phase in the direction of applied magnetic field. This kind of alignment was explained in term of coalescence and growth between the γ phase nuclei under the dipolar interactions regarded as magnetic holes in the background of the ferromagnetic α phase medium.

Later, the high magnetic field effect on ferrite alignment during the austenite to ferrite transformation was investigated in Nb containing steel and Fe-0.4C (wt%) [OHTS00a]. Whereas no alignment was observed in the Nb containing samples, an aligned microstructure was obtained in the Fe-0.4C (wt%) samples both during slow continuous cooling and isothermal holding above Curie temperature [HAO03]. A similar result was confirmed in Fe-0.25C (wt%) steel during slow cooling [WANG08]. In the case of Fe-0.4C (wt%), the degree of elongation was found to increase with increasing transformation temperature below the Curie temperature, and decreased above the Curie point. It was shown that the degree of elongation is determined by the competition between the demagnetisation effect and the chemical driving force for ferrite nucleation and their combined effects results in a peak value at approximately Tc. During the transformation, the degree of elongation increased monotonically, showing that the aligned structure is the result of preferential grain growth. In [SHMA03], the formation mechanism of aligned structure was also discussed from the view point of the nucleation and growth of ferrite grains in austenite phase. It was shown that the shape of aligned ferrite grains was determined by a balance of the magnetostatic and the interfacial energies.

Besides, Zhang et al. [ZHAN04] investigated the effect of cooling rate on the obtention of aligned microstructure. When cooling at a rate of 10 K/min, the nucleation occurs preferentially along austenite grain boundaries. Due to the inhomogeneous deformation of the previous hot rolling and the dipolar attraction between ferrite nuclei in the magnetic field, the final microstructure of alternately distributed ferrite grains and pearlite colonies along the magnetic field direction is obtained, as shown in Figure 1.23. On the contrary, when the cooling rate is higher (46 K/min), the final microstructure is characteristic of randomly distributed ferrite grains and pearlite colonies with smaller sizes, because the nucleation at higher temperatures is greatly inhibited and more sites inside austenite grains in addition to those on grain boundaries are available for the ferrite nucleation at lower temperatures. A more recent study showed that an alignment of pearlite could be obtained without any elongation of ferrite grains [SONG08]. Pearlite colonies were elongated and aligned along the field direction due to the preferential nucleation of proeutectoid ferrite in the late stage of proeutectoid transformation. In addition, the magnetic field also reduced the amount of pearlite. However, no clear elongation of proeutectoid ferrite grains was observed.
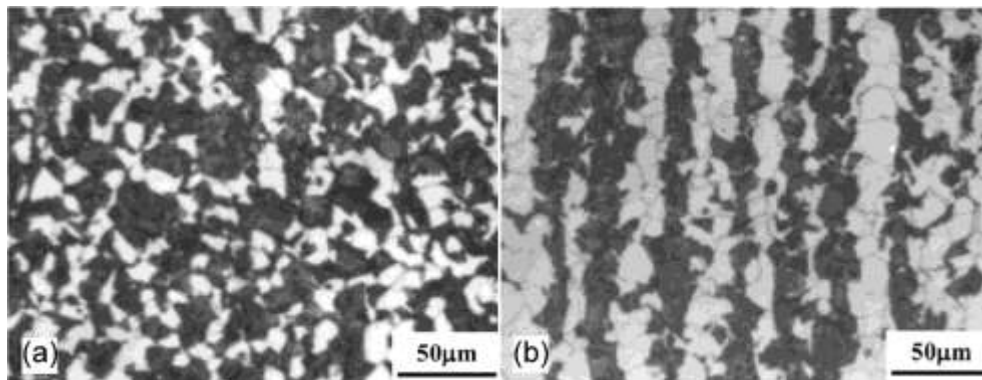
Figure 1.23   Optical micrograph of a Fe-0.4C-1Cr-0.2Mo (wt%) after heating at 1153 K for 33mn and cooling at 10 K/s (a) without and (b) with a 14T magnetic field (2% Nital) [ZHAN04]

Finally, Koyama et al applied a phase field modelling of structural elongation and alignment in Fe-0.4C (wt%) and simulated the influence of an anisotropic carbon diffusion on the occurrence of the two phase aligned microstructures [KOYA07]. However, this point has to be confirmed experimentally.

However, the microscopic mechanism of elongation remains difficult to explain because the growth rate depends on several factors, such as boundary energy, chemical driving force for transformation, demagnetisation effect and carbon diffusion.

Magnetic field effect in martensitic transformation

The influence of the magnetic field on the martensitic transformation in various kinds of alloys is well documented and is not the subject of this section.

The studies of magnetic field effect on martensitic transformation in steels were first performed with pulsating fields [KAKE99]. Kakeshita and co-workers have observed a rise toward higher temperature in the martensitic start transformation temperature (Ms) as illustrated for some ferrous alloys in Figure 1.24. The sample used were Invar Fe-Ni-C alloys [KAKE85], disordered and ordered Fe-Pt Invar alloys [KAKE84] and Fe-Mn-C alloys [KAKE87]. They used magnetisation changes to establish the modification of the percentage of martensite formed as well detailed in [KAKE86].

In order to predict the shift of the Ms with the magnetic field, they assumed that the change between Gibbs free energies under the magnetic field was the same as that under no magnetic field at Ms. This assumption on the effect of a magnetic field is analogous to that of the effect of uniaxial stress and hydrostatic pressure made by Patel and Cohen [PATE53] and has been confirmed later by [OTSU79] by showing that the martensitic transformation temperature dependence of uniaxial stress calculated by this assumption was in good agreement with the experimental one in many materials.

The volume fraction of martensite formed during quenching in a static field of 1.6 T was increased between 4 and 9 % when a magnetic field was super imposed as illustrated in Figure 1.25 [SATY68].

Both the change in the M_s and modification of the percentage of martensite were explained by a simple thermodynamic treatment with only one additional term referred as $B \cdot \Delta M$ and accounting for the observed effect (ΔM is the difference in saturation magnetisation of the parent and product phases). Four years later, isothermal martensitic transformation was studied under the application of a magnetic field of 2 T [PETE72]. Acceleration of the transformation rate by a factor of 3 was experimentally evidenced and theoretically demonstrated by a thermodynamic model. No elongation or alignment of transformed structure has been observed up to now for transformations to lath martensite.
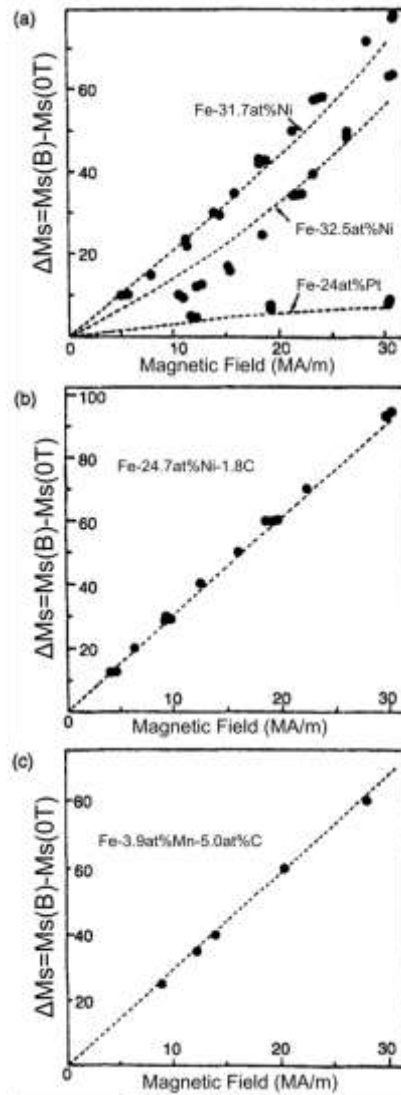
Figure 1.24   Comparison between calculated (---) and measured (●) ΔMs as a function of the magnetic field strength, relations for Invar FeNi and Fe-Pt alloys (a), and non Invar Fe-Ni-C (b), and Fe-Mn-C alloys (c) [KAKE84, KAKE85, KAKE87]
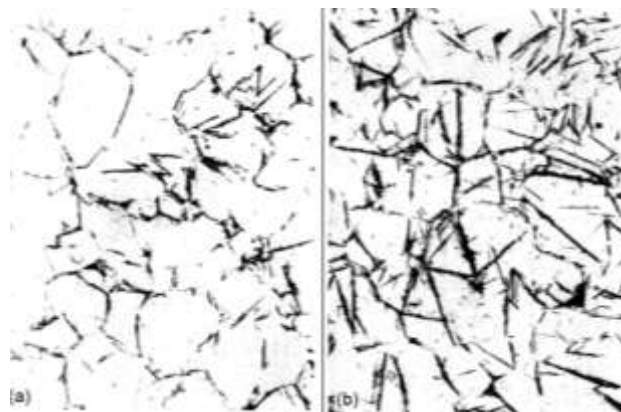
Figure 1.25   Optical micrograph of a Fe-1C-1.5Cr-0.5Mn-0.2Si (wt%) after cooling at 368 K (a) without and (b) with a 1.6T magnetic field (2% Nital) x150 [SATY68]

Effects of a high magnetic field on bainitic transformation in steels

There are very few reports that show the effect of magnetic fields on bainitic transformation. However the magnetic field is expected to affect this transformation due to the change in the magnetisation of phases.

It has been recently verified that magnetic field effectively influences the bainitic transformation in the same way as it influences the decomposition of austenite into martensite [OHTS06a]. In a Fe-3.6Ni-1.5Cr-0.5C (wt%), the bainitic transformation temperature was increased by more than 40 K by applying a magnetic field of 10 T and this increase was larger than for ferrite transformation in low alloyed steels. Moreover it has been found that the isothermal transformation behaviour was accelerated by applying 10 T. Figure 1.26 shows the optical micrographs for the specimen transformed at 763 K for 10 min in magnetic field with and without magnetic field. Bainite was not observed in the specimen transformed without magnetic field, but small volume of bainite plates were observed both at grain boundaries and grain interiors in the specimen transformed for 10 min in 10 T.
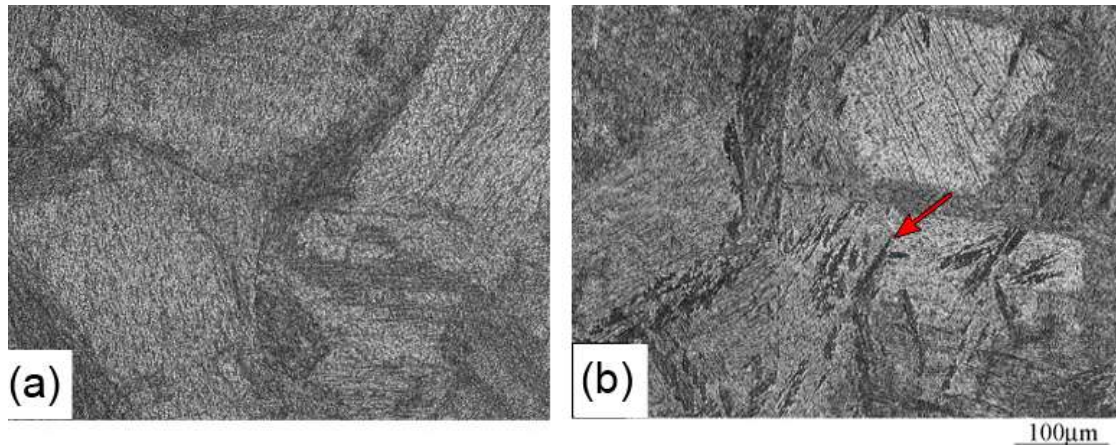
Figure 1.26   Optical micrograph showing the transformed structure in an Fe-3.6Ni-1.5Cr-0.5C (wt%)alloy. Specimens were austenitised at 1423 K for 15 min and transformed at 763 K for 10 min with magnetic field of: (a) 0 T and (b) 10 T.

Recently, novel bainitic steels have been developed with very high strength [CABA01]. The particularity of these steels is that they transform at such low temperatures that bainite plates can be as thin as 30 nm. This microstructure is obtained during isothermal transformation around 473 K for more than 400 h. It has been found that the addition of cobalt

or aluminium could accelerate the rate of transformation in increasing the free energy change accompanying the decomposition of austenite. It reduces the time required for transformation by a factor of 4. With the same goal, magnetic field was expected to influence the rate of transformation in increasing the change in free energy during the austenite decomposition into ferrite. Experiments were performed under a magnetic field of 30 T during a continuous cooling [JARA05a, JARA05b]. It has been found that magnetic field completely change the microstructure obtained, from a mixture of bainite and martensite to one containing a very fine pearlite with an interlamellar spacing of about 50 nm. Isothermal transformation experiments have shown similar austenite decomposition characteristics as those of continuous cooling conditions.

Recrystallisation studies in static magnetic field

Smoluchowski and Turner were probably the first to study the texture formation during magnetic annealing in 1949 [SMOL49]. Fe-35Co samples were annealed at 700ºC in the presence of a magnetic field, each sample having a different orientation of the rolling direction with respect to the field direction. The influence of the magnetic field appeared to be a strong enhancement of the grains with their (100) planes parallel to the surface of the sample and [110] directions parallel to the rolling direction, i.e., (100)[110] recrystallized texture. This texture was probably strong enough to produce the saturation magnetisation.

In a continuation to this study, the grain boundary misorientation as a function of the boundary misorientation angle has been studied in an iron-cobalt polycrystalline alloy [WATA90]. A 0.5 T magnetic field increased the frequency of low-angle boundaries, being 3 to 4 times larger than the prediction for a random polycrystalline material.

In 1981, Maritikainen and Lindroos [MART81] showed that the recrystallisation of the samples annealed in a 1.5 T field was retarded thanks to hardness measurements and metallographic analysis. The retard in recrystallisation was explained to be due to three reasons: the first one is the low mobility of the grain boundaries between the magnetically oriented nuclei and the deformed matrix due to magnetic ordering. The second one is that the domain walls act as a barrier against grain boundary migration and the third one is the change in the structure of grains due to the magnetic field. The authors have also found texture change as an effect of magnetic field.

More recently, it was found in Interstitial Free steels that the magnetic annealing retards the recrystallisation process, but promotes the nucleation at the initial stage of recrystallisation

[WUHE07]. In non-oriented 3% silicon steels, effects of a strong magnetic field on recrystallisation and coarsening of grains after primary recrystallisation were studied [OHTS00b]. It was found that primary recrystallisation process is retarded by applying a strong magnetic field, and this retardation effect is affected by the degree of cold rolling.

1.2.3. Summary on field effect on processing of steels

To summarise 20 years of results concerning the effect of magnetic fields on solid/solid transformation in iron based alloy, the main achievements are presented below:

- Equilibrium phase diagrams in a magnetic field have been calculated with the Molecular field model and can be found in literature.
- Experimental measurements of phase transformation temperatures in the presence of a magnetic field have been performed for some special composition. The change in the average γ/α transformation temperature was almost proportional to the magnetic field when the ferrite phase is ferromagnetic at the transformation temperature whereas it was proportional to the square of the magnetic field when the ferrite phase was paramagnetic.
- Magnetic field effect on kinetics of the austenite decomposition has been confirmed experimentally and is thought to be due to an increase in the nucleation rate. However, the effect on growth kinetics is not clarified yet.
- Alignment and elongation of ferrite grains along the magnetic field lines have been observed in different alloy composition. It was shown that the shape of aligned ferrite grains was determined by a balance of the magnetostatic and the interfacial energies.
- Rise toward higher temperature of the martensitic start transformation temperature has been measured. Acceleration of the martensitic transformation rate was experimentally evidenced and theoretically demonstrated.
- The bainitic transformation temperature was increased by applying a magnetic field and this increase was larger than for ferrite transformation in low alloyed steels.
- Change in the microstructure obtained, from a mixture of bainite and martensite without field to one containing a very fine pearlite in magnetic field has been observed in novel bainitic steel.

- Retard in recrystallisation process in a magnetic field has been observed and explained to be due to the low grain boundaries mobility between nuclei and deformed matrix due to difference magnetic ordering. It was also found texture changes as an effect of a magnetic field.

Chapter 2

Experimental means

- 54 -

With the recent development of superconducting technology, magnetic fields of high strength have been available in large volume. Besides, microstructure analysis resulting from high magnetic field processing has become necessary to design experimental setups for the in-situ control of phase transformations. Therefore, high temperature experiments have been designed in the last decade to simulate at the laboratory scale, steels processing routes in order to evidence any magnetic field impact that could be interesting for the functional properties of those materials.

The technology of high temperature furnaces in a static magnetic field has been well established for several years now at laboratory scale, even if no device has been commercialized yet. CNRS/CRETA Laboratory in Grenoble was a precursor in this skill and still owns a number of heating facilities inserted in several room temperature bores of superconducting magnets and possesses the technical know-how for the design of new devices. The existing furnaces in magnetic fields installed in CRETA are based on direct induction [BONV95, LEGR98], induction through a susceptor [GAUC01], or resistive heating [BRAI91]. Similar equipments are described elsewhere in a non exhaustive way [YASU00, FUKU06, ZHAN06, OHTS08].

Most of the time, and as it is the case in the devices described above, the specimen has a fixed and constant position relatively to the furnace and to the magnet. The possibility to move the sample during the treatment is used in other devices built [SHMA03, SHIM03, VILL07]. However, because of the strong forces induced on the magnet by the displacement of any electrically conductive piece inside a magnet, the use of such a device is limited to specific cases. In this work, a new device has been developed for the treatment of materials requiring high cooling rates. It is based on the following innovative concept: the sample has a fixed and constant position relatively to the magnetic field during the whole process. To enable rapid shift from the heating to cooling system, the furnace and the quenching bath are moved with an external jack. This new apparatus is described in paragraph 2.3. Together with processing, characterisation is also needed in a magnetic field. Several techniques have already been used to evidence the magnetic field dependence of solid state phase transformations, such as magnetometry [GAUC01], resistivity measurement [FUKU06], dilatometry [RIVO09], and thermal analyses [OHTS08].

This chapter is devoted to the technical description of three different home-made devices used in this work and dedicated to magneto annealing of inorganic materials. The first

device is a high temperature magnetisation measurement setup. It is a powerful tool to probe phase transformations by the monitoring of magnetic susceptibility of a material during its processing. The second experiment is a high temperature furnace installed in a 16 T superconducting magnet. A laser interferometer is coupled with this furnace to follow the dilatation of the sample. Dilatometry is a powerful and common technique to follow the solid state phase transformations. It is based on the measurement of sample length changes as a function of time and temperature, which are directly correlated to changes in the specific volume. The third device has been specifically developed during this work to enable very high cooling rates, usually obtained by water, oil and gas quenching. This apparatus opens the way to a number of innovative studies in metallic materials and more specifically to a better understanding of the effect of magnetic fields in industrial processing of steels and out of equilibrium structure formation.

In the last part, material preparation, metallography and hardness measurement and methods are briefly reviewed.

2.1. High temperature balance in high magnetic field

The High Temperature Balance is used to measure the magnetic susceptibility of materials during their processing. Melting, solidification, and solid state phase transformations can be evidenced and quantitatively monitored by this technique [GAUC01]. Moreover, this device is of capital importance to measure the magnetic properties of multiphase materials or of multi-element crystallographic compounds for which any prediction of the magnetisation hasn't been checked experimentally or simply does not exist yet. The maximum magnetic field can reach 3.8 T. Maximum heating and cooling rates are about 1 K/s up to 1800 K.

2.1.1. Experimental setup

The whole system is schematically shown in Figure 2.1. It consists in a high frequency induction furnace, an alumina sample holder and a weight measuring device, installed in the vertical room temperature bore of an 8 T superconducting magnet.
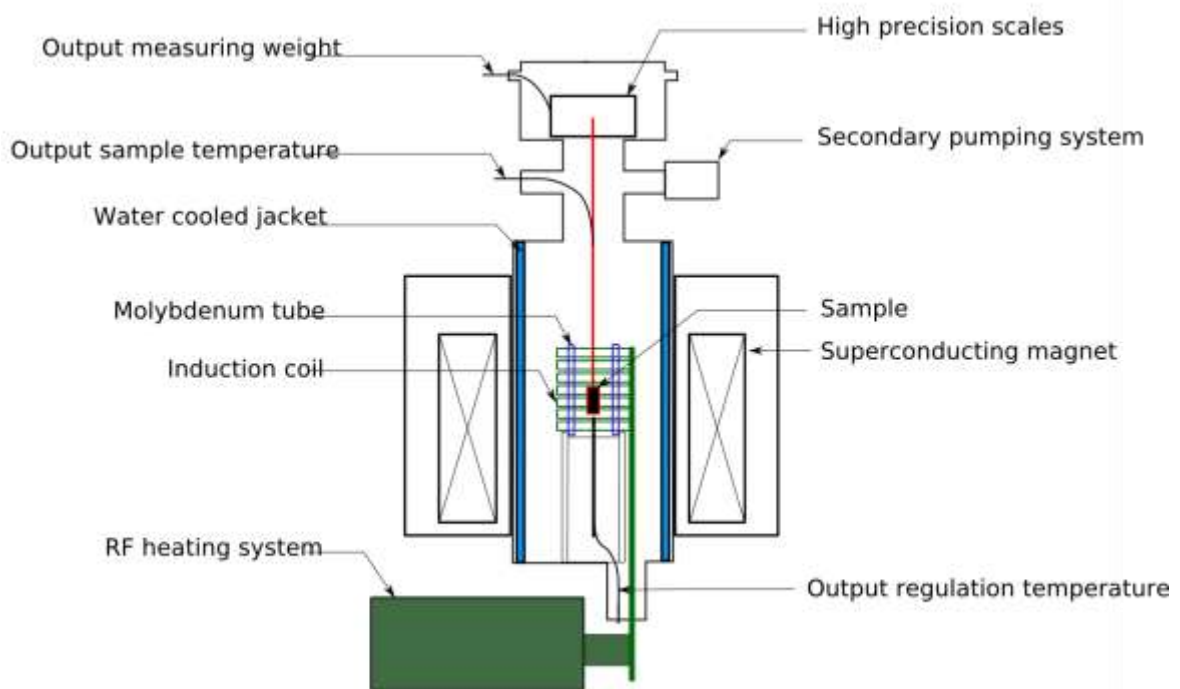
Figure 2.1   Schematic illustration of the high temperature balance

The whole system is under controlled atmosphere, i.e. secondary vacuum or inert gas (Ar, He, …). The electronic part of the scales is kept away from the influence of the magnetic field. The sample, suspended to the scales, is centred inside a hollow molybdenum tube heated by a radio-frequency induction coil (120 kHz, 6 kW) as described in the first chapter. The whole system is screened by a copper water-cooled jacket. Special care must be taken for the position of the heating element. Homogeneous temperatures must be applied to the sample placed in the maximum field gradient. Therefore, the heating element can be vertically translated to meet this requirement. The sample holder is an alumina cylindrical crucible suspended below the scales by two alumina rods also containing the thermocouples.

2.1.2. Magnetic field zones in a solenoid coil

Figure 2.2 shows the magnetic force acting on ferromagnetic or paramagnetic materials ($\chi > 0$) along the vertical axis of the magnet bore (blue) and radial to the axis (red). These forces derived from the calculation of $F_{xyz} \propto \chi \Delta B^2$ for a cylindrical solenoid.
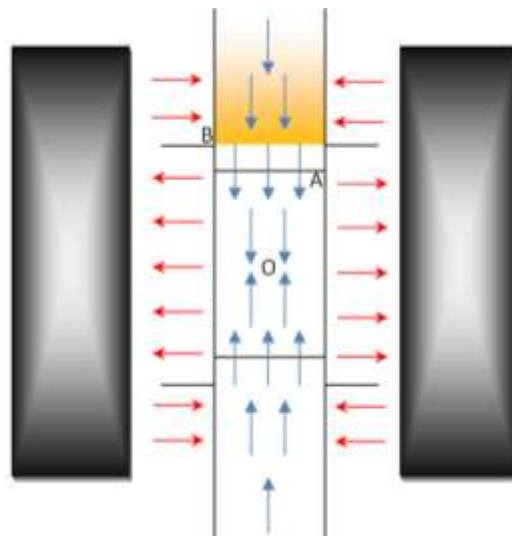
Figure 2.2   Schematic illustration of radial (red) and axial (blue) forces applied on a ferromagnetic or paramagnetic materials, in the room temperature bore of a superconducting magnet.

In the magnet centre region (point O), the higher field is located near the edges of the superconducting coil. A sample with positive magnetic susceptibility (ferromagnetic or paramagnetic) is expelled away from the magnet vertical axis by radial forces and goes into

contact with the furnace heating element. In this case and because of friction, any accurate measurement of the vertical magnetic force exerted on the sample is impossible. However, above the centre field region, the magnetic field gradient along the vertical axis is maximal at point *A*. Furthermore, at this point the radial force still expels the sample from the vertical axis of the magnet. But, there is an inversion point of the radial forces, marked as *B*, where the magnet is seen as a dipole so that the maximum field is on the vertical axis. As a consequence, a ferromagnetic (or paramagnetic) sample is self-centred on the axis of the magnet, so that it does not go into contact with the heating element. In this position, the sample is submitted to a much smaller magnetic field but the corresponding downward vertical force is still high. This is the position which is chosen as sample position in the high temperature scales.

2.1.3. Principe of the magnetisation measurement

The magnetisation is measured by the magnetic force exerted on the sample placed in a field gradient. The measurement of the magnetic force F_z (in dyne) derives from the weighting of the sample being freely suspended to the scales as:

$$F_z = \frac{\chi}{2\mu_0} V B \frac{dB}{dz} = mM \frac{dB}{dz} \tag{34}$$

where χ is the magnetic susceptibility (cgs), *M* is the magnetisation per unit of mass (cgs), *V* and *m* are respectively the volume and the mass of the sample. In these expressions, the magnetic field gradient is expressed respectively in $Oe^2.cm^{-1}$ and $Oe.cm^{-1}$ When the magnetic field is applied, the measured weight corresponds to the addition of the sample holder contribution and the sample magnetic force contribution. The signal of the sample holder is measured for background removal:

$$F_z = (m_{measured} - m_{bg})g \tag{35}$$

where $m_{measured}$ and m_{bg} are respectively the weight measured with a sample and the weight measured with an empty crucible. *g* is the gravity constant in $cm.s^{-2}$. The background signal mainly corresponds to the negative contribution of the diamagnetic alumina sample

holder. Therefore, it is negligibly low compared to the measured ferromagnetic sample. Because the steel sample becomes ferromagnetic in the ferritic state, very large forces arise in high fields and special care must be taken to suspend it in the field gradient. However, the background signal may not be negligible any longer when a weak paramagnetic behaviour is measured.

2.1.4. Calibration of the measurement

<u>Temperature map of the heating element</u>

On the one hand, the temperature map along the axis of the heating element is measured for a regulation temperature of 1220 K. The homogeneous temperature zone is found 2 cm above the bottom of the Molybdenum tube. The result is shown in Figure 2.3. In the insert, the calibrating curve at this particular sample position is shown. The calibration curve consists of the measurement of the sample temperature as a function of the regulation temperature during a thermal cycle at 2 K/min up to 1200 K.
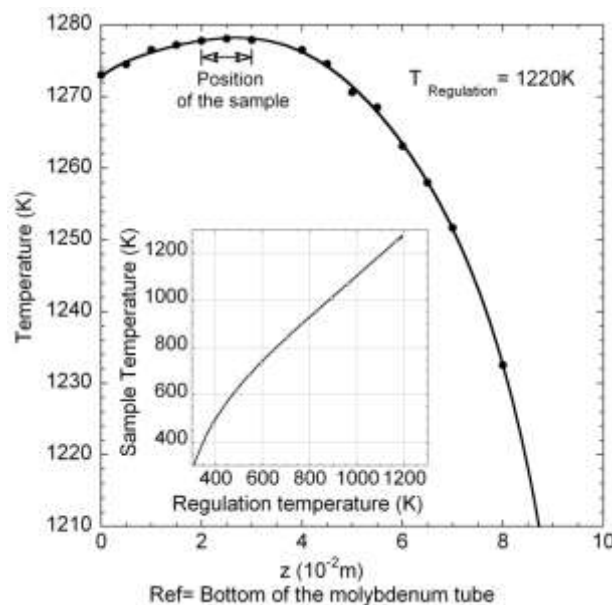
Figure 2.3   Temperature map of the heating element during a soaking at 1220 K. The reference point ($z = 0$ cm) is fixed at the bottom of the molybdenum tube. Insert: calibrating curve for sample positioned at $z = 2$ cm

Magnetic field map

On the other hand, the magnetic field strength along the axis of the magnet is experimentally measured in order to determine the position of the homogeneous magnetic field corresponding to point O on Figure 2.2. Measurements are done with a "Hall Effect" sensor which can measure a magnetic field up to 2 T with a sensitivity of 1 mT. Results are shown in Figure 2.4. Point O is found at z = 43.5 cm from the top of the magnet flange. The magnetic field gradient BdB/dz is calculated by the derivative of the measurement. This gives a first indication of the maximum magnetic field gradient position.
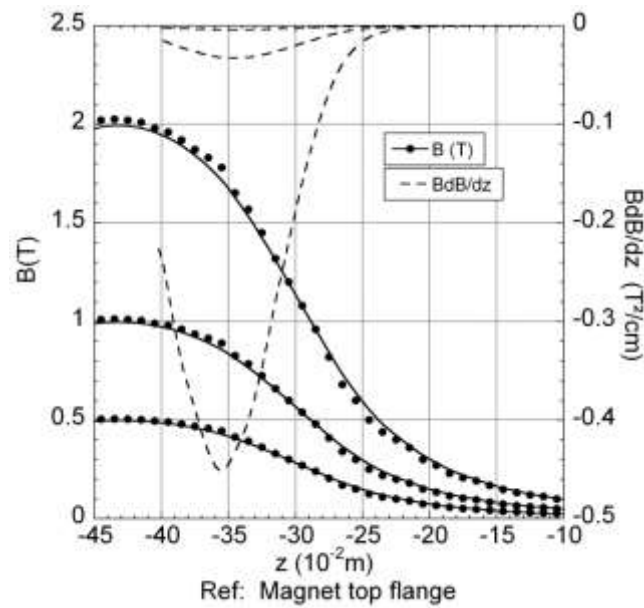
Figure 2.4   Variation of the magnetic field strength along the vertical axis of the magnet bore, z, and calculation of the magnetic field gradient. z = 0 cm at the magnet top flange.

The position of the maximum magnetic field gradient, together with its strength along the vertical axis is then experimentally confirmed as follows.

The force acting on a ferromagnetic sphere of high purity Ni with a saturation magnetisation M_0^{Ni} =54.35 A.m^2.kg^{-1} at 300 K, a mass m_{Ni} = 2.0733 g, and a diameter of 7.63 mm, is measured as a function of the z position. The force arising from the background is removed from the signal and the dB/dz value is obtained by:

$$\frac{dB}{dz} = \frac{(m_{measured} - m_{bg})g}{M_0^{Ni} m_{Ni}}$$

(36)

In the same way, the force acting on a paramagnetic sphere of Cr with a magnetic susceptibility χ_{Cr} = 4.35 10^{-8} $m^3.kg^{-1}$ at 300 K, a mass m_{Cr}=13.3476 g and a diameter of 15.20 mm is measured and the magnetic field gradient BdB/dz is calculated after background removal as:

$$B \frac{dB}{dz} = \frac{(m_{measured} - m_{bg})g}{\chi_{Cr} m_{Cr}}$$

(37)

These measurements are shown in Figure 2.5. The position of the maximum magnetic field gradient is precisely determined at z = 35 cm from the top of the magnet flange.
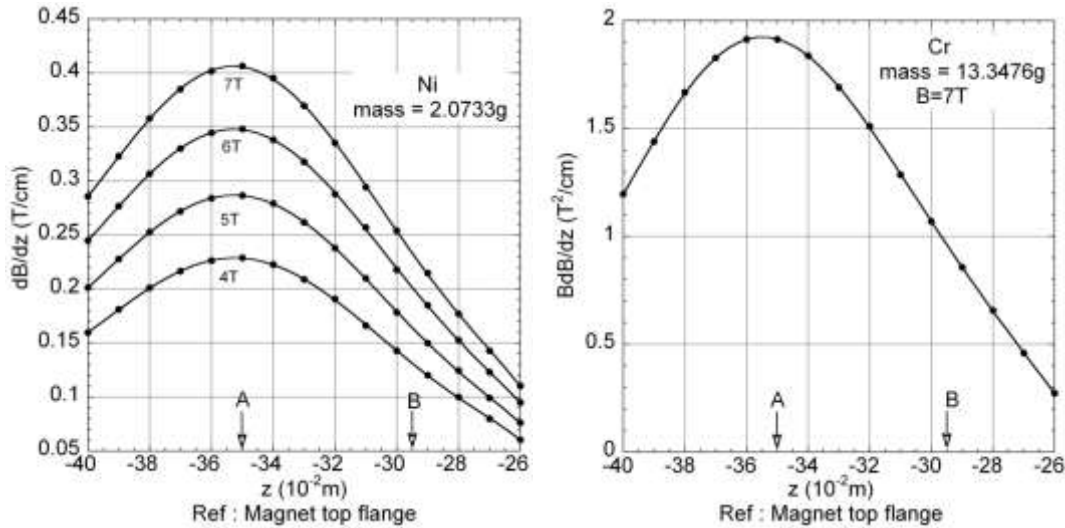
Figure 2.5   *dB/dz* and *BdB/dz* measured along the z- axis of the magnet bore.

The inversion point, noted as *B*, is first manually experienced using a ferromagnetic Ni sample suspended to a thin non-magnetic wire. The coordinate where the sample is self-centred on the magnet axis is measured at a distance of 14.5 cm from the homogenous field position. The bottom of the crucible is then positioned 0.5 cm above the *B* position to ensure the stability of the sample along the magnet axis.

The calibration shown in Figure 2.5 is sufficient for most of the usual measurements. However, for the measurement of weak magnetic properties, such as the paramagnetic behaviour of Fe-based alloys at high temperature, for example, and/or to account for samples with different sizes or shapes, a more accurate calibration is necessary because the magnetic field gradient can no longer be assumed to be constant along the 20 mm height of the crucible.

In this case, a smaller sphere of ferromagnetic substance, such as iron enables a more accurate measurement of the z axis magnetic field gradient within the crucible. Iron has a saturation magnetisation $M_0^{Fe} = 218$ A.m^2.kg^{-1} at 300 K, a mass $m_{Fe} = 0.2194$ g, and a diameter of 3.76 mm. The force acting on the sample for three different z-positions of the sphere center in the crucible is determined as a function of the magnetic field strength. As for Ni, the expression for dB/dz (in Oe.cm^{-1}) is derived as a function of z_S the sample size (in cm) and of B_C, the magnetic field strength in the centre of the magnet (in T) as:

$$\frac{dB}{dz} = \left[2236.2 - 80.427 \left(\frac{z_s}{2}\right) - 24.162 \left(\frac{z_s}{2}\right)^2 \right] B_C \qquad (38)$$

With the "Hall Effect" sensor, the variation of the magnetic field in the sample region B_s (in T) is accurately measured along the axis of the crucible as a function of the magnetic field strength in the centre of the magnet, B_C (in T) as:

$$B_s = \left[0.55159 - 0.06896 \left(\frac{z_s}{2}\right) + 0.0348 \left(\frac{z_s}{2}\right)^2 \right] B_c \qquad (39)$$

Finally, the background signal, m_{bg} (in g) is measured as a function of temperature T and the following expression is determined as a function of the magnetic field in the centre of the magnet, B_C:

$$m_{bg} = \left[(-2.72 - 0.0007 * T)/7 \right] * B_c \qquad (40)$$

Sensitivity of the measurement

For B_C=7 T, a 1 g sample, with positive magnetic susceptibility, positioned 1 mm above the bottom of the crucible, will be submitted to a 5.95 T^2/cm field gradient and a 3.81 T magnetic field. 0.05 g being the resolution of the scales, the minimal magnetic susceptibility change that can be measured is 1.04 10^{-8} m^3/kg and the minimal magnetisation change is 3.14 10^{-3} A.m^2.kg^{-1}. Hence, the device resolution is 5.01 10^{-8} m^3.kg^{-1}.g.T, for the susceptibility and 2.20 10^{-2} A.m^2.kg^{-1}.g.T for the magnetisation.

2.2. In-situ dilatometry in magnetic field

The second part contains the description of the dilatometry experimental setup used for the in-situ monitoring of structural transformations in magnetic fields. It consists in a laser interferometer coupled with a high temperature furnace. This apparatus fits an 18 T superconducting magnet with a 32 mm diameter room temperature bore. The optical method was chosen for dilatation measurements because it is not perturbated by the magnetic field. The measured sample can be heated up to 1500 K under controlled atmosphere. Heating and cooling rates can be varied within a range of 10 K/s. The resolution is below 50 nm.

2.2.1. Experimental Setup

As shown in Figure 2.6, the experimental setup consists of four main parts that are : a high temperature resistive furnace, a laser interferometer measuring the sample dilatation, both installed in a closed chamber, itself placed in the vertical room temperature bore of the superconducting magnet.
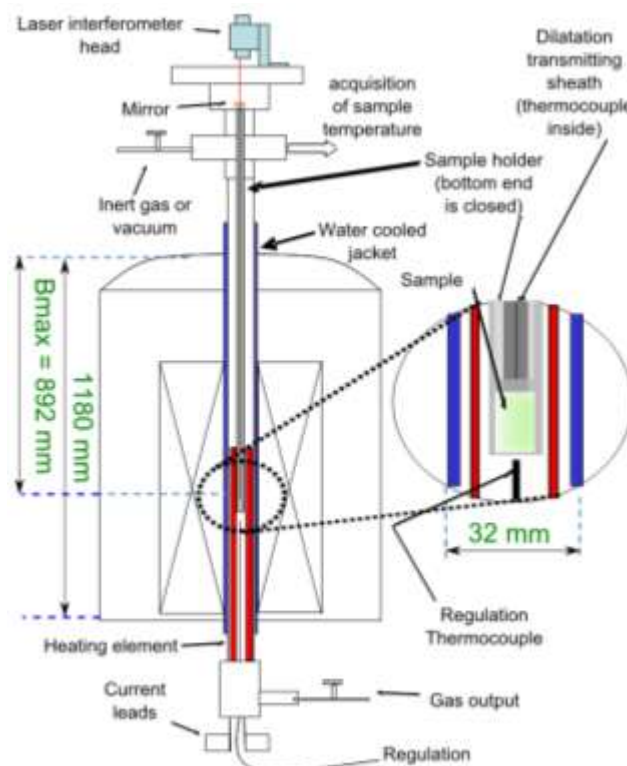
Figure 2.6   Schematic illustration of the dilatometer [RIVO09]

2.2.2. Resistive heating element

The furnace consists of a spiralling, hollow, Silicon Carbide heating element with an inner diameter of 9.5 mm. To protect the magnet from the furnace heating, a water cooled jacket with a 26 mm inner diameter is adjusted along the whole vertical bore of the magnet. The heating element is inserted in the magnet from the bottom of the magnet bore and fixed to the water jacket. The electrical source is a direct current rather than an alternative current power supply to avoid the strong vibrations due to the coupling between the magnet field and the current. In the few millimetres between the cold jacket and the heater, a 2 mm thickness alumina wool sheet provides a sufficient thermal insulation. The upper part of the jacket is closed by a Pyrex window and the lower part is sealed so that the furnace can operate under secondary vacuum or controlled atmosphere. The temperature is controlled through a Eurotherm controller and can reach 1500 K with a maximum heating rate of 10 K/s and a cooling rate of 1 K/s corresponding to the natural cooling of the furnace.

Figure 2.7 shows the temperature map of the heating element along its z vertical axis with an imposed temperature of 1173 K in the centre of the heating zone of resistive element. This map is used to set the position of the 1 cm long sample in order to minimize temperature gradients.
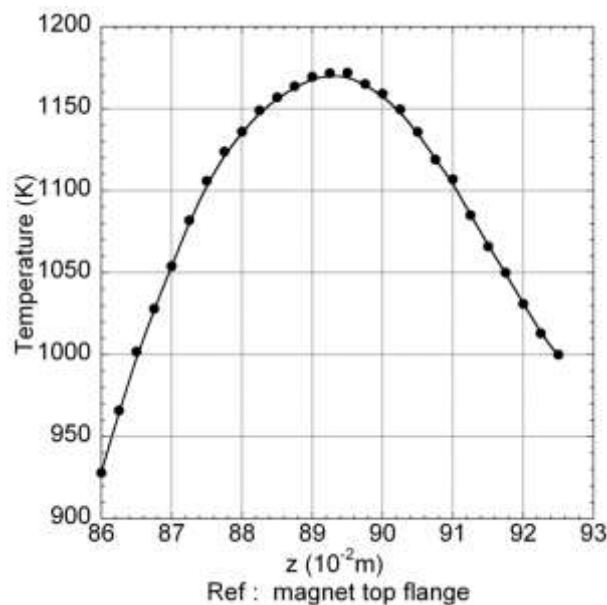
Figure 2.7   Temperature map of the heating element during soaking at 1173 K. $z = 0$ cm is the magnet top flange.

2.2.3. Dilatation measurement

The dilatation measurement of the sample during the processing is measured by interferometry. In the magnetic field vicinity, an optical technique for dilatation measurements seems to be a natural choice. To our knowledge, laser dilatometry has never been used in high magnetic field experiments. The high resolution Michelson laser interferometer is a HC 500 micro-model (by Sageis-CSO, Grenoble, France). A schematic illustration of the measurement setup is shown in Figure 2.8.
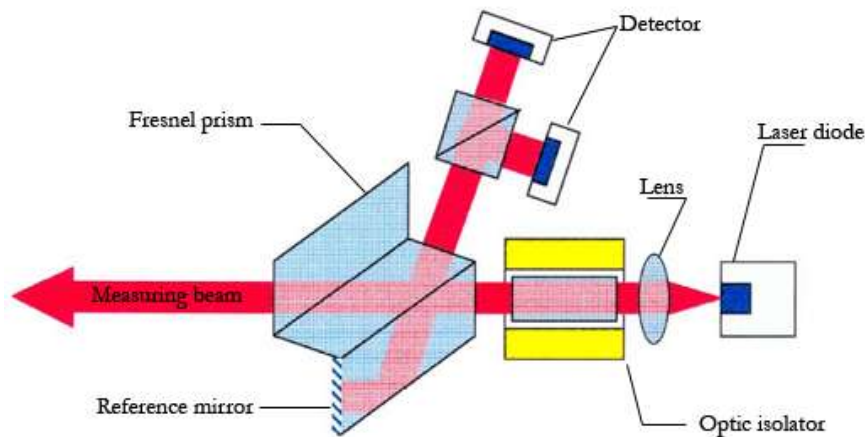
Figure 2.8   Schematic illustration of the measurement principle with the HC500 laser interferometer ([®]Sageis CSO).

The laser diode, the optical parts and the detectors are integrated in a pen-size head (about 10 cm in height and 1 cm in diameter) placed above the magnet entrance. The laser beam has a wavelength of λ = 780 nm and a diameter of 1 mm. The measuring beam (one of the two branches of a Michelson interferometer) crosses the Pyrex furnace windows and is reflected by a spherical mirror connected to the sample through an alumina sheath. The dilatation of the sample vertically displaces this sheath together with the mirror screwed on top of it. The reflected measuring beam interferes with the reference beam located in the interferometer head itself and the relative dimensional change of the sample is measured through the displacement of the interference fringes between the reflected beam and the reference beam. The reference beam never leaves the interferometer head. As a result, the changing interference pattern comprises both the sample dilatation itself and other

contributions (sample holder, alumina connecting sheath, furnace's frame). Reference experiments (without sample and with standard probes such as silicon or alumina replicas) are regularly performed, to measure the apparatus contribution to the dilatation measurement. These reference measurements enable to obtain the background signal, by subtracting the standard probe dilatation coefficient expected from literature data. This background contribution is found to have a linear variation with temperature, which amounts to around 150 μm over the full temperature range of the instrument. This background contribution is then further removed from the measured signal to recover the dilatation of the sample.

The alumina sheath enables not only the deformation of the sample to be transmitted but also the temperature of the sample to be measured. A Pt/Pt-Rh thermocouple at the bottom end of this sheath is in close contact with the sample to measure its temperature (accuracy is ±1K).

The interferometer control unit provides several outputs: a high frequency digital connection to a computer allows the continuous measurement of the mirror displacement and two analogue outputs provide the cosine and the sine of the phase delay between the measuring and reference beams. These two outputs are connected to an oscilloscope to conveniently monitor the signal strength and stability. From the signal width on the scope, the resolution in our operating conditions is estimated to be below 50 nm. The final accuracy depends on the whole furnace dilatation compensation.

2.2.4. Superconducting magnet

The superconducting magnet (Oxford Instrument) can reach 16 T at 4.2 K. When operating at 2 K by pumping the helium bath, the maximum field is 18.5 T. The available experimental space inside the magnet is a vertical cylindrical room temperature bore with a 32 mm diameter. The vertical size of the bore is 118 cm, and the maximum field is located at 89.2 cm below the magnet top flange. The magnetic field map along the vertical axis of the magnet is shown on Figure 2.9.
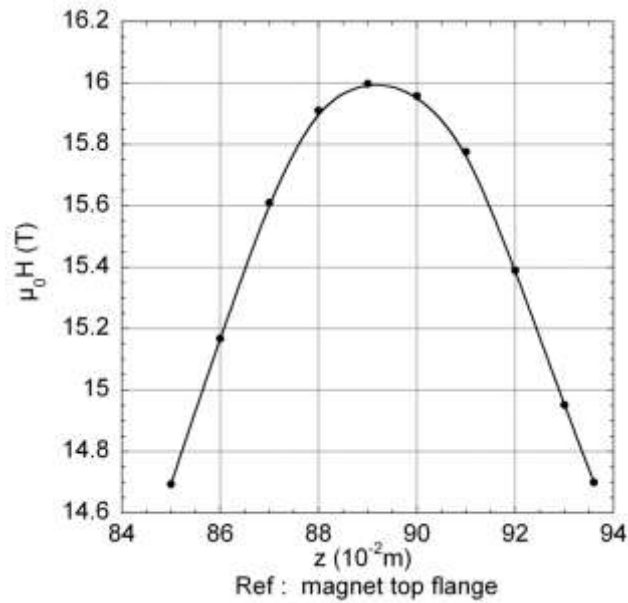
Figure 2.9   Magnetic field measured along the z-axis of the magnet. z = 0 cm on the magnet top flange

2.2.5. Sample holder

The sample holder consists of a brass tube connected to the top of the jacket, and of an alumina tube, which is suspended below, with its lower part inside the hollow heating element. The sample, 4 mm in diameter and 10 mm in length, stands on the bottom closed end of the alumina tube and is positioned in the homogeneous temperature region of the heating element. This position coincides with the homogeneous magnetic field zone, so that the bottom of the sample never changes position during measurements. Special care must be taken to set up the sample in the position where the vertical magnetic forces balance near zero. If the position is too low, the sample is lifted and a contribution is added to the dilatation signal. If the position is too high, the magnetic force pushes the sample towards the bottom of the sample holder and induces an additional elastic deformation contribution. By recording the dilatation signal at room temperature while raising the field, any small variation of the sample position due to the magnetic force shows up immediately. This helps to adjust the sample equilibrium position before starting the experiment. In order to avoid the movement of the sample due to the magnetic torque, the 10 mm sample length is vertical and parallel to the magnetic field. In this case, no torque is induced by the sample shape anisotropy (the ratio of length over diameter is much higher than 1). As a second precaution, the inner diameter of the alumina tube (sample holder) is adjusted to the sample diameter. Thus, neither magnetic

forces nor torques are a cause of perturbation during measurements (within experimental resolution). On top of the sample holder, an evacuation pipe is connected to a secondary vacuum pump and an electro-valve enables the furnace chamber to be filled with purified gas: He, Ar, Ar/H_2 or N_2 can be chosen as the experimental environment. A Pirani-Penning vacuum gauge, together with a manometer is also connected to the furnace chamber through this upper part. On the sample holder and above the vacuum/gas connections, a stand with a xyz fine-motion stage is fixed to maintain the laser head in the vertical position. This set stands 25 cm above the entrance of the magnet bore. At this position, no perturbation due to the magnetic field has been observed in the signal delivered by the laser head detectors. The xyz fine-motion stage is used to set the operating point and to adjust the alignment of the laser beam.

2.3. Process for the thermal treatment of a material under magnetic field.

During this work and through discussions with scientific and industrial partners, the need has emerged for a thermo-magnetic set-up able to simulate a wide range of cooling rates that could be of more specific interest for steel industry. As a result, specifications for a new furnace in high magnetic fields [GARC09b] have been established in order to fit the project requirements. These requirements are:

-a cooling rate greater than 100 K/s from the austenite temperature region,

-a static magnetic field environment higher than 10 T.

-a normalized sample geometry: such as cylindrical dilatometry specimen and A25 (10 cm in length) tensile sheets

Sample position kept constant in the magnetic field during the whole thermal cycle (heating and rapid cooling). (By this way, the magnetic field strength applied to the work piece does not change during the different steps of the treatment).

2.3.1. Design of the system and technical choices

In order to meet the above mentioned requirements, the design of the furnace has been chosen as follows:

- The high cooling rates are obtained thanks to a quenching bath, fixed below the furnace. Various liquids can be used, but water leads to the most severe quenching conditions. Intermediate cooling rates are obtained from gas injection.

- A 11 T superconducting magnet available at CNRS/CRETA with a 120 mm room temperature bore has been used but the device can also fit a 20 T magnet (160 mm) available at NHMFL in Grenoble.

- Due to the cylindrical geometry of the available magnets, a cylindrical geometry has been chosen in a first version for the whole set-up. However, a second heating element dedicated to the treatment of sheet samples is also available.

- The set-up consists of a water-cooled jacket, a mobile furnace, a quenching bath and a sample holder. In order to keep the sample in a constant position in the field during the whole treatment, it is decided to move the furnace and the quenching bath instead. These two elements are fixed to each other and are vertically translated thanks to an external jack. The sample, once its position has been chosen (homogeneous field zone or field gradient), never moves within the magnet bore during the experiment. This set-up is shown in Figure 2.10.

In this configuration, the sample always remains in a constant position, while the whole heating and cooling device can move up and down thanks to an external jack. In the lower position of the jack, the sample is heated in air or under argon flow in the homogeneous heating zone of the furnace and submitted to a homogeneous magnetic field. In the upper position of the jack, the sample, no longer in the hot zone but still in the homogeneous magnetic field, is quenched in the moving up cooling bath. In both cases, the sample remains in a constant magnetic force zone while the furnace is moved: in the ferromagnetic state, any displacement of the sample from this position would lead to extremely high forces which could not be accommodated.

Thanks to this specific design, the work piece is always cooled in the magnetic field (its position never changes) and various cooling rates are available depending on the quenching medium: water, oil (in the quenching bath), air or injection of any other gas (from the top, through the sample holder). The sample diameter should not exceed 8 mm in this design.
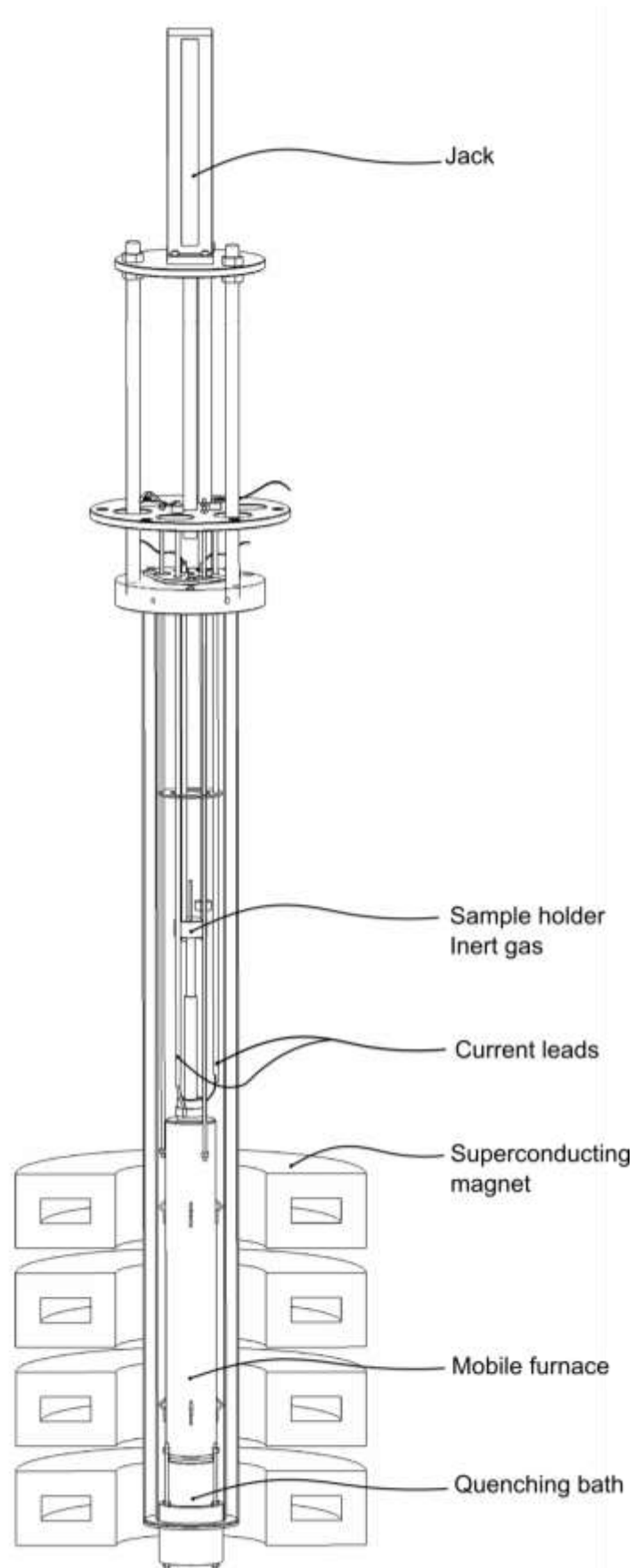
Figure 2.10   Schematic drawing of the mobile furnace with quenching bath [GARC09b]

2.3.2. Details of the design

<u>**Materials selections**</u>

Application of a high magnetic field induces important constraints in the design of this furnace. An electrically conductive piece moving in a magnetic field is submitted to Lorentz forces in the opposite direction of the motion $d\vec{F} = q.\vec{v} \wedge \vec{B}$. An electrically conductive wire submitted to electrical current is subjected to Laplace forces as $d\vec{F} = I.d\vec{l} \wedge \vec{B}$. The ferromagnetic sample and the magnet can then be coupled. Moreover, the motion of a ferromagnetic work piece can disturb or even damage the magnet which is submitted to mechanical stresses. Other secondary problems have to be solved.

- A ferromagnetic sample is submitted to radial magnetic forces in the centre of the magnet bore.
- The size of a bore is often small in high field magnet facilities. In the superconducting magnet used for our experiments, the diameter cannot exceed 120 mm.
- A large gap exists between the magnet top flange and the homogeneous magnetic field zone where the sample is placed (more than 1600 mm).
- High thermal stresses due to high temperature gradients are induced on the sample holder meanwhile rapid cooling.

All these technical problems have led to a specific design, and to a precise selection of the materials constituting the various pieces of the devices. Generally speaking, for each part of the system, the materials used have to be non-magnetic or at least weakly magnetic in order to reduce the coupling with the magnetic field provided by the magnet. In practice, a compromise has to be found between the magnetic response of the material and its electrical conductivity, thermal conductivity, dilatation and its shape forming ability.

The heating element, the quenching bath, and the thermal insulator are made of ceramics: Silicon carbide, Boron Nitride and alumina are used respectively. Brass is used for the current leads and any part which doesn't move during processing. Non-magnetic stainless steel, i.e. austenitic steel, is used for the mobile parts, for the parts which are submitted to high temperature.

Cylindrical configuration

This configuration is dedicated to the heat treatment of a specimen with cylindrical shape and a length and diameter of around 15 mm and 8 mm respectively and is schematically shown n Figure 2.11.
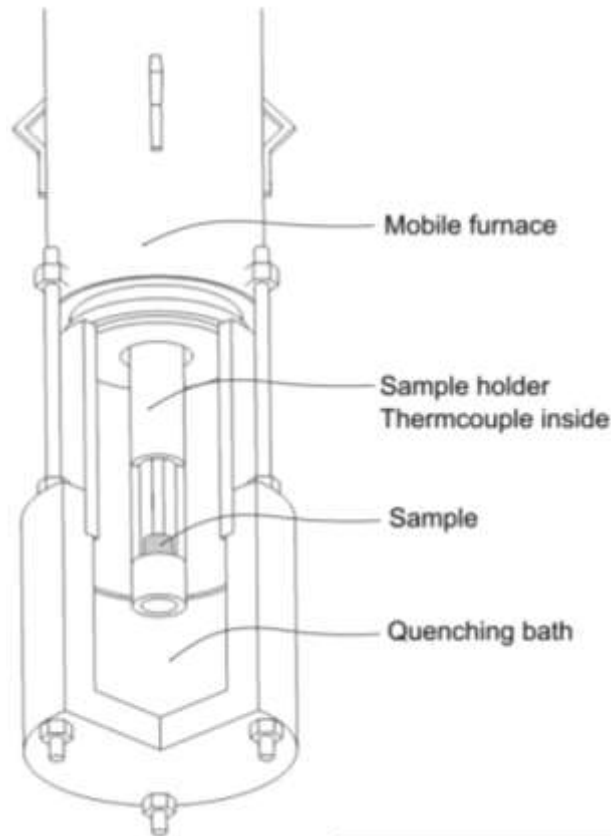
Figure 2.11   Lower part of the set-up with sample in the quenching bath (upper position of the jack) [GARC09b]

The sample is placed inside a SiC tubular resistive heating element with a resistance of 2.2 Ω. A ceramic collar is fixed on the upper part of the heating element. The tubular resistive element is placed inside an alumina cylinder for thermal insulation and finally, both are inserted in a metallic tube (Stainless steel 304L), which constitutes the outside furnace envelope. The size of the heating element has been chosen to ensure temperature homogeneity along the work piece. Note that the distance between the homogeneous temperature zone of the heating element and the centre of the quenching bath has been set to correspond exactly to the displacement length of the external jack. In Figure 2.12, the temperature map of the heating zone on the left and a picture of the silicon carbide element on the right are shown.
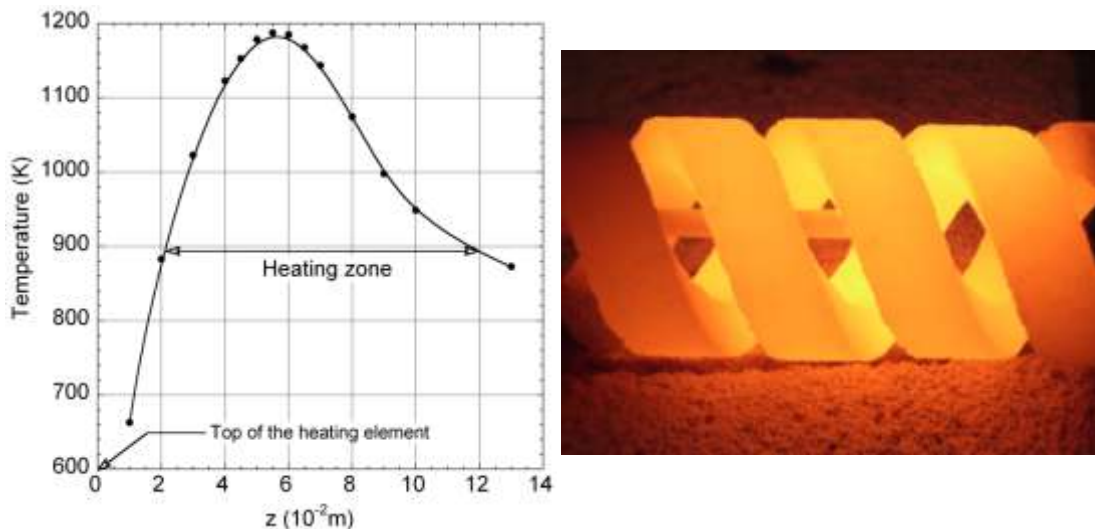
Figure 2.12   Left: Temperature map of the resistive heating used in the cylindrical configuration. Right: Picture of the hot zone of the heating element used in the furnace.

Plane configuration

The plane configuration allows the processing of sheets with large dimensions of about 100 mm in length, 10 mm in width and 5 mm in thickness. The SiC tubular heating element is replaced by two graphite heating plates. These two plate heating elements ($^{®}$MCSE) are placed on both sides of the work piece, as shown in Figure 2.13. The plates are made of sintered boron nitride (BN) with an imprint graphite track for the current transport. These elements have a limit upper temperature of use of 1173 K under oxidizing atmosphere. The heating part with the two heating plates installed in an alumina insulator tube is shown in Figure 2.13. The current leads are divided into two parts and are connected to the heating elements by intermediate molybdenum pieces screwed onto the heating plates with Mo screws. Molybdenum is used because its expansion coefficient, similar to that of ceramics, avoids any differential dilatation on the heating plates and it thus prevents the ceramics element from destruction. The Molybdenum pieces are prolonged by stainless steel current leads, which serve different purposes. They supply power to the heating device. They support the whole heating device which is hanging up below. They show a very good resistance to high temperatures under oxidizing atmosphere and present a well-known non-magnetic character.

As in the cylindrical configuration, the vertical upwards displacement of the heating plates is possible to enable quenching of the sheet specimen. This version is well adapted to the treatment of normalized A25 tensile sample (10 cm in length).
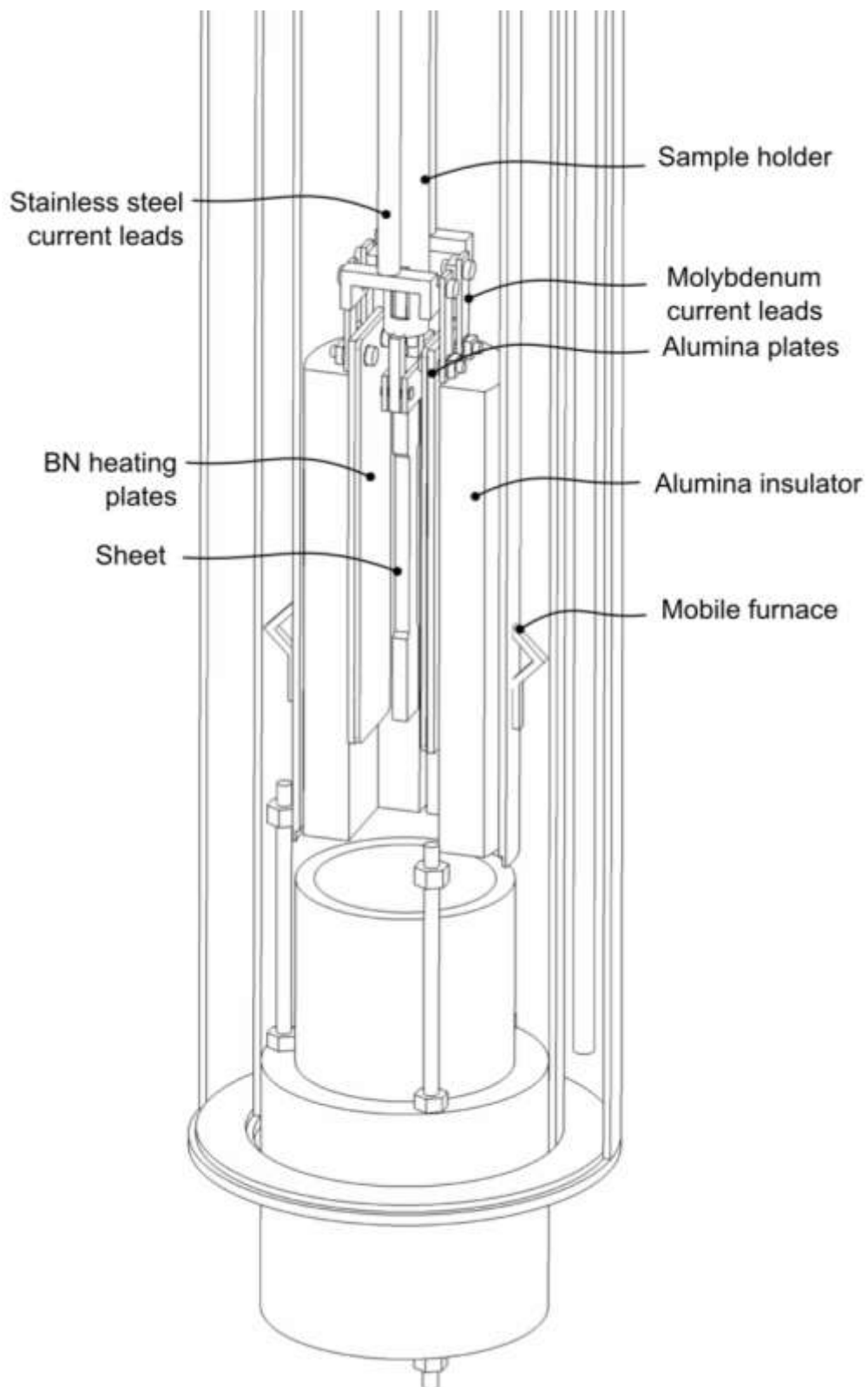
Figure 2.13   Schematic view of the heating system in the plane configuration for the heat treatment of sheet [GARC09b].

Power supply and Instrumentation

The electrical source is a Direct Current Sorensen® power supply (80 V, 37 A), with an output power of 2960 W. In the system, the heating elements are supposed to move in the magnetic field. For that reason, an electrical security relay is installed in the electrical circuit which allows automatic power shutdown when motion is started. A current flow of several tens of amps during the heating element motion in the magnetic field would be very damaging to the magnet.

Two S-type (Pt/Pt 10% Rh) thermocouples allow the temperature measurement. One is placed near the heating element and measures the "regulation" temperature. It is used as a feedback for regulation. The other one is spot welded on the sample and allows the accurate measurement of sample temperature. An ®Eurotherm controller monitors the regulation of temperature in the sample region. A ®Labview interface allows the data acquisition as a function of time: two temperatures and the power supplied.

Work piece positioning in magnetic field

The sample holder is a rigid piece that allows the centring of the sample along the axis of the magnet that counters the important radial magnetic forces in the bore, and that ensures the concentricity of the various moving parts. A quick fixation system, on its upper part, able to adapt the sample holder to the two different (plane and cylindrical) configurations and to switch easily from one to the other.

The lower part of the sample holder containing the sample is a stainless steel tube coated by boron nitride for its electrical insulation. This lower part is subjected to strong temperature gradients during quenching and steel is more resistant than alumina to thermal shocks. However, the alumina sample holder is especially designed to be used for intermediate cooling rates. On the upper side, the sample holder is fixed to a brass flange that ensures thermocouples and gas connections.

External jack

The use of a pneumatic jack allows the translation of the "furnace + quenching bath". The jack axis is a stainless steel rod with strong magnetic properties. For that reason, the jack

is fixed more than 1.5 m above the top flange of the magnet. An extension of the rod has been machined using a non-magnetic stainless steel (304L) in order to deport the jack stroke.

Cooling means

Heat transfer between the materials and the fluid during a rapid cooling is a very complex process. However, three components in the heat transfer can be qualitatively distinguished that are: transfer in the solid media, at the interface between solid and cooling fluid and in the fluid itself. Because the work pieces are usually metallic materials, have a large thermal conductivity and are of relatively small thicknesses, thermal gradients in the solid are assumed to be negligible. Indeed, as a piece of evidence for this assumption, a very good homogeneity in the microstructure of water quenched samples has been obtained. Concerning the heat transfer at the interface and in the fluid, the temperature of the bath is maintained constant and near 300 K during quenching and the volume of the evaporated fluid is found to be very small. Finally, to avoid any pre-heating of the bath by the furnace radiation, the fluid is injected only a few seconds before quenching. The cooling rate measured during water quenching a 10 mm length, 5 mm diameter cylindrical sample, is higher than 200 K/s in the range 1100K to 300K.

Apart from the liquid bath, an injection gas system is adapted to obtain intermediate cooling rates. The gas flow is regulated by several valves. The output pressure, governing the rate of flow (and thus the cooling power), is between 0.1 and 3 bar, which corresponds to cooling rates experimentally measured between 1 and 100 K/s in the temperature range 1200-900 K.

2.3.3. Magnetic field environment

The whole system has been designed to be inserted in two magnets available in Grenoble. The first is a superconducting magnet permanently available at CNRS/CRETA with a vertical room temperature bore of 120 mm and a maximum field of 11 T. The homogeneity of the field on the vertical axis is better than 3% within 32 mm (useful length of an A25 tensile sample) (see Figure 2.13). The second high field facility is a resistive Bitter magnet available at CNRS/Grenoble National High Magnetic Field Laboratory (GNHMFL) with a room temperature bore of 160 mm, a maximum field of 20 T and field homogeneity on

the vertical axis of 0.25 % within 32 mm [MOSS04]. Magnetic field map along the vertical axis of the magnets bore is shown on Figure 2.14

The mobile furnace set-up is permanently installed in the first magnet (11 T) but has been installed for two months in the second magnet (20 T) after proposal application and selection by an external scientific committee at the GNHMFL. The main advantage of this magnet is fast field sweeping rate. This property can be useful to apply the magnetic field for short periods of time and to test for the magnetic field effects at particular moments during the full process.
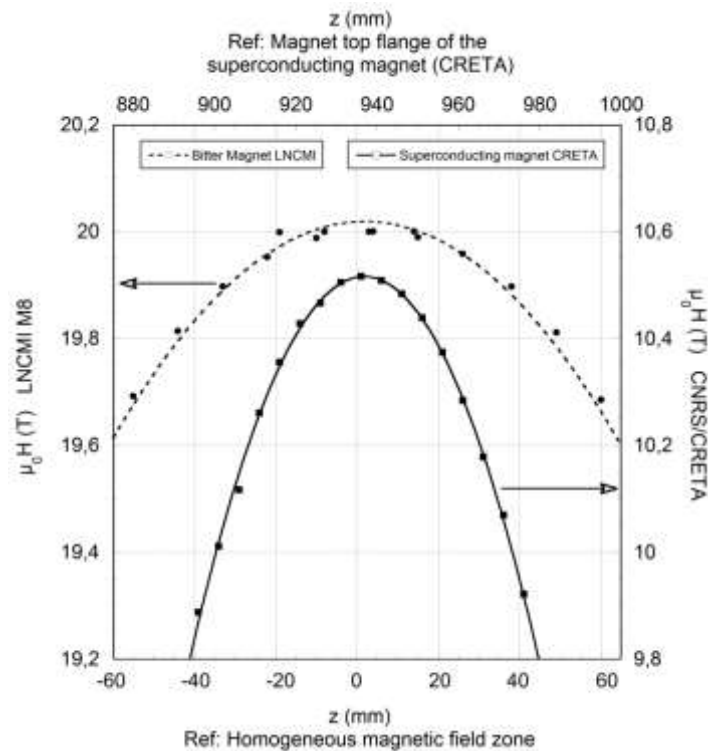
Figure 2.14   Magnetic field map along the vertical axis of the two magnets used in this project.

2.4. Microstructures characterisation

The following part is designed to introduce typical post treatment characterisation techniques that have been used in this work.

After material processing, microstructure characterisation is always highly required in metallurgy, because the functional properties, (i.e. physical and mechanical properties) are directly correlated to the microstructure at different levels. Wide information is already obtained by this simple investigation, such as the determination of the phases involved in the

structure and their volume fractions, the possible occurrence of any texture, phase alignment or shape modifications, or also the evaluation of typical length scales (i.e. grain size, inter-lamellar distances, number of nuclei). In this work, Optical Microscopy (OM) together with Scanning Electron Microscopy (SEM) is used for microstructure observation. Besides, hardness testing is widely used in the characterisation of materials because it completes microstructural characterisation and gives a rough estimation of the mechanical properties. The hardness number is not really a true property of the material but is an empirical value. The Vickers hardness (HV) is usually measured because it is proportional, in first approximation, to the uniaxial yield stress of the material. Finally, the Residual Stress measurement technique by X-Ray Diffraction (RSXRD) is briefly described. This characterisation method is used (see chapter 5) for the investigation of magnetic field effect on recovery and recrystallisation in an IF steel.

2.4.1. Metallurgy and Metallographic Techniques

Microscopes

Metallography consists in examining and determining the constitution and the underlying structure in metals, alloys and materials. The examination of structure may be done over a wide range of length scales or magnification levels, ranging from low-magnification (~20×) examination to magnifications over 1,000,000× with electron microscopes. Metallography may also include the examination of crystal structure by techniques such as x-ray diffraction. However, the most familiar tool for metallography is the light microscope.

In regards to the presentation done in the first chapter on the phases involved in steels, a large range of scales is observed in the various structures. From a macroscopic scale in the solidification structure or in the massive transformation structure, it goes to the microscopic scale in the vast majority of industrial ferrito-pearlitic steels up to the nanometric scale in the substructure of pearlite or thin plates of bainite and martensite often found in high strength steels.

The Optical Microscope used in this study is a Zeiss® SIP 40715 light Microscope with magnifications ranging from 50x to 500x and the ability to resolve microstructural features of

~ 0.5 μm or larger. The SEM is a JEOL 5600LV instrument equipped with EDS (Energy Dispersive Spectrometry, Silicon Drift Detector, 138 eV, PGT®).

Material Preparations (Sectioning, Polishing, Etching)

Sectioning consists in the removal of a conveniently sized and representative specimen from a larger piece and is the first major operation in the preparation of metallographic specimens. By its nature, metallography is a destructive test, and extreme care must be taken in this operation. Sectioning can cause microstructural changes, due to residual stresses, that may lead to erroneous conclusions. In practice, the damage to the specimen during sectioning depends on the nature of the material, the cutting device used, the cutting speed, the feed rate and the amount and type of coolant used. In any case, the user develops a habit of checking every single specimen for burn or deformation damage at the area of interest before any further investigation.

After the metallographic specimen is cut to an appropriate size, mounting of the specimen is often desirable or necessary for subsequent handling and metallographic polishing. Mounting is often done by encapsulating the specimen in a polymeric material. Advantages of encapsulating specimens include the edge retention of mounted specimens, the easier handling of specimens that are too small, fragile, or awkwardly shaped, the containment of sharp edges or corners that may damage the papers and cloths used in polishing equipment, the convenient and uniform configuration for either manual or automatic polishing machines, and the filling of holes and cracks in the specimen with mounting material to prevent "bleeding" of water, alcohol, and etching solutions.

Characterisations of the structure of a metal are generally carried out on sections that have been cut from the bulk specimen. The techniques often involve the reflection of some form of radiation from the section surface. An image of the surface is formed from the reflected radiation. Visible light is used for this purpose in the optical microscope and it is usually necessary to treat section surface by some chemical or physical process that changes the way light reflects in the various structural constituents that have been exposed. The purpose of this chemical of physical etching is to enhance the contrast between different phases or grains and thus to reveal the microstructure by an optical mean. A carefully polished plane area of the material is required for etching. A complete list of chemical etching solutions are given in [ASMH04] as a function of the nature of the materials

In this work, the samples are polished using a series of increasingly fine sandpapers (P320 (46 µm), P600 (26 µm), P1200 (15 µm) together with 95% purity ethanol to clean the samples during polishing. Then a series of crystal solutions of decreasing crystal size (15 µm, 9 µm, 3 µm, 1 µm) are used with special nylon polishing discs. After each individual polishing step, the sample is cleaned in an ultrasonic bath and then dried with a nitrogen gas flux.

For etching, a small quantity (2-4 ml) of nital solution (96% ethanol, 4% nitric acid) is deposited on the surface of the sample in order to highlight the grain boundaries for about 10 second.

2.4.2. Hardness Testing

The term Hardness is defined as the ability of a material to resist permanent indentation or plastic deformation when in contact with an indenter under load. The test consists of pressing an indenter of known geometry and mechanical properties into the test material. The hardness is quantified using one variety of scales related to the contact pressure involved in deforming the test surface. The indenter may be spherical (Brinell test), pyramidal (Vickers test) or conical (Rockwell test). In the Brinell and Vickers tests, the hardness value is the load supported by a unit area of the indentation in [kgf/mm²] whereas in the Rockwell tests, the depth of indentation at a prescribed load is determined and converted to a dimensionless hardness number [ASMH00].

For macrohardness tests, indentation loads are 1 kgf or greater: Vickers testing may use loads from 1 to 120 kgf. The microhardness tests use smaller loads ranging from 1 gf to 1 kgf, the most common being 100 to 500 gf and suited for material layers that are thicker than about 3 mm. After the forces have reached a static or equilibrium condition and further penetration ceases, the force remains applied for a specific time (10 to 15 s for normal test times) and is then removed. The resulting unrecovered indentation diagonals are measured and averaged to give a value in millimetres. These length measurements are used to calculate the Vickers hardness number (HV).

- 82 -

Chapter 3

Diffusional transformations in plain carbon steels in magnetic field

This chapter deals with the presentation studies investigated during this work and relating to the effect of high magnetic field on the diffusional transformation in iron and iron based alloys.

In the first two studies, the effect of magnetic field on both the $\alpha \rightarrow \gamma$ and $\gamma \rightarrow \alpha$ transformation temperature is experimentally investigated by dilatometry up to 16T in pure iron and Fe-xNi alloys. The Molecular Field model, which described the influence of a strong magnetic field on the saturation magnetisation of iron and iron substitutional alloys, is directly tested by high temperature magnetic measurements up to 3.5T. In pure iron the equilibrium temperature between α-Fe and γ-Fe is experimentally defined and compared with calculations. In Fe-xNi alloys, non-equilibrium transformation temperatures are measured and thermodynamically analysed.

Then, the non-isothermal decomposition of austenite into ferrite and pearlite in Fe-xC-1.5wt%Mn steels with x = 0.1, 0.2 and 0.3wt%C is experimentally investigated by *in situ* dilatometry and microstructure characterisation in magnetic fields up to 16T. The global shift towards higher temperatures of the respective austenite, ferrite+austenite and ferrite+pearlite stability regions is experimentally confirmed. A systematic characterisation of microstructure in term of ferrite volume fraction and Vickers hardness is done. The steels' magnetisations, measured up to 3.5T and 1200 K are used to calculate the magnetic contribution to the free energy of the transformation and to account thermodynamically for the field dependence of the transformation temperature.

In the fourth part, the magnetic field impact on the austenite to ferrite + pearlite transformation in four Fe-C-Mn-xSi steels with increasing silicon content from 0.015 wt% to 1.75 wt% is investigated. Magnetostatic contribution to the free energy is determined by experimental measurements. Quantitative correlation is done between the effect of silicon (reducing the stability domain of austenite) and magnetic field (enlarging the stability domain of ferrite).

In a last part, isothermal transformation in pure iron is monitored by dilatometry up to 16T. The kinetics of the $\gamma \rightarrow \alpha$ transformation is studied in terms of Avrami exponent, interface mobility and driving force for transformation.

3.1. Experimental evidence of the magnetic field effect on the α/γ equilibrium in pure iron

In this paragraph, the measurements of phase transformation temperatures in pure iron in the presence of magnetic field are described. Dilatation measurements up to 16 T are used. This study has two main purposes. The first one is to discuss the effect of high magnetic field on the α/γ equilibrium in pure iron. The second one is to check the validity of the calculated phase diagram in magnetic field based on the Molecular Field model. For this last purpose, high temperature magnetic measurements are achieved up to 3.55 T.

3.1.1. Experimental details

The experimental setup used to measure transformation temperatures is the in-situ dilatometry measurement setup described in part 2.2 and in [RIVO09]. The whole device is operating under magnetic fields up to 16 T. Specimen of high purity iron (99.999%) are prepared by induction melting in a cold crucible induction furnace. After melting, the iron is cast into a cylindrical copper mould with an inner diameter of 4 mm. Then, cylinders of 10 mm in height are cut from this ingot. After that, specimens are kept at 1223K for 30 min for homogenization before the measurements.

Then, the samples are heated under various magnetic field strength with a heating rate of 3 K/min between 1163 and 1213 K. The same rate is applied on cooling between 940 K and 1163 K. The magnetic field is applied during the whole thermal treatment and the furnace is under pure argon atmosphere. Both α/γ and γ/α transformations are studied and each measurement is repeated twice. Below 1163 K, the cooling rate is about 30 K/min down to room temperature.

3.1.2. Dilatation measurements

Figure 3.1 shows the change of the sample length (ΔL) relative to the initial length at room temperature, L_0. In this Figure, the dilatation signal monitored for a high purity iron sample is observed in the transformation temperature range on heating and on cooling. The α/γ transition shows up as a sharp volume reduction of the sample. The γ/α transition shows

up as a sharp expansion of the sample.

Expansion coefficients measured during cooling are 11.1 10^{-6} K^{-1} for α-Fe and 25.6 10^{-6} K^{-1} for γ-Fe are deduced from this measurement. The measured volume change during the transformation is evaluated at 1.7%.
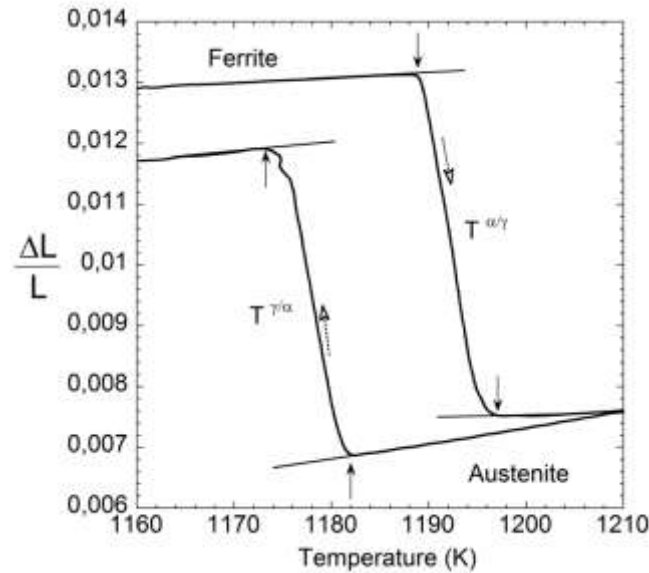
Figure 3.1   Change of the sample length relative to the initial (room temperature) length as a function of temperature recorded during the γ-Fe to α-Fe transformation without applied magnetic field.

The effect of magnetic field on pure iron was tested for several values between 0 Tesla and 16 Tesla. The transformation temperatures are noted $T_{\alpha\rightarrow\gamma}$ on heating and $T_{\gamma\rightarrow\alpha}$ on cooling. The temperature at which the linear thermal expansion, graphically represented by the $\Delta L/L_0 = f(T)$ function in Figure 3.1, deviates from linearity is evaluated as illustrated with the black arrows in Figure 3.1. The location of the points at which the deviation occurs is obtained by extrapolating the linear portions of the thermal expansion curve. $T_{\alpha\rightarrow\gamma}$ (respectively $T_{\gamma\rightarrow\alpha}$) is then defined by the average value of point corresponding to the start and to the end of the respective transformation. The equilibrium temperature is finally calculated as $T_{\alpha/\gamma} = (T_{\alpha\rightarrow\gamma} + T_{\gamma\rightarrow\alpha})/2$. The change in the equilibrium temperature is plotted as a function of the magnetic field intensity in Figure 3.2. The average α/γ transformation temperature for pure iron is increased with increasing magnetic field strength as also reported by [FUKU06, HAOO04]. The variation relative to the equilibrium temperature in the absence of magnetic field amounts to 17 K in pure Fe, in a magnetic field of 16 T. The α-Fe phase is

stabilized at the expense of γ-Fe.

The effect of a high magnetic field on the respective stability of the α-Fe and γ-Fe phases can be qualitatively explained in term of the magnetic contribution to the total Gibbs energy of each phase. When a magnetic induction, B, is applied, the respective Gibbs free energy of α-Fe and γ-Fe is lowered due to the contribution of a magnetic energy term, ΔG_{mag}, to the total energy of each phase as detailed in equation (17). These respective contributions are proportional to the field dependence of the magnetisation of each phase. As α-Fe is more magnetic than γ-Fe, this phase is stabilized, so that a shift in the equilibrium temperature is observed towards higher temperatures.
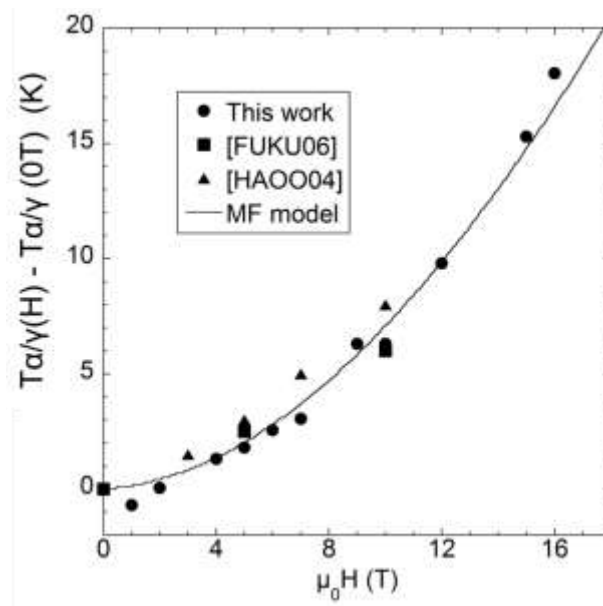
Figure 3.2   Relative change in the austenite/ferrite equilibrium temperature, $T_{\alpha/\gamma}$ as a function of applied magnetic field: a) (circles): our experimental data b) (square): Experimental data from [FUKU06] c) (triangle) Experimental data from [HAOO04]

When the γ/α transition occurs below the Curie temperature of the α-Fe phase, the magnetisation of this phase, M^{α}, is rapidly saturated so that the magnetic energy is roughly linear with the applied magnetic field value. On the contrary and as it is the case here, when the γ/α transition occurs above the Curie temperature, the α-Fe phase is formed in the paramagnetic state and hence M^{α} is almost linearly dependent on B. Since the magnetic energy is proportional both to the applied field and to the magnetisation, the temperature shift is roughly proportional to the square of the field value.

3.1.3. <u>Calculation of the equilibrium temperature's shift by the magnetic field</u>

The average γ/α transformation temperature measured experimentally can then be easily compared to the calculated γ/α equilibrium temperature because the hysteresis of the transformation temperature is very narrow (see later on Figure 3.14).

On Figure 3.3 is shown the equilibrium temperature $T_{\alpha/\gamma}$ calculated as the mean values of $T_{\alpha \to \gamma}$ and $T_{\gamma \to \alpha}$. This equilibrium temperature is directly compared with the predicted shift of the γ/α equilibrium calculated using either the Molecular Field (MF) model or the Curie Weiss (CW) law by [CHOI00, GUOE00, ENOM01] (see chapter 1) and illustrated on Figure 1.19.
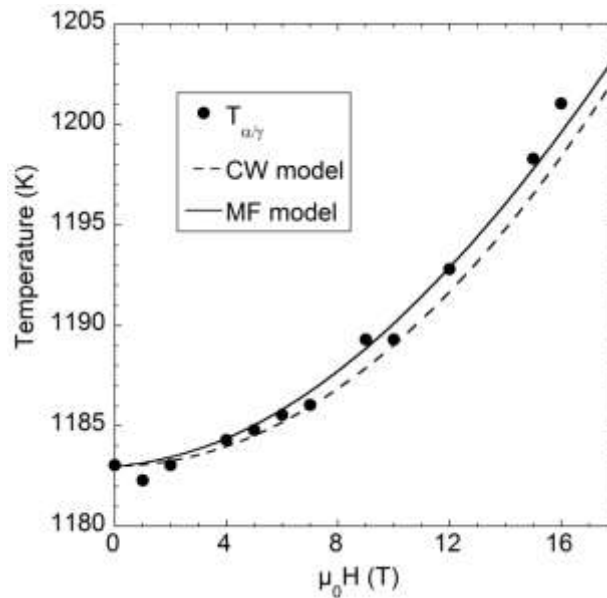
Figure 3.3   Variations in the austenite/ferrite equilibrium temperature, $T_{\alpha/\gamma}$ as a function of applied magnetic field: a) (circles): our experimental data b) (solid line): calculation with Molecular Field (MF) model c) (dotted line) Calculation with Curie Weiss (CW) model

In a first approach, the magnetic free energy term of the α-Fe phase $\mu_{Fe}^{\alpha B}$ is calculated with the MF model with with J=0.5, T_C =1043 K and M_{Fe}^0=1.73 10^6 A.m^{-1}. The magnetic free energy of the γ-Fe phase $\mu_{Fe}^{\gamma B}$ is calculated with the Curie-Weiss Law given by eq. (21). At $T_{\alpha/\gamma}$, the term $\Delta\mu_{Fe}^{tot}$ is zero and in this way, the equilibrium temperature is deduced. The experimental data are found to be in very good agreement with the calculated ones (solid line), as seen in Figure 3.3.

In a second approach, the magnetic free energy contribution is calculated by evaluating the magnetisation of α-Fe with the Curie Weiss Law given from eq. (20) valid above about 1100 K (dotted line) in [ARAJ60]. In this approach, the agreement with experimental measurements is less good than that of the MF model. As discussed in chapter 1, this Curie Weiss law is no longer valid in a temperature region very close to the Curie point (1043 K) and only MF model can be used in such a case.

3.1.4. <u>Magnetic properties of pure iron</u>

Because the $T_{\alpha \to \gamma}$ (respectively $T_{\gamma \to \alpha}$) transformation occurs above but close to the Curie point of the α-Fe phase, the magnetic susceptibility of α-Fe deviates from the Curie-Weiss law due to the magnetic transition. Therefore, it is most commonly adopted to estimate the α-Fe magnetisation with the Molecular Field model [BOZO78, CHOI00, GUOE00, ENOM01, ZAHE05, ZHAN07]. However, how close is this calculation to experimental measurements of magnetisation? On the basis of magnetic measurements, the purpose of this part is to discuss the use of the Molecular Field Theory to calculate the magnetisation of the α-Fe phase.

In Figure 3.4 are shown the magnetic measurements done for high purity iron under various magnetic field strength (black lines). In this figure are added the calculated values given by the MF theory with J=0.5, T_C =1043 K and M_{Fe}^0=1.73 10^6 A.m^{-1} (red lines). In insert, the high temperature region is enlarged in order to show the magnetic signal corresponding to the structural transformation from α-Fe to γ-Fe on heating and the reverse on cooling. The Molecular Field model gives a correct estimation of the saturation magnetisation near the transformation point of pure iron, i.e. at temperatures around 1100 K. However, at lower temperatures the calculated curve does not agree well with the experimentally measured values. To highlight this discrepancy, the predicted magnetisations values obtained with the MF model are plotted as a function of the measured data on Figure 3.5a. In addition Figure 3.5b gives the error made for each measurement calculated as follows:

$$Error\ (\%) = 100 * \frac{M_{meas} - M_{calc}}{M_{calc}} \tag{46}$$
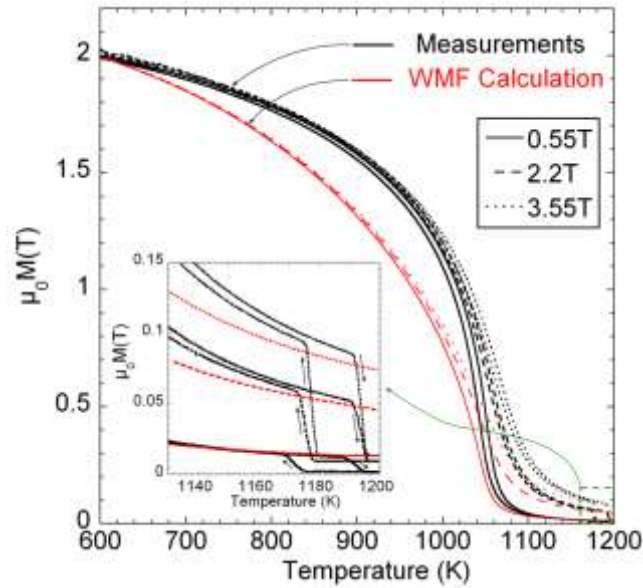
Figure 3.4   Saturation magnetisation of high purity iron as a function of temperature (black lines) measured and (red lines) calculated with the MF model for 0.55, 2.2 and 3.55 T.
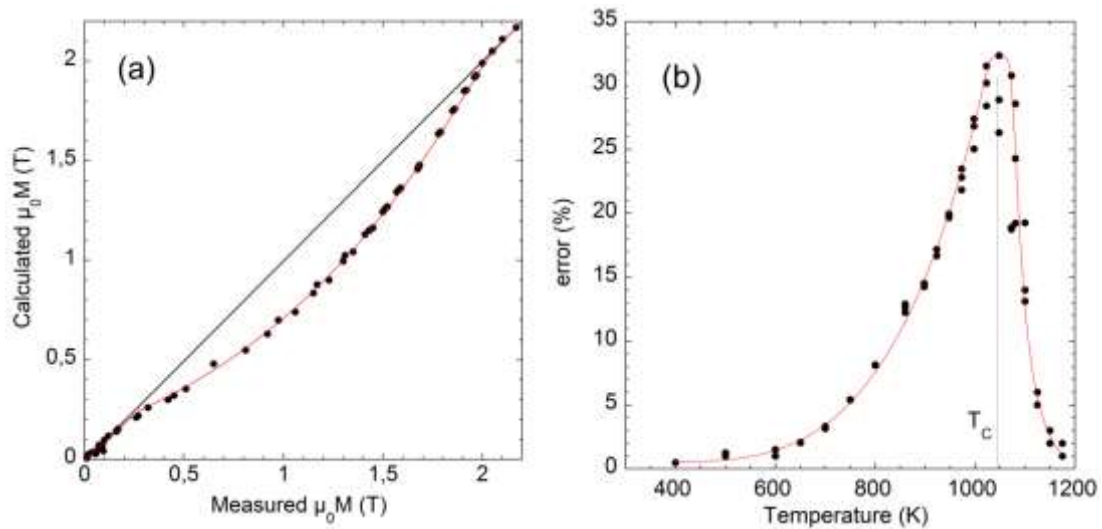
Figure 3.5   (a) Calculated values of magnetisation of iron as a function of measured data up to 3.55 T and 1200 K (b) Error in % as a function of temperature calculated with equ. (46)

It appears that the error in the estimation of the magnetisation of pure iron presents a maximum around the Curie point. It is proposed in [KUBL07] that this discrepancy is due to an improper treatment in the MF model of the magnon excitations. According to [KUBL07], the collective excitation of the electrons' spin structure in the crystal lattice should not be described in the mean field approximation as it is the case in the MF model but rather in a local moment. To our knowledge and because the transformations that are studied under high

magnetic field in literature usually occur around or above the Curie point, no attempts have been made so far to introduce the local moment approximation in the calculation of the α-Fe phase magnetisation.

3.1.5. <u>Conclusion</u>

The results obtained with pure iron constitute strong experimental evidence of the predicted calculations of the shift of the equilibrium temperature under magnetic field and validates the use of high field laser dilatometry for such investigations.

3.2. Characterisation of phase transformations in Fe-Ni alloys in magnetic field

Fe-Ni alloys in which the alloying Ni content is relatively small (less than several percents) are of special interest in the study of the effect of magnetic field on the $\alpha \rightarrow \gamma$ and $\gamma \rightarrow \alpha$ phase transformations for 2 main reasons.

The first reason is that any substitutional alloying elements may influence the magnetic properties of the two phases (α-Fe and γ-Fe) via their influence on the magnetic moment and on the Curie temperature of the iron solid solution. Thus, the addition of Ni to the Fe lattice is expected to decrease the Curie point of the ferrite (α-Fe) phase [GUOE00]. At the same time, the addition of Nickel also influences both the $\alpha \rightarrow \gamma$ and $\gamma \rightarrow \alpha$ transformation temperatures as Ni acts towards the stabilisation of the gamma phase. The resulting phase diagram (up to 6 wt%) is shown in Figure 3.6, together with the variation of the Curie point with Ni content. As shown in Figure 3.6, the $\alpha \rightarrow \gamma$ (respectively $\gamma \rightarrow \alpha$) transformation is spread on a wide range of temperatures when the Ni content is increased. In the same time, the Curie temperature (T_C) of ferrite is slightly decreased. As a consequence, and depending on the Ni content, T_C can be found below, within or even above the ($\alpha + \gamma$) stability region. Therefore it is expected that the magnetic field's impact on the transformation temperature (T_T) will differ depending on the value of $T_C - T_T$ or in other words depending on the magnetisation of the ferrite phase at the transformation point.

The second point of interest is the possibility to obtain polycrystalline but single phase material. It is thus possible to test the validity of the Molecular Field model in relatively

simple and well defined cases. Since the austenite transforms completely into ferrite on cooling, no secondary phases are involved in such a transformation and only the magnetisation of ferrite and austenite will contribute to the measurements.
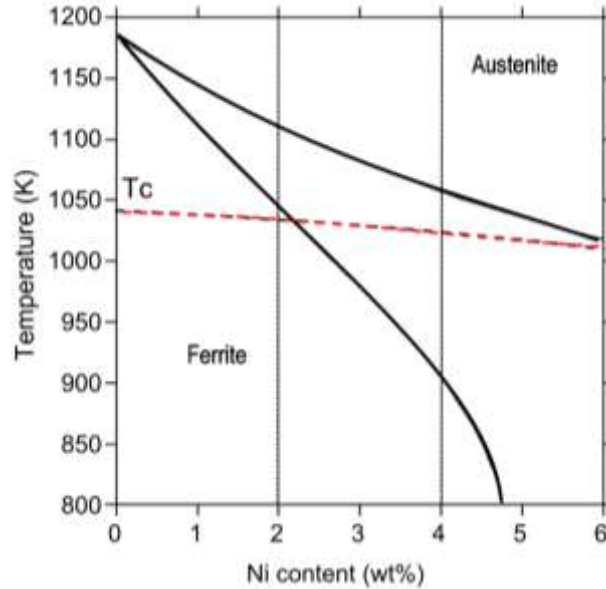
Figure 3.6   Equilibrium phase diagram of the Fe-Ni in the range of composition interesting in this study.

In the present study, the alloy compositions are Fe-xNi with x = 0, 2, 4 wt%. Magnetic measurements at high temperatures are done to follow the magnetic behaviour of ferrite during a complete heat treatment. $\alpha \rightarrow \gamma$ and $\gamma \rightarrow \alpha$ transformation temperatures are examined by dilatometry measurements up to 16 T and are compared with calculated values based on the Molecular Field theory.

3.2.1. Experimental procedure

Ingots of Fe-Ni alloys with Ni content of 0, 2 and 4 wt% are prepared by induction melting in a cold crucible under argon atmosphere and cast into a 10 mm diameter copper mould. The alloys are treated for 48 h at 1173 K under vacuum for homogenization. Finally the ingots are cold worked down to a diameter of 4 mm and cut into cylindrical specimens of 10 mm in length. Before heat treatment in magnetic field, they are subjected to a final heat treatment at 973 K for 1 h in order to start with a fully recrystallized structure. The magnetic properties of each alloy expected from literature data [GUOE00, ISHI75] and the onset

transformation temperature on heating $T_{\alpha \to \gamma}$ and on cooling $T_{\gamma \to \alpha}$ measured by dilatometry under 0T are summarized in Table 3.1.

Fe-Ni (x wt%)	0	2	4
T_C (K)	1043	1036	1029
m (µb per atom) (0K)	2.22	2.23	2.25
$T_{\alpha \to \gamma}^{B=0T}$(K)	1189	1113	1061
$T_{\gamma \to \alpha}^{B=0T}$(K)	1175	1048	968

Table 3.1: Magnetic properties of each alloy expected from literature data [GUOE00, ISHI75] and the onset transformation temperature on heating $T_{\alpha \to \gamma}^{B=0T}$ and on cooling $T_{\gamma \to \alpha}^{B=0T}$ measured by dilatometry under 0 T

In a first hand, the variation of the magnetisation as a function of temperature for different magnetic field strength is measured by the Faraday method for the different alloys composition using the magnetic balance described in the part 2.1. Results are compared with those predicted by the Molecular Field theory. The thermal treatment is the following. Temperature is increase up to 1250 K at a rate of 3 K/min and the same rate is imposed on cooling. Measurements are performed under three different values of magnetic field strength.

In a second hand, isothermal magnetisation measurements $M(H)$ as a function of magnetic field up to 3.55 T and around the transformation temperature are done for Fe-2Ni wt% and for Fe-4Ni wt%. Specimens are heated at a slow rate of 0.1 K /min up to various isothermal temperatures around the transformation point. The dimensions and weights of the specimens used for these measurements are specified in Table 3.2. The internal magnetic field value is corrected by the demagnetisation coefficient, N_D for a cylinder [SATO89] as :

$$N_D = \frac{1}{2\left(\frac{2n}{\sqrt{\pi}}\right) + 1} \qquad (47)$$

where n is a dimensional ratio of the long axis over the diameter.

In a third hand, the three alloy compositions are heat treated in the dilatometer up to their respective austenitisation temperature with a heating rate of 3 K/min. The temperature is then kept constant for 10 min. The same rate is applied on cooling. The austenitisation

temperatures are set 30 K above the upper boundary of the two phase $\gamma + \alpha$ region respectively for each composition. This corresponds to 1213 K for pure Fe, 1173 K for Fe-2Ni wt% and 1123 K for the Fe-4Ni wt% alloys. The transformation temperatures from ferrite to austenite on heating and from austenite to ferrite on cooling are measured in several magnetic fields up to 16T by dilatometry.

Based on existing thermodynamics databases (Thermocalc®) and on the above mentioned magnetic measurements, the measured changes in the phase boundaries due to the application of a magnetic field are discussed.

	Long axis c (mm)	Diameter a (mm)	Demagnetisation factor (N_D)	Weight (g)
Fe-2Ni wt%	10	1.5	0.062	0.255
Fe-4Ni wt%	10	2	0.081	0.292

Table 3.2: Dimensions, demagnetisation factor and weight of specimens for isothermal magnetic measurements.

3.2.2. Magnetic measurements in Fe-Ni alloys

Magnetic properties of Fe-Ni (2 and 4wt%) alloys as a function of temperature

Figure 3.7 shows the magnetisation curves as a function of temperature measured for both Fe-Ni (2 and 4 wt%) alloys upon (a) heating and (b) cooling under a magnetic field of 0.55, 1.5 and 3.5 T. These curves are compared with those of pure iron measured under 3.5T. According to Table 3.1, the addition of 4 wt% of nickel in iron reduces the T_C of 15K and increases the Fe magnetic moment m from 2.2 to 2.25. The corresponding Curie temperature calculated with equation (32) is added to the figure.

On heating, the magnetisations of the three respective alloys measured under the same magnetic field intensity coincide probably due to the weak impact on the magnetisation of iron of a small Ni amount. The continuous decrease of the magnetic signal in all the cases is attributed to the Curie transition. At higher temperatures, the $\alpha \rightarrow \gamma$ transformation is observed as a sharp decrease in the magnetic signal. This effect can hardly be seen in the Fe-

4Ni wt% alloy because the magnetic transition occurs in the same temperature range as the $\alpha \rightarrow \gamma$ transformation.
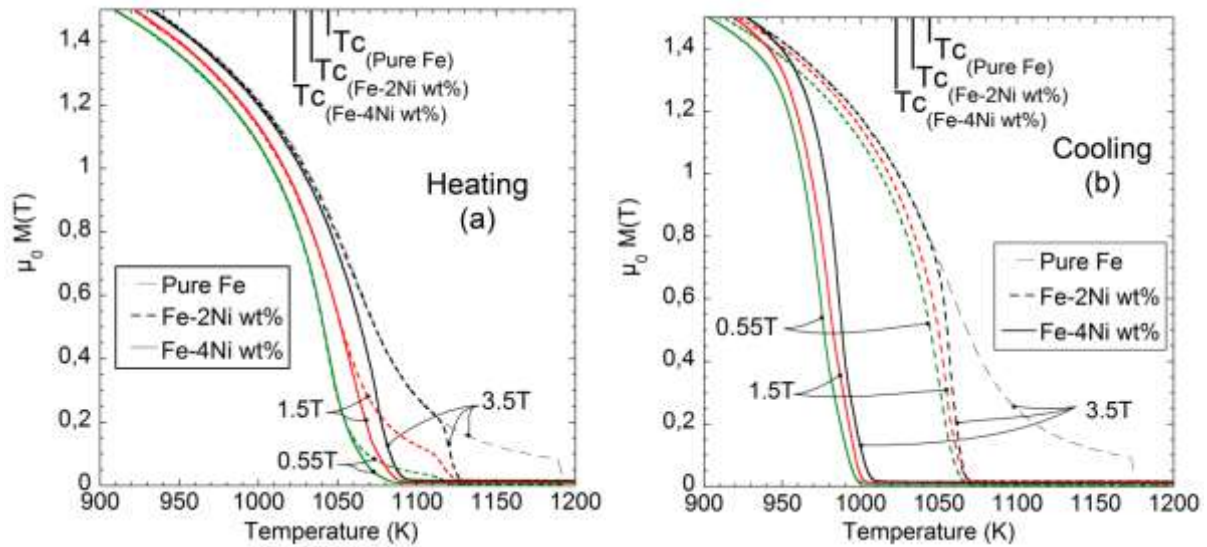
Figure 3.7   Magnetisation curves as a function of temperature at 3 K/min for Fe-Ni (0, 2 and 4 wt%), upon (a) heating and (b) cooling under 0.55, 1.5 and 3.5T

On cooling, the $\gamma \rightarrow \alpha$ transformations and the magnetic transitions are well dissociated in pure Fe as it has been already shown in Figure 3.4. However for nickel alloys, no $\gamma \rightarrow \alpha$ transformation shows up before reaching the Curie point. The $\gamma \rightarrow \alpha$ transformations occur around the T_C of ferrite both for Fe-Ni 2 and 4 wt%. The magnetic and structural transitions are both mixed in the measured magnetic signal. That is, the sharp increase on cooling corresponds both to the formation of ferrite from austenite and to the paramagnetic to ferromagnetic transition of ferrite.

To sum up, these M(T) magnetic measurements constitute a rough experimental evidence of the Molecular Field model up to 3.5T. The magnetisation of ferrite is not zero above the Curie point and its magnetisation value increases with the magnetic field intensity as shown in Figure 3.7. Moreover, the paramagnetic susceptibility of ferrite is found to be much higher than the susceptibility of austenite as reported in [GAOB06]. The shift towards lower temperatures with increasing Ni content of the respective $\alpha \rightarrow \gamma$ and $\gamma \rightarrow \alpha$ transformations is evidenced. However, the magnetic properties of ferrite seem to be not really affected by Ni alloying. This behaviour is totally consistent with the small values of the a and b parameters reported in Table 1.1 and controlling the influence of the substitutional alloying element on the Curie temperature and on the magnetic moment of iron. Finally, the

experimental shift of the transformation temperature by the application of a magnetic field (up to 3.55T) can also be seen in Figure 3.7b.

Isothermal M(H) magnetic measurements close to the transformation temperature

During the isothermal holding, the magnetisation is measured as a function of applied magnetic field. Figure 3.8 shows the results obtained for different temperatures between 898 K and 1081 K for both Fe-2Ni wt% and Fe-4Ni wt% alloys. These measurements are of special interest to calculate the magnetic contribution to the free energy of ferrite. Indeed, in equation (17), the magnetisation is needed as a function of magnetic field.

On applying a magnetic field, the average direction of the magnetic moments is modified, and an induced magnetisation parallel to the field progressively appears. Below the Curie temperature, spontaneous magnetisation appears at very low field. At higher temperature, due to the larger thermal agitation, the magnetisation is lower and becomes progressively linear well above the Curie point.
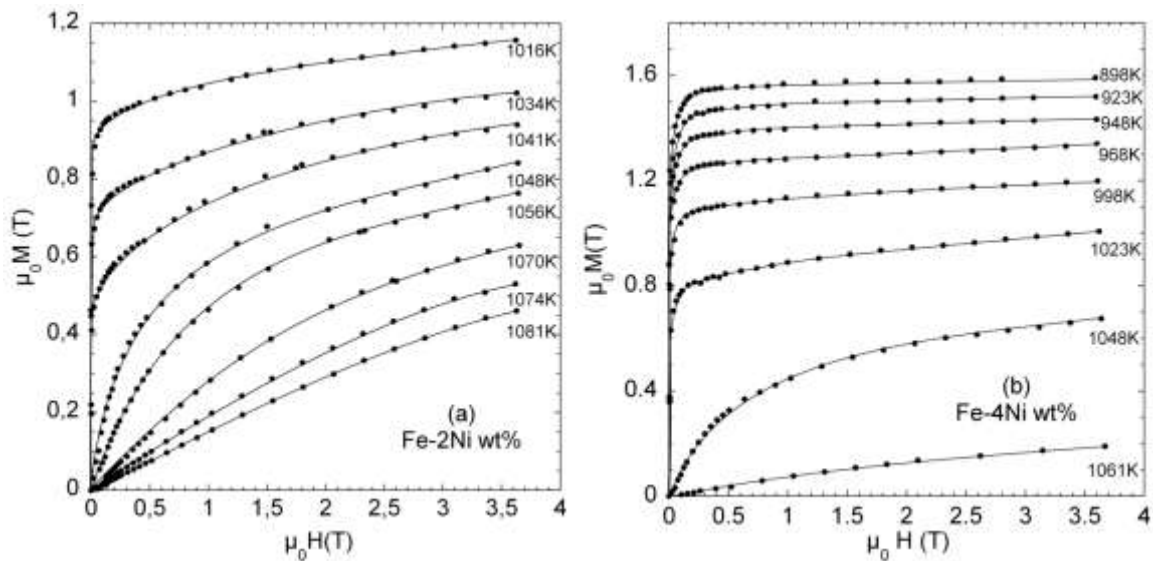
Figure 3.8   Magnetisation curves measured at isothermal temperature around the Curie point for Fe-2Ni and Fe-4Ni (wt%) as a function of magnetic field

Comparison with magnetisation data calculated from the MF Model

The above measured magnetisation values of the ferrite phase for each alloy composition are compared in Figure 3.9 with the magnetisation of the alpha-Fe phase

calculated from the Molecular Field Model. The measured values of magnetisation are plotted as a function of the predicted data calculated with the Molecular Field theory and the error is reported as a function of temperature. Similarly to pure Fe, a discrepancy between the measured and calculated values is observed and this discrepancy exactly fits this for pure iron. The MF model underestimates the experimental measurement, especially around the Curie point where an error close to 30%-is found.
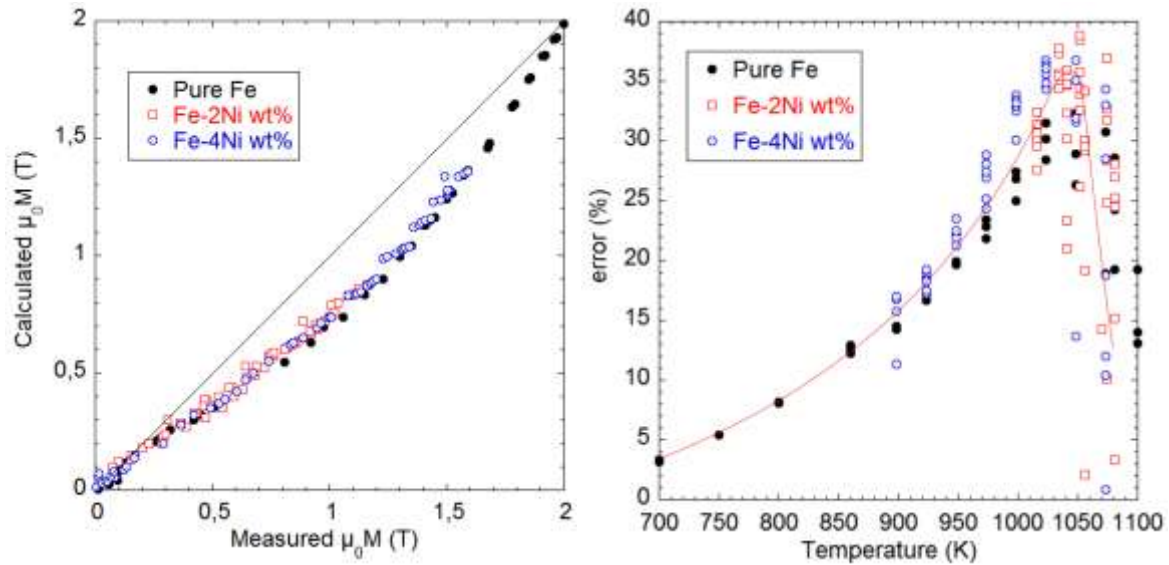
Figure 3.9 (a) Comparison between measured values of the magnetisation of iron around the *Tc* and calculated data given by the MF theory (b) Error in % as a function of temperature calculated with equ. (46)

3.2.3. Dilatometry investigation under magnetic field in Fe-Ni alloys

Similarly to the measurements achieved on pure iron, the dilatometry measurements enable us to measure in Fe-Ni alloys the respective transformation temperatures both on heating and cooling and to study the influence of the applied magnetic field on the phase transformation.

Dilatation curves and phase fraction

As an illustration to the various measurements completed in the dilatometer in magnetic fields of 16T, the change of the sample length (ΔL) relative to the initial length at room

temperature, L_0 obtained during the heat treatment of the Fe-2Ni wt% sample in 16T is shown in Figure 3.10.
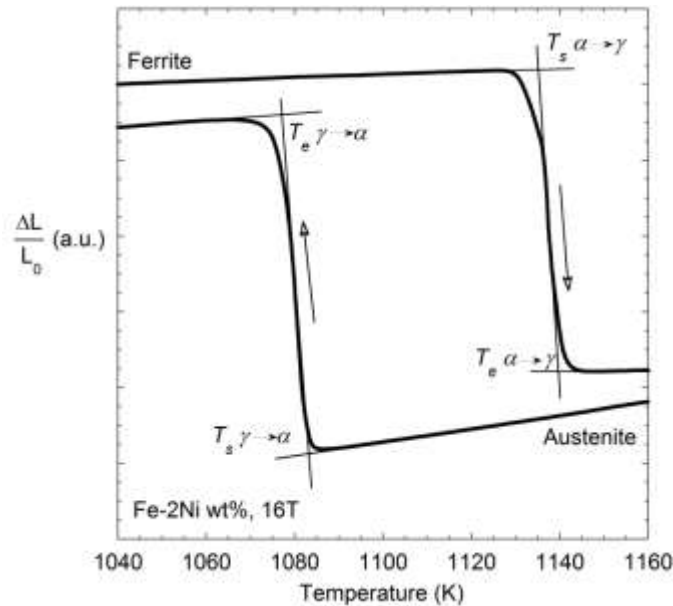
Figure 3.10   Dilatation measurement of Fe-2Ni wt% as a function of temperature in 16T
The transformation temperatures are defined as $T_{\alpha \to \gamma}$ on heating and $T_{\gamma \to \alpha}$ on cooling.

The $\alpha \to \gamma$ phase transformation appears as a sharp contraction of the sample whereas the $\gamma \to \alpha$ phase transformation exhibits a sharp expansion in the dilatometric signal. At each magnetic field strength, the onset of the transformation temperature (T_s) and the end of the transformation temperature (T_e) are evaluated by the tangents method as shown in Figure 3.10 and already described in paragraph 3.1.2. The $\gamma \to \alpha$ and $\alpha \to \gamma$ transformation temperatures are then calculated as the mean value between T_s and T_e and are referred as $T_{\alpha \to \gamma}$ on heating and $T_{\gamma \to \alpha}$ on cooling.

The volume fraction of ferrite is deduced from the dilatometry signal. A widely used method to analyze the phase fraction from dilatometric signal [GARC02] is the lever rules method. It consists in the evaluation of the BC/AC ratio as illustrated in Figure 3.11. The ferrite fraction as a function of temperature during continuous heating and cooling is shown in Figure 3.12 for 0, 5, 10 and 16 T. The shift toward higher temperature appears clearly for all alloys compositions.

It is very interesting to notice that the curves are parallel one to one another even if the transformation temperature is not the same. Because the heating and cooling rates are kept constant, we can deduce that the time needed to achieve the transformation (100 % ferrite) is

always the same for a given composition, whatever the magnetic field intensity is. This means that the rate of the transformation does not seem to be influenced by the magnetic field. The transformation rate obtained by the derivative of the phase fraction has been evaluated for all the dilatometric signals under various magnetic field intensities as illustrated on Figure 3.13 for the $\gamma \rightarrow \alpha$ transformation in pure iron.
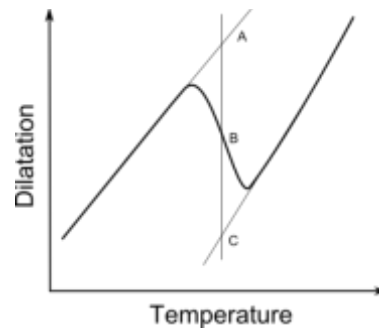
Figure 3.11   Lever rule method for the evaluation of phase fraction from dilatometric signal.

The mean transformation rate is progressively reduced by the Ni addition both for the $\gamma \rightarrow \alpha$ and $\alpha \rightarrow \gamma$ transformations. A maximum is found around 0.5 of the ferrite volume fraction which tends to be smoothed when the Ni content increases. The magnetic field does not change the way how the diffusional transformation proceeds.

No specific relationship can be found between the transformation rates and the magnetic field strength. As a consequence, a mean transformation rate is preferentially calculated by the average value of the rates measured during the $\gamma \rightarrow \alpha$ (respectively $\alpha \rightarrow \gamma$) transformation. After statistical analysis, standard deviation never exceeds 10 % of the mean values. Because the heating and cooling rates are constant, the mean transformation rate is a percentage of the product phase per second. This means that the various transformation rates measured under different magnetic field strengths between 0 and 16 T do not differ more than 10% from one to one anothers. The rate of the transformation is not strongly influenced by the magnetic field.

As introduced in the first chapter, the rate of transformation is associated to the interfaces velocity (eq. 12) and the latter is proportional to the total driving force for transformation ∆G. Consequently, if the rate of the transformation is not influenced by the magnetic field, we may deduce and further assume in the calculations that the driving force for the transformation during continuous heating or cooling is the same with and without magnetic field.
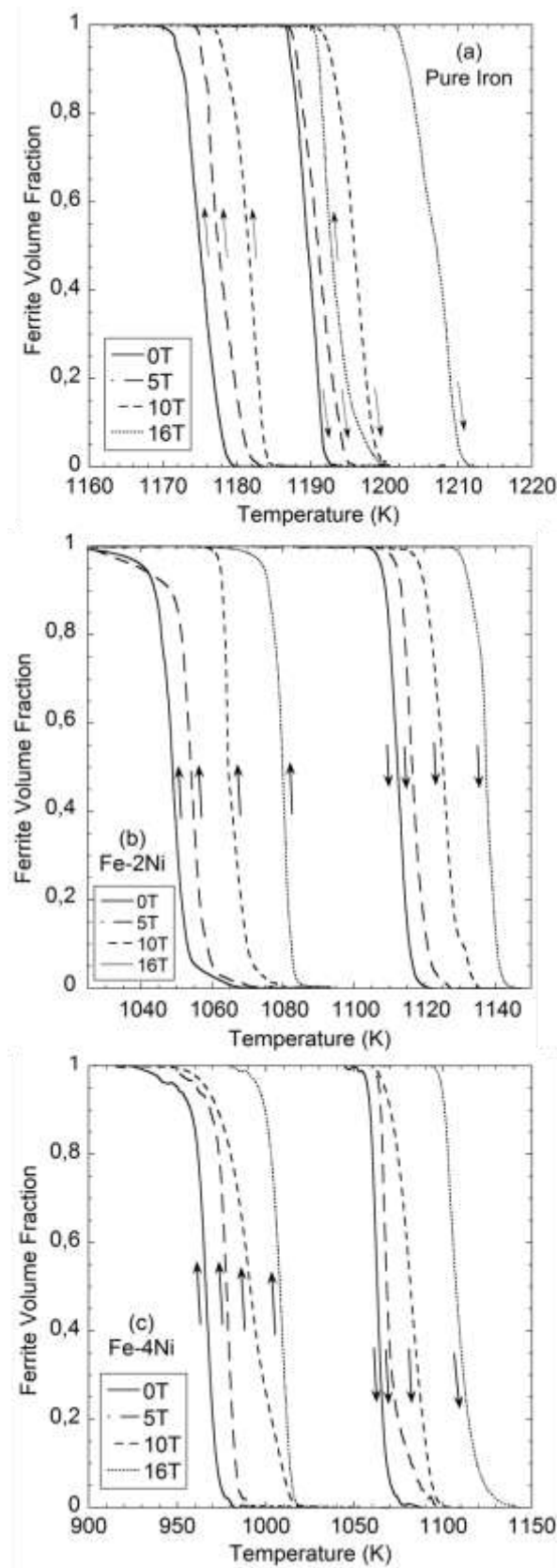
Figure 3.12   The fraction curves obtained from the lever rules method for the Fe-xNi alloys with x = 0, 2 and 4 wt% treated in 0, 5, 10 and 16T.
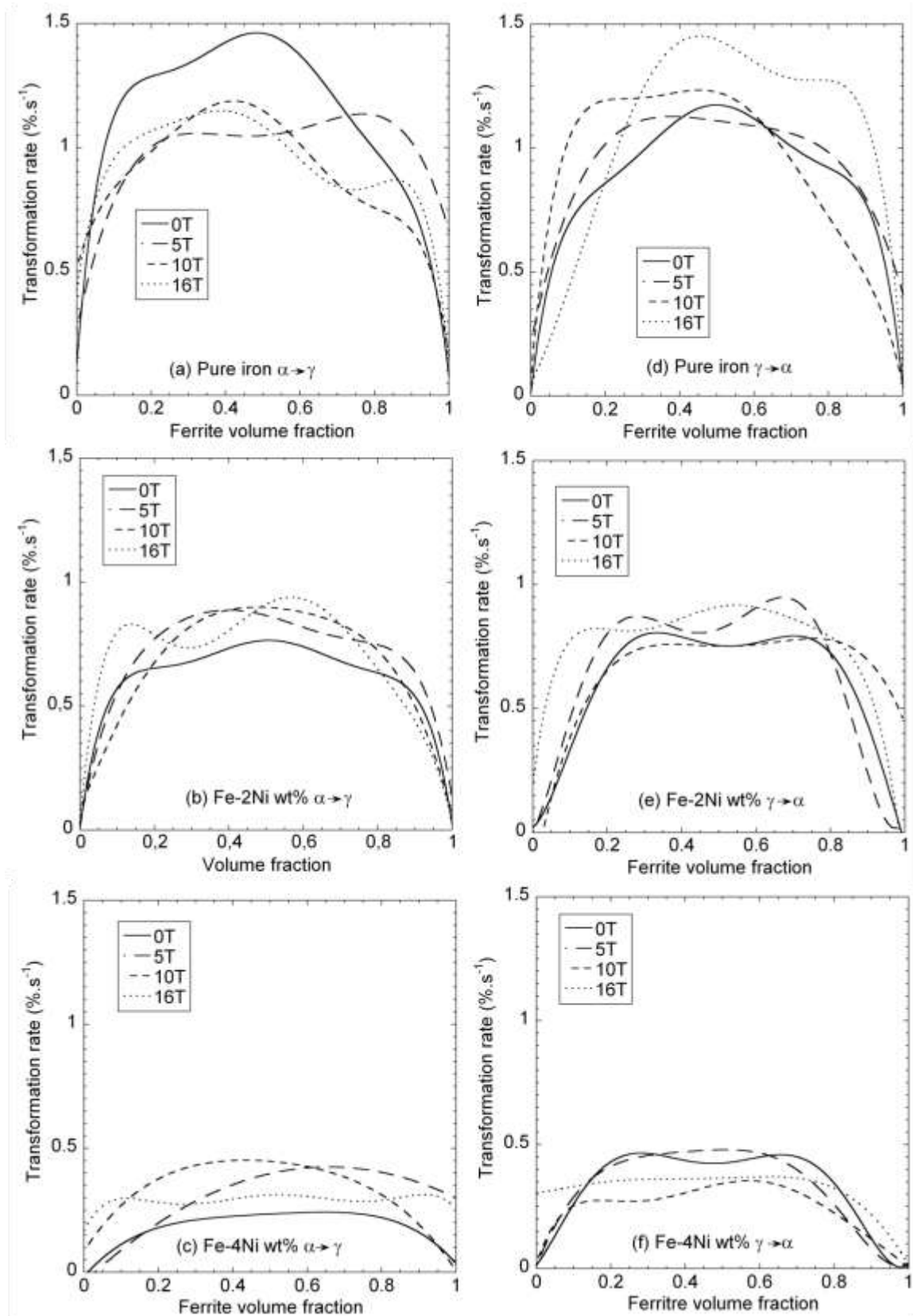
Figure 3.13   Transformation rates measured during $\alpha \rightarrow \gamma$ and $\gamma \rightarrow \alpha$ transformations for (a, d) pure iron, (b, e) Fe-2Ni and (c, f) Fe-4Ni (wt%). under 0, 5, 10 and 16T.

Shift of the transformation temperature in magnetic field

The magnetic field dependences of $T_{\alpha \to \gamma}$ and $T_{\gamma \to \alpha}$ for the three alloys are plotted with solid marks in Figure 3.14. The solid lines correspond to calculations based on the MF model. The dotted lines correspond to the shift predicted with *in-situ* magnetic measurements. These calculations will be discussed in details in part 3.2.4.
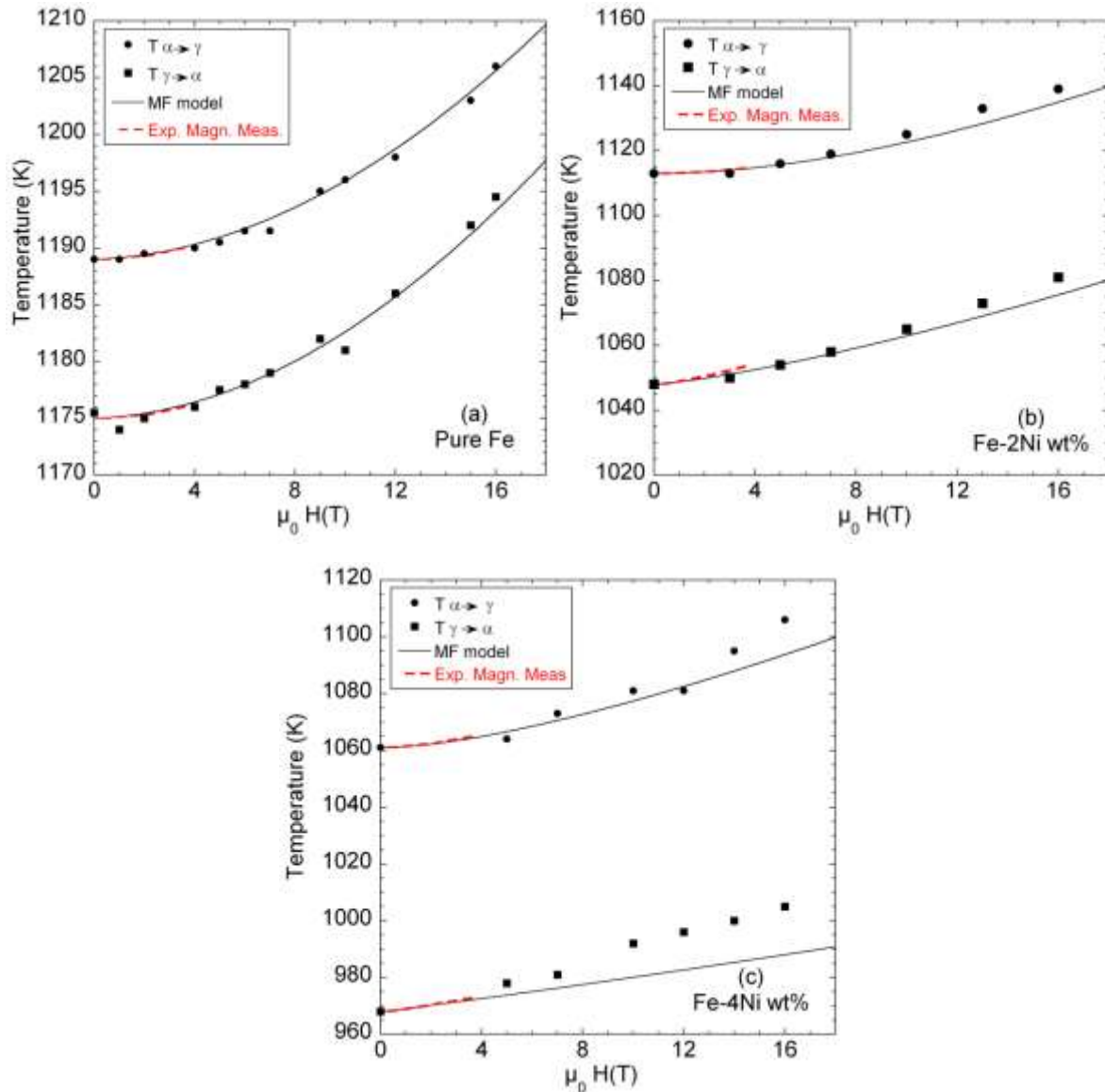
Figure 3.14   Change in the transformation temperature in (a) pure iron (b) Fe-2Ni wt% and (c) Fe-4Ni wt% in the presence of magnetic field.

Obviously, $T_{\alpha \to \gamma}$ and $T_{\gamma \to \alpha}$ increase with increasing the magnetic field intensity for the three alloys. The increase of $T_{\alpha \to \gamma}$ amounts to 17 K in pure Fe, 27 K in Fe-2Ni wt% alloy and

40 K in the Fe-4Ni wt% alloy in a magnetic field of 16 T. These increases seem to be proportional to the square of magnetic field for the three alloys compositions. The $T_{\gamma \to \alpha}$ is increased by 19 K in pure Fe, 33 K in the Fe-2Ni wt% alloy and 39 K in the Fe-4Ni wt% alloy in 16T. However the increase is proportional to B² for pure iron, whereas it tends towards a linear behaviour for the 2wt% and 4wt% Ni alloys.

3.2.4. Calculation method for non equilibrium temperature determination in magnetic field

The effect of magnetic field on the non-equilibrium $T_{\alpha \to \gamma}$ and $T_{\gamma \to \alpha}$ transformation temperature is calculated, applying a thermodynamics analysis and using high temperature, high field magnetic measurements.

Up to now and in order to evaluate the magnetostatic energy supplied by the magnetic field, the γ/α transformation temperature at equilibrium was mainly considered as Figure 3.3 for pure iron. In order to compare the calculated shift by the field of the equilibrium temperature with experimental transformation temperatures data, the average of the temperature for austenite to ferrite and its reverse transformation temperatures was usually taken as the equilibrium temperature [FUKU06]. However, this approximation leads to discrepancies between experimental results and calculated data.

In this work, an approach is proposed to discuss the magnetic field dependence of diffusional phase transformation temperatures taking into account the existence of temperature hysteresis due to the relatively large driving force required for the transformation. In this approach the shift of non-equilibrium transformation temperature in magnetic field is considered. This approach is similar to that taken by Kakeshita et al. for the prediction of the martensite start transformation temperature in magnetic field and is based on an analogy with the effect of uniaxial stress or hydrostatic pressure [PATE53, KAKE99]. Applied to diffusional transformation in iron based-alloy, this method has been validated for Fe-Rh alloys very recently in [KAKE09] and is applied both to Fe-Ni alloys and plain carbon steels (see part 3.3 and 3.4) in this work for the first time.

As it has been shown by experimental dilatometry measurements (Figure 3.14), $T_{\alpha \to \gamma}$ and $T_{\gamma \to \alpha}$ are non-equilibrium transformation temperatures which involve a necessary driving force for the diffusional transformation. This driving force is given by the difference in the

total Gibbs free energy ΔG_{tot}^B of the two phases α and γ at the transformation point and is composed of the chemical contribution, ΔG_{chem} and of the magnetic contribution ΔG_{mag} by:

$$\Delta G_{tot}^B = \Delta G_{chem} + \Delta G_{mag} \tag{48}$$

$$\Delta G_{tot}^B = \Delta H_{i \to j} - T_{i \to j}^B \Delta S_{i \to j} - \frac{M^{mol}}{\rho \mu_0} \int_0^B (M^\alpha - M^\gamma) dB \tag{49}$$

where M^{mol}, ρ and μ_0 are respectively the atomic weight, the density and the magnetic permeability of vacuum. $\Delta H_{i \to j}$ and $\Delta S_{i \to j}$ are respectively the latent heat of transformation and the entropy change from the phase i to j. $T_{i \to j}^B$ with i and j being α and γ, corresponds to the temperature at which the $\alpha \to \gamma$ (respectively $\gamma \to \alpha$) transformation starts under a magnetic field B. M^α and M^γ are the magnetisation of ferrite and austenite respectively at $T_{i \to j}^B$.

At equilibrium and without the application of a magnetic field, the total Gibbs free energy $\Delta G_{tot}^{B=0}$ is zero, so that the entropy change can be expressed by:

$$\Delta S_{i \to j}^{equ} = \frac{\Delta H_{i \to j}^{equ}}{T_{i \to j}^{equ}} \tag{50}$$

where $T_{i \to j}^{equ}$ is the equilibrium temperature between phases i and j. Out of equilibrium but for low overheating and overcooling, the free energy difference between the two phases is assumed to be linearly proportional to the difference between the transformation temperature $T_{i \to j}^{B=0T}$ and the equilibrium temperature $T_{i \to j}^{equ}$ [JACK04] and can be written as:

$$\Delta G_{tot}^{B=0T} = \Delta H_{i \to j}^{equ} \left(\frac{T_{i \to j}^{equ} - T_{i \to j}^{B=0T}}{T_{i \to j}^{equ}} \right) \tag{51}$$

The similar expression for the free energy difference between the two phases under the application of a magnetic field is obtained in adding the magnetic contribution as shown with the right hand term of equ.(49).

As an similar manner as the effect of hydrostatic pressure or uniaxial stress applied to phase transformation, the total driving force for the transformation, ΔG_{tot}^B is assumed to be

unchanged by the application of a magnetic field in the same cooling conditions. However, the relative contributions of the chemical term and the magnetic term to this energy vary as illustrated in Figure 3.15 so that:

$$\Delta G_{tot}^{B=0T} = \Delta G_{tot}^{B \neq 0T} \tag{52}$$
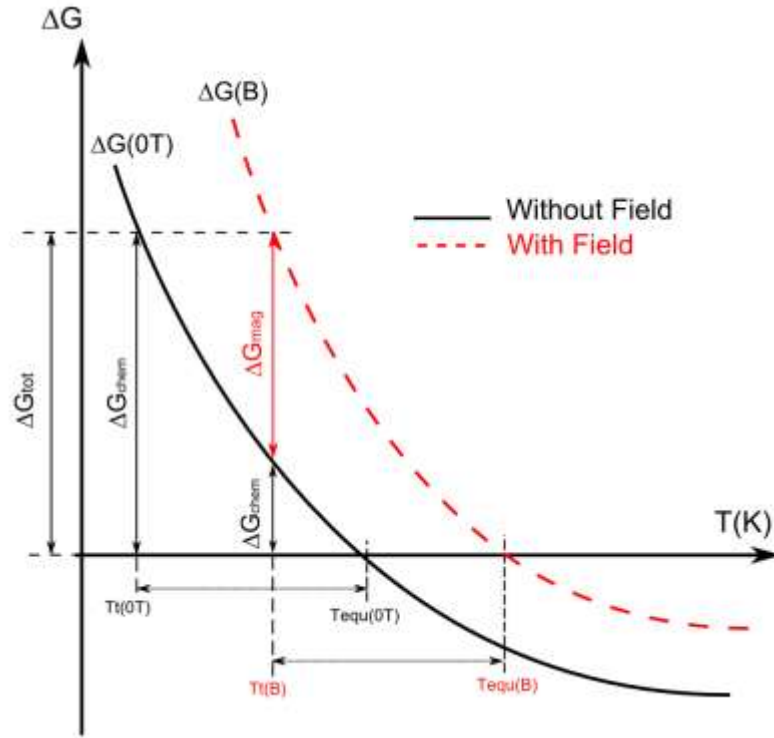
Figure 3.15   Schematic free energy-temperature diagram representing the effect of magnetic field on the relative contribution of the chemical and the magnetic free energy in the case of the $\gamma \rightarrow \alpha$ transformation on cooling. Same total driving force for transformation and same undercooling are assumed with and without the application of external magnetic field.

If the change in transformation temperature induced by magnetic field is not too large, the latent heat for transformation $\Delta H_{i \rightarrow j}^{equ}$ and the entropy change $\Delta S_{i \rightarrow j}^{equ}$ are assumed to be uninfluenced by the application of magnetic field. From equ. (52), the change in the transformation temperature $T_{i \rightarrow j}^{B \neq 0T}$ can be calculated as a function of magnetic field as:

$$T_{i \rightarrow j}^{B \neq 0T} = T_{i \rightarrow j}^{B=0T} + \frac{T_{i \rightarrow j}^{equ}}{\Delta H_{i \rightarrow j}^{equ}} \frac{M^{mol}}{\rho \mu_0} \int_0^B (M^\alpha - M^\gamma) dB \tag{53}$$

The values for $\Delta H_{i \to j}^{equ}$ are obtained at the respective equilibrium temperature $T_{i \to j}^{equ}$ from thermodynamics databases contained in the database of Thermocalc® and are reported in Table 3.3. It is interesting to notice the small difference between the non-equilibrium temperatures $T_{i \to j}^{B=0T}$ measured by dilatometry and reported in Table 3.2 and the respective equilibrium temperature $T_{i \to j}^{equ}$ reported in Table 3.3.

Fe-Ni (x wt%)	0	2	4
$T_{\alpha \to \gamma}^{equ}$ (K)	1183	1107	1056
$\Delta H_{\alpha \to \gamma}^{equ}$ (J.mol^{-1})	1026	1605	1646
$T_{\gamma \to \alpha}^{equ}$ (K)	1183	1040	902
$\Delta H_{\gamma \to \alpha}^{equ}$ (J.mol^{-1})	1026	2364	4637

Table 3.3: Equilibrium temperature $T_{\alpha \to \gamma}^{equ}$ and $T_{\gamma \to \alpha}^{equ}$ for the $\alpha \to \gamma$ and $\gamma \to \alpha$ transformation and respective enthalpy change $\Delta H_{\alpha \to \gamma}^{equ}$ and $\Delta H_{\gamma \to \alpha}^{equ}$ obtained in Thermocalc® for pure iron, Fe-2Ni wt% and Fe-4Ni wt%.

The magnetisation of ferrite is evaluated by two different ways. On the one hand, Molecular Field model is used to evaluate the variation of M^α with composition and magnetic field in the determination of ΔG_{mag} at the temperature $T_{i \to j}^{B=0T}$. On the other hand, experimental magnetisation data for M^α are used in the calculation of ΔG_{mag}. The magnetisation of austenite is taken from the data of Arajs et al. [ARAJ60].

The corresponding results of the magnetic field dependence of $T_{\alpha \to \gamma}^{B \neq 0T}$ and $T_{\gamma \to \alpha}^{B \neq 0T}$ are shown in Figure 3.14. The black lines correspond to the calculation with the Molecular field model and the red lines are calculated using experimental magnetic measurements.

The calculated data are in relatively good agreement with the experimental temperatures measured by dilatometry. Underestimation is observed when the transformation occurs around and below the Curie point which is in good agreement with the experimental check of the non validity of the MF model shown in Figure 3.9b around the Curie point. In addition, the use of experimentally measured M^α to calculate the magnetic contribution to the total free energy of the transformation constitutes a very accurate approach, as well, however, limited in our device to 3.55T.

3.2.5. Conclusion

In pure iron, Fe-2Ni and Fe-4Ni wt% alloys, magnetisation and dilatometry measurements were used to explore the effect of magnetic field on the austenite/ferrite transformation temperatures during continuous heating and cooling up to 16T.

The transformation temperature is shifted towards higher temperatures under magnetic field. Against magnetic field intensity, this change shifts from a linear to a quadratic behaviour depending on the position of the transformation temperature relatively to the Curie temperature.

Experimental determination of the magnetisation of ferrite at high temperature in various field values up to 3.5 T is achieved and has allowed a direct comparison between the MF predictions and the experimental data. The MF model is found to underestimate the magnetisation of ferrite especially around the Curie temperature.

The shift towards higher temperatures of the respective $\alpha \rightarrow \gamma$ and $\gamma \rightarrow \alpha$ transformations temperature is experimentally and theoretically calculated by thermodynamics analysis. The model is based on an analogy with the effect of uniaxial stress on phase transformation and is found to describe correctly the experimental measurement.

3.3. Experimental evidence of the high magnetic field effect on the austenite to ferrite transformation in Fe-xC-Mn Alloys.

Proeutectoid ferrite and pearlite are the main constituents of the microstructure of plain carbon steels when subjected to relatively slow cooling rates from the austenite region. It is thus of great interest to study the effect of strong magnetic field in the transformation behaviours and structures in order to evidence interesting features of magnetic field in metallurgical process. During the austenite decomposition in steels and related Fe based materials, the magnetisation of ferrite is higher than that of austenite, therefore the transformation is promoted and the ferrite phase is stabilized by the presence of a magnetic field.

In this approach, and similarly to the previous study on Fe-Ni alloys, the magnetic field dependence of the respective γ/α onset and end transformation temperatures is investigated (instead of equilibrium temperature) for Fe- xC-1.5wt%Mn plain steels with x = 0.1, 0.2 and

0.3 wt%C by means of dilatometry measurements. Experimental magnetic measurements are used to obtain magnetisation data at high temperatures and high fields. Finally, the experimental dilatometry results are compared to the calculated data. In the case of proeutectoid steels and contrary to the previous part (3.2), the alloys are composed of a mixture of ferrite and pearlite. Thus, the microstructures are investigated toward the determination of phase fractions and the Vickers hardness values are measured. The results are discussed as a function of both applied magnetic field and C content.

3.3.1. Alloys compositions and experiments

Materials preparation

The Fe-1.5 wt%Mn-xC plain steels with x = 0.1, 0.2 and 0.3 wt%C were cast using CRM laboratory [CRMLab] casting facility. The materials used in this study are three alloys referred as 0.1C, 0.2C and 0.3C. They were prepared by hot rolling in 5 passes down to a thickness of 5.9 mm and then homogenized for 48 h at 1573 K followed by a natural cooling before the experiments. From each hot rolled sheet, cylindrical specimens of 4 mm in diameter and 10 mm in height were cut out with their revolution axes parallel to the rolling direction. They were then annealed to further homogenize the composition and microstructure. Initial microstructures and corresponding phase fractions and Vickers hardness values are shown on Figure 3.16. The three alloys studied here are composed of a mixture of ferrite with equiaxed grains and pearlite. The amount of ferrite is higher in the lower carbon content (0.1C) and decreases when the carbon content increases. The corresponding macro-hardness value increases with carbon content.

Experimental procedure

The dilatometry measurements were achieved during a complete annealing treatment of the specimens under various magnetic field strengths up to 16 T. That is, in the dilatometer device, the specimens were treated up to 1173 K for 5 min with heating rate of 10 K/s and cooling rate of 0.5 K/s with the magnetic field applied along the rolling direction.

Microstructural observations were performed by optical microscopy after polishing and etching with Nital 2% and the ferrite volume fraction was measured by image analysis.

Specimen magnetisations were measured as a function of both temperature (up to 1200K) and magnetic field intensity (up to 3.5T) in the high sensitivity magnetometer described in the second chapter and in [GAUC01].
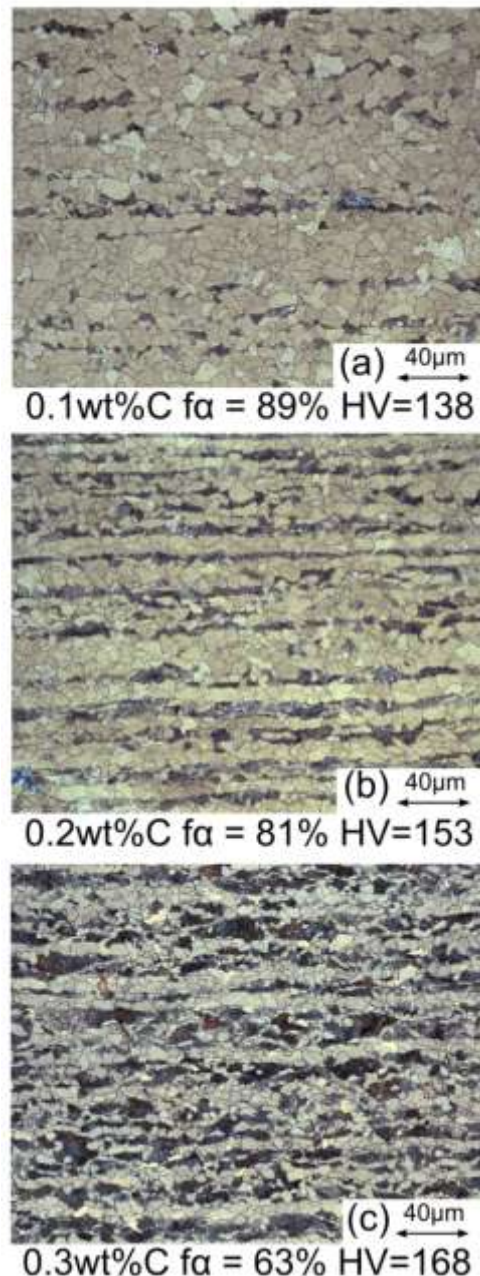
Figure 3.16   Optical micrographs of hot rolled specimen used in the following study for (a) 0.1 wt%C, (b) 0.2 wt%C and (c) 0.3wt%C alloy. Microstructure is composed of equiaxed ferrite grains (grey) and pearlite colonies (black), Original magnification 200x 2% nital etch

3.3.2. Dilatometry analysis

Dilatometry curves and transformation temperatures

Figure 3.17 shows the change of the sample length (ΔL) relative to the initial length at room temperature, L_0, during cooling under various magnetic field intensities for the 0.3C steel.
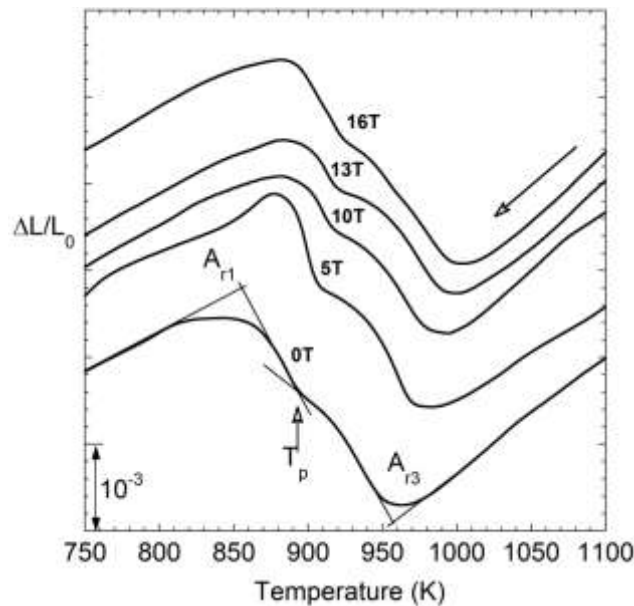
Figure 3.17   Dilatometry cooling curves of the 0.3C steel obtained in 0, 5, 10, 13 and 16T.

Starting from 1200K, the first decrease in the dilatometry signal is related to the austenite contraction on cooling. Then, the austenite decomposition during continuous slow cooling is associated to a significant expansion on the dilatometry curve occurring in two steps. During the first step, proeutectoid ferrite is formed. During the second step, when the concentration of C in the austenite reaches the eutectoid composition (≈ 0.8wt%C), the remaining austenite transforms into pearlite. This two-steps expansion behaviour has been mainly attributed to the difference in the ferrite and pearlite atomic volumes [KOPS01, GARC02]. Similarly, the austenite formation on heating (not shown here) shows a two-step contraction.

In Figure 3.17, the A_{r3} and A_{r1} temperatures correspond respectively, to the start and finish transformation temperatures of the non-isothermal decomposition of austenite into ferrite + pearlite. They are evaluated by the tangents method, as shown in Figure 3.12. In

addition, and according to [GARC02], we choose to record point T_P as the start of the pearlite precipitation.

The variations of A_{r3}, A_{r1} and T_P as a function of magnetic field are shown in Figure 3.18 for the three steel grades.
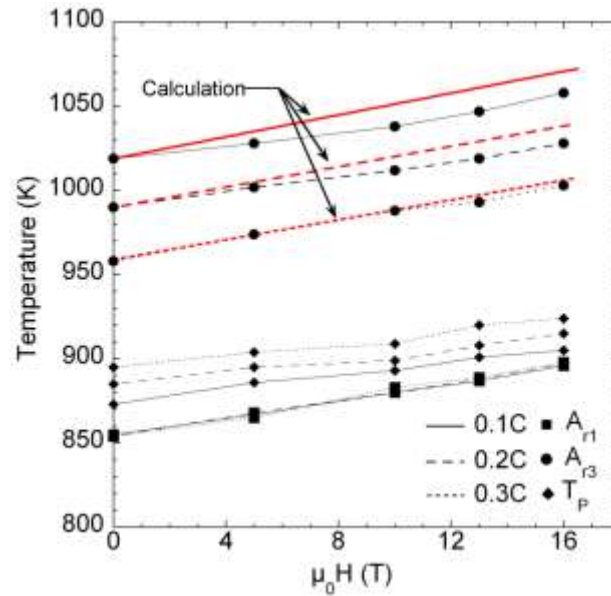
Figure 3.18 A_{r3} (circles), A_{r1} (squares) and T_P (rhombus) temperatures as a function of magnetic field intensity measured on cooling for the Fe-1.5wt%Mn-xC plain steels with x = 0.1, 0.2 and 0.3wt%C.

As expected from the Fe-C phase diagram, the A_{r3} temperature is progressively lowered by the addition of carbon and the A_{r1} temperature is independent of the carbon content. The transition temperature T_P is found to increase with the addition of carbon which may indicate that the volume fraction of pro-eutectoid ferrite is simultaneously reduced.

The application of a magnetic field during cooling leads to a linear shift towards higher temperatures of the whole pro-eutectoid region of the phase diagram as A_{r3}, A_{r1} and T_P are increased. The experimental data are first linearly fitted (the linear regression is not shown on the Figure). The shift of the A_{r3} temperature amounts to 2.2, 2.4 and 2.7 K/T respectively for the 0.1, 0.2 and 0.3 wt%C steel grades. A_{r1} temperature is increased by 2.5 K/T and T_P is increased by 1.8 K/T whatever the carbon content. The error bars estimated for each measurement never exceed 0.1 K/T. Thus, the effect of magnetic field on the experimental A_{r3} temperature is found to be greater for higher carbon content.

Ferrite volume fraction

The most widely used method to analyze dilatometry data is the lever-rule method. The fraction transformed determined by this method is the sum of the ferrite and pearlite fractions. It is assumed in this method that the effect of carbon enrichment on the cell parameter of the austenite phase and the difference between the density of ferrite and pearlite are neglected [AGRE82]. Under these assumptions, the fractions of ferrite and pearlite derived from dilatometry curves are shown in Figure 3.19 for the three steel grades as a function of temperature.

The two-step ferrite formation behaviour shows up again. The respective transition (from ferrite to pearlite) point T_P is marked with a cross in the corresponding curves. It appears on this graph that the volume fraction of ferrite is increased by the application of magnetic field and that this increase is enhanced by the increase in the carbon in the alloy.

Besides, the mean transformation rate and its corresponding standard deviation are systematically evaluated and shown on Figure 3.20. As it was already found in Fe-Ni alloys, no variation of the transformation rate is observed against magnetic field strength. The standard deviation is lower than about 10% of the mean value for the three alloys that may indicate that, the total driving force can be assumed to be unchanged by the application of magnetic field. Similarly to the Ni addition, the transformation rate is decreased by the addition of carbon which may indicate that the kinetics of the interface is controlled by carbon redistribution.
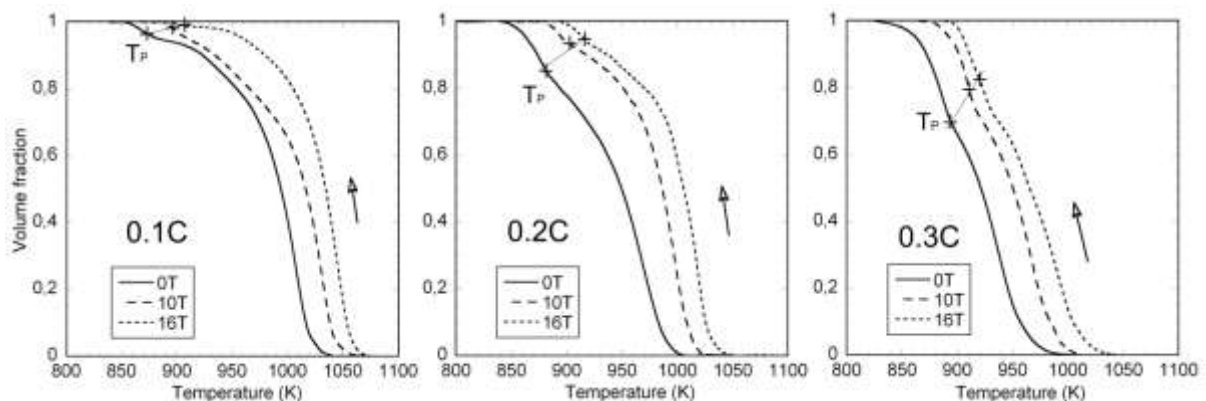
Figure 3.19   The fraction curves obtained from the lever rules method for the Fe-xC-1.5wt%Mn alloys treated in 0, 10 and 16T. The crosses indicate the transition temperature T_P from ferrite to pearlite transformation.
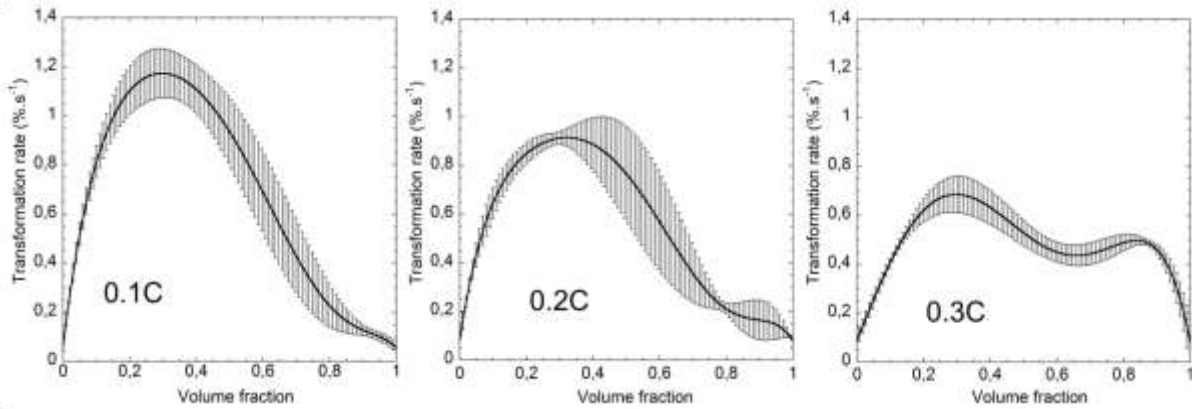
Figure 3.20   Mean transformation rate measured during the austenite decomposition the Fe-1.5Mn-xC (wt%) where x=0.1, 0.1 and 0.3 wt%. Error bar correspond to the standard deviation obtained for 0, 10 and 16T.

3.3.3. Effect of magnetic field on transformed microstructures

After each dilatomety measurement, the corresponding microstructures of the three alloys submitted to different magnetic field intensities have been observed both by optical and SE Microscopy. The pictures are shown below and the results are discussed as a function of both magnetic field intensity and carbon content.

Increase in ferrite fraction under magnetic field

Figure 3.21 shows optical micrographs to illustrate the effect of magnetic field on microstructures obtained by non-isothermal decomposition of austenite in the three Fe-1.5wt%Mn-xC plain steels with x= 0.1, 0.2 and 0.3wt%C.

The direction of applied magnetic field is horizontal in the figure and corresponds to the hot rolling direction. As predicted by the phase diagram, for low cooling rates, a mixed microstructure of ferrite (light grey) and pearlite (dark grey) is observed.

The corresponding area fractions of ferrite are determined by statistical image analyses of five optical micrographs for each specimen and are shown in Figure 3.22a. The fraction of ferrite is systematically increased by the application of magnetic field. Moreover, it is found that the impact of the magnetic field is more important when the steel carbon content increases, i.e. when the ferrite volume fraction is lower. This increase in the ferrite volume fraction is associated to a corresponding proportional reduction of the steel Vickers hardness values as shown in Figure 3.22b.
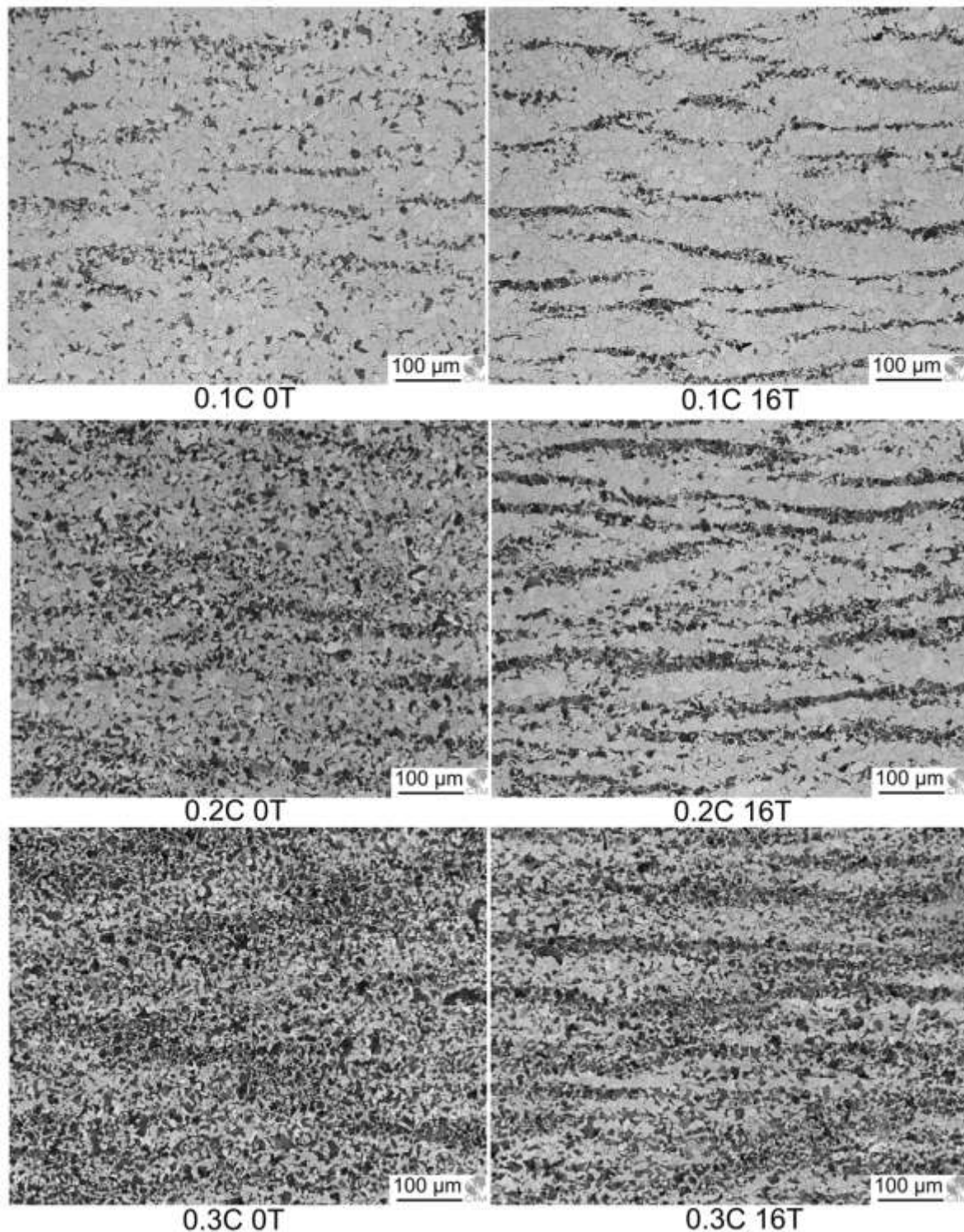
Figure 3.21   Optical micrographs showing the ferrite + pearlite structure obtained after continuous cooling at a rate of 0.5 K/s for the Fe-xC-1.5wt%Mn steels with x= 0.1, 0.2 and 0.3wt%C respectively treated in 0T (a,b and c) and 16T (d, e and f). Original magnification 200x, 4% nital etch
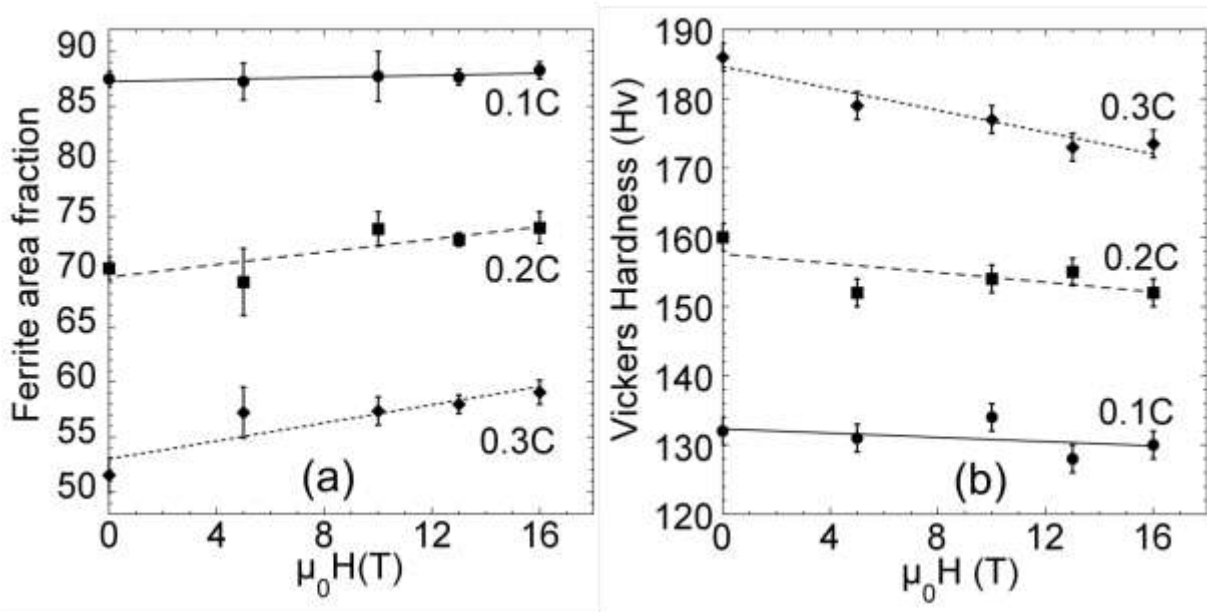
Figure 3.22   a) Area fraction of ferrite. b) Vickers hardness as a function of magnetic field intensity for the Fe-C-1.5wt%Mn steels with x= 0.1, 0.2 and 0.3wt%C.

Aligned structures in magnetic field

Figure 3.21 also shows a strong alignment of pearlite colonies in the direction of the magnetic field. From the analysis of the samples treated in intermediate magnetic field intensities (not shown here), this tendency is found to increase with the magnetic field strength. This alignment (also referred as "banded" microstructure) already exists in specimens before thermal treatment under the form of alternating ferrite and pearlite bands aligned parallel to the hot rolling direction (Figure 3.16). This microstructure is well known in hot rolled Mn-steels [BHAD83] and is related to the solidification process of the steel in which the alloying element (Mn in this study) lowers the melting point of iron. In this case, Mn micro-segregations can be found at the dendrite scale during solidification. On further hot rolling, plastic deformation leads to the alternation of high Mn and low Mn-content regions, resulting, in turn, in preferential growth of primary ferrite in the Mn-depleted regions and pearlite in the Mn-rich areas (Mn stabilizes austenite).

The application of a magnetic field during subsequent cooling promotes this alignment, as it has also been reported by other groups [CHOI00, SHMA03, ZHAN05]. According to these studies, the aligned structure of pearlite colonies is thought to be mostly formed during

ferrite grain growth and maybe explained by a balance of the dipolar energies and the interfacial energies.

Pearlite microstructure

Scanning Electronic Microscopy (SEM) has also been used to check for other modifications in the sub-structure of pearlite colonies resulting from the application of a magnetic field. The 0.3C alloy composition is chosen for this analysis since this composition is the most impacted by the magnetic field in terms of transformation temperatures and phase fraction. Representative SEM images of two samples treated under 0 and 16T are shown in Figure 3.23.

The microstructure of pearlite is very similar in both cases. Apart from the alignment of colonies described above, no specific orientation of the pearlite lamellae is observed at the SEM scale. The interlamellae distance in each pearlite colony is measured with ImageJ freeware. Change in the contrast between cementite (white appearing constituent) and ferrite (dark appearing constituent) is used for the determination of the interlamellae spacing of about 30 grains of pearlite in each specimen. A total of about 1100 lamellae is measured for each sample and the mean spacing is determined as being (0.29±0.11) μm and (0.27±0.09) μm respectively for the sample treated in zero field and under 16T. Therefore, no impact of the magnetic field on the pearlite microstructure arises from this analysis.
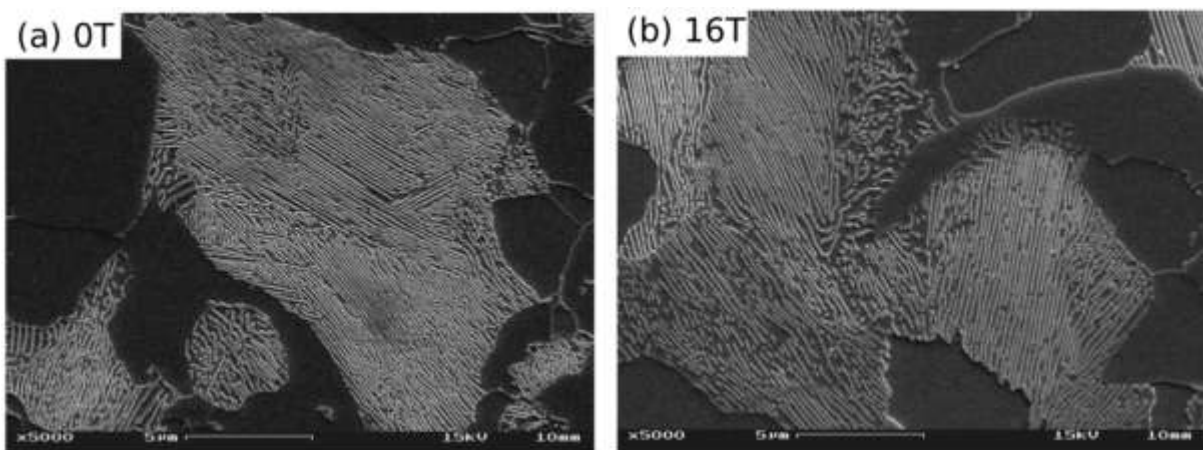
Figure 3.23   SEM images of pearlite colonies in the Fe-1.5Mn-0.3C (wt%) treated under (a) zero field and (b) 16T.

3.3.4. Thermodynamics analysis based on magnetic measurement

In this section, the effect of magnetic field on the A_{r3} austenite-ferrite transformation temperature is calculated, applying a thermodynamics analysis and using high temperature, high field magnetic measurements.

The starting temperature of the pro-eutectoid ferrite formation process (A_{r3}) is a non-equilibrium transformation. The calculation method for the estimation of the shift of the transformation temperatures in magnetic field is described in paragraph 3.2.4 of this present chapter for Fe-xNi alloys and is now tested for these alloy compositions.

Usually, the Molecular Field model [CULL72] provides a theoretical method to estimate the high-field ferrite magnetisation, M^{α}. It has been shown in the previous study related to pure iron and Fe-Ni alloys, that the MF model underestimates the magnetisation of ferrite especially around and below the Curie point. It is then proposed to use experimental magnetisation data in order to estimate the magnetic free energy term of ferrite. For this purpose, magnetic properties of alloys as a function of temperature and magnetic field are accurately investigated.

<u>**Effect of C and Mn addition on the magnetic properties of steels**</u>

The saturation magnetisations of the three steels are measured as a function of temperature (up to 1200K) in 3.5T. In order to evidence the effect of C and Mn addition on the magnetic properties of steels, these measurements are compared with that of high purity iron and with the saturation magnetisation given by the Molecular Field theory with J=0.5, T_C =1043 K and M_{Fe}^0=1.73 10^6 A.m^{-1} (Figure 3.24). The magnetic signal measured in the three steels corresponds to the addition of the respective magnetic contributions of ferrite and cementite. Due to the fact that the amount of cementite is very low (cementite is only present in pearlite) in the three steels and that cementite is paramagnetic above 483K [CHAI09], its magnetic contribution is negligibly small compared to that of ferrite in the temperature range of the transformation. This could explain why the magnetisation curves of the Fe-C-Mn steels appear almost independent of the carbon content. Therefore, it is considered that these measurements are a good approximation of M^{α}.
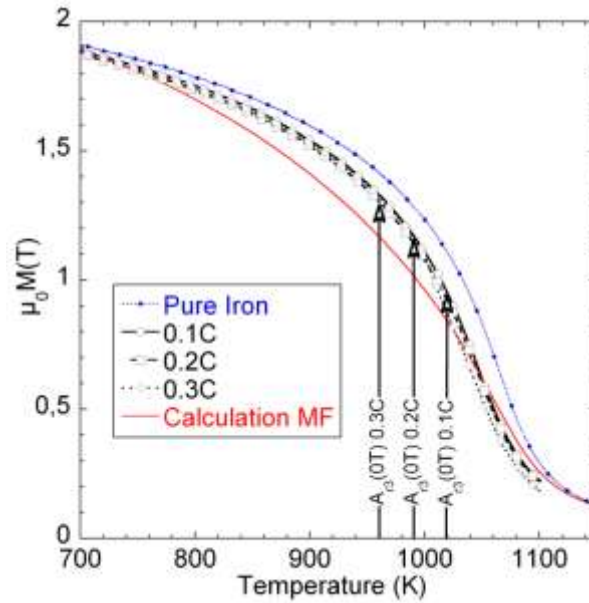
Figure 3.24   Saturation magnetisation as a function of temperature in 3.5T of high purity Iron and Fe-C-1.5wt%Mn steels with x= 0.1, 0.2 and 0.3wt%C. The solid red line corresponds to the values predicted by the Molecular Field Model

The magnetic signals corresponding to the Fe-C-1.5wt%Mn steels with x = 0.1, 0.2 and 0.3wt%C are lower than the measured magnetisation of iron. This result is in good agreement with [GUOE00, ISHI75], where the addition of 1.5wt%Mn to iron is found to reduce its saturation magnetisation to 2.18 μ_B per atom and the Curie point to 1020 K instead of 2.22 μ_B and 1043 K respectively for pure iron. Moreover, A_{r3} temperatures of each steel grade measured under zero magnetic fields are found to be lower than the Curie point as shown on Figure 3.24. Accordingly, a linear shift of the transformation temperature by the field is expected and measured by dilatometry measurements (Figure 3.18).

Isothermal magnetisation data and magnetic free energy contribution

Because the Molecular Field theory is not suitable to describe the magnetisation of ferrite close to the transformation temperatures, as seen in Figure 3.24, it was decided to use experimental magnetisation data for M^α instead for the calculation of ΔG_{mag}. For that purpose, magnetisation measurements as a function of magnetic field strength have been realized for the three steel grades at their respective A_{r3} temperatures, namely 958 K, 990 K and 1019 K. The results are shown in Figure 3.25.
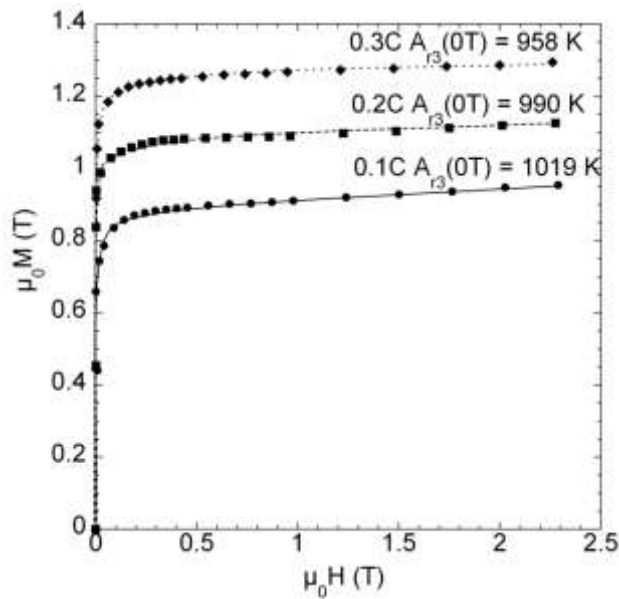
Figure 3.25   Magnetisation curves of the Fe-C-1.5wt%Mn steels with x= 0.1, 0.2 and 0.3wt%C measured at their respective A_{r3} temperature.

The resulting M^{α} was obtained up to 2.3 T. For higher field intensities, we extrapolated the linear relation of $M^2 \; vs \; H/M$ (Arott plot [BOZO78]) obtained for H < 2.3T to higher fields and deduced M^{α} up to 16 T. The magnetic contribution to the total free energy is determined from the measurement using equ.(17) and is 5.13 J/mol/T for the Fe-0.1C-1.5wt%Mn, 6.16 J/mol/T for Fe-0.2C-1.5wt%Mn and 7.13 J/mol/T for the Fe-0.3C-1.5wt%Mn indicating that on continuous cooling from the austenite phase, the impact of magnetic field is stronger when the carbon content is increased.

Evaluation of the magnetic field dependence of the A_{r3} temperature

According to equ.(50), the entropy change is determined by the ratio of the Latent heat for transformation to the equilibrium temperature. The equilibrium temperature A_{e3} obtained in Thermocalc is 1093 K, 1070 K and 1050 K respectively for the 0.1, 0.2 and 0.3 wt%C alloy. The corresponding $\Delta H_{\gamma \rightarrow \alpha}^{equ}$ are 1730 J.mol^{-1}, 2180 J.mol^{-1} and 2540 J.mol^{-1} respectively for the 0.1, 0.2 and 0.3 wt% C alloy. Applying equ.(53), the magnetic field dependence of the A_{r3} temperatures is calculated and shown in Figure 3.18 with red lines. The calculated data are in relatively good agreement with the experimental A_{r3} temperatures measured by dilatometry [GARC09c]. However, the proposed model seems to slightly overestimate the

measured data. This discrepancy is expected to be mainly due to an improper determination of the entropy change at the transformation temperature.

3.3.5. <u>Conclusion</u>

In Fe-xC-1.5wt%Mn steels with x= 0.1, 0.2 and 0.3wt%C dilatometry measurements is used to explore the effect of magnetic field on the austenite/ferrite + pearlite transformation temperatures during continuous cooling up to 16T. The shift towards higher temperatures of the respective austenite, ferrite + austenite and ferrite + pearlite stability regions is experimentally confirmed. The experimental A_{r3} temperature increases linearly by 2.2, 2.4 and 2.7 K/T respectively for the 0.1, 0.2 and 0.3wt%C steels. The A_{r1} temperature increases by 2.5 K/T. and the T_P temperature corresponding to the start of the pearlite precipitation shifts by 1.8 K/T toward higher temperatures.

Because the Molecular Field theory is found to be not accurate enough to describe the magnetisation of ferrite close to the transformation temperatures, experimental magnetisation data are used to calculate the magnetic contribution to the Free energy of the transformation. This magnetic contribution to the total free energy is found to be 5.13 J/mol/T for the Fe-0.1C-1.5wt%Mn, 6.16 J/mol/T for Fe-0.2C-1.5wt%Mn and 7.13 J/mol/T for the Fe-0.3C-1.5wt%Mn. These data are used for a correct determination of the magnetic field dependence of the A_{r3} temperatures using a simple thermodynamic analysis.

Microstructure analyses show a systematic increase in the ferrite volume fraction with the increase of the applied magnetic field, which is associated to a proportional reduction of the Vickers hardness values. Besides, the alignment of pearlite colonies is observed along the rolling direction and seems to be promoted by the application of a magnetic field but no specific change is found in the sub-structure of pearlite.

Values of magnetic contributions for the three steels indicate that the impact of magnetic field is stronger when the steel carbon content is increased. This is consistent with the observed field effect on the transformation temperature measured experimentally by dilatometry and with the increase of the ferrite volume fraction with carbon content.

3.4. Influence of Silicon content in the austenite decomposition in high magnetic field in Fe-C-Mn-xSi alloys

Fe-C-Mn-Si steels are known as TRansformation Induced Plasticity (TRIP) steels. They are a new generation of low-alloy steels that exhibit an enhanced combination of strength and ductility. After special thermal treatment, a triple-phase microstructure is obtained, consisting of ferrite, bainite and retained austenite [ZHUW06]. The TRIP effect results from the transformation of retained austenite into martensite during the deformation of the workpiece. Therefore, the stabilization of retained austenite has great impact on the TRIP effect. Presently, the typical TRIP steel contains silicon. This element contributes to the stabilization of the retained austenite through the inhibition of carbide precipitation (mainly cementite) during the bainite reaction [ZHUW08]. Consequently, even if Si is not an austenite stabilizing element, an increase in the silicon content leads to an increase of the retained austenite volume fraction. However, steels with high Si contents lead to difficulties in welding and may also result in the formation of a very strong oxide layer during hot rolling.

In the previous part of this chapter (3.3), ferrite phase stability domain has been found to be enlarging by the application of a magnetic field and the volume fraction of carbide was reduced (pearlite in proeutectoid Fe-C-Mn alloys, see 3.3). We may then wonder what could be the impact of a magnetic field in the stabilisation of retained austenite in TRIP steels. Quantitative comparison of the effect of Si content and magnetic field are thus needed. In a first step toward this goal, in this part, the shift of the A_{r3} line due to the application of magnetic field is compared with the shifts due to the increase in silicon content. In the next chapter further results about the martensitic and bainitic transformation will be considered.

3.4.1. Materials and experiments

The materials used in this study are cast using Arcelor laboratory casting facility. They are prepared by hot rolling in 5 passes down to a thickness of 5.9 mm and then homogenized at 1473 K for 48 h followed by an air cooling before the experiments. Based on a low carbon and manganese composition, the four steel grades differ only from their Si content. The chemical compositions of these steels are reported in Table 3.4.

Test specimens are cylindrical ingot pulled out from the hot rolling sheet with their axis parallel to the rolling direction. Their dimensions are 4 mm in diameter and 10 mm in height. In order to determine the austenitisation temperatures, the temperatures for complete transformation into austenite ($T_{\alpha \to \gamma}$) have been first determined by dilatometry and the temperatures for the austenitisation (T_γ) have been chosen around 30 K above the transformation temperatures. The obtained values are reported in Table 3.4.

Alloy	C	Mn	Si	Fe	$T_{\alpha \to \gamma}(K)$	$T_\gamma(K)$
A	145	1450	15	Balance	1143	1173
B	145	1455	530	Balance	1168	1198
C	145	1430	1050	Balance	1178	1208
D	140	1430	1730	Balance	1218	1248

Table 3.4: Composition of the 4 cast alloys (Alloy compositions in 10^{-3} wt%); Temperatures for complete transformation into austenite with 10 K/s heating rate and chosen austenitisation temperatures.

After preparation, the samples are heat treated in the dilatometer. Temperature is increased up to T_γ at a rate of 10 K/s where the temperature is kept constant for austenitisation during 5 min. Finally, the samples are continuously cooled at a rate of 0.5 K/s. Experiments are reproduced under various magnetic field strengths up to 16T. The magnetic field is imposed during the whole thermal treatment.

3.4.2. Dilatometry results

Dilatation curves and transformation temperature

As an illustration of the dilatation measurements, the length changes of steel A (lowest silicon content) are shown as a function of temperature and magnetic field intensity in Figure 3.26. The austenite decomposition into a ferrito-perlitic structure appears as a sharp dilatation of the specimen.

The onset of the transformation A_{r3} and the end of transformation A_{r1} are evaluated by the tangents method in the same way as illustrated in Figure 3.17 and the values are reported in Figure 3.27. The beginning of pearlite precipitation associated to point T_P in Figure 3.17 is not determined in this part because the signal remains noisy in this region.
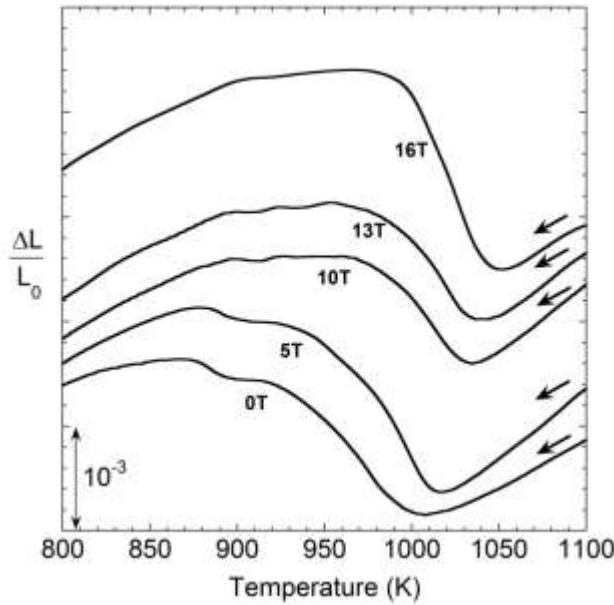
Figure 3.26   Dilatation measurement of the Fe-0.145C-1.5Mn-0.015Si (wt%) referred as A as a function of temperature for 0, 5, 10, 13 and 16T.
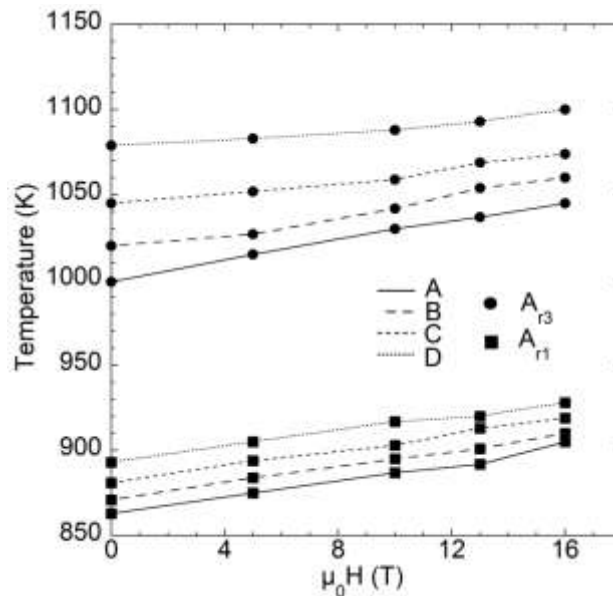
Figure 3.27 A_{r3} (circles), A_{r1} (squares) temperatures as a function of magnetic field intensity measured on cooling for the Fe-0.145C-1.5Mn-xSi (wt%) plain steels with x = 0.015 (A), 0.55 (B), 1.05 (C) and 1.75 (D) wt%.

It appears clearly in Figure 3.27 that an increase in the silicon content (from A to D) leads to an increase of the A_{r3} and A_{r1} temperatures due to the ferrite stabilizing effect of silicon (in zero field). The application of a magnetic field during cooling leads to a linear shift towards higher temperatures of the whole pro-eutectoid region of the phase diagram as A_{r3} and A_{r1} are increased.

Experimental data are linearly fitted for each alloy composition (regression lines are not shown on the Figure). The shift of the A_{r3} temperature amounts to 2.9, 2.6, 1.8 and 1.3 K/T respectively for the alloy containing 0.015 (A), 0.55(B), 1.05(C) and 1.75(D) wt%Si. In a similar way, A_{r1} is increased by 2.5, 2.4, 2.3 and 2.2 K/T respectively for the 0.015, 0.55, 1.05 and 1.75 wt%Si alloy. The error bars estimated for each measurement never exceed 0.1 K/T. These experimental investigations show that the impact of magnetic field on the A_{r3} and A_{r1} temperature seem to be lower when the silicon content in steel increases.

Magnetic measurement and magnetic free energy contribution

There is no predictive model for the prediction of the influence of alloying elements in Fe-C-X-Y alloys where X and Y are substitutional elements which can both interact with the Curie point and the spontaneous magnetisation of iron. As for the Fe-xC-Mn steels studied in part 3.3, the saturation magnetisation of the four steels are thus measured as a function of temperature in 3.5 T. High temperature magnetic measurements are shown in Figure 3.28 in comparison with the measurement done for pure iron in 3.5T.

The magnetic signal corresponding to the Fe-1.5Mn-0.15C-xSi (wt%) with x = 0.015 (A), 0.55(B), 1.05(C) and 1.75 (D)wt% is found to be lower than the measured magnetisation of iron. Increase in the silicon content in steel reduces the saturation magnetisation in good agreement with [ISHI75]. The A_{r3} temperature measured by dilatometry without the application of magnetic field is added in Figure 3.28 with solid arrows. The magnetisation of ferrite is reduced at this respective A_{r3} temperature when the silicon content is increased. In addition to these magnetic measurements, magnetisation curves are done at the respective A_{r3} temperature of the alloys. Results are shown in Figure 3.29(a) up to 3.5 T.
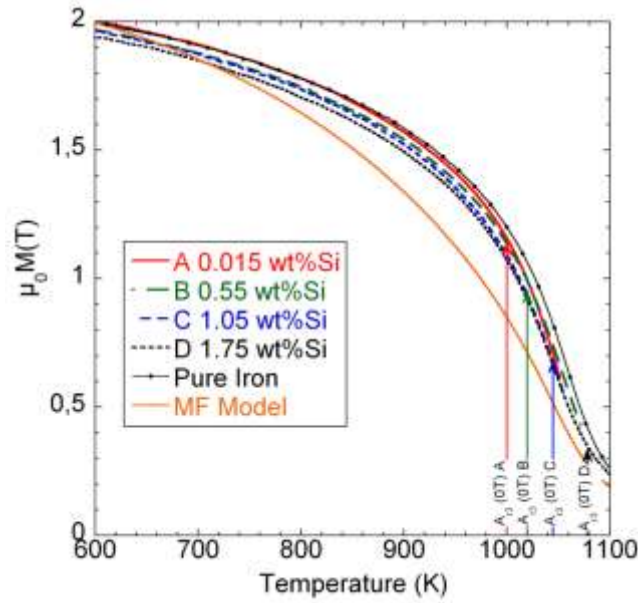
Figure 3.28   Saturation magnetisation as a function of temperature in 3.5 T of high purity iron and Fe-1.5Mn-0.15C-xSi (wt%) with x = 0.015 (A), 0.55(B), 1.05(C) and 1.75 (D)wt%
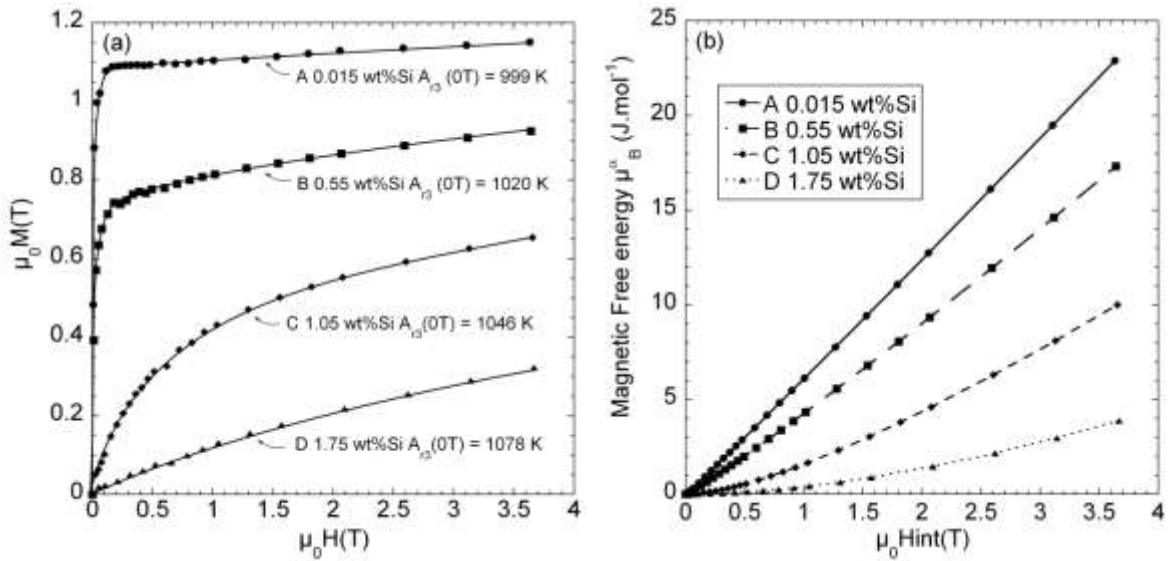
Figure 3.29   (a) Magnetisation curves of the Fe-1.5Mn-0.15C-xSi (wt%) with x = 0.015 (A), 0.55(B), 1.05(C) and 1.75 (D)wt%Si measured at their respective A_{r3} temperature. (b) Absolute value of the magnetic free energy determined according to equ (17) with the experimental magnetisation data.

The linear relation of M^2 vs H/M is obtained only for the alloy A in which the A_{r3} temperature is well below the Curie point. According to equ (17), these magnetisation data are used for the determination of the magnetic free energy contribution. The results are shown in Figure 3.29(b). The magnetic contribution to the total free energy is found to be 5.55 J/mol/T

for the alloy A with 0.015 wt%Si. For other alloys, since the magnetic dependence of the magnetic free energy term does not follow a linear behaviour, magnetisation measurements at higher fields are needed for extrapolation. However, these measurements are an accurate experimental determination of the magnetic contribution to the free energy of ferrite up to 3.5T.

Ferrite volume fraction

The fraction of phase formed during the transformation is evaluated for the four steel grades. The method and assumptions for calculation are described in details in the paragraph 3.4.2. The ferrite volume fraction is shown in Figure 3.30 for the four steel grades as a function of temperature and for 0, 10 and 16T.
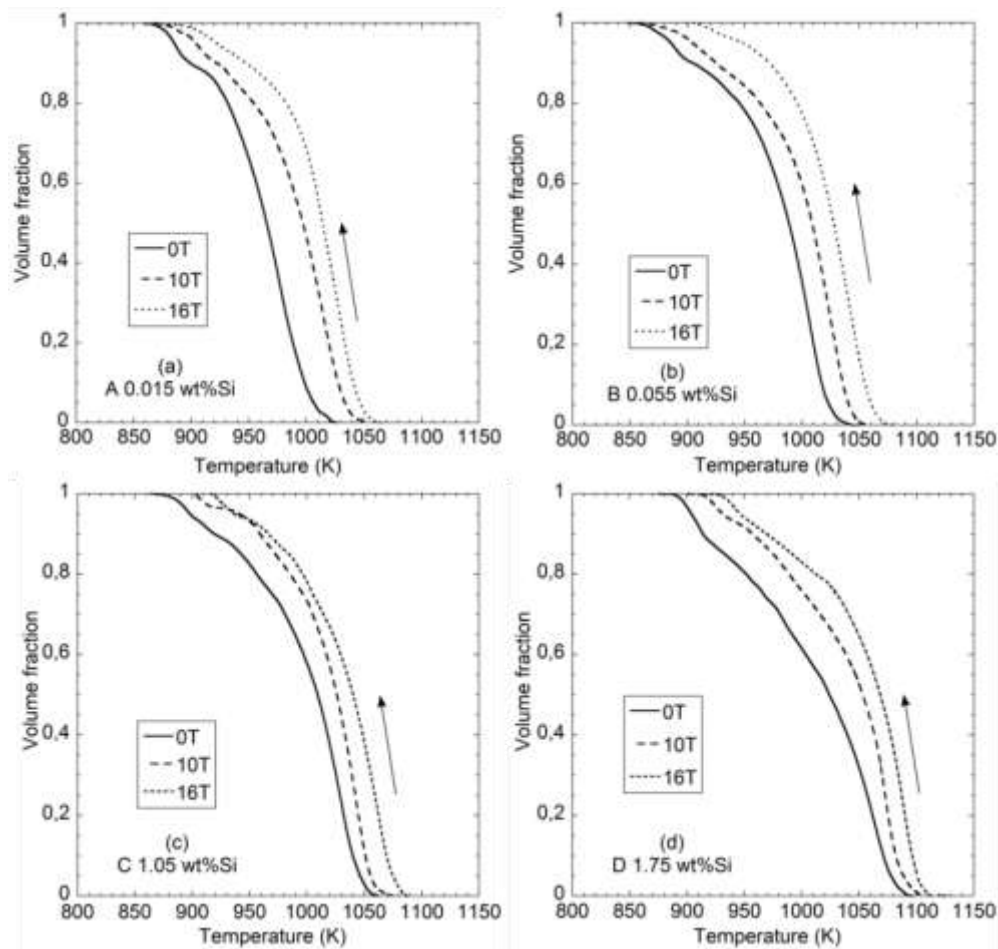
Figure 3.30   The fraction curves obtained from the lever rules method for the Fe-0.145C-1.5Mn-xSi (wt%) plain steels with x = 0.015 (A), 0.55(B), 1.05(C) and 1.75 (D)wt% treated in 0, 10 and 16T.

In each case, the curves corresponding to the various thermal treatments under 0, 10 and 16T are parallel one to the others. As for the previous studies, the mean transformation rate and its corresponding standard deviation are then deduced and shown on Figure 3.31. As it was already found in Fe-Ni alloys and Fe-1.5Mn-C steels, no variation of the transformation rate is observed against magnetic field strength. The standard deviation is lower than about 15% of the mean value for the four alloys. Contrary to the previous alloys studied, the transformation rate seems to be weakly influenced by the addition of silicon which may indicate that the transformation occurs in local equilibrium without partitioning of the silicon element.
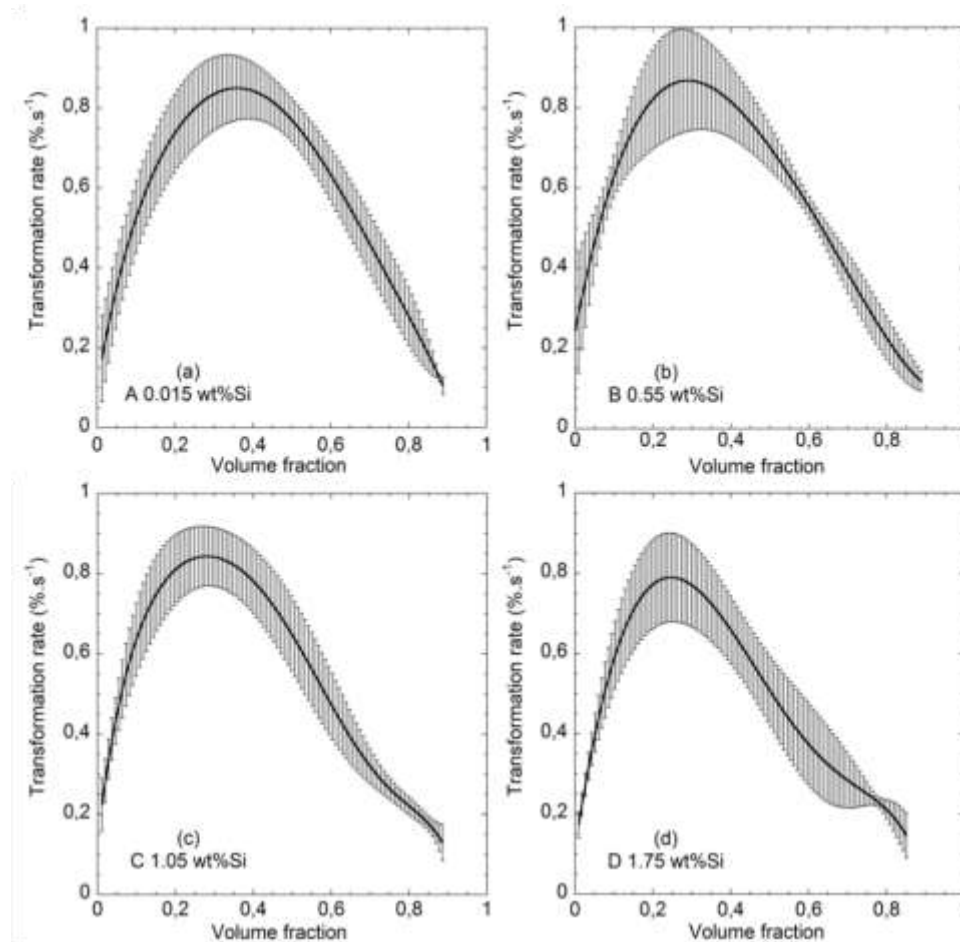
Figure 3.31   Mean transformation rate measured during the austenite decomposition the Fe-1.5Mn-1.45C-xSi (wt%) where x=0.015 (A), 0.55(B), 1.05(C) and 1.75 (D) wt% Error bars correspond to the standard deviation obtained for 0, 10 and 16T.

3.4.3. Effect of magnetic field on transformed microstructures

Figure 3.32 shows optical micrographs to illustrate the effect of magnetic field on microstructures in the four Fe-1.5wt%Mn-0.15wt%C-xSi plain steels, obtained by the non-isothermal decomposition of austenite. The direction of applied magnetic field is horizontal in the figures and corresponds to the hot rolling direction. As predicted by the phase diagram, for low cooling rates, a mixed microstructure of ferrite (light grey) and pearlite (dark grey) is observed.

The corresponding area fractions of ferrite are determined by statistical image analyses of five optical micrographs for specimens treated under zero fields (ZF) and 16 T and are reported in Figure 3.32. The ferrite volume fraction is systematically increased by the addition of silicon. The magnetic field slightly increases the ferrite volume fraction in agreement with the stabilisation of the ferrite phase measured by dilatometry. However, this effect is less visible when the silicon content in steel increases. This result is consistent with the lower shift due to the field of the A_{r3} temperature observed in higher silicon content.

3.4.4. Correlation between Si effect and magnetic field effect

The variations of the A_{r3} temperatures against magnetic field strength measured by dilatometry are smoothed with the red lines shown in Figure 3.33. In the same figure, the variation of the A_{r3} temperature versus silicon content is also shown (dotted line).

It can be observed that the black dashed line (transformation temperature versus Si content) crosses the solid lines (transformation temperature versus field). It means that similar transformation temperatures are measured in both low Si alloys under high magnetic field and high Si alloy without field. As an example, alloy C with 1.05%Si presents the same transformation temperature A_{r3} in zero fields as the transformation temperature measured under 15.5T in the alloy A with 0.015%Si.

Based on this example, some equivalence can be found between the transformation temperature values measured either with different Si content samples or with different applied magnetic field intensities. This observation leads to build the graph in Figure 3.34. This figure represents, for each steel grade, the magnetic field value necessary to obtain the same transformation temperature that would be measured in an alloy with equivalent Si content.
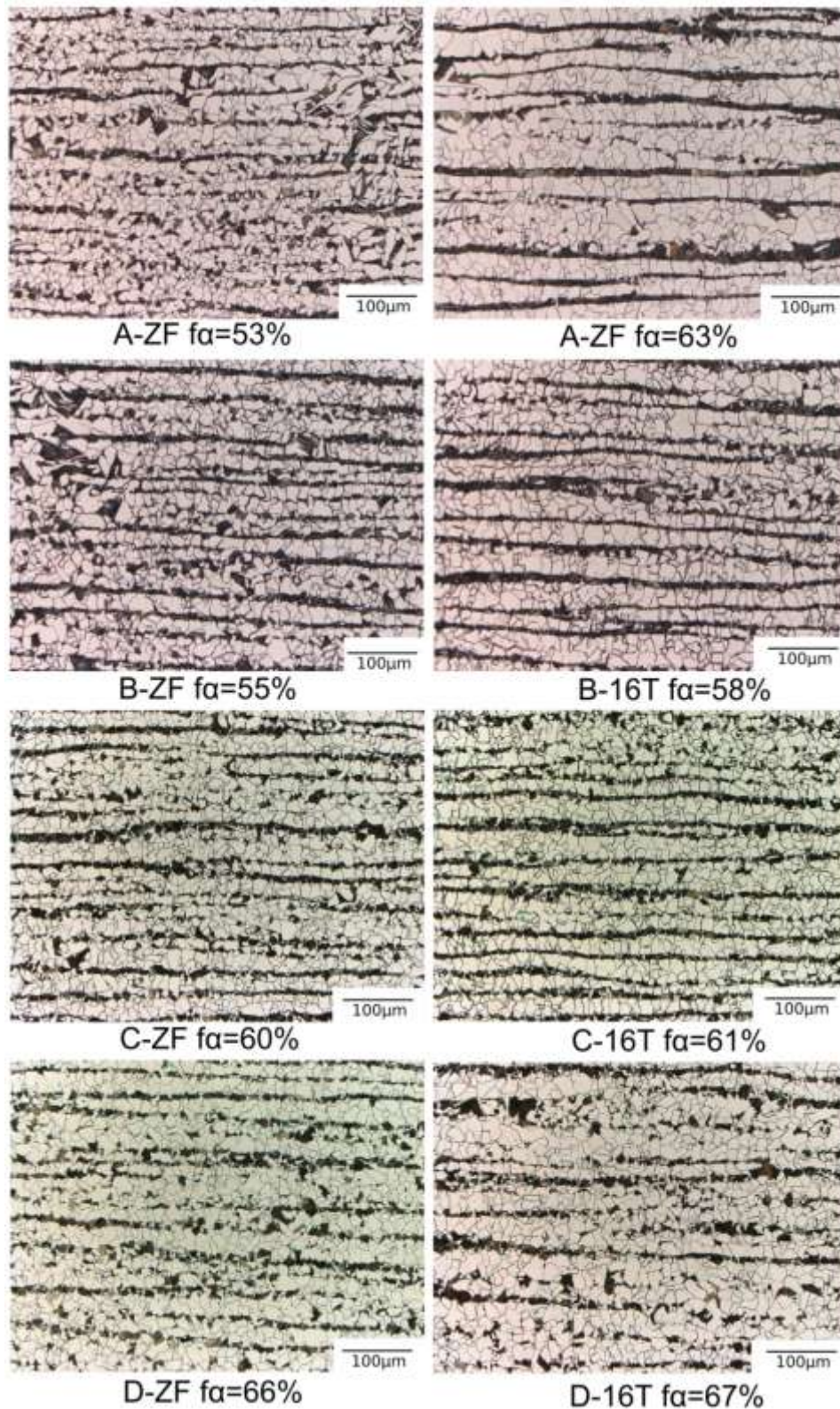
Figure 3.32   Optical micrographs showing the ferrite + pearlite structure obtained after continuous cooling in zero field (ZF) or 16T at a rate of 0.5 K/s for the the Fe-1.5Mn-0.15C-Si steels A (0.015%Si), B (0,53%Si), C (1.05%Si) and D (1,75%Si) Original magnification 200x, 4% nital etch
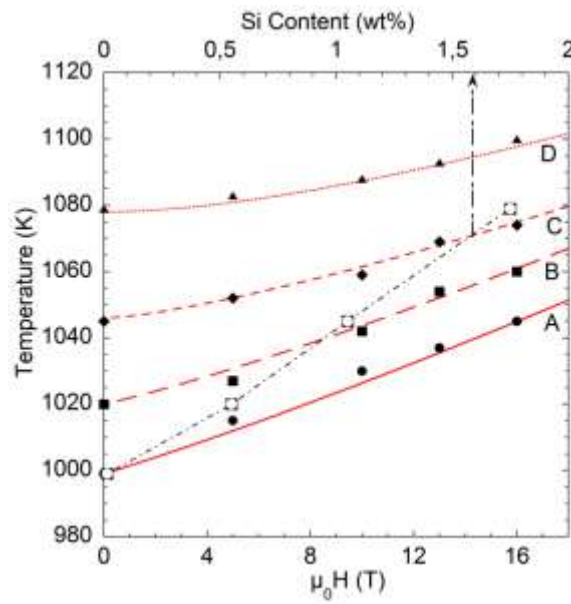
Figure 3.33 $\gamma \rightarrow \alpha$ transformation temperature as a function of the Si content (dotted line) and applied magnetic field (grey line) for the four steel grades.
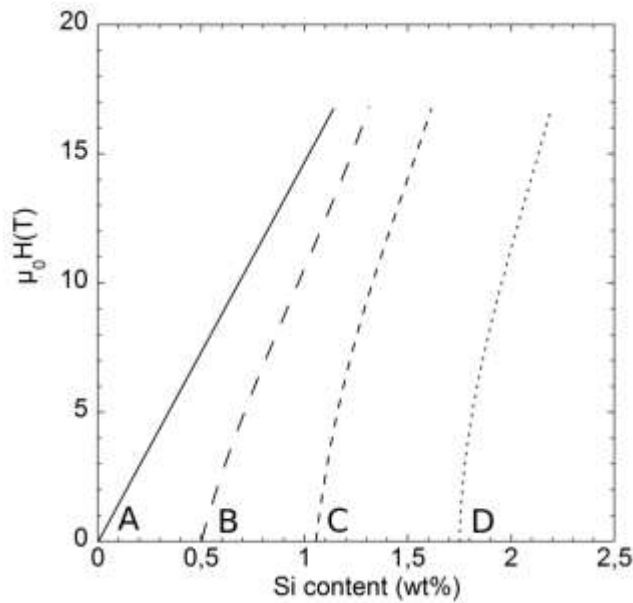
Figure 3.34   Equivalence between the Si content and the magnetic field intensity derived from transformation temperature measurements

In Figure 3.34, vertical lines can be drawn. Along these lines, the Si content is constant. The intersection points between one given vertical line and the experimental straight lines stand for the same transformation temperature. Therefore, vertical lines with a constant step of

0.2wt%Si have been drawn and the corresponding intersection points have been collected. The results are reported in Figure 3.35.

In this figure, the above-mentioned intersection points are extrapolated into "iso-transformation temperatures" lines plotted against both applied magnetic field and silicon content. The solid marks correspond to experimental points whereas the open marks are extrapolated from Figure 3.34 to higher field values and higher Si content. As an illustration, the Si content of a given alloy can be varied without any transformation temperature change by changing the applied magnetic field following any "iso-line".

This result opens the way to an interesting application of the magnetic field in steel processing. If the application of a magnetic field has a similar effect as Si addition on A_{r3}, then high Si content alloys could be advantageously replaced by very low Si grades provided a magnetic field is applied during processing. However, further analysis is needed to link the effect on the A_{r3} temperature to the resulting microstructure of the alloys and to the functional properties.
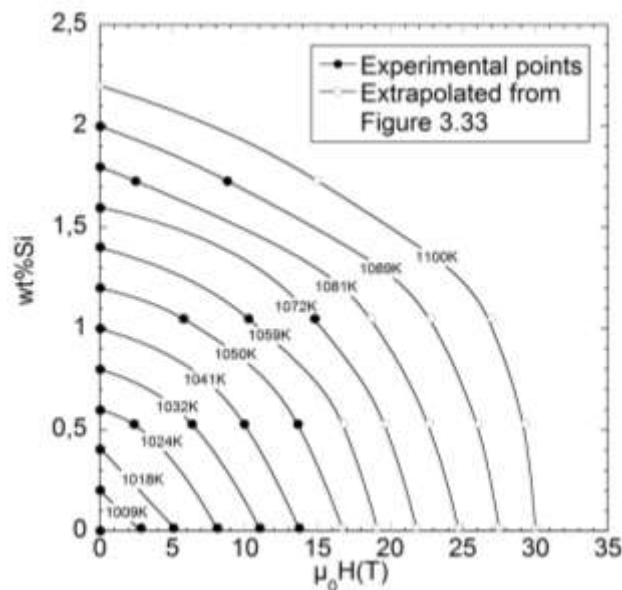
Figure 3.35   Two dimensions-diagram of "iso-transformation temperatures" lines against applied magnetic field and silicon content.

3.4.5. Conclusion

Continuous cooling experiments under magnetic field were performed with four Fe-C-Mn-(Si) with increasing Silicon content. Dilatation measurements allowed the precise

evaluation of the transformation temperature. Shift toward higher temperature between 2 and 3 K/T have been evidenced in these cases. Magnetisation measurements at high temperature are done for the determination of the magnetic contribution to the total free energy in each alloy.

The correlation found between the effect of the magnetic field and of the Si content on the A_{r3} transformation enables to extent the experimental results obtained on four samples, to a wider range of Si content. The equivalence between the Si content in the alloy and the applied magnetic field suggested in this work has to be confirmed by structural analysis. As a perspective for this work, it could be interesting to achieve, under various magnetic field intensities, the conventional treatment used for TRIP steel. In this case, a direct evaluation of the TRIP functional properties would be possible and may validate the use of the magnetic field as a substitution for Si addition.

3.5.   Effect of magnetic field on the kinetics of austenite/ferrite transformation in pure iron

The kinetics of the $\gamma \rightarrow \alpha$ transformation in pure iron is assumed to be only controlled by the interface reaction since there is no long-range diffusion of the components that could influence the kinetics. It is proposed in this study to use experimental data from dilatometry experiments to study the effect of magnetic field on the kinetics of $\gamma \rightarrow \alpha$ isothermal transformation in pure iron. A Free energy-temperature diagram in magnetic field is used to set the driving force for transformation. The JMAK analysis of the time dependence of ferrite fraction gives information about the impact of field on growth mode. Then spherical growth assumption is taken with respect to the shape of the ferrite grain for the estimation of the field dependence of interface mobility.

3.5.1.   Driving force for transformation and experiments

Control of the driving force during isothermal transformation

In the previous studies presented in this chapter, the austenite decomposition occurred

during continuous cooling from the austenite state. The transformation thus took place in a certain range of temperature in which the free energy of austenite and of ferrite respectively varied continuously. In this study, it is proposed to carry out isothermal transformation investigations in order to fix the free energy of each phase during the transformation.

The total free energy change $\Delta\mu_{Fe}^{tot}$ between α-Fe and γ-Fe as a function of temperature and magnetic field in pure iron has been calculated in part 1.2.2. The data of [DINS91] for the chemical free energy terms and from the MF model for the magnetic free energy terms have been used in the calculation. Figure 3.36 shows the variations of the total free energy change $\Delta\mu_{Fe}^{tot}$ between α-Fe and γ-Fe as a function of temperature for a magnetic field strength of 0, 10 and 16T. It is indeed a zoomed view of Figure 1.19. In this figure, the γ/α equilibrium temperatures correspond to the respective intersections of each curve with the x-axis ($\Delta\mu_{Fe}^{tot} = 0$). On each curve, any other non-zero value of the total free energy change represents the driving force for the $\gamma \rightarrow \alpha$ transformation. Therefore, in a given magnetic field strength, the necessary driving force for the $\gamma \rightarrow \alpha$ transformation is increased when the temperature is decreased below the equilibrium temperature.
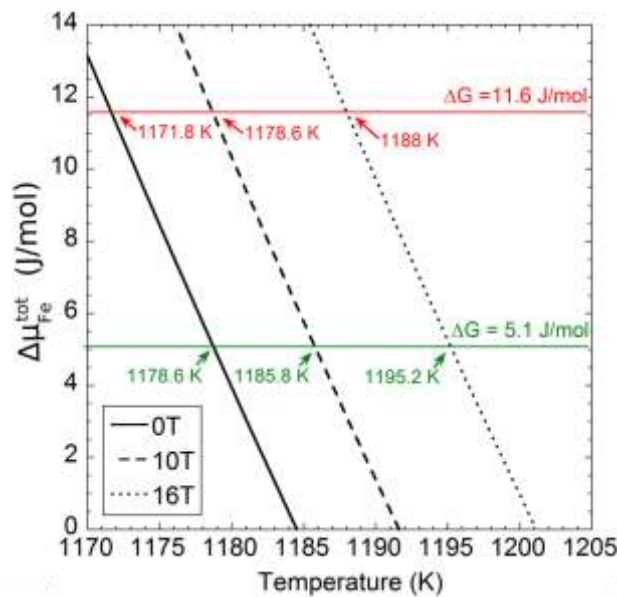
Figure 3.36   Variations of the Gibbs free energy difference between ferrite and austenite as a function of temperature and magnetic field strength for pure iron. Calculated from MF model and [DINS91]

The validity of this diagram has been experimentally checked for pure iron in part 3.1. It is proposed to use these thermodynamical calculations for the determination of the isothermal

transformation temperature imposed during the thermal treatment, so called T_α in the present study. By this way, the total driving force for transformation is known in each case at a given temperature. Along any vertical line in Figure 3.36, i.e. at a given temperature, the driving force is increased with the magnetic field strength. Each intersection along any horizontal line in Figure 3.36, gives the holding temperature T_α that has to be applied in respectively 0 T, 10 T and 16 T in order to allow equal driving force for ferrite transformation.

In order to distinguish, the magnetic field impact on the transformation kinetics, it is suggested to tune the isothermal temperature T_α with respect to the magnetic field strength in order to enable the same driving force whatever the magnetic field value. It is thus proposed to use these thermodynamical calculations along any horizontal line in Figure 3.36, to determine each holding temperature T_α, needed to keep the total driving force ΔG_m for transformation equal under various field intensities. The Red line represents the case where a relatively "high" driving force of 11.6 J.mol^{-1} is set. This implies that T_α is chosen as 1171.8 K, 1178.6 K and 1188 K respectively under 0, 10 and 16T. The Green line corresponds to the "low" driving force of 5.1 J.mol^{-1}. In this second case, T_α is set at 1178.6 K, 1185.8 K and 1195.2 K respectively for the 0, 10 and 16T experiments.

Sample preparation and profile of the thermal treatment

Specimens of high purity iron (99.999%) are prepared by induction melting in a cold crucible induction furnace. After melting, the iron is cast into a cylindrical copper mould with an inner diameter of 4 mm. Then, cylinders of 10 mm in height are cut from this ingot. After that, the specimens are kept at 1223 K for 30 min for homogenization before the measurements.

Then, the samples are heat treated in the dilatometer. Magnetic field is applied during the whole thermal treatment and the furnace is under pure argon atmosphere. Temperature is increased at a rate of 1.7 K/s up to 1250 K where it is kept constant for 2 min. The sample is then cooled down to the holding temperature T_α at a rate of 17 K/s for the $\gamma \rightarrow \alpha$ isothermal transformation to proceed. After 5 min at T_α, sample is cooled down to room temperature at a rate of 3 K/s. The resulting profile of the thermal treatment is schematically shown on Figure 3.37 for a set of experiments done in 0, 10 and 16T.
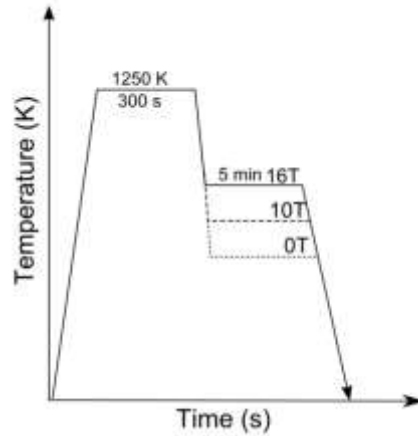
Figure 3.37   Thermal treatment profile for the ferrite isothermal transformation under equal Gibbs free energy conditions (or equal driving force).

3.5.2. Kinetics analysis of the $\gamma \to \alpha$ isothermal transformation based on dilatometry measurements

Ferrite volume fraction and transformation rate

In Figure 3.38(a), the ferrite volume fraction as a function of time $f(t)$, monitored during the isothermal growth under 11.6 and 5.1 J.mol^{-1} respectively, is shown for 0, 10 and 16T. The origin of time corresponds to the beginning of the isothermal holding. The time needed to achieve complete transformation seems to be quite similar in various magnetic field intensities and for a given total driving force as if the increase in the isothermal transformation temperature was compensated by the application of the magnetic field.

The corresponding transformation rates $df(t)/dt$ are shown in Figure 3.38b. They are plotted as a function of the ferrite volume fraction in order to evidence the different steps of the transformation associated to the variation of the transformation rates. At low degrees of transformation, i.e. below 0.05 % of ferrite, the transformation rate is very low in all the cases which may indicate a settling time for nucleation and for the progressive increase in the number of ferrite nuclei. Similarly, at high degrees of transformation the rates fall down to zero which could be associated to ferrite coarsening. The fastest transformation rate occurs earlier when the driving force is low. It is measured around 50% of transformation in the case of the higher driving force, and around 20% for the lower driving force. According to expectations, it is also found to be higher with the higher driving force.
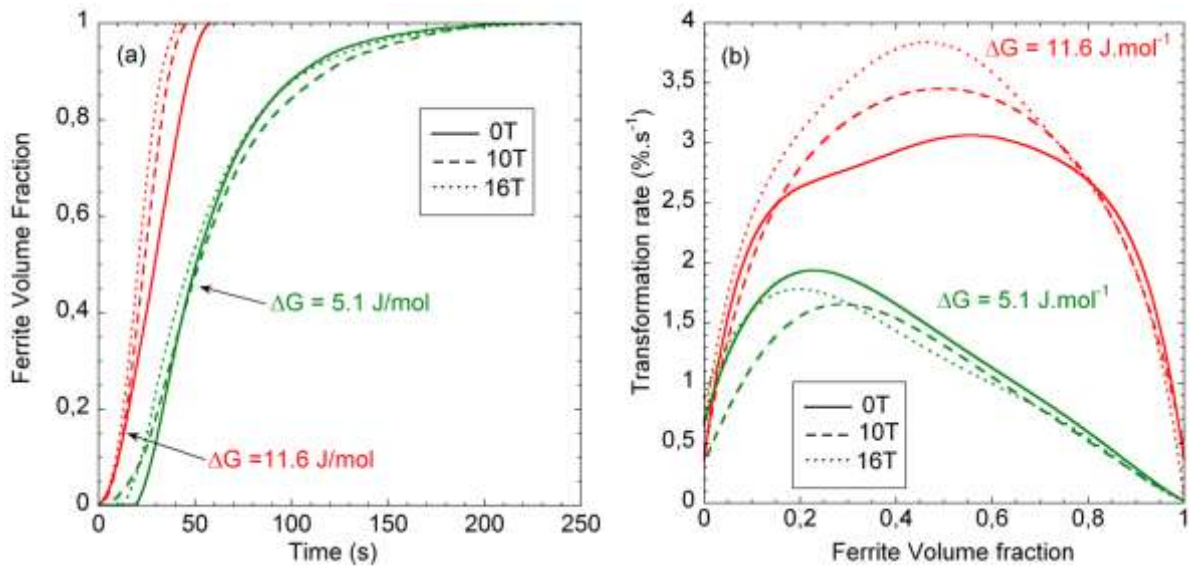
Figure 3.38   (a) Variation of the fraction of ferrite during the $\gamma \to \alpha$ transformation in pure iron for 0, 10 and 16T for respective total free energies of 11.6 J/mol (red lines) and 5.1 J/mol (green lines). (The corresponding transition temperatures are indicated in Figure 3.36. (b) Transformation rate as a function of ferrite volume fraction measured for both driving forces and for 0, 10 and 16 T.

The effect of the magnetic field is to gradually increase the transformation rate in the experiments performed under the "high" driving force. However, this behaviour is not found in the case of the low driving force where the same order of transformation rate is measured whatever the magnetic field strength.

Kinetics parameters of the transformation in the JMAK analysis

In order to quantify the transformation kinetics, a conventional method is the Jonhson-Mehl-Avrami-Kolmogorov theory (JMAK). In this theory the fraction of ferrite formed corresponds to:

$$f(t) \approx 1 - \exp(-k\,t^n) \tag{54}$$

where $f(t)$ is the ferrite fraction formed after time t, k is a temperature dependent constant and n is the Avrami exponent. The Avrami exponent reflects the nucleation rate and

the growth morphology. Unlike n, it is generally dangerous to associate a specific role to the k value [PHIL98] but their values are however determined systematically for information.

Plotting $\ln(-\ln(1-f(t)))$ as a function of $\ln(t)$ leads to a linear behaviour with n being the slope of this straight line and k determined for $\ln(t) = 1$, as illustrated in Figure 3.39.
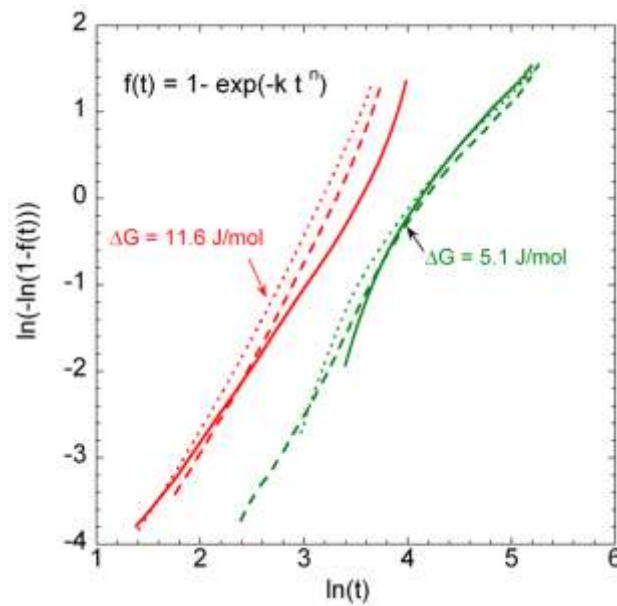
Figure 3.39   Determination of the temperature dependant constant k and the Avrami exponent n for the isothermal transformation from austenite to ferrite in pure iron at 5.1 and 11.6 J.mol^{-1}

Table 3.5 summarizes the results obtained for the two n and k parameters at the different magnetic field strength. Under conditions of equal free energy, a very small variation of the Avrami exponent is measured when the magnetic field strength is changed. This indicates clearly that the growth behaviour is not drastically changed by the application of a magnetic field.

The mean value and the standard deviation are also given Table 3.5. The Avrami exponent is around 2 for the high driving force experiment and about 3/2 for the low driving force experiment.

Besides, no effect of magnetic field is observed on the k parameter which is found to fluctuate in a relatively large range for the various experiments probably due to incertitude in the dilatometry signal.

	n ΔG_m=11.6 J.mol^{-1}	n ΔG_m=5.1 J.mol^{-1}	k (.10^{-4}) ΔG_m=11.6 J.mol^{-1}	k (.10^{-4}) ΔG_m=5.1 J.mol^{-1}
0T	1,95	1,65	9.5071	10.047
10T	2,38	1,72	4.0218	6.0881
16T	2,34	1,55	6.1635	15.383
Mean value	2.22	1,64	6,56	10,51
Std Deviation	0,23	0,08	2,76	4,66

Table 3.5: Avrami exponent n and temperature dependant constant k for the isothermal transformation from austenite to ferrite in pure iron at 5.1 and 11.6 J.mol^{-1}

This analysis proved that when the total driving force for the transformation is the same, the nucleation and growth rate is not influenced by the application of a magnetic field as high as 16T. This means that, whatever the respective amounts of the chemical contribution and the magnetic contribution to the total driving force, the transformation kinetics is related only to the total energy available for transformation whatever its origin.

3.5.3. Interface controlled reaction and interface mobility

It is now proposed to estimate the γ/α interface mobility in order to observe an eventual modification induced by the application of a magnetic field. According to the most common version of the model for interface controlled reaction [HILL75, HILL06], the amount of free energy dissipated at the interface is related to the interface velocity v as shown in equ (12) and the instantaneous interface position $r(t)$ can be deduced by:

$$r(t) = \int_0^t Mob\frac{\Delta G_m}{V_m}\,dt = Mob\frac{\Delta G_m}{V_m}t + t_0 \qquad (55)$$

where Mob is the γ/α interface mobility expressed in m^4.J^{-1}.s^{-1}, V_m is the volume for one mole of material (typically $V_m = 7.10^{-6}$ m^3.mol^{-1}) and t_0 is taken as zero since it correspond approximately to the start of transformation.

In this study, we will consider a spherical growth mode which is a realistic case under our experimental condition. In spherical growth conditions, as illustrated in Figure 3.40, the

volume fraction of ferrite *f(t)* can be expressed in terms of the instantaneous interface position *r(t)* and of the initial austenite grain size R_0 as:

$$f(t) = 1 - \frac{r(t)^3}{R_0{}^3}$$ (56)
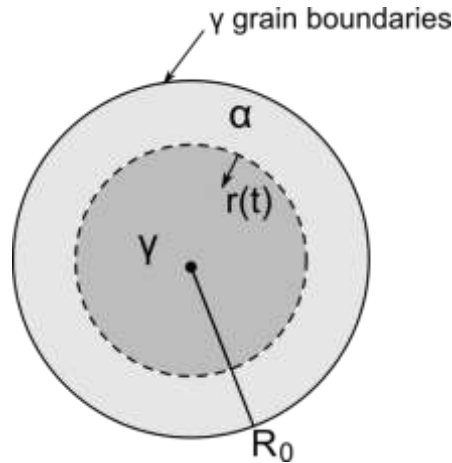
Figure 3.40   Schematic representation of an austenite grain during isothermal growth of ferrite in the case of planar growth conditions.

From equ.(55) and (56) the term Mob/R_0 called, in this present study, the reduced interface mobility can be calculated as :

$$\frac{Mob}{R_0} = \frac{V_m \sqrt[3]{1 - f(t)}}{\Delta G_m t}$$ (57)

This term is expressed in m^4.J^{-1}.s^{-1}.m^{-1}. From the experimental data shown in Figure 3.38(a), the reduced interface mobility Mob/R_0 is systematically calculated and plotted as a function of time, ferrite volume fraction, magnetic field and driving force in Figure 3.41.

The reduced interface mobility is found to slightly decrease during isothermal holding for both driving forces studied. The variation is important at the very beginning and end of the transformation. The reduced interface mobility should not vary during the isothermal transformation since it is an intrinsic parameter only depending on temperature. Indeed, the simple spherical model does not seem to be very realistic at low and high degrees of transformation where the term Mob/R_0 is somewhat divergent. However, according to [HILL06], the model would be reasonably accurate around 50% of transformation. In Figure

3.41(a), the value for 50% transformation is marked with crosses. In this case, the magnetic field does not seem to change drastically the measured value of Mob/R_0. Moreover, it is totally consistent to find similar values (around 2.10^{-8} $m^4.J^{-1}.s^{-1}.m^{-1}$ at 50%) whatever the amount of driving force (curves red and green).
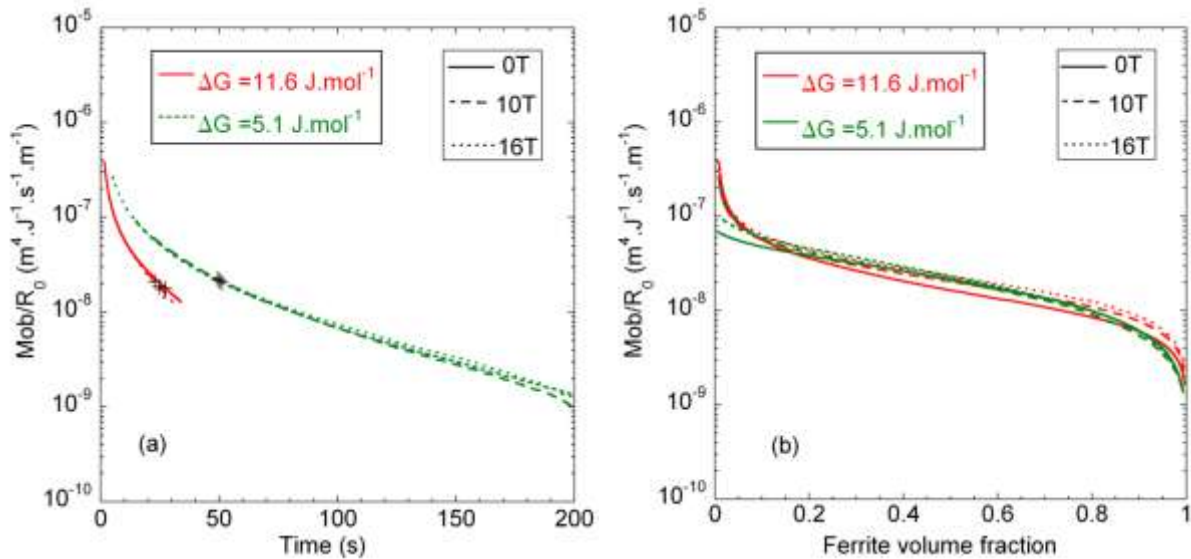
Figure 3.41 Reduced interface mobility Mob/R_0 as a function of (a) time and (b)ferrite volume fraction calculated in the case of spherical growth. Crosses in Figure (a) represent the points corresponding to 50% transformation

From the value of Mob/R_0 obtained at 50% transformation, an attempt is now made for the determination of the temperature dependence of the interface mobility for each experiments. According to [HILL75], the reduced interface mobility in our case is expressed as:

$$\frac{Mob}{R_0} = \frac{Mob_0}{R_0} \exp\left(-\frac{Q}{RT}\right)$$

(58)

where Q is an activation energy in J.mol^{-1} and Mob_0 is the intrinsic mobility. Plotting $ln(Mob)/ln(10)$ as a function of $10000/T$ lead to a linear behaviour with a and b being the coefficient of the straight line as:

$$\frac{ln(Mob)}{ln(10)} = a\frac{10000}{T} + b$$

(59)

where Mob_0 and Q are deduced by :

$$Mob_0 = \exp(b \ln(10) + \ln(R_0)) \tag{60}$$

$$Q = 10000 R ln(10) a \tag{61}$$

The R_0 value is unknown in the model. However, through this analysis, it is evident that an improper choice in the initial austenite grain size R_0 will not change the slope of the straight line (a coefficient). It will shift the line vertically, leading to an improper value of the intrinsic mobility Mob_0. According to several attempts to evaluate Mob_0 for the γ/α interface by several groups [HILL75, KRIE97, WIST00], values between 0.0350 and 4.10^{-7} m^4.J^{-1}.s^{-1} were found. In this work, it is thus decided to give an arbitrary value of $R_0 = 100$ μm for the austenite grain size in order to discuss the values of the activation energy for interface mobility (through a) and compare them with the value obtained in literature.

The Mob values obtained at 50% by dilatation experiments in each case are plotted in Figure 3.42. The green points correspond to the experiments performed under the "low" driving force and red one correspond to the "high" driving force experiments. In this Figure is added the well accepted temperature dependence of the mobility obtained respectively by Hillert et al. [HILL75], Krielaart et al. [KRIE97], and Wits et al. [WITS00] which are discussed in details in [HILL06].

The experimental points are all aligned along one straight line whatever the magnetic field strength and whatever the driving force for transformation. Application of a 16T magnetic field during isothermal transformation seems to influence weakly the activation energy for the interface mobility. It is thus decided to fit linearly all the experimental data in order to compare the activation energy with those of literature. The result deduced from this linear regression is 158144 J.mol^{-1} which is in relatively good agreement with the data of [HILL75] (147000 J.mol^{-1}) and with the data of [KRIE97] and [WIST00] (140000 J.mol^{-1}). This last result validates the use of all sets of experiments for the calculation of the activation energy for the interface mobility, whatever the magnetic field intensity.
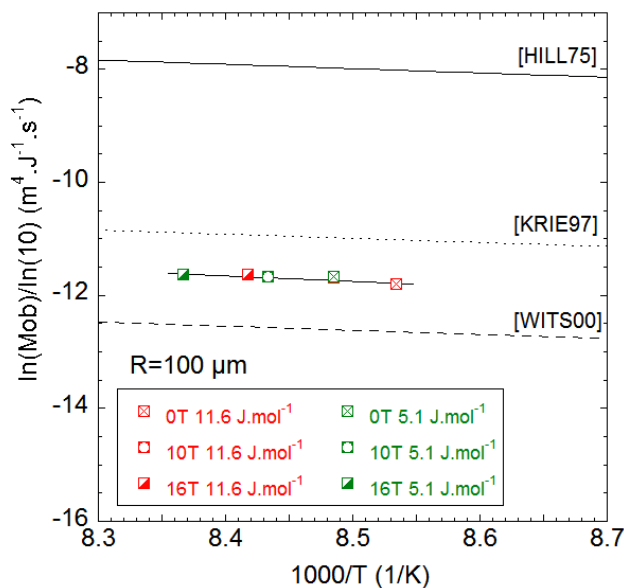
Figure 3.42   Apparent mobility evaluated with equ (57) for the isothermal transformation from austenite to ferrite in pure iron under a driving force of 5.1 (green line) and 11.6 J.mol^{-1} (red line) for 0, 10 and 16T.

3.5.4. <u>Conclusions</u>

For the first time, isothermal transformation from γ-Fe to α-Fe is in situ monitored by dilatometry in high magnetic field up to 16 T. The isothermal temperature T_α is tuned with respect to the magnetic field strength in order to enable the same driving force whatever the magnetic field value.

The duration to achieve a complete transformation seems to be quite similar for a given driving force as if the increase in the isothermal transformation temperature was compensated by the application of the magnetic field.

JMAK analysis of the time dependence of the ferrite fraction proved that when the total driving force for the transformation is the same, the nucleation and growth rate is not influence by the application of a 16T magnetic field. This means that whatever the part of chemical or magnetic contribution in the total driving force, transformation kinetics is not changed.

Finally, the systematic estimation of the activation energy for the interface mobility confirmed the weak impact of magnetic field on the kinetics of transformation.

3.6. <u>Summary</u>

The austenite to ferrite transformation under the influence of a strong magnetic field has been investigated in this chapter for several alloys compositions. High purity iron, Fe-(2 and 4)Ni (wt%) substitutional alloys, Fe-1.5Mn-(0.1, 0.2 and 0.3)C (wt%) plain carbon steels and Fe-1.5Mn-0.15C-(0.015, 0.55, 1.05 and 1.75)Si (wt%) plain carbon steels have been investigated.

The austenite to ferrite transformation temperature has been accurately measured by *in-situ* dilatometry up to 16T. Magnetisation measurements at high temperature have been performed up to 3.55T to study the impact of alloying element on the magnetic properties of iron. These measurements have been used to test the validity of the Molecular Field Model. Thermodynamic calculations have been finally performed for the prediction of the non-equilibrium transformation temperature in magnetic field. It is generally possible to predict the shift of the transformation temperature using only two important parameters. The first one is the enthalpy change accompanying the transformation which can be found in databases or measured by Differential Scanning Calorimetry. In this work, this term (through the change in the entropy between ferrite and austenite) has been assumed to be uninfluenced by the magnetic field. However, in-situ DSC experiments are needed to check for this assumption. The second parameter is the magnetisation of the ferrite phase. This term can be evaluated by direct in-situ magnetic measurement or can be estimated using MF model. The hypothesis that the magnetic field does not influence the total driving force for transformation is validated by the relatively good agreement found between the measured and predicted shift of the austenite to ferrite transformation temperature in magnetic field.

The important results obtained are summarized here:

- The MF model is found to underestimate the magnetisation of ferrite especially around the Curie temperature.
- The austenite to ferrite transformation temperature in Fe, Fe-2Ni and Fe-4Ni wt% alloys is shifted towards higher temperatures under magnetic field. Against magnetic field intensity, this shift shifts from a linear to a quadratic behaviour depending on the $T_C - T_T$ temperature range.

- Thermodynamics calculations based on the Molecular field Model and on magnetic measurements are found to describe well the measured shift of the transformation temperature in magnetic field.

- In Fe-xC-1.5wt%Mn steels, the shift towards higher temperatures of the respective austenite, ferrite + austenite and ferrite + pearlite stability regions is experimentally confirmed.

- Experimental magnetisation data are used to calculate the magnetic contribution to the Free energy of the transformation and to calculate the magnetic field dependence of the A_{r3} temperatures.

- Impact of magnetic field on the A_{r3} temperature experimentally measured, ferrite volume fraction and Vickers hardness values are found to increase with the increase in the carbon content. This behaviour is confirmed by the evaluation of the magnetic free energy contribution based on magnetic measurement.

- In Fe-1.5Mn-0.15C-xSi (wt%), the shift toward higher temperature of the A_{r3} temperature is found to decrease with increasing silicon content in alloy.

- The correlation found between the effect of the magnetic field and of the Si content on the A_{r3} transformation enables to extent the experimental results obtained on four samples, to a wider range of Si content.

- In plain carbon steels the alignment of pearlite colonies is observed along the rolling direction and seems to be promoted by the application of a magnetic field but no specific change is found in the sub-structure of pearlite.

- In isothermal conditions in pure iron, it was found that when the total driving force for the transformation is the same, the nucleation and growth rate are not influenced by the application of a magnetic field as high as 16T.

- The systematic estimation of the activation energy for the interface mobility confirmed the weak impact of magnetic field on the kinetics of transformation.

Chapter 4

Martensitic and bainitic transformations in plain carbon steels in magnetic field

Ch 4- Martensitic and bainitic transformations in plain carbon steels in magnetic field

As an introduction to this chapter, the first part is dedicated to the calculation of the magnetic field dependence of the T_0 line in the Fe-C system. This line sets the thermodynamics limits for displacive transformations. The Molecular Field Model for the magnetisation of ferrite together with the Curie-Weiss law for the magnetic susceptibility of austenite are used to quantify the magnetic free energy as a function of temperature and magnetic field strength. This new contribution is added to the partial molar free energy terms for ferrite and austenite and the new T_0 is determined.

The next parts deal more specifically with the influence of magnetic field on the martensitic and bainitic transformations. The experimental work is carried out in the new processing device developed during this work and that allows the rapid cooling of materials in magnetic field.

Both Fe-xC-Mn alloys with increasing carbon content (part 4.2) and Fe-C-Mn-xSi plain carbon steels with increasing silicon content (part 4.3) are used to test the influence of a strong magnetic field applied during water quenching from the austenite state. Microstructure changes due to the application of the magnetic field are described.

4.1. Shift of the T_0 line in magnetic field in the Fe-C system

This first part deals with the theoretical evaluation of the magnetic field dependence of the T_0 line in the Fe-C system. Along this temperature-composition line, the free energies of austenite and of ferrite are equal for the same composition. Moreover this line defines the limit beyond which it is thermodynamically impossible to get displacive transformation. By the evaluation of the magnetic contribution to the free energy curves of ferrite and austenite, new free energy-composition diagrams are obtained and the T_0 line is determined as a function of magnetic field.

4.1.1. Criteria for displacive mechanism and importance of the T_0 line in the iron-based alloys

In steels, the T_0 line is of capital importance in the transformation that involves displacive mechanisms. As an illustration of this fact and in addition to the description given in part 1.2.1 of this work, the conditions for martensitic transformation are briefly listed in this paragraph.

Martensite in steels is a phase which forms athermally at low temperature, with a very high kinetics of growth (more than 1000 m.s^{-1} in some cases) and that implies no changes in the composition (carbon atoms are trapped by the moving interface). Therefore, in the very fast motion of the interface, unconservative processes are not allowed, such as the creation of vacancies or the climb of dislocations. The interface has to be able to move without any thermal activation. It is possible in a conservative process where the interface between austenite and martensite is glissile [BALL05]. There is thus a lot of coherence in the interface between austenite and martensite with a low interfacial energy (typically 0.2 J.m^{-2} compared to 0.8 J.m^{-2} for an incoherent boundary).

The crystallography of this transformation and the orientation relationships between austenite and martensite are predictable in most of cases [BHAD01]. It consists of a combination of two shears and one rotation of the austenite lattice. The two shears are knows as the Bain strain which is a compression in one direction and an expansion in the

perpendicular one. These cumulated operations leave a completely unchanged line between the austenite and martensite lattice called the Invariant Line Strain (ILS). In addition to the ILS, twin and slip deformations are regularly introduced in the lattice to compensate the macroscopic shape deformation. This change in the tetragonal orientation does not modify the crystal structure and is called a Lattice Invariant Deformation (ILD).

Thermodynamics has to be used to predict the temperature at which the martensite can form [PALU08]. On Figure 4.1 is shown a free energy diagram for ferrite and austenite and the corresponding part of the Fe-C phase diagram.
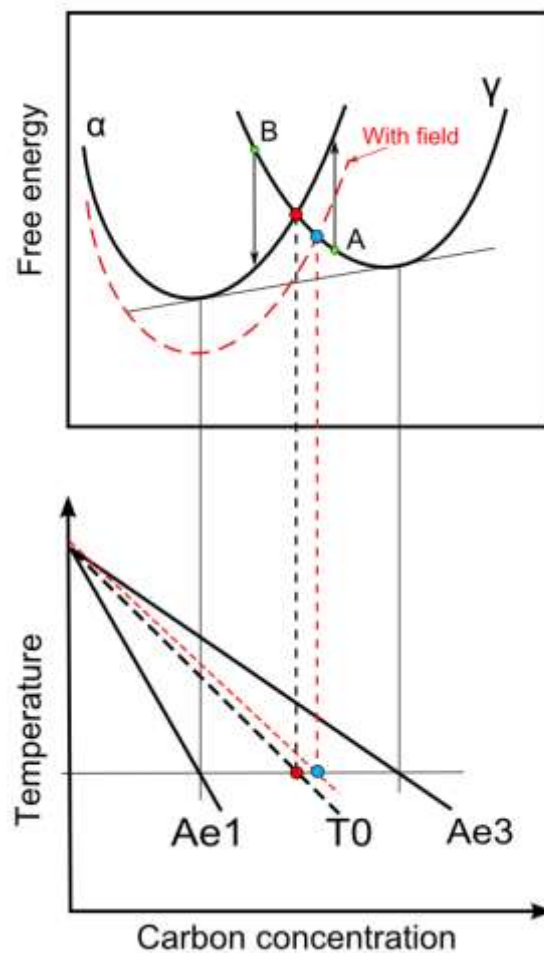
Figure 4.1   Schematic illustration of the T0 line construction. The red lines correspond to the diagram under magnetic field. Modification induced by magnetic field in the free energy of austenite is not represented in the diagram.

As previously introduced the equilibrium phase diagram is built by the evaluation of the common tangent to the two free energy curves because it gives the minimum free energy state. But, there is another important point in the free energy diagram which is usually not

plotted in the equilibrium phase diagram. This is the point where the free energies of austenite and of ferrite are equal for the same composition. This point is called the T_0 point and is extrapolated for several temperatures in the phase diagram to obtain the T_0 line. The importance of this line is illustrated below: if the austenite is at a composition given by point A in Figure 4.1, richer in carbon content than the T_0 point, it is theoretically impossible to transform because it will lead to an increase in the free energy. On the other hand, if the austenite is at a composition given by point B, lower in carbon content than the T_0 point, the martensitic transformation can occurs because it leads in this case to a decrease in the free energy. This is the reason why, the T_0 line defines the limit beyond which it is thermodynamically impossible for the martensitic transformation to proceed. Generally speaking, this line sets the thermodynamics limits for the displacive transformations.

In practice, when the austenite is cooled down, the martensitic transformation does not occur at equilibrium temperature, T_0 but occurs at the so called martensitic start transformation temperature M_s, which is below T_0. This is because some interfacial energy and strain energy are needed to initiate the transformation, and this additional energy (typically 600 J/mol for Fe based alloys) is supplied by the excess cooling, i.e., from T_0 down to M_s. When the magnetic field is applied, the Gibbs free energy of the martensite decreases mainly due to the addition of the magnetostatic energy. Therefore, the equilibrium temperature T_0 under the magnetic field increases. According to [KAKE99], it is assumed for ferrous alloys, that the driving force for martensitic transformation in magnetic field is the same than that without magnetic field. Also, temperature M_s under the magnetic field increases with respect to the equilibrium temperature T_0 under the magnetic field. The validity of this assumptions has been established in [KAKE99] for the martensitic transformation in Fe-based alloys and tested for the austenite to ferrite transformation in chapter 3 of this work.

In the following part, it is proposed to evaluate theoretically the change in the T_0 line by the application of an external magnetic field by the evaluation of the magneto-static contribution added to the free energy of ferrite.

4.1.2. Calculations and discussion

Method for calculation and conditions

The calculation method for the evaluation of the magnetic free energy term for ferrite in the Fe-C system has been explained in details in the first chapter (part 1.2.2).

The saturation magnetisation as a function of temperature and magnetic field strength is given by the Molecular Field theory with J=0.5, T_C =1043 K and M_{Fe}^0=1.73 10^6 A.m^{-1}. The effect of carbon content in the magnetisation of ferrite is assumed to be negligible due to the very low diffusivity of carbon in ferrite. The magnetic susceptibility of austenite is calculated with the values of Arajs et al. [ARAJ60] (equ. (21)) and the effect of carbon content in the magnetic susceptibility value of austenite is neglected.

The partial molar free energy curves for ferrite and austenite as a function of carbon at isothermal temperatures between 1183 K and 1023 K are obtained from thermodynamics databases with Thermocalc software. The calculated magnetic contribution is added to the chemical free energy curves of respectively austenite and ferrite as illustrated with red line in Figure 4.1. The cross section of the curves for austenite and for ferrite in the new free energy-composition diagram corresponds to the T_0 point at a given temperature and magnetic field. The evaluation of this point for several temperatures and fields give the dependence of the T_0 line as a function of carbon content and magnetic field.

Discussions

Figure 4.2 shows the results obtained when magnetic field change between 0 and 40 T. The T_0 line is shifted toward higher carbon content. As an illustration of the use of such a diagram, the upper horizontal lines drawn in Figure 4.2 at T = 1150 K represents the shift of the line toward higher carbon content under 40 T. The T_0 composition is 0.02 wt%C under zero field at this temperature, and becomes 0.10 wt%C under 40T. It corresponds thus to a shift of 0.08 wt%C towards higher carbon content. Let us now consider the reverse situation: how high has the magnetic field to be imposed for an equivalent change in the T_0 composition but at a lower temperature? Segments of 0.08wt%C in length are drawn at 1100 K and 1050 K. It appears that lower magnetic field than 40 T is needed to shift the T_0 composition of 0.08wt%C such as 36T and only 31T at respectively at 1100 K and 1050 K. It means that at a given magnetic field strength, the shift of the T_0 line increases when the temperature is reduced. This effect, mainly due to the rapid increase of the magnetisation of ferrite at the

Curie temperature, has been experimentally evidenced for the A_{r3} line in Fe-C-Mn alloys in the part 3.3.
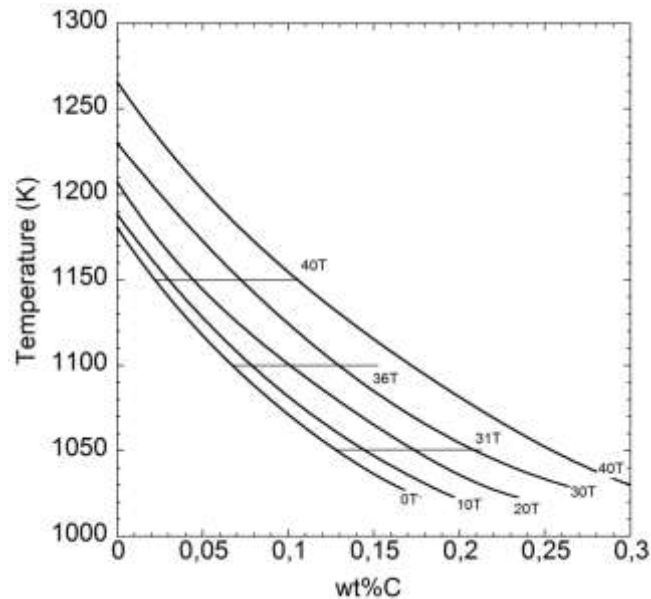
Figure 4.2   Calculation of the shift of the T_0 line under strong magnetic field in the Fe-C system.

The possibility to tune the T_0 line by the application of magnetic field can be useful in various fields of metallurgy. As an example, the T_0 line plays an important role in the bainitic transformation because this reaction exhibits features of both diffusive and displacive transformation. Supposing that the plates of bainite form without diffusion (by displacive mechanism) but that any excess of carbon is rapidly rejected into the residual austenite, the carbon concentration is progressively increased in the parent phase. It means that, while the nucleation mechanism of bainite can be diffusionless, the nucleation rate of bainite is controlled by carbon diffusion [QUID01, QUID02]. Because diffusionless transformation can only occur below the T_0 curve, the bainite reaction must cease when the austenite concentration reaches the T_0 point. According to the calculation, the effect of magnetic field is to shift the T_0 curves towards higher carbon content. Assuming that the magnetic field does not affect the other contributions, such as the strain energy, or carbon partitioning kinetics, it is theoretically expected that the fraction of bainite for given temperature and additive content conditions could be tuned in changing the magnetic field strength. This result has been experimentally observed by [OHTS06a] in a Fe-3.6Ni-1.5Cr-0.5C (wt%) alloy.

4.1.3. Conclusion

Thermodynamic calculation for the quantification of the impact of magnetic field on the T_0 composition line of the Fe-C system is shown in this study. An important shift towards higher carbon content is calculated in the presence of a magnetic field. This shift is found to be higher when temperature decreases. This result can be in practice directly used for the determination of the martensitic start transformation temperature taking in account the other contributions coming from the interfacial and strain energy.

4.2. Changes in the microstructure resulting from high cooling rate in Fe-xC-Mn alloys in strong magnetic field

In the previous chapter (part 3.3), the modifications induced by the application of a strong magnetic field in the diffusional decomposition of austenite was studied in Fe-xC-Mn alloys with increasing carbon content from 0.1 to 0.3 wt%C. Austenite was transformed into a ferrite + pearlite microstructure due to the relatively low cooling rate (0.5 K/s). In this part, it is proposed to use the same set of alloys but for the observation of the microstructures changes resulting from a rapid cooling in magnetic field.

For this purpose, the new device developed during this work and described in the second chapter (part 2.3) is used to allow thermal treatments followed by water quenching (rapid cooling) in magnetic field up to 16 T.

4.2.1. Alloy composition and experiments

The alloys compositions of the three plain steels, their preparations and initial microstructures are described in part 3.3.1. Cylindrical specimens of 4 mm in diameter and 10 mm in height are used for experiment in magnetic field. For the experiments in 16 T, a 160 mm bore diameter resistive-magnet is used at the National High Magnetic Field Laboratory in

Grenoble. A key component of the experimental work is the ability to water cool the specimen inside the bore of the magnet in the homogeneous magnetic field zone. The magnetic field is imposed during the whole thermal treatment and temperature measurements are made using a type "S" (Pt-10%Rh) thermocouple spot welded on the surface of the specimen. The atmosphere is maintained by purging with argon.

Thermal treatment is as follows. The specimen is heated up to 1173 K at a rate of 5 K/s where the temperature is kept constant for 5 min. Then, the power is switched off and the sample is quenched by the cooperative displacement of both the furnace and the quenching bath along the vertical axis of the high field magnet. The rapid cooling rate is obtained by filling the quenching bath with cold water a few seconds before the quench. After that, the microstructures are characterised using optical and Scanning Electron Microscopy after applying standard polishing and etching techniques (4% Nital). The Vickers hardness of each specimen is measured to complete characterisation.

4.2.2. Microstructure resulting from high cooling rate in magnetic field

Temperature monitoring during fast cooling

The measured cooling curves from 1173 K are presented in Figure 4.3. More than 200 K/s is obtained by water quenching between 1173 K and 373 K. This measurement has to be taken with care since it corresponds to the temperature at the surface of the sample. However, due to its small thickness, thermal gradients inside the sample are assumed to be small. Moreover, the temperature of the bath is maintained constant and near 300 K during quenching and the volume of evaporated water is very small. In addition, no microstructure gradient from the surface to the centre of the specimen is found in the different samples treated by this way.

It is now proposed to observe the resulting microstructures. To this aim, optical microscopy and SEM are systematically used and attempts are done for the identification of phases involved in the different cases. The Figures correspond to micrographs of the microstructures at mid length of the longitudinal plane for each specimen. The magnetic field is always vertical in the Figures. It is in some cases not obvious to distinguish between martensite and bainite. However, we propose identification based on the phases morphology, neighbouring constituents and reaction with etching solution.
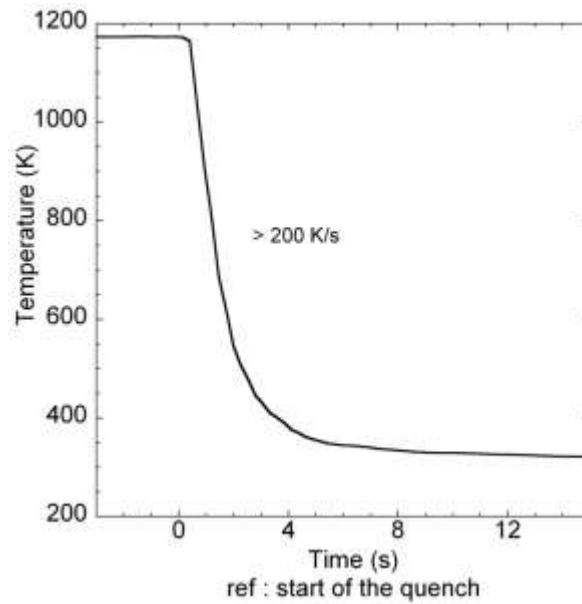
Figure 4.3   Temperature versus time signal monitored during the quench by water

The microstructures constituents are first described in details and the effect of magnetic field is then commented on [GARC09d, GARC09e].

Fe-1.5Mn-0.1C (wt%) cooled by water in magnetic field

Figure 4.4 shows optical microstructures corresponding to the Fe-1.5Mn-0.1C (wt%) plain steel quenched by water without and with 16T magnetic field. Figure 4.5 show SE Micrograph at higher magnification. Microstructure resulting from the experiment done in 10T magnetic field is not shown here.

First of all, the structure corresponding to the sample treated without magnetic field contains a large number of allotriomorphic ferrite grains (α) probably due to an insufficiently high cooling rate in the high temperature range. The grains are more or less equiaxed and appear in white on the optical micrograph after Nital etching. Typically, the allotriomorphic ferrite nucleates along the prior-austenite grain boundaries and then grows into the interior of the austenite grain [BRAD81, INDE03]. As the austenite transforms into ferrite (with less capacity than austenite to dissolve carbon), the excess carbon in the remaining austenite is available for eventual formation of cementite carbide. At low cooling rate, these carbides are usually formed of pearlite with a lamellar mixture of ferrite and cementite [HILL62].

However due to the high cooling rate, precipitation of pearlite (P) is not expected but martensite (α') and bainite (α_b) may be present in the structure [ASMH04].

Figure 4.4   Optical micrographs showing the structure obtained after water quenching for the Fe-0.1C-1.5Mn (wt%) under 0 and 16T magnetic field. Original magnification 500x, 4% nital etch.

Like pearlite, bainite is a two-phase structure that contains ferrite-cementite regions formed from the eutectoid decomposition of austenite [BHAD01]. However, the cementite particles in bainite are small and chunky, as compared to the cementite platelets of p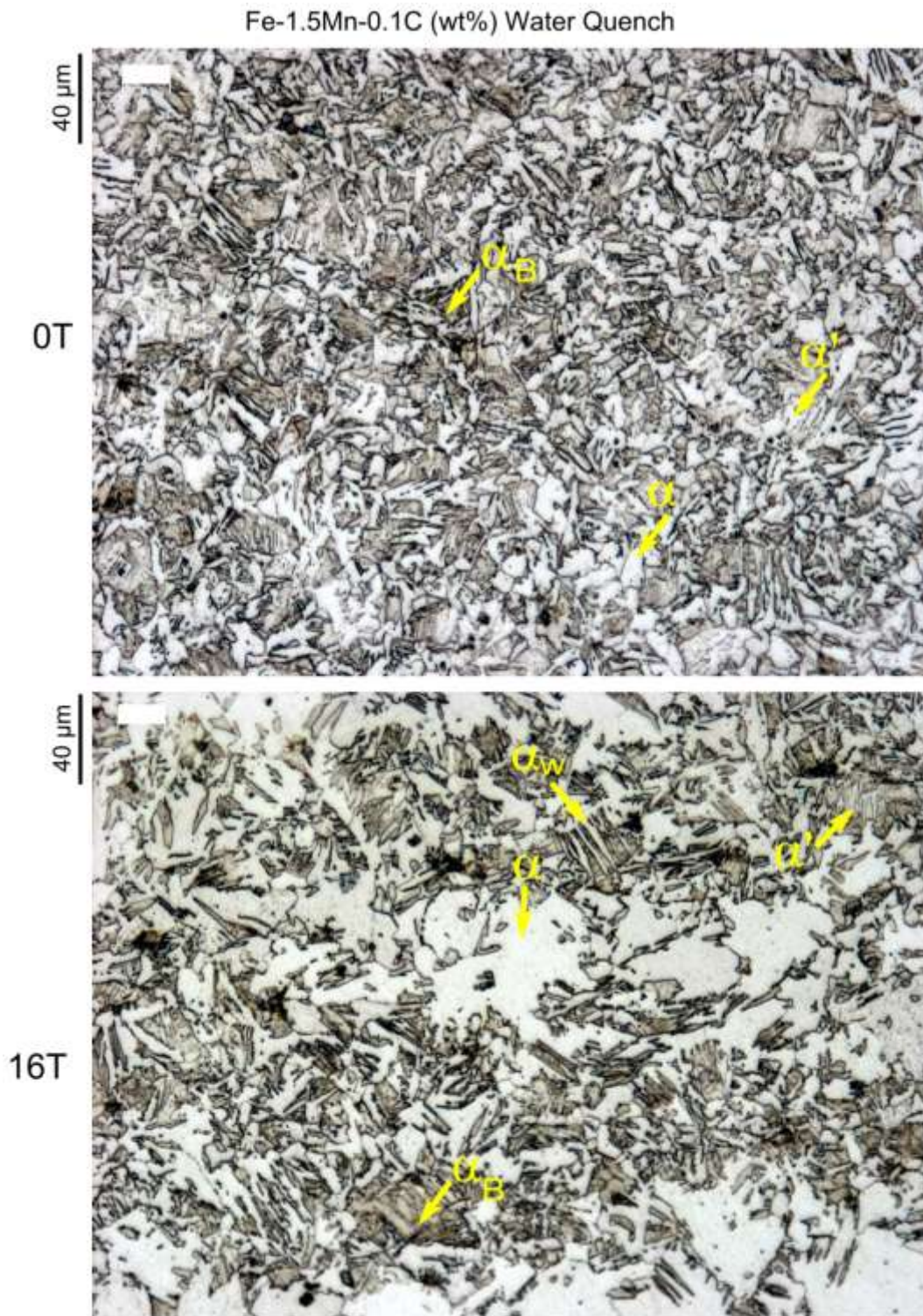earlite. The two-phase structure of bainite may appear similar to martensitic plates in light microscopy, while the small and chunky carbide particles are more apparent at higher magnification. The bainite usually etched dark because it is a mixture of ferrite and cementite, and the bainitic ferrite/cementite (α_b/θ) interfaces are easily attacked by the nital etchant used [ASMH04]. The residual phase is martensite which etches lighter because of the absence of carbide precipitates. It follows that it could be easy in some cases, using optical microscopy, to distinguish bainite and martensite as long as both phases are present in the microstructure.

In the micrograph shown in Figure 4.4 for the sample treated in zero fields, the remaining phases in between the ferrite grains seem to appear mainly as dark region which may thus correspond to bainite. Small regions which have not the morphology of equiaxed ferrite grain appear lighter and may be associated to the presence of martensite.

For confirmation, SE micrographs shown in Figure 4.5 helped for the identification of those phases. Contrary to optical micrographs, ferrite appears dark in a SEM and the presence of carbides is detected as lighter regions in the structure. As expected, no regular lamellar structure which could be characteristics of a pearlite colony is found in between the ferrite grains. This confirms that no pearlite has formed during the rapid cooling. However, parallel laths or needles of ferrite appear in Figure 4.5 which is a characteristic of upper bainite (α_b).

Upper bainite is a form of bainite that nucleates and grows at high transformation temperatures (near or in the lower-temperature region of pearlite formation). Nucleation of ferrite typically starts at the grain boundaries, and cementite (white phase in the micrograph) grows as elongated particles that are generally oriented parallel to the direction of growth of the ferrite laths [BHAD01, ASMH04]. The cementite forms near the ferrite, because the nucleation ability of the ferrite in this temperature range is much greater than the diffusion of excess carbon near the newly formed ferrite.
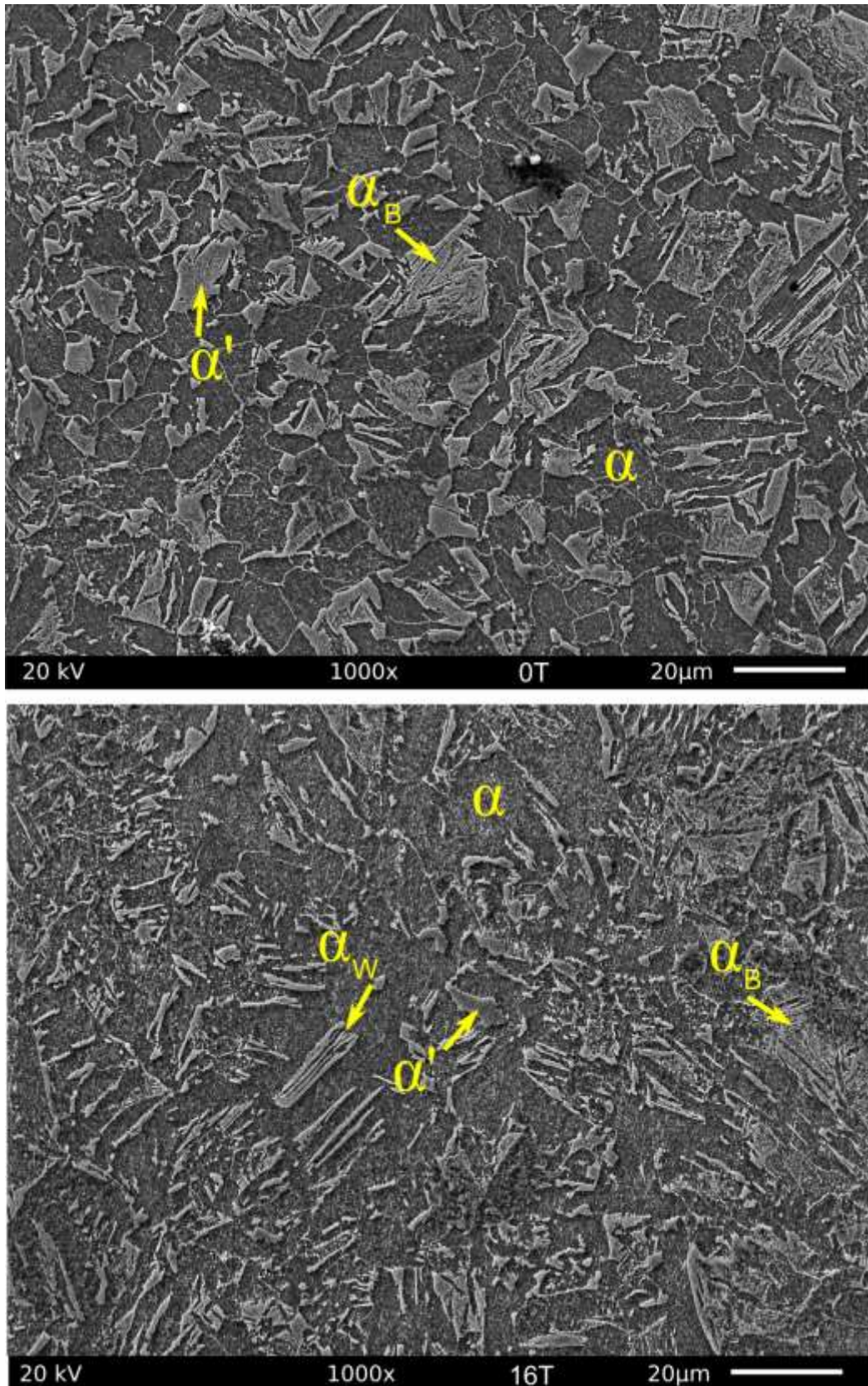
Figure 4.5   SEM micrographs showing the structure obtained after water quenching under 0 and 16 T for the Fe-0.1C-1.5Mn (wt%) Original magnification 1000x, 4% nital etch

Beside allotriomorphic ferrite grains and upper bainite, the remaining phase in Figure 4.5 may be either associated to martensite since no carbide or any substructure is observed inside or either associated to retained austenite which may still be present in a rapidly cooled carbon steel when the transformation ceases [ASMH04]. Martensite is expected by the presence of lighter regions detected by optical micrograph in Figure 4.4. However, the morphology of this remaining phase does not appear as lath or plates of martensite so that further investigations such as High Resolution Electronics microscopy (FEG) are needed for a correct description of this remaining phase.

The effect of magnetic field is evidenced in the optical micrograph shown in Figure 4.4. The amount of ferrite is drastically increased in the 16T sample. Moreover, in addition to the stabilisation of allotriomorphic ferrite, Widmanstätten ferrite (α_w) can also be observed in the 16 T micrograph shown in Figure 4.4 [PHIL98]. This white-etching wedge-shaped Widmanstätten ferrite plates have grown from the prior-austenite boundaries in rejecting any excess of carbon into austenite. This phase is not observed in the 0 T sample. The presence of small spherical precipitates of carbide dispersed inside the ferrite grains is not well understood yet but is probably due to oxide precipitation during polishing.

As a summary for this microstructure analysis of the 0.1%C alloy, it appears that ferrite is promoted by the magnetic field since the fraction of ferrite grain is increased.

Fe-1.5Mn-0.2C (wt%) cooled by water in magnetic field

Figure 4.6 shows the optical micrographs corresponding to the Fe-1.5Mn-0.2C (wt%) alloy water quenched without magnetic field and under 16 T magnetic field. In the 0 T sample, the amount of allotriomorphic ferrite (α) is very low compared to the previous 0.1wt%C alloy.

Only several islands of allotriomorphic ferrite are observed in the 0 T sample. The allotriomorphic ferrite grows rapidly along the austenite grain boundary (which is an easy diffusion path) but thickens more slowly [HILL60]. This may explain the elongated shape of some allotriomorph grains. Besides, the microstructure is composed of a mixture of bainite (α_B) and martensite (α'). As explained before, the bainite is etched dark in optical micrograph and the martensite appears lighter. However, any accurate distinction between the two phases is not obvious.

Figure 4.6   Optical micrographs showing the structure obtained after water quenching under 0 and 16 T for the Fe-0.2C-1.5Mn (wt%) Original magnification 500x, 4% nital etch

Application of 16T magnetic field leads to a considerable increase in the allotriomorphic ferrite fraction along the prior austenite grains boundaries. In addition, a large amount of Widmanstätten ferrite (α_w) is detected by the presence of thin-wedge plates which

have grown from the prior austenite grain boundaries. The Widmanstätten ferrite plates are white because of the lack of structure within the plates, whereas bainite etches relatively dark.

Figure 4.7 and Figure 4.8 show SE micrographs of the samples treated with and without 16 T magnetic fields. In the 0 T sample, the allotriomorphic ferrite grains (α) are easily identified. The matrix appears more clearly than by optical means but the distinction between bainite and martensite is not obvious. Inter-particles of cementite (light grey in the SE micrograph) are however well identified between the ferrite plates which may indicate the presence of bainite. The martensite can be seen here as a structure in which no internal structure appear. But extreme care must be taken to this distinction since the morphology of martensite depends on the carbon content and formation temperature which are unknown parameters in the experiment. In the 16T sample, the allotriomorphic ferrite and Widmanstätten ferrite plates (dark constituents in the SE micrographs) are well defined and are located in the prior austenite grain boundaries. The cementite precipitates due to the presence of bainite appear less clearly than for the 0 T sample and it is still very complex to distinguish martensite and bainite. However, the matrix has incontestably not the same morphology after cooling in magnetic field and a modification in its formation temperature is highly expected from this difference.

In Figure 4.8, the different morphologies of the ferrite grains appear clearly. From small allotriomorphic ferrite grains present in the 0 T sample, large ferrite grains with Widmanstätten ferrite (α_w) plates are observed in the 16 T sample. In between the plates of Widmanstätten ferrite, no precipitate or substructure is observed even at high magnification probably due to the absence of carbide precipitation which may indicate the presence of martensite.

These modifications in the resulting microstructure by the application of a static magnetic field may be interesting from an industrial point of view when a mixture of ferrite, bainite and martensite is desired. Indeed magnetic field plays a role similar to that of an alloying element often adding in the alloy for the stabilisation of ferrite even at high cooling rate.

In the same idea, the possibility to obtain a structure composed of ferrite, martensite and bainite at a very high cooling rate may be interesting from an economic point of view. These structures are regularly obtained at an intermediate cooling rate. Application of magnetic field allows the imposition of higher cooling rate without changing the resulting structure and thus reduced the time for cooling a workpiece.

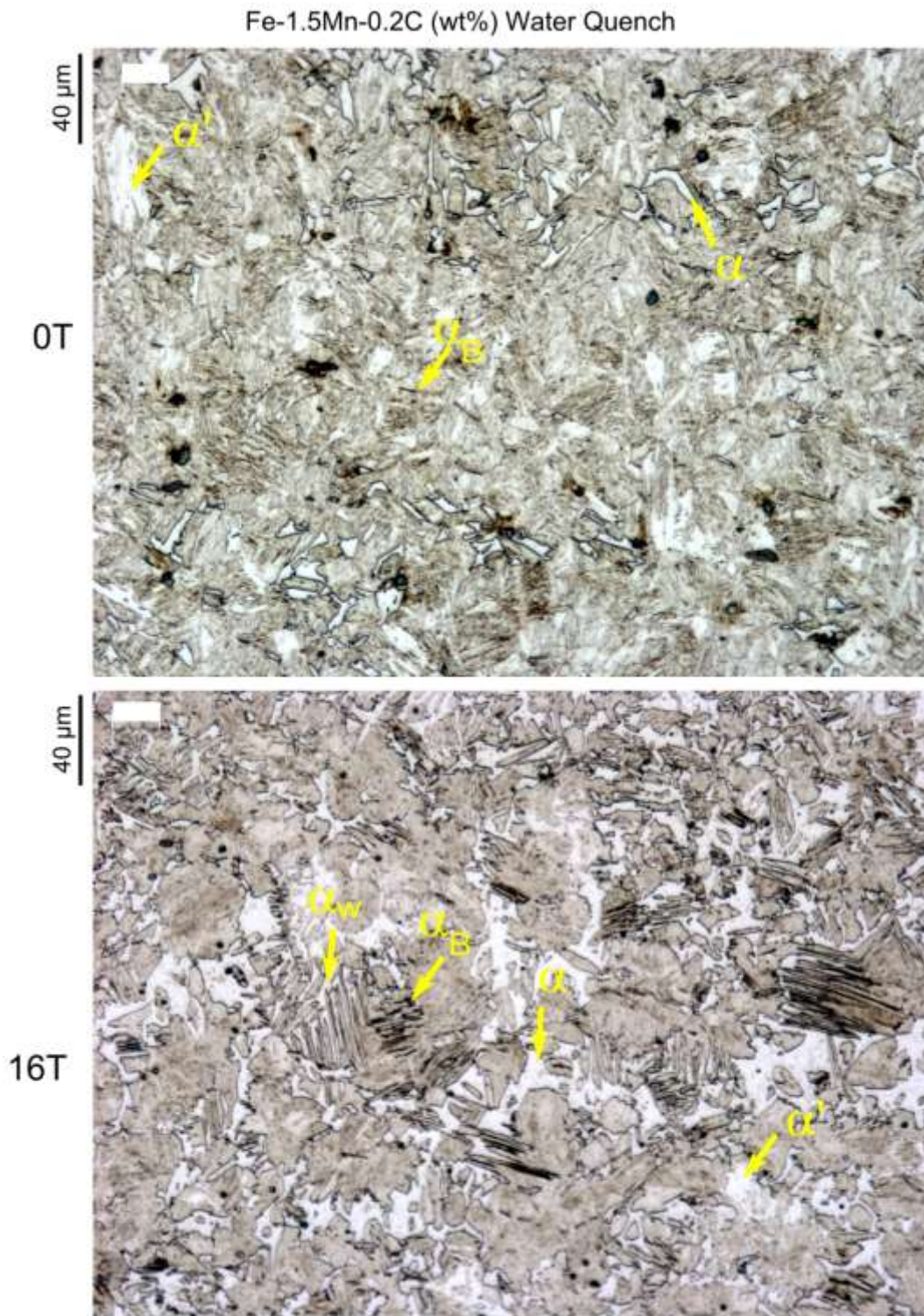Figure 4.7   SEM micrographs showing the structure obtained after water quenching under 0 and 16 T for the Fe-0.2C-1.5Mn (wt%) Original magnification 1000x, 4% nital etch
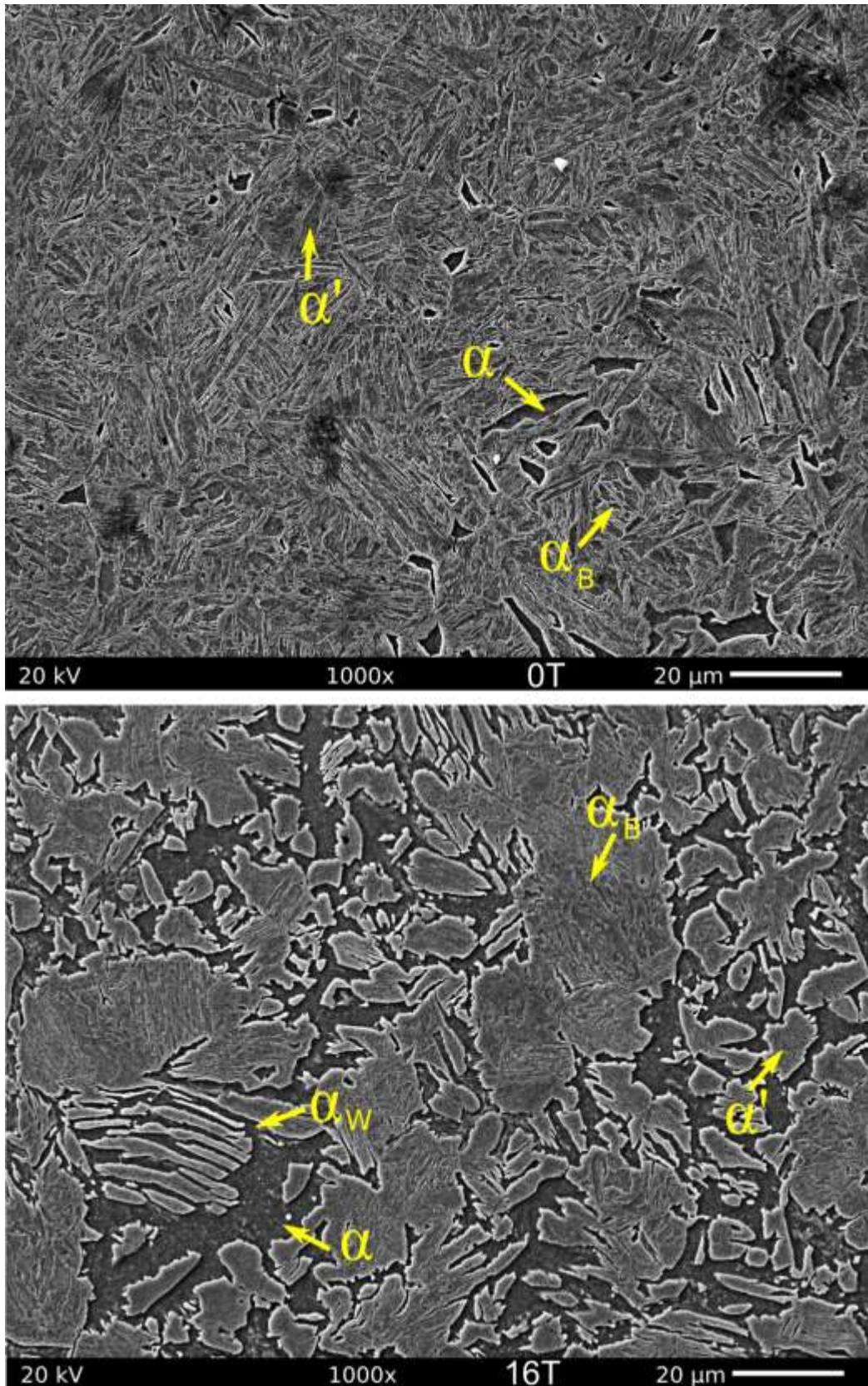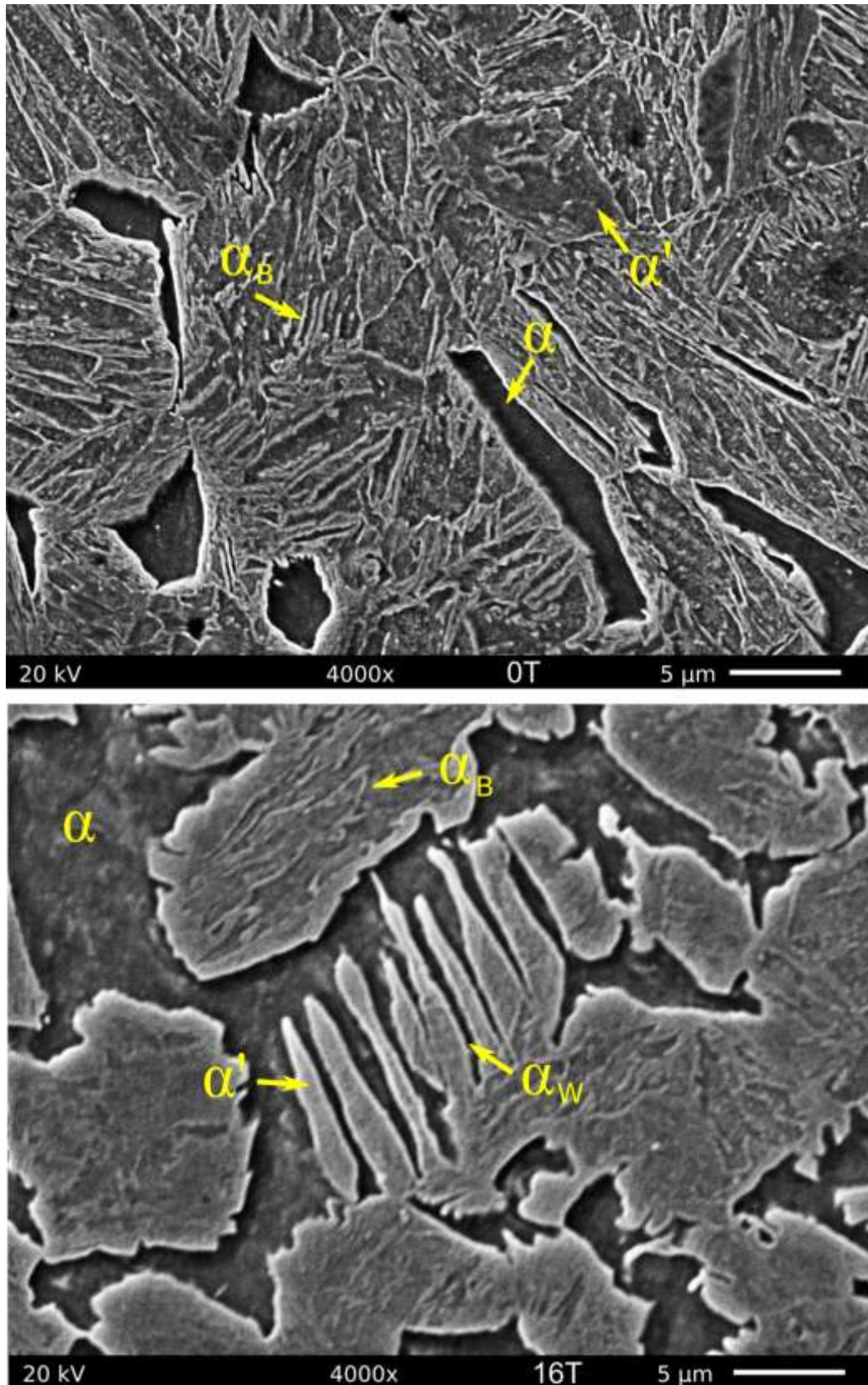
Figure 4.8   SEM micrographs showing the structure obtained after water quenching under 0 and 16 T for the Fe-0.2C-1.5Mn (wt%) Original magnification 4000x, 4% nital etch

Fe-1.5Mn-0.3C (wt%) cooled by water in magnetic field

Figure 4.9 shows optical micrographs of the Fe-1.5Mn-0.3C (wt%) steel grades cooled by water with and without 16T magnetic field. In the 0 T sample, no allotriomorphic ferrite is observed probably due to the relatively high carbon content in alloy. The microstructure is composed of a mixture of bainite and martensite. As usual, the martensite region appears lighter in optical micrograph but boundaries between martensite and bainite are not well defined. When the transformation occurs with 16T magnetic field, the microstructure is predominantly martensite but also has allotriomorphic ferrite, Widmanstätten ferrite, bainite and even pearlite. The martensite structure can be here referred to as lath martensite which consists of martensite needles with different but well-defined orientations. Notice that the spherical shape of pearlite colonies is obvious in this sample because of the lack of impingement with other pearlite colonies. Notice also that pearlite, unlike bainite, grows across the austenite grain boundaries.

Figure 4.10 shows SE micrographs of the sample treated without magnetic and with 16T magnetic field. In the 0 T sample, cementite precipitates are visible within the plates which may indicate the predominance of bainite in the microstructure but martensite is also expected under the form of large plates growing across the austenite grain. In the sample treated with 16 T magnetic fields, the morphology of the matrix is again totally different than that for the 0 T sample. Non-negligible amount of allotriomorphic ferrite has grown along the prior austenite grain boundaries. In some cases, plates of Widmanstätten ferrite have grown from the allotriomorphic ferrite. In other, needles with a distinctly more lenticular shape could be associated to bainite. In addition, pearlite colonies are well visible.

The third picture of Figure 4.11 shows a complete set of Widmanstätten ferrite plates growing form the allotriomorphic ferrite at a prior austenite grain boundary. It is interesting to notice the thickness of the plates. The strain energy due to the shape deformation when an individual plate of Widmanstätten ferrite forms is generally very high and cannot be tolerated at the low driving-force where it grows. As a consequence, two back-to-back plates which accommodated each other's shape deformation grow simultaneously in some cases (indicated by a black arrow) and dramatically reduce the strain energy. However, this phenomenon requires the simultaneous nucleation of appropriate crystallographic variants and thus the probability of nucleation is reduced. This can often lead to the coarse character of this structure [WATS73].
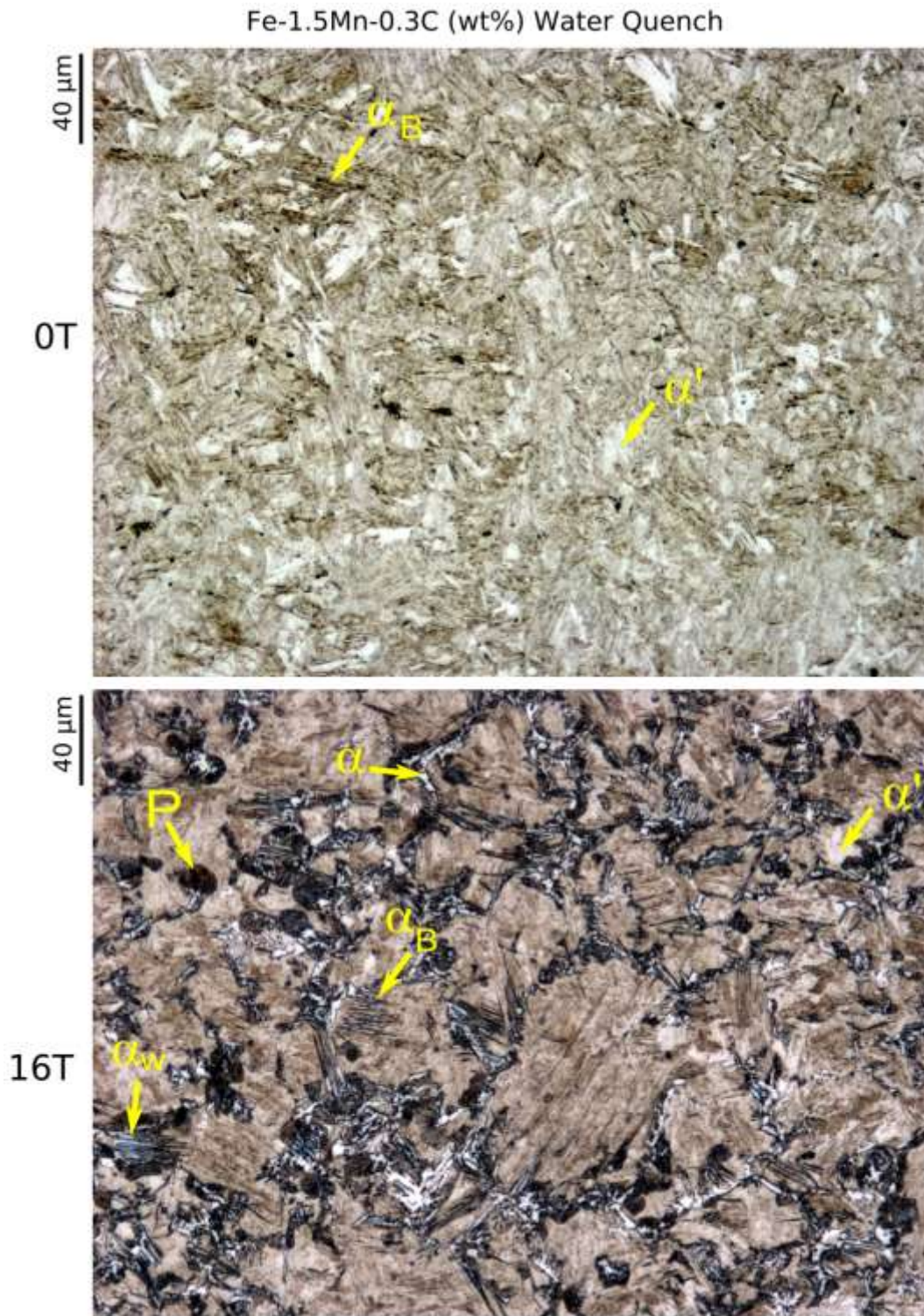
Figure 4.9   Optical micrographs showing the structure obtained after water quenching under 0 and 16 T for the Fe-0.3C-1.5Mn steels (wt%) . Original magnification 500x, 4% nital etch
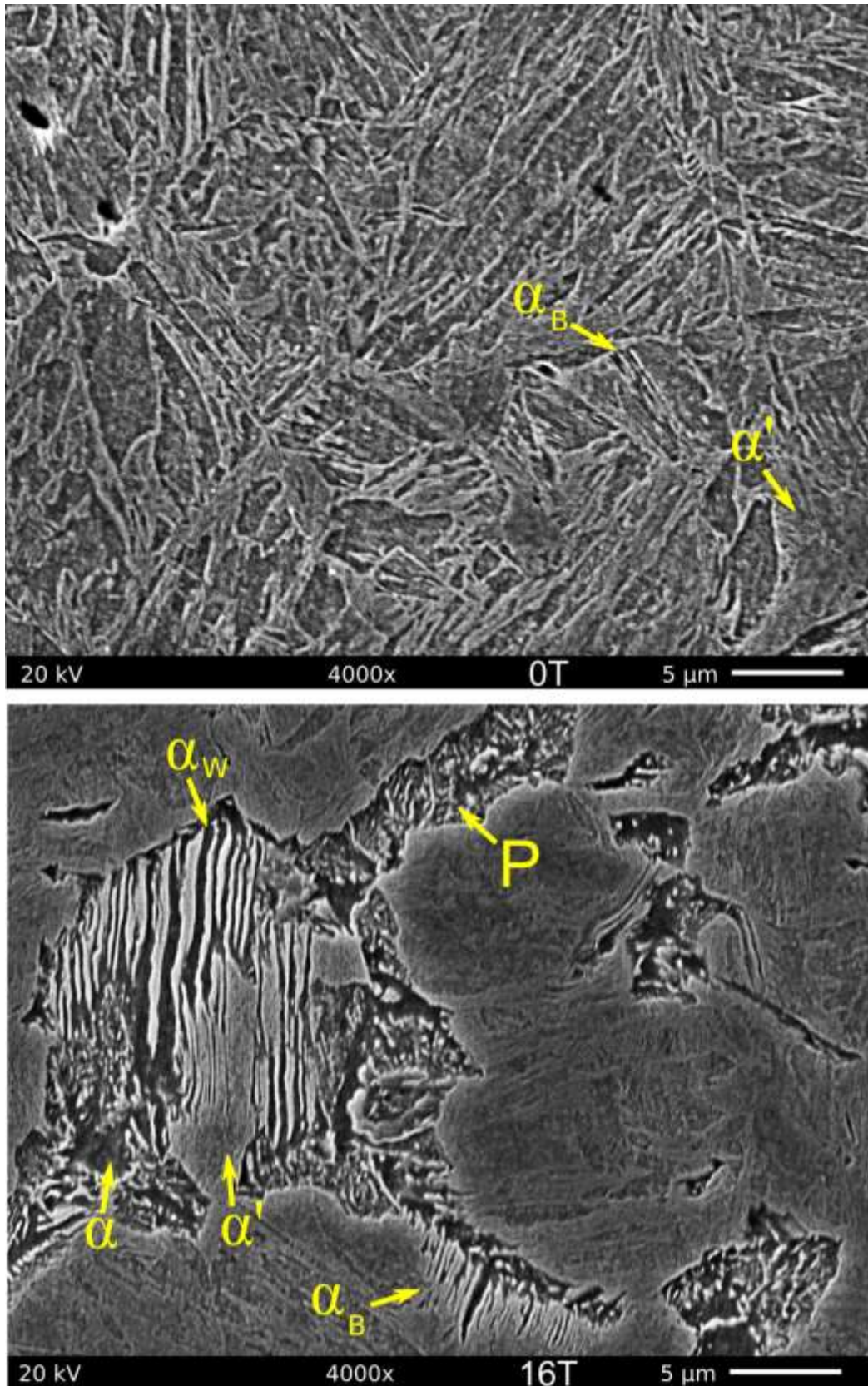
Figure 4.10   SEM micrographs showing the structure obtained after water quenching under 0 and 16 T magnetic field for the Fe-0.3C-1.5Mn steels (wt%) . Original magnification 4000x, 4% nital etch
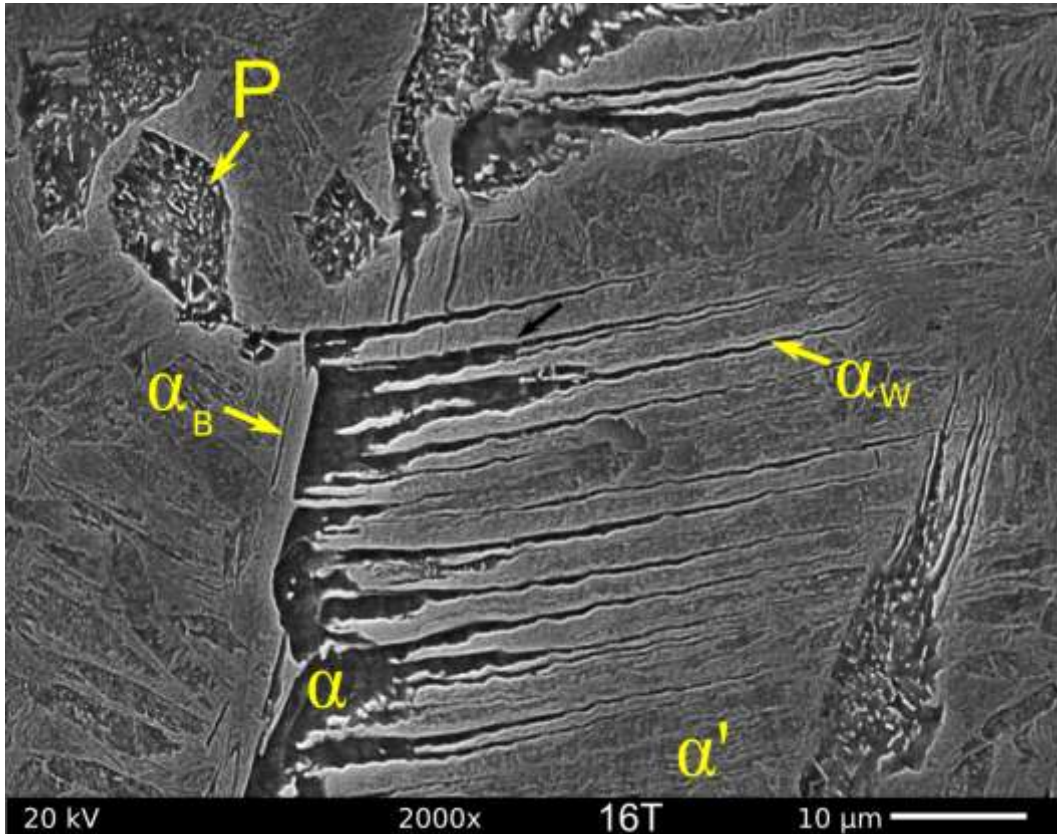
Figure 4.11   SEM micrographs showing the structure obtained after water quenching under 16 T for the Fe-0.3C-1.5Mn steels (wt%) . Original magnification 2000x, 4% nital etch

Impact of field on the resulting Hardness of structure

In Figure 4.12 is shown the Vickers hardness measurement performed for the different alloys composition after thermal treatment with and without the presence 10 and 16T magnetic field. First of all, increase in carbon content leads to an increase in the resulting hardness. The red circle shown the data obtained after thermal treatment under 1.2T in the CRM laboratory with an electro-magnet. Good agreement is found with our data that may validate the conditions obtained in the new furnace.

The application of a strong magnetic field during the thermal treatment results in a general decrease in the hardness values. This reduction of the hardness is due to the enhancement of the precipitation of ferrite in the alloys treated in magnetic field.
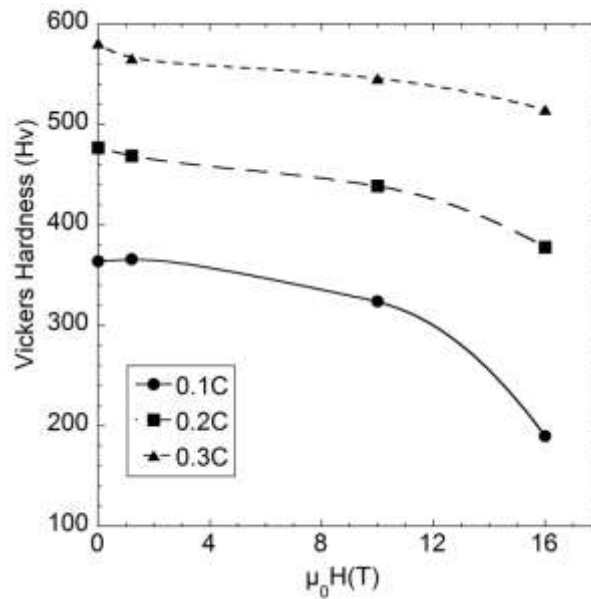
Figure 4.12   Vickers Hardness value of the Fe-xC-1.5Mn (wt%) steels with x = 0.1, 0.2 and
0.3 wt%C water cooled in zero field and under 16T magnetic field.

4.2.3. Conclusion

Fe-1.5wt%Mn-xC with x = 0.1, 0.2, 0.3 wt% steels have been water quenched in a setup especially designed to be inserted in a 16T magnet.

Under normal cooling conditions (zero fields), in the 0.1wt%C alloy, the cooling rate seems to be not sufficiently high for the complete decomposition of austenite into a bainite and martensite structure and a large amount of allotriomorphic ferrite is observed. However, this amount is still enlarged drastically by the application of a magnetic field. In the 0.2wt%C alloy, the microstructure is almost fully martensitic and bainitic in the sample treated without magnetic field and is composed of an intimate mixture of ferrite, Widmanstätten ferrite, bainite and martensite when a magnetic field is applied during transformation. In the 0.3wt% carbon, the microstructure is fully martensitic under normal conditions and the application of magnetic field leads to the formation of allotriomorphic ferrite in the prior austenite grain, thin-shape Widmanstätten ferrite plates and spherical shape pearlite colony in a matrix constituted of a mixture bainite and martensite.

Even if the distinction between bainite and martensite is not obvious in each case, the morphology of the mixture is incontestably modified by the application of magnetic field which seems to indicate a large modification in the formation temperature and the promotion of stable phases. Hardness measurements are consistent with image analysis.

4.3. Changes in the microstructure resulting from high cooling rate in Fe-C-Mn-xSi alloys in magnetic field

Magnetic field impact on the austenite decomposition into ferrite + pearlite has been investigated in part 3.4 with a set of four Fe-0.15C-1.5Mn-xSi (wt%) steels, with x = 0.015 (A), 0.55(B), 1.05(C) and 1.75(D) wt%Si. It is proposed in this part to study the impact of magnetic field on the microstructure resulting from a rapid cooling in these four alloy compositions. Resulting microstructures are described in terms of phase fraction and Vickers hardness.

4.3.1. Alloy composition and experiments

The alloy compositions are shown in Table 3.3 in part 3.4.1. The alloy preparation is described in part 3.4.1. Test specimens are cylindrical ingots with dimension of 4 mm in diameter and 10 mm in height. The magnetic field is imposed during the whole heat treatment. Temperature measurements are performed using a type "S" (Pt-10%Rh) thermocouple spot welded onto the top surface of the specimen.

The samples are heated at 5 K/s up to 1173, 1198, 1208 and 1248 K respectively for the steels grades A, B, C and D and held for 5 min in order to achieve complete austenitisation. They are then cooled down to room temperature in a 300 ml water bath ~~at 300 K~~. Thermal treatments are reproduced under 0, 10 and 16 T magnetic field. The microstructures are characterized using optical and SE microscopy applying standard polishing and etching techniques (4% Nital).

4.3.2. Effect of magnetic field on transformed microstructures

Temperature monitoring during fast cooling

The end of a typical thermal treatment in the experimental setup is shown in Figure 4.13. The measured cooling rates are higher than 200 K/s. No recalescence in the temperature measurement associated with austenite decomposition is observed in the signal.
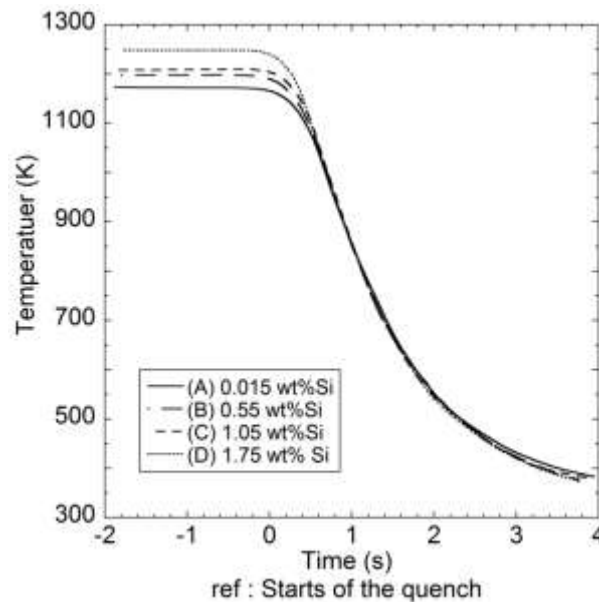
Figure 4.13   Temperature versus time signal monitored during the water quench

Magnetic field impact on microstructure observed by image analysis

Figure 4.14 shows optical micrographs of the Fe-1.5Mn-0.15C-0.015Si (wt%) steel A cooled by water without magnetic field and in 10 and 16 T magnetic field. In the sample treated without magnetic field, the microstructure is composed mainly of a mixture a bainite and martensite. The prior austenite grain boundaries are well detected since very small grains of ferrite (α) have begun to grow from the boundary. As previously described, in part 4.2.2, the bainite appears in dark and martensite is relatively lighter. The application of a magnetic field during the thermal treatment leads to an increase in the thickness of the allotriomorphic ferrite grains. Widmanstätten ferrite is also observed in the 10 and 16 T samples.

The SE micrographs of the samples treated without and with 16T magnetic field are shown in Figure 4.15. Ferrite needles surrounded by cementite precipitates are visible in the 0 T sample and correspond to the presence of bainite. The dark region without any precipitate of cementite (white regions in optical micrograph) is probably martensite because it is

relatively easy to distinguish from bainite regions. The small and spherical-shape allotriomorphic ferrite grains are visible along the prior austenite grain boundaries together with the thin and characteristic shape of the Widmanstätten ferrite plates. In the micrographs corresponding to the 16 T sample in Figure 4.15, the increase in ferrite fraction appears clearly. The Widmanstätten ferrite plates are coarser than without magnetic field. The growth rate of the plate may thus have been increased by the presence of magnetic field. However some martensite and bainite regions are still observed in the structure.

In Figure 4.16 and Figure 4.17 are shown respectively the optical and SE micrograph of the Fe-1.5Mn-0.15C-0.55Si (wt%) steel B treated with and without magnetic field. The phases involved in the sample treated without application of magnetic field are similar to those described in the previous paragraph for steels A. Application of magnetic field also leads to a similar effect that is a general increase in the allotriomorphic ferrite fraction and in the thickness of Widmanstätten ferrite plates.

Figure 4.18 and Figure 4.19 show the microstructure for the Fe-1.5Mn-0.15C-1.05Si (wt%) steel C. Again in this composition, the application of a magnetic field leads to an important modification of the resulting microstructure as already observed in alloys A and B. From a mixture of martensite and bainite in the sample treated without magnetic field, the structure composition shifts to allotriomorphic ferrite, coarse Widmanstätten ferrite, bainite and martensite when cooling occurs under the application of a 16T magnetic field. Figure 4.20 allows the fine observation of the morphology in the sample treated without and with 16T magnetic field. The bainitic ferrite plates of several micrometers in length are observed in the 0 T sample surrounded by cementite precipitates parallel to the ferrite plates. In the 16T sample large grains of allotriomorphic ferrite are predominant in the structure. White appearing precipitates elongated in between the Widmanstätten ferrite plates may be associated to the precipitation of cementite.

The optical microstructures corresponding to the Fe-1.5Mn-0.15C-1.75Si (wt%) steel D are shown in Figure 4.21 for 0, 10 and 16T. Due to the relatively high silicon content and contrary to the three previous alloys, some allotriomorphic ferrite grains have grown from prior austenite boundary in the sample treated without any magnetic field. However, the ferrite fraction is as usually increased by the application of a magnetic field. Both allotriomorphic ferrite and Widmanstätten ferrite are seen in the structure. Corresponding SE micrograph are shown in Figure 4.22 for the sample treated without and with 16T magnetic field. The increase in the allotriomorphic ferrite fraction appears clearly.

A Fe-0.15C-1.5Mn-0.015Si (wt%) Water Quench

Figure 4.14   Optical micrographs of the Fe-1.5Mn-0.15C-0.015Si (wt%) steels A water quench under 0, 10 and 16T. Original magnification 500x, 4% nital etch

Figure 4.15   SEM micrographs of the Fe-1.5Mn-0.15C-0.015Si (wt%) steels A water quench under 0 and 16T. Original magnification 1000x, 4% nital etch

Figure 4.16   Optical micrographs of the Fe-1.5Mn-0.15C-0.53%Si (wt%) steels B, water quench under 0, 10 and 16T. Original magnification 500x, 4% nital etch

Figure 4.17   SEM micrographs of the Fe-1.5Mn-0.15C-0,53%Si (wt%) steels B, water quench under 0, 10 and 16T. Original magnification 1000x, 4% nital etch

C Fe-0.15C-1.5Mn-1.05Si (wt%) Water Quench
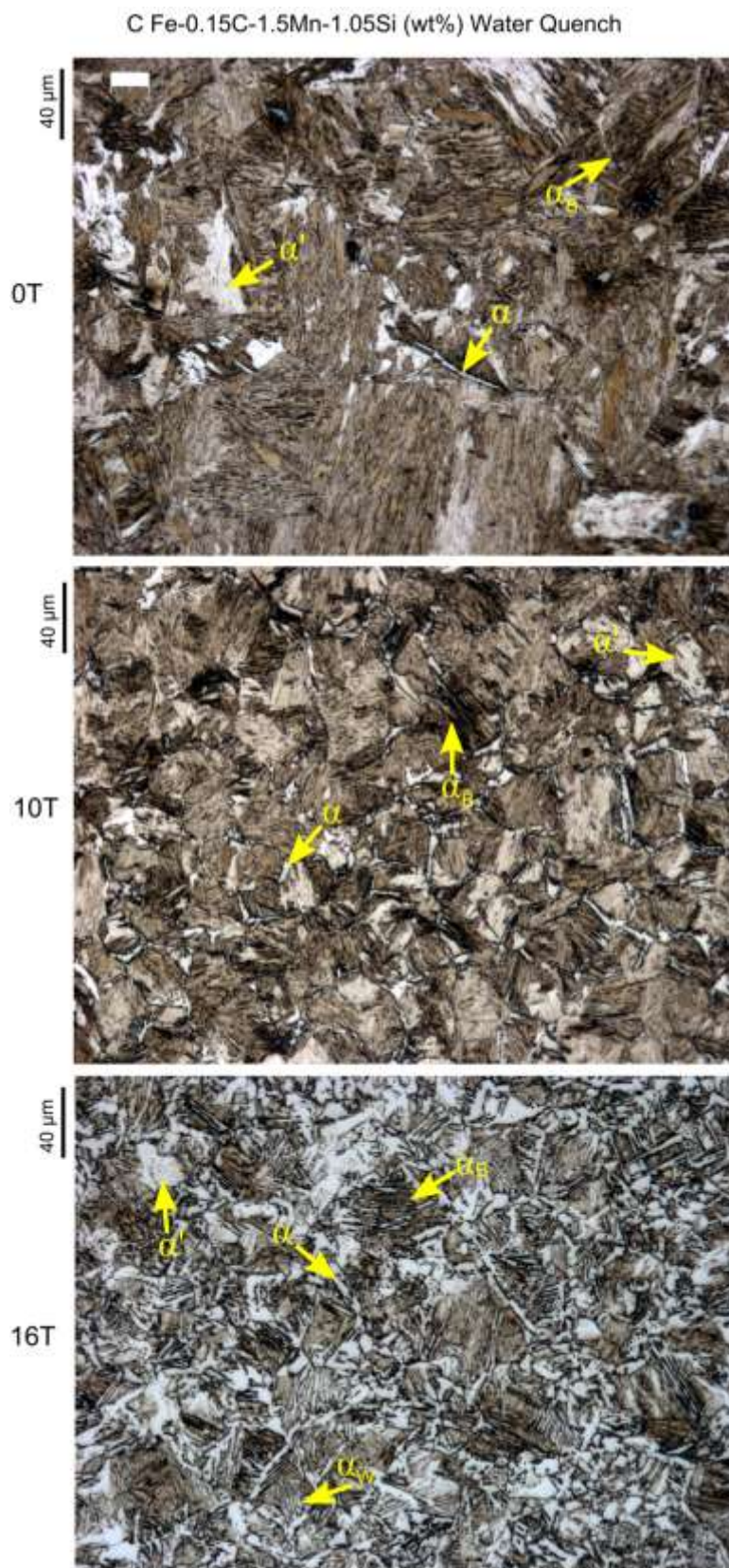
Figure 4.18   Optical micrographs of the Fe-1.5Mn-0.15C-1.05Si (wt%) steels C water quench under 0, 10 and 16T. Original magnification 500x, 4% nital etch
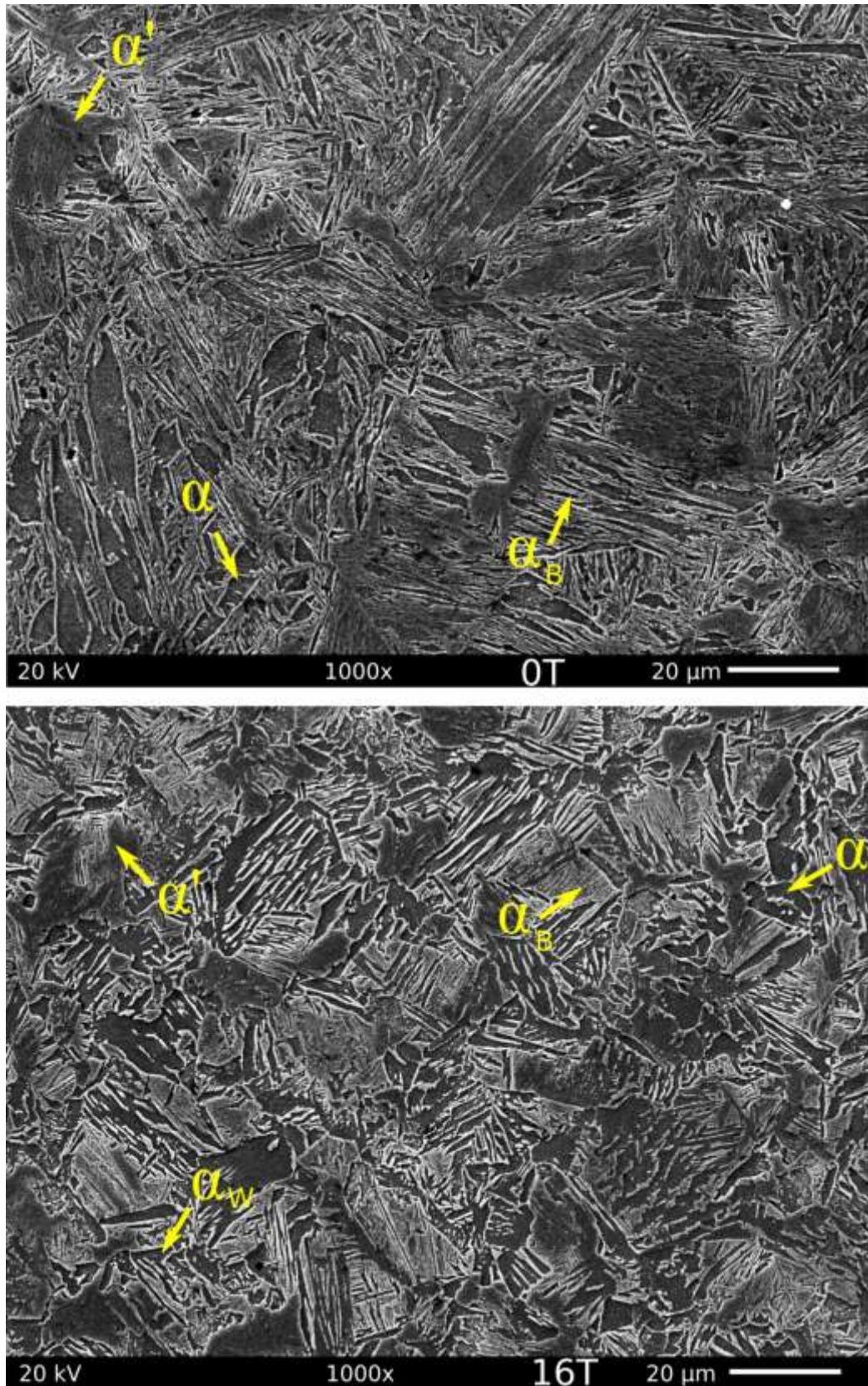
Figure 4.19   SEM micrographs of the Fe-1.5Mn-0.15C-1.05Si (wt%) steels C water quench

under 0 and 16T. Original magnification 1000x, 4% nital etch
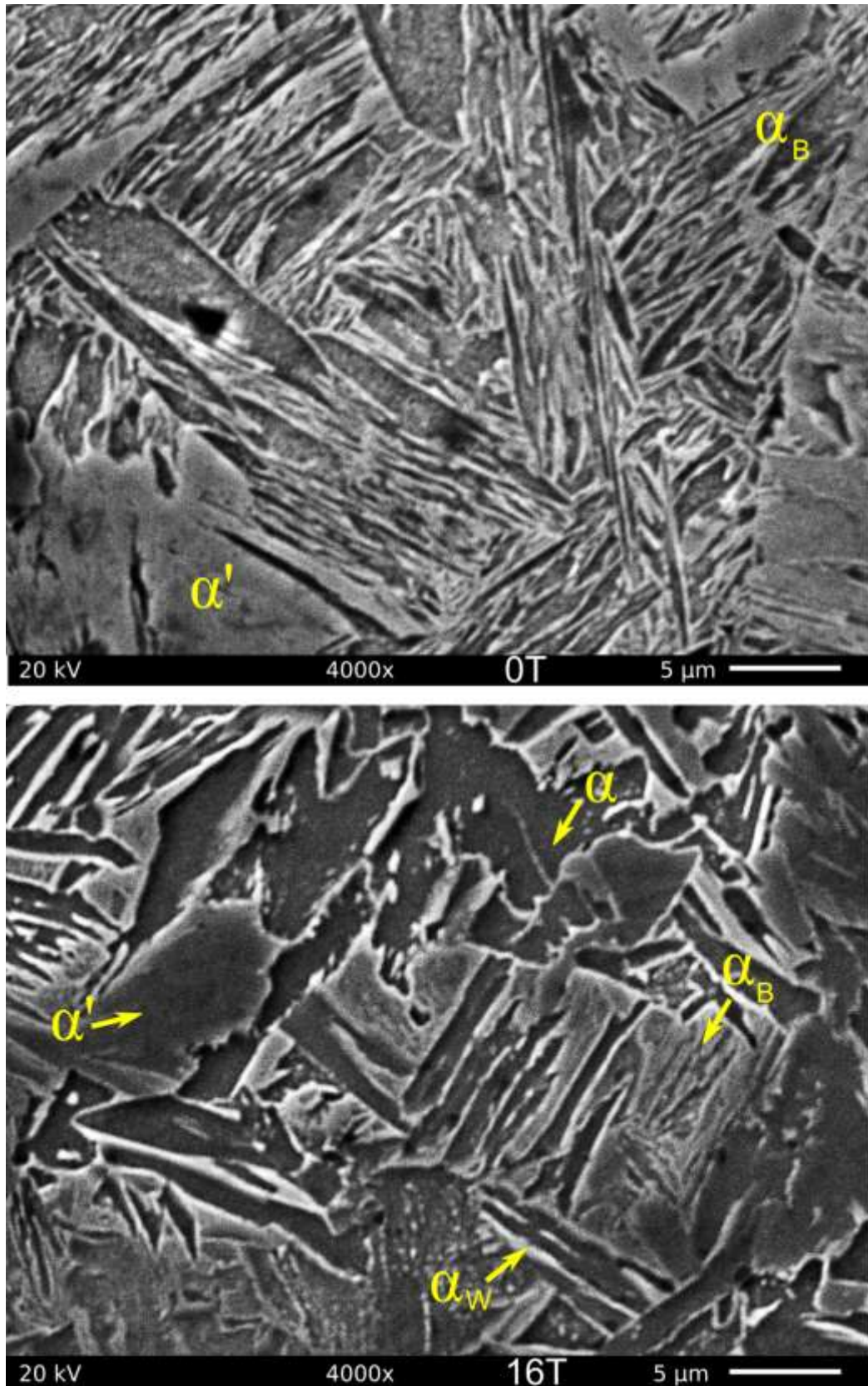
Figure 4.20   SE micrographs of the Fe-1.5Mn-0.15C-1.05Si (wt%) steels C water quench

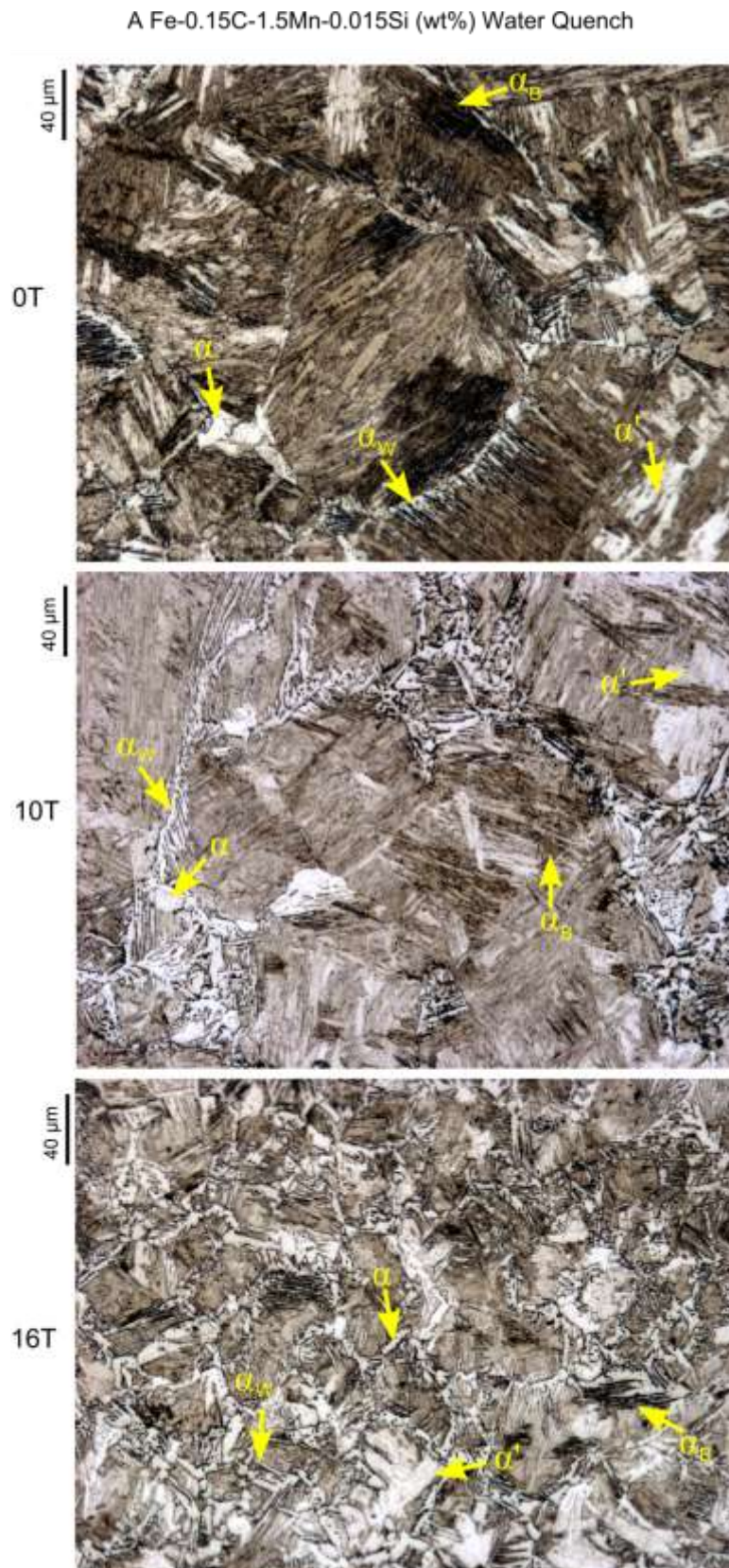under 0 and 16T. Original magnification 4000x, 4% nital etch
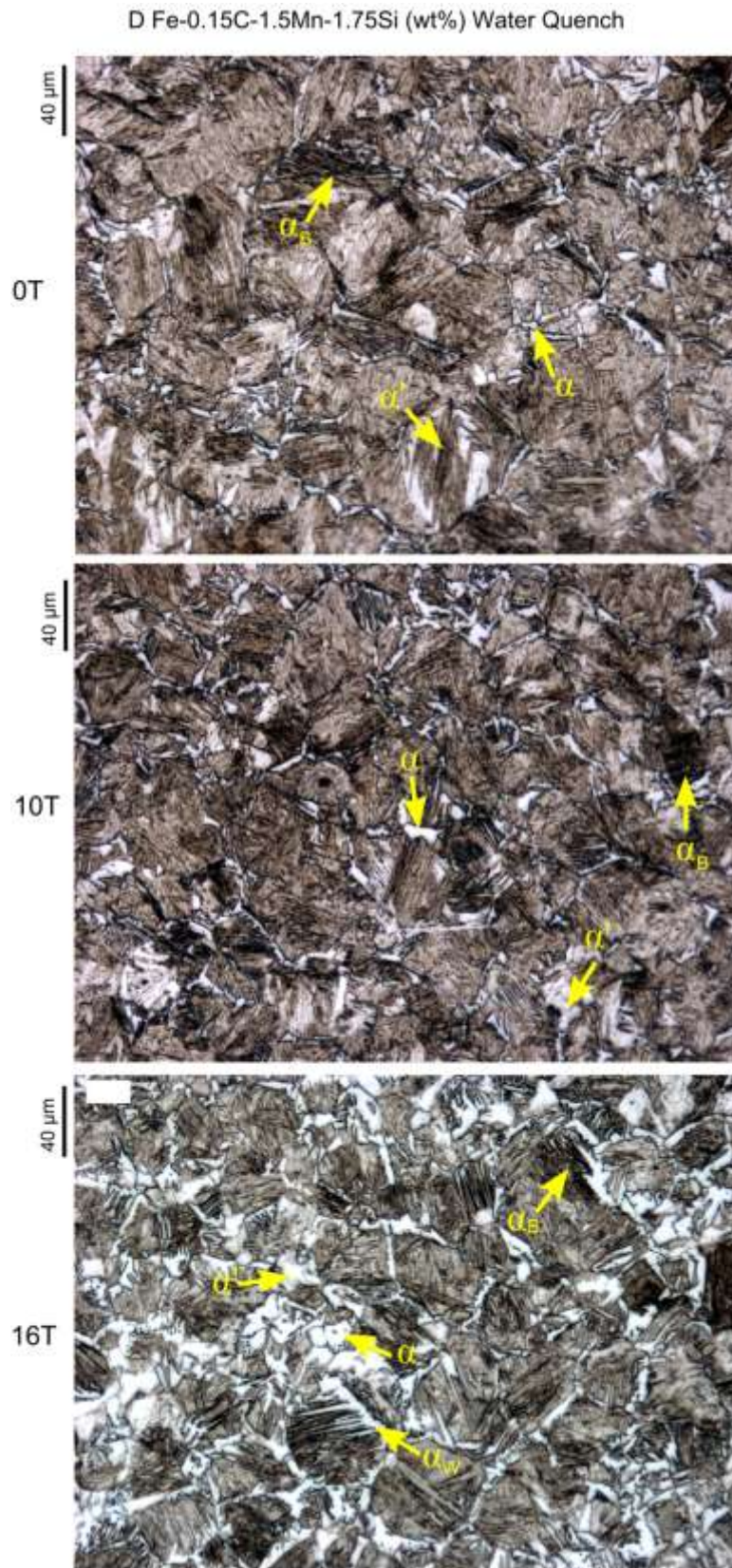
Figure 4.21   Optical micrographs of the Fe-1.5Mn-0.15C-1.75Si (wt%) steels D water quench under 0, 10 and 16T. Original magnification 500x, 4% nital etch
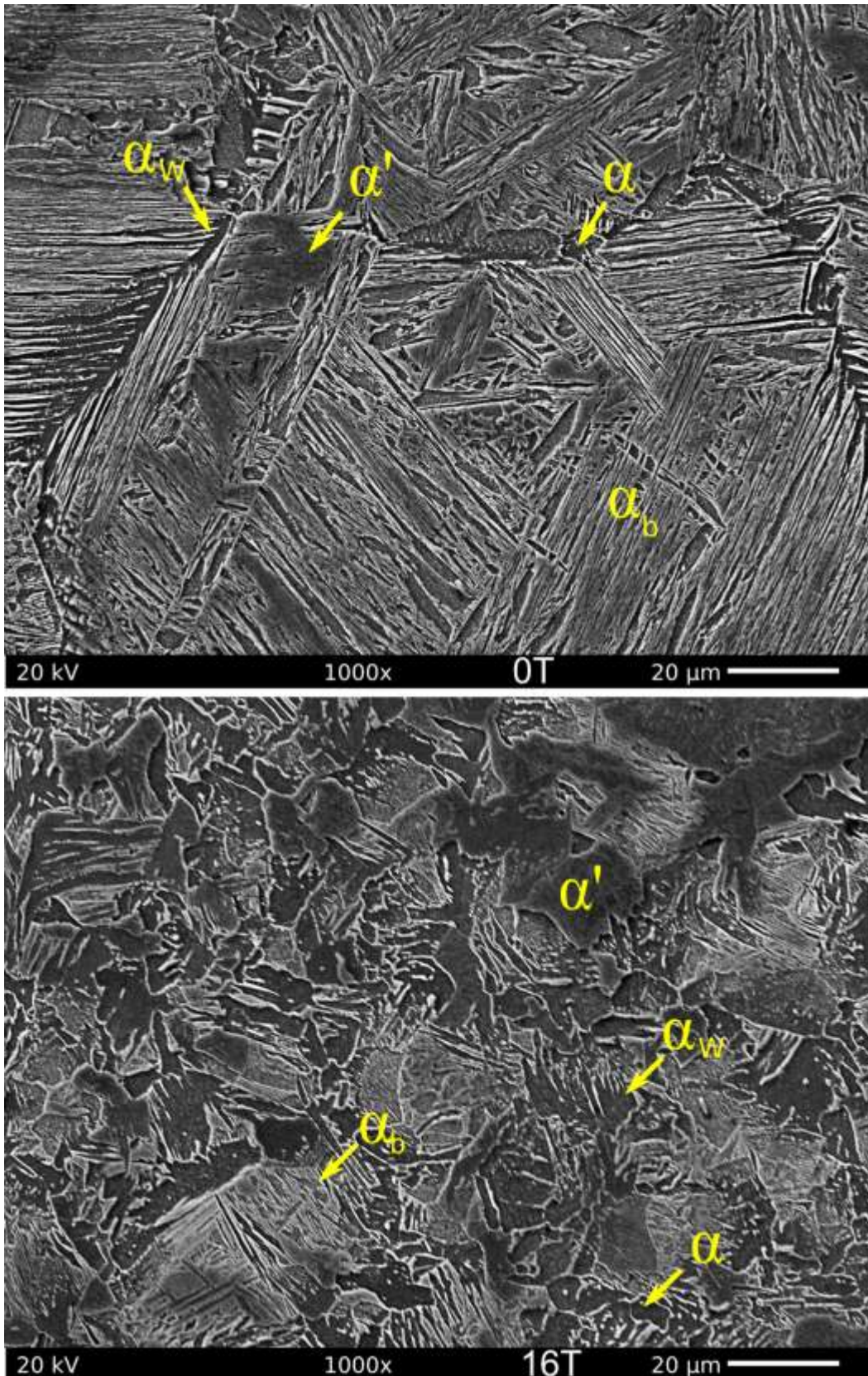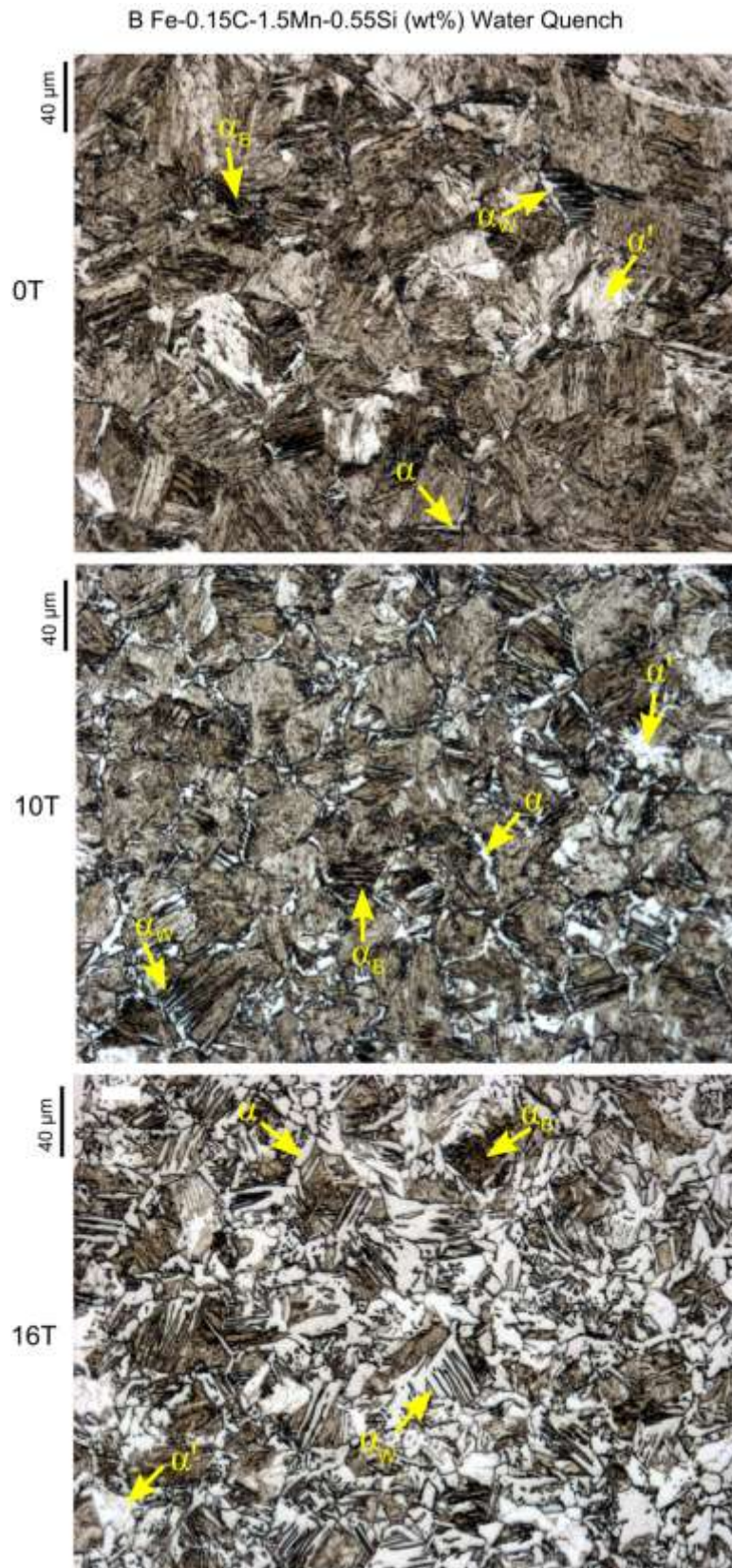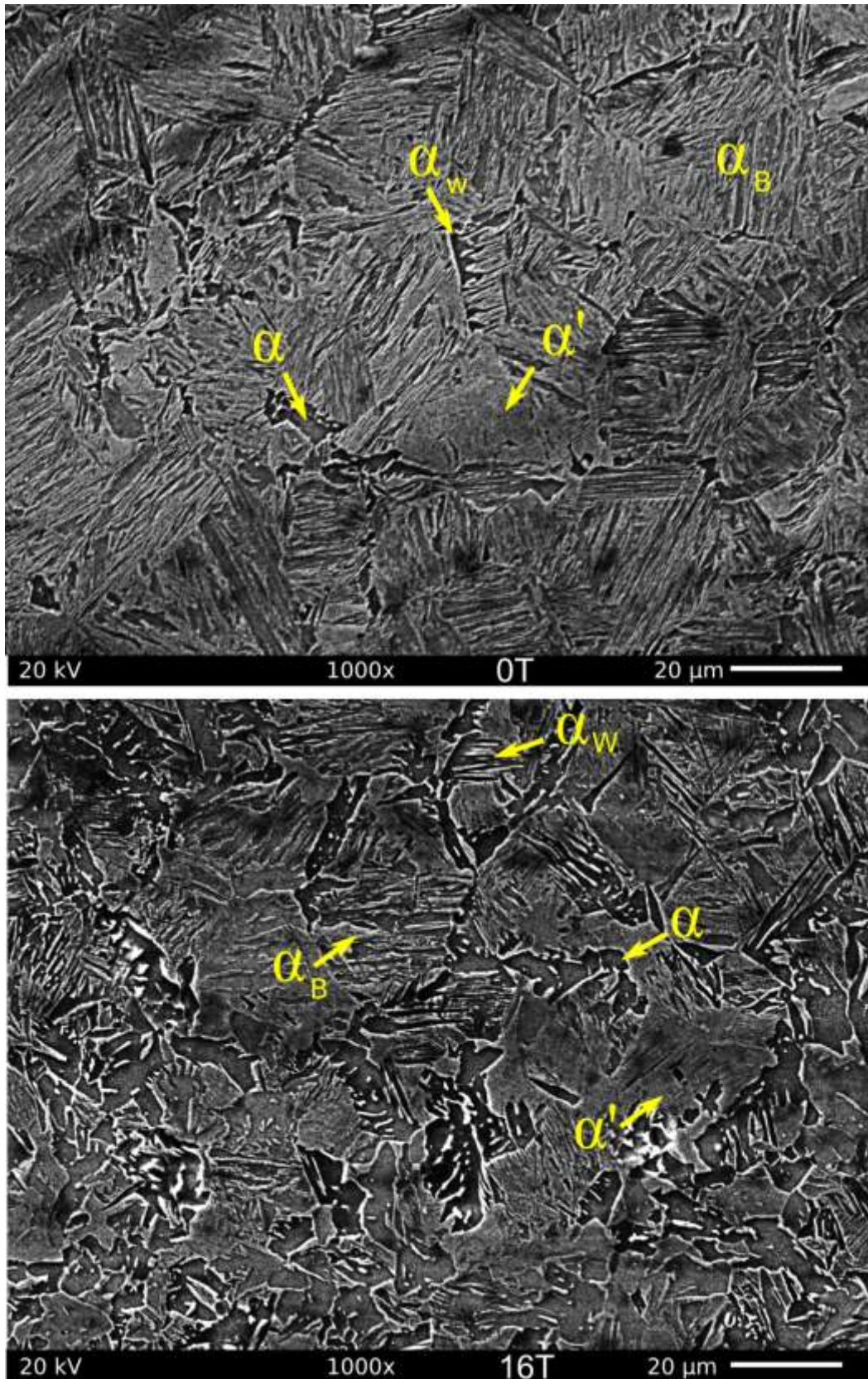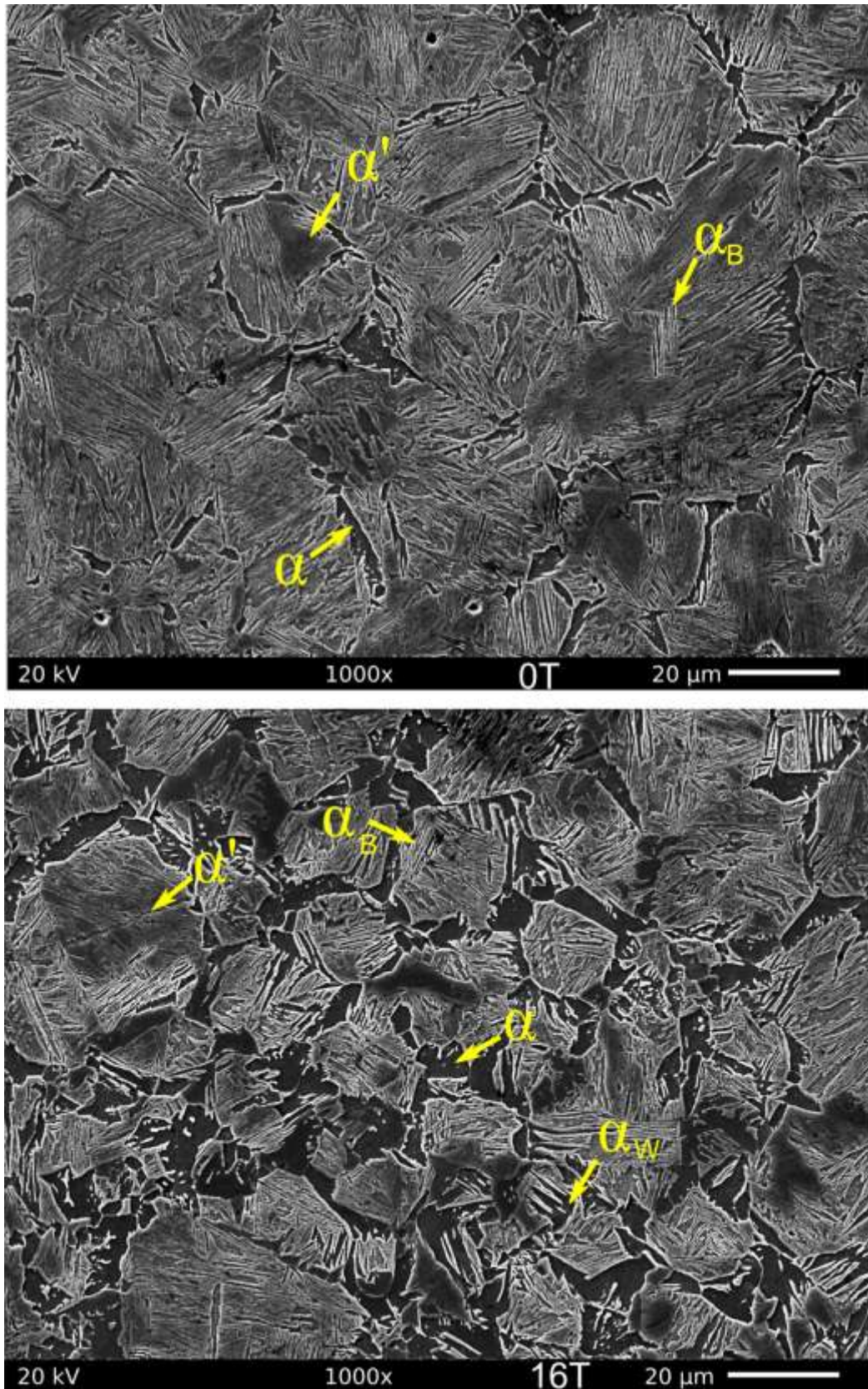
Figure 4.22   SE micrographs of the Fe-1.5Mn-1.75C-xSi steels D (1.75%Si) water quench under 0 and 16T. Original magnification 1000x, 4% nital etch

Resulting ferrite fraction and Vickers hardness

In Figure 4.23, is shown on the left, the ferrite area fraction evaluated by image analysis of 5 pictures for each specimen.

This result indicates that the application of a 16T magnetic field during water-quenching increased the ferrite volume fraction from several percent to more than 20% ferrite. The increase in the ferrite volume fraction does not have a linear dependence with the magnetic field strength in any cases. It is obvious that the free energies of the phases involved have been altered by the application of a 16T magnetic field.

It is not clear if the increase in the Silicon content from alloy A to D changes the effect of the magnetic field during the water cooling. On Figure 4.23, on the right, are plotted the corresponding average hardness values of the steels grades A to D as a function of magnetic field. In the sample treated without magnetic field, the increase in the silicon content leads to an increase of the hardness. This can be well explained by the increase of strain energy deformation in the lattice due to the presence of substitutional solute. A general decrease in the average hardness is measured when the field intensity applied during cooling is increased. This can be related to the increase in the ferrite volume fraction.
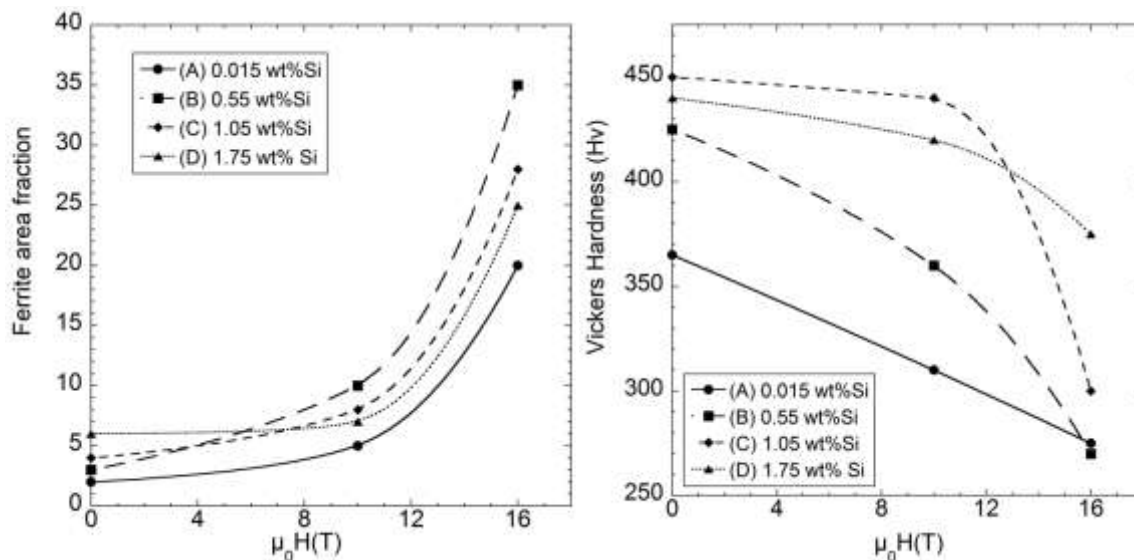
Figure 4.23   (Left) Estimate allotriomorphic ferrite area fraction as a function of magnetic field intensity for alloy A to D (right) Measured Vickers hardness of the sample A to D as a function of magnetic field.

These experiments show the opportunity to obtain a rapidly cooled structure containing a mixture of martensite, bainite and allotriomorphic ferrite without the use of decarburizing elements such as Silicon. The stabilisation of ferrite by the application of a high magnetic field is demonstrated even at cooling rates as high as 200K/s.

4.3.3. Conclusion

High cooling rate transformation experiments both with and without the influence of a magnetic field have been conducted on high-strength steels with increasing Si content.

From microstructural observations, the effect of magnetic field is to shift the austenite decomposition from the formation of out of equilibrium phases such as martensite of bainite, to the formation of more stable phases. In this sense, it is as if the magnetic field could ("decrease the cooling rate") and slow down the transformation. Under normal cooling condition (zero fields) all steels transform to a fully martensite structure. Application of a magnetic field during the fast cooling results in a mixture of martensite, bainite and ferrite. A corresponding reduction of the hardness is measured with the increased of the field strength.

4.4. Conclusions on the effect of magnetic field on martensitic and bainitic transformations

The important observations concerning the effect of static magnetic field applied during the water quench of Fe-xC-Mn and Fe-C-Mn-xSi alloys are summarized here:

- In the several alloys tested, the amount of allotriomorphic ferrite is enlarged drastically by the application of a magnetic field whatever the alloy composition. Hardness measurements are consistent with image analysis (corresponding reduction in hardness when the ferrite volume fraction increases).

- When magnetic field is applied during the treatments, an intimate mixture of ferrite, Widmanstätten ferrite, bainite and martensite is obtained compared to an almost fully martensite structure observed without magnetic field.

- In the Fe-0.3C-Mn (wt%) alloy, even pearlite colonies are observed in the matrix constituted of a mixture bainite and martensite.

- Large modifications in the formation temperature are expected by the different morphology of martensite and bainite.

- From microstructural observations, the effect of magnetic field is to shift the austenite decomposition from the formation of out of equilibrium phases such as martensite of bainite, to the formation of more stable phases. In this sense, it is as if the magnetic field could ("decrease the cooling rate") and slow down the transformation.

As a summary of these observations, an attempt is made for the prediction of the effect of magnetic field on a CCT diagram. The effect of field is to generally shift the stability domain of ferrite toward higher temperature and also higher cooling rate. A schematic CCT diagram corresponding to these two criteria is proposed in Figure 4.24.
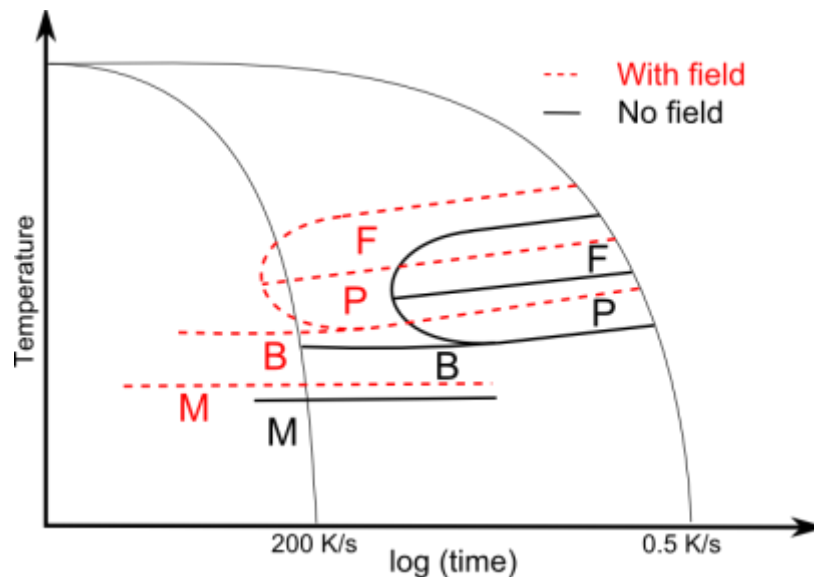
Figure 4.24   Schematic illustration of the effect of magnetic field on the stability domains of the various phases involved in steels.

On this diagram two lines are drawn corresponding to a cooling rate of 0.5 K/s applied in the chapter 3 and to a cooling rate of about 200 K/s corresponding to the rapid cooling of the alloy. Without magnetic field (black lines), a mixture of bainite and martensite is obtained at high cooling rate. By the application of magnetic field, the stability domain of ferrite and pearlite is shifted upwards and towards higher cooling rates. Ferrite is thus expected to be able to grow at high cooling rate when a magnetic field is applied.

General Conclusions

This work has been devoted to the quantification of the effect of magnetic field on the phase transformation in iron based alloys and steels. Pure iron, Fe-Ni substitutional alloys, Fe-xC-Mn steels with increasing carbon content and Fe-C-Mn-xSi steels with increasing silicon content have been used to explore a wide range of transformations and microstructures. Based on the results obtained in the literature, three axes of research have been mainly developed that are:

- The construction of a new device for the rapid cooling of inorganic materials in magnetic field.
- The development of experimental and theoretical tools for the prediction of diffusional phase transformation temperature in magnetic field in iron based alloys.
- The study of the impact of magnetic field on the martensitic and bainitic transformation in plain carbon steels.

1/ First of all, a new device for the process of material in high magnetic field has been developed during this work. In this apparatus the main advantage is that the ferromagnetic sample, submitted to strong forces due to high magnetic field, remains in a constant position, while the whole heating and cooling devices can move up and down thanks to an external jack. This apparatus enables, for the first time, very high cooling rates from the high temperature in magnetic field. Through its flexibility, it opens the way to a number of innovative studies in metallic materials and to a better understanding of the effect of magnetic fields in the industrial processing of steels and out of equilibrium structure formation. Since there is no physical problem for the upscale of this new system to an industrial scale, the authors have proposed a new process based on the same ideas but adapted to the continuous treatment of finite pieces in strong magnetic field. (Information about this process is not given in this work but can be found in [GARC09b])

2/ The second axis of development was mainly devoted to the diffusional decomposition of austenite in magnetic field. The validity of Molecular Field predictions are first checked for several alloys composition since this model is widely used for theoretical predictions of phase diagram in magnetic field and very few experiments were performed before this work. A large number of measurements at high temperature and high magnetic field has thus been performed and data are directly compared with Molecular Field predictions. The main result

is that the model underestimates the experimental data and that the discrepancy is maximized around the Curie point. For that reason, experimental magnetisation data have been used for the determination of the magnetostatic energy added by the application of an external magnetic field. A physically based model has been then proposed for the prediction of the non-equilibrium transformation temperatures and those predictions are finally compared with in-situ dilatometry experiments.

As a summary of the results obtained, it is generally possible to predict the shift of the transformation temperature from austenite to ferrite in plain carbon steel and iron substitutional alloys using only two important parameters:

- The first one is the magnetisation of ferrite and austenite phases. Usually, the magnetisation of austenite or more specifically its high temperature magnetic susceptibility is obtained in literature but can be in most cases neglected when its value is well below that of ferrite. The magnetisation of ferrite can be estimated using the Molecular Field model which only gives a correct estimation well above the Curie point of ferrite. In the vast majority of cases, this term has to be evaluated by direct *in-situ* magnetic measurements that allow a correct estimation of the magnetostatic energy. More in details, well below the Curie point, magnetic measurements up to about 2 T are enough for an extrapolation of the magnetostatic energy at higher magnetic fields. Around the Curie point and above, it is not possible to extrapolate at higher field since the magnetic field dependence of the magnetostatic energy does not follow a linear behaviour.

- The second parameter is Latent heat accompanying the transformation which can be found in databases or measured by Differential Scanning Calorymetry. A proper determination of this term is of capital importance for correct prediction of the shift of the transformation temperature in magnetic field. In this work, in a first approximation this term or more specifically the change in the entropy between ferrite and austenite has been assumed to be uninfluenced by the magnetic field. However, *in-situ* DSC experiments in magnetic field are highly needed to check for this assumption.

3/ The third research axis investigated during this work has been possible thanks to the new process and devices developed for the treatment of metallic material in magnetic field. The rapid cooling of plain carbon steels in magnetic field has shown that the resulting microstructure was totally modified by the field. From a mixture of bainite and martensite in the sample treated without the application of magnetic field, the austenite transforms into

allotriomorphic ferrite and Widmanstätten ferrite in a matrix of bainite and martensite. The formation of ferrite by diffusional process is able even at very high cooling rate under the influence of magnetic field. Important modifications in the morphology of martensite and of bainite have indicated that the formation temperature of these phases has been modified by the field. This modification in the formation temperature was highly expected by previous experimental works [KAKE99] and by the theoretical evaluation of the shift of the T_0 line in magnetic field in the Fe-C system proposed in this work.

References:

[AGRE82] A. Agren, *"Computer simulation of the austenite/ferrite diffusional transformation in low alloyed steels"*, Acta Materialia **30**, 841-851 (1982)

[AHAR98] A Aharoni, *"Demagnetizing factors for rectangular ferromagnetic prisms"*, Journal of Applied Physics **83**, 3432 (1998)

[ANTR99] V. P. Antropov, B. N. Harmon, and A. N. Smirnov, *"Aspects of spin dynamics and magnetic interactions",* Journal of Magnetism and Magnetic Materials **200** (1-3), 148-166 (1999)

[ARAJ60] S. Arajs and D.S. Miller, *"Paramagnetic Susceptibilities of Fe and Fe-Si Alloys"*, Journal of Applied Physics **31** (6), 986-991 (1960)

[ASMH91] ASM Handbook *"Heat Treating",* **4**, 398 (1991)

[ASMH93] ASM Handbook *"Properties and Selection: Irons, Steels, and High-Performance Alloys",* **1**, 2521 (1993)

[ASMH00] ASM Handbook *"Mechanical Testing and Evaluation"*, **8**, 2235 (2000)

[ASMH04] ASM Handbook *"Metallography and Microstructures",* **9**, 1437 (2004)

[ASAI03] S. Asai, *"Crystal orientation of non-magnetic materials by imposition of a high magnetic field"* Science and Technology of Advanced Materials **4**, 455-460 (2003)

[BACA03] C. M. B. Bacaltchuk, G. A. Castello-Branco, M. Ebrahimi, H. Garmestani and A. D. Rollett, *"Effect of magnetic field applied during secondary annealing on texture and grain size of silicon steel"*, Scripta Materialia **48** (9), 1343-1347 (2003)

[BAIN39] E. C. Bain, *"Function of the alloying elements in steel"*, Pittsburgh, (1939)

[BALL05] R. W. Balluffi, S. M. Allen, C. W. Carter and R. A. Kemper, *"Kinetics of Materials"* 672 (2005)

[BEAU91] E. Beaugnon and R. Tournier, *"Levitation of organic materials"*, Nature **349** (6309), 470-470 (1991)

[BEAU06] E. Beaugnon, S. Rivoirard, T. Garcin, and O. Bouaziz, *"Dilatometry of the austenite/ferrite transformation on a high magnetic field",* ISIJ International,

The 5th International Symposium on Electromagnetic Processing of Materials, 604-607 (2006)

[BHAD79] H. K. D. H. Bhadeshia and D. V. Edmonds, *"The Bainite Transformation in a Silicon Steel",* Metallurgical Transaction A **10**, 895-907 (1979)

[BHAD80] H. K. D. H. Bhadeshia and D. V. Edmonds, *"The Mechanism of Bainite Formation in Steels ",* Acta Metallurgica **28**, 1265-1273 (1980)

[BHAD83] H. K. D. H. Bhadeshia, "*Ferrite formation in heterogeneous dual phase steels"*, Scripta Materialia **17**, 857-860 (1983)

[BHAD85] H. K. D. H. Bhadeshia, *"Diffusionnal formation of ferrite in iron and its alloys"*, Progress in Materials Science **29**, 321-386 (1985)

[BHAD01] H. K. D. H. Bhadeshia, *"Bainite in Steels",* Institute of Materials (2001)

[BHAD06] H. K. D. H. Bhadeshia, *"Worked examples in the Geometry of Crystals"*, Institute of Materials, (2006)

[BIRA83] J.P. Birat and J. Chone, *"Electromagnetic Stirring on Billet, Bloom and Slab Continuous Casters: State of the Art",* Ironmaking and Steelmaking **6**, 269-281 (1983).

[BONV95] M. Bonvalot, P. Courtois, P. Gillon and R. Tournier, *"Magnetic levitation stabilized by eddy currents",* Journal of Magnetism and Magnetic Materials **151** (1-2), 283-289 (1995)

[BOZO78] R. M. Bozorth, *"Ferromagnetism"*, New York, (1993)

[BRAD77] J. Bradley, J. Rigsbee, and H. Aaronson, *"Growth kinetics of grain boundary ferrite allotriomorphs in Fe−C alloys"* Metallurgical and Materials Transactions A **8** (2), 323-333 (1977)

[BRAD81] J. R. Bradley and H. I. Aaronson, *"Growth Kinetics of Grain Boundary Ferrite Allotriomorphs in Fe-C-X Alloys"*, Metallurgical Transaction A **12A**, 1729-1741 (1981)

[BRAI91] D. Braithwaite, E. Beaugnon, and R. Tournier, *"Magnetically controlled convection in a paramagnetic fluid"*, Nature **354** (6349), 134-136 (1991)

[BRIA72] M. Briane, *"Réalisation d'une balance de translation pour la mesure des susceptibilités magnétique à haute températures",* C.R.Acad.Sci. Paris **275** (B), 673-676 (1972)

[BUDD03] E. Buddy Damm and M. J. Merwin, A Symposium on the *"Thermodynamics, Kinetics and Modelling of Austenite Formation and Decomposition",* TMS, Chicago, (2003)

[CABA01]   F. G. Caballero, H. K. D. H. Bhadeshia, K. J. A. Mawella, D. G. Jones and P. Brown, *"Design of novel high strength bainitic steels: Part 1",* Materials Science and Technology **17** (5), 512-516 (2001)

[CAHN63]   J. W. Cahn, *"Magnetic Aging of Spinodal Alloys"*, Journal of Applied Physics **34** (12), 3581-3586 (1963)

[CHAI09]   D. Chaira, B. K. Mishra, and S. Sangal, *"Magnetic properties of cementite powder produced by reaction milling"*, Journal of Alloys and Compounds **474** (1-2), 396-400 (2009)

[CHAU97]   X. Chaud, E. Beaugnon, and R. Tournier, "*Magnetic susceptibility during the peritectic recombination of YBaCuO"*, Physica C: Superconductivity **282-287** (Part 2), 525-526 (1997)

[CHOI00]   J.K. Choi, H Ohtsuka, Y. Xu and W. Y. Choo, *"Effects of a strong magnetic field on the phase stability of plain carbon steels"*, Scripta Materialia **43**, 221-226 (2000)

[CRMLab]   Centre for Research in Metallurgy, Gent: Technologies park 903c, B-9052 Zwijnaarde

[CULL72]   B. D. Cullity and C. W. Allen, *"Accelerated stress relaxation caused by an alternating magnetic field"* Acta Metallurgica **13** (8), 933-935 (1965)

[DERA91]   P. De Rango, M. Lees, P. Lejay, A. Sulpice, R. Tournier, M. Ingold, P. Germi and M. Pernet, *"Texturing of magnetic materials at high temperature by solidification in a magnetic field",* Nature **349**, 770-772 (1991),

[DINS91]   A. T. Dinsdale, *"SGTE data for pure elements"* Calphad **15** (4), 317-425 (1991)

[ENOM01]   M. Enomoto, H. Guo, Y. Tazuke, Y. Abe and M. Shimotomai, *"Influence of Magnetic Field on the Kinetics of Proeutectoid Ferrite Transformation in Iron Alloys",* Metallurgical and Materials Transactions A **32** (A), 445-453 (2001)

[FILA05]   P. Filar, E. Fornalik, M. Kaneda, T. Tagawa, H. Ozoe and J. S. Szmyd, *"Three-dimensional numerical computation for magnetic convection of air inside a cylinder heated and cooled isothermally from a side wall",* International Journal of Heat and Mass Transfer **48** (9), 1858-1867 (2005)

[FUKU06]   T. Fukuda, M. Yuge, T. Terai and T. Kakeshita, *"Magnetic field dependence of γ-α equilibrium temperature in Fe-Co alloys",* Journal of Physics: Conference Series **51**, 307-310 (2006)

[GAIN75]   R. Ya Gainutdinov, V. G. D'Yakonov, and A. G. Usmanov, *"Heat transfer in forced convection in high-frequency electromagnetic fields",* Journal of Engineering Physics and Thermophysics **28** (6), 686-690 (1975)

[GALI07]   V. Galindo, I. Grants, R. Lantzsch, O. Pätzold and G. Gerbeth, *"Numerical and experimental modelling of the melt flow in a travelling magnetic field for vertical gradient freeze crystal growth"* Journal of Crystal Growth **303** (1), 258-261 (2007)

[GAMS06]   E. Gamsjäger, M. Militzer, F. Fazeli, J. Svoboda, and F.D. Fischer, *"Interface mobility in case of the austenite-to-ferrite phase transformation",* Computational Materials Science **37**, 94-100 (2006).

[GAOB06]   M. C. Gao, T. A. Bennet, A. D. Rollet and D. E. Laughlin., *"The effect of applied magnetic field on the ferrite/austenite phase boundary in the Fe-Si system"* J.Phys.D: Appl Phys **39**, 2890-2896 (2006)

[GARC98]   C. García de Andrés, F. G. Caballero and C. Capdevila, *"Dilatometric characterization of pearlite dissolution in 0.1C-0.5Mn low carbon low manganese steel"* Scripta Materialia **38** (12), 1835-1842 (1998)

[GARC02]   C. García de Andrés, F. G. Caballero, C. Capdevila and L. F. Alvarez, *"Application of dilatometric analysis to the study of solid-solid phase transformations in steels",* Materials Characterization **48**, 101-111 (2002)

[GARC09a] T. Garcin, S. Rivoirard, and E. Beaugnon, *"In situ characterization of phase transformation in a magnetic field in Fe-Ni alloys",* Journal of Physics: Conference Series **156**, 012010 (2009)

[GARC09b] T. Garcin, S. Rivoirard, E. Beaugnon and P. F. Sibeud, 955380: Priority patent of invention filed on July 31, 2009 and entitled *"Process for the thermal treatment of a material under magnetic field",* 02736-01, France, 2009

[GARC09c] T. Garcin, S. Rivoirard, C.Elgoyhen, E. Beaugnon *"Experimental evidence and thermodynamics analysis of high magnetic field effects on the austenite to ferrite transformation temperature in Fe-C-Mn Alloys",* Acta Materialia, in press: http://dx.doi.org/10.1016/j.actamat.2009.11.045 (2009)

[GARC09d] T.Garcin, S.Rivoirard, R.Morgunov, E.Beaugnon, F.Debray, *"Martensitic transformation in Fe-0.2C-1.5Mn Alloy in intense magnetic fields"* GHMFL Annual Reports, 2008

[GARC09e] T.Garcin, S.Rivoirard, R.Morgunov, E.Beaugnon, F.Debray, *"Changes in the microstructure resulting from high cooling rate in Fe-xC-Mn alloys in strong magnetic field"* GHMFL Annual Reports, 2009

[GAUC01] F. Gaucherand and E. Beaugnon, *"Magnetic susceptibility of high-Curie temperature alloys near their melting point",* Physica B **294**, 96-101 (2001)

[GELF03] Y. Gelfgat, *"The use of combined magnetic field for controlling the characteristics of motion and heat/mass transfer in electrically conducting liquid media"*, in: Electromagnetic Processing of Materials, Lyon, France, (2003)

[GUOE00] H. Guo and M. Enomoto, *"Influence of magnetic fields on α/γ equilibrium in Fe-C(-X) alloys",* Materials Transactions **41** (8), 911-916 (2000)

[GUST85] P. Gustafson, *"Thermodynamic evaluation of the Fe--C system",* Scandinavian Journal of Metallurgy **14**, 259-267 (1985)

[HAOO03] X.J. Hao, H. Ohtsuka, and H. Wada, *"Structural Elongation and Alignment in an Fe-0.4C Alloy by Isothermal Ferrite Transformation in High Magnetic Fields",* Materials Transactions **44** (12), 2532-2536 (2003)

[HAOO04] X.J. Hao and H. Ohtsuka, *"Effect of magnetic field on Phase Transformation Temperature in Fe-C Alloys",* Materials Transactions **45** (8), 2622-2625 (2004)

[HAOO06] X. Hao and H Ohtsuka, *"Effect of high magnetic field on transformation Temperature in Fe-based alloys",* ISIJ International **46** (9), 1271-1273 (2006)

[HILL53] M.Hillert, *"Paraequilibrium"* (1953) in Thermodynamics and Phase Transformations, The selected works of Mats Hillert, J. Agren, Y. J. M. Brechet, C. Hutchinson, J. Philibert, G. R. Purdy 7-24 (2006)

[HILL58] M. Hillert, *"Thermodynamics of Martensitic Transformations",* (1958), in Thermodynamics and Phase Transformations, The selected works of Mats Hillert, J. Agren, Y. J. M. Brechet, C. Hutchinson, J. Philibert, G. R. Purdy 87-110(2006)

[HILL60] M. Hillert, *"The growth of ferrite, bainite and martensite",* (1960), in Thermodynamics and Phase Transformations, The selected works of Mats Hillert, J. Agren, Y. J. M. Brechet, C. Hutchinson, J. Philibert, G. R. Purdy 111-158(2006)

[HILL62] M. Hillert, *"The Formation of Pearlite",* (1962) in Thermodynamics and Phase Transformations, The selected works of Mats Hillert, J. Agren, Y. J. M. Brechet, C. Hutchinson, J. Philibert, G. R. Purdy 177-229 (2006)

[HILL75]   M. Hillert, *"Diffusion and interface control of reactions in alloys",* Metallurgical and Materials Transactions A **6** (1), 5-19 (1975)

[HILL06]   M. Hillert and L. Höglund, *"Mobility of α/γ phase interfaces in Fe alloys",* Scripta Materialia **54** (7), 1259-1263 (2006)

[IDOG93]   A. Idogawa, M. Sugizawa, S. Takeuchi, K. Sorimachi and T. Fujii, *"Control of molten steel flow in continuous casting mould by two static magnetic fields imposed on whole width",* Materials science & engineering. A, Structural materials: properties, microstructure and processing **173** (1-2), 293-297 (1993)

[INDE03]   G. Inden and C. R. Hutchinson, *"Interfacial Condition at the Moving Interface During Growth of Ferrite from Austenite in Fe-C-(X) Alloys",* The Minerals, Metals & Materials Society: Austenite Formation and Decomposition, 65-79 (2003)

[INMA65]   C.H. Inman, *"Proceedings of the Physical Properties of Martensite and Bainite Conference"*. (The Iron and Steel Institute, Scarborough, 1965

[ISHI75]   Y. Ishikawa, *"Handbook of Magnetic substance"*, Asakura Shoten, Tokyo, (1975)

[JACK04]   K.A. Jackson, *"Kinetics Processes: Crystal Growth, Diffusion, and Phase Transitions in Materials",* Wiley-VCH, 263-264

[JACO97]   A. Jacot and M. Rappaz, *"A two-dimensional diffusion model for the prediction of phase transformations: Application to austenitization and homogenization of hypoeutectoid Fe-C steels",* Acta Materialia **45** (2), 575-585 (1997)

[JARA05a]   R.A Jaramillo, S.S. Babu, M.K. Miller, R G. M. Ludtka, R. A. Kisner, J. B. Wilgen, G. Mackiewicz-Ludtka, D. M. Nicholson, S. M. Kelly, M. Murugananth and H. K. D. H. Bhadeshia, *"Effect of 30T magnetic field on transformations in a novel bainitic steel",* Scripta Materialia **52**, 461-466 (2005)

[JARA05b]   R.A. Jaramillo, S.S. Babu, M.R. Miller, G. M. Ludtka, G. Mackiewicz-Ludtka, R. A. Kisner, J. B. Wilgen and H. K. D. H. Bhadeshia, *"Investigation of austenite decomposition in high carbon high strength Fe-C-Si-Mn Steel under 30Tesla magnetic field",* Solid-Solid Phase Transformations in Inorganic Materials, TMS **1**, 873-878 (2005)

[JILE91]   D. Jiles, *"Introduction to Magnetism and Magnetic Materials"*, London: Chapman and Hall, (1991)

[KAKE84] T. Kakeshita, K. Shimizu, S. Funada, and M. Date, *"Magnetic field-induced martensitic transformations in disordered and ordered Fe-Pt alloys"*, Trans. Jpn. Inst. Met. **25** 837 (1984)

[KAKE85] T. Kakeshita, K. Shimizu, S. Funada, and M. Date, *"Composition dependence of magnetic field-induced martensitic transformations in Fe-Ni alloys"*, Acta Metallurgica **33** (8), 1381-1389 (1985)

[KAKE86] T. Kakeshita, S. Furikado, K. Shimizu, S. Kijima and M. Date, *"Magnetic field-induced martensitic transformation in single crystals of Fe-31.6at%Ni alloy"*, Trans. Jpn. Inst. Met. **27** 477 (1986)

[KAKE87] T. Kakeshita, H. Shirai, K. Shimizu, K. Sugiyama, K. Hazumi, and M. Date, *"Magnetic field-induced martensitic transformation from paramagnetic austenite to ferromagnetic martensite in an Fe-3.9Mn-5.0C (at%) alloy"*, Trans. Jpn. Inst. Met. **28** 891 (1987)

[KAKE99] T. Kakeshita, T. Saburi, K. Kind, and S. Endo, *"Martensitic transformations in some ferrous and non-ferrous alloys under magnetic field and hydrostatic pressure"* Phase Transitions **70**, 35-113 (1999)

[KAKE06] T. Kakeshita and T. Fukuda, *"Magnetic field control of microstructure and function of materials exhibiting solid-solid phase transformation"*, Science and Technology of Advanced Materials **7**, 350-355 (2006)

[KAKE09] T. Kakeshita and T. Fukuda, *"Effect of magnetic field on solid-solid phase transformations in iron-based ferromagnetic alloys"*, Journal of Physics: Conference Series **156**, 012012 (2009)

[KHRI03] R.M. Khristinich, V.N. Timofeyev, V.V. Stafievskaya and A. V. Velenteyenko, *"Molten Metal Electromagnetic Stirring in Metallurgy"* presented at the International Scientific Colloquium on the Modelling for Electromagnetic Processing Hannover, 29-34, (2003)

[KITT98] C. Kittel, *"Introduction to solid state physics"*, Univ. of California, Berkeley, 1998.

[KOPS01] T.A. Kop, J. Sietsma, and S. Van Der Zwaag, *"Dilatometric analysis of phase transformations in hypo-eutectoid steels"* Journal of Materials Science **36**, 519-526 (2001)

[KOYA07] T. Koyama and H. Onodera, *"Phase-field Modelling of Structural Elongation and Alignment of $(\alpha + \gamma)$ Microstructure in Fe-0.4C Alloy during Thermomagnetic Treatment"*, ISIJ International **46** (9), 1277-1282 (2006)

[KRIE97] G P. Krielaart, J Sietsma, and S van der Zwaag, *"Ferrite formation in Fe-C alloys during austenite decomposition under non-equilibrium interface conditions"*, Materials Science and Engineering A **237** (2), 216-223 (1997)

[KUBL07] J. Kübler, *"Handbook of Magnetism and Advanced Magnetic Materials: Fundamentals and Theory"* **1** 323-355 (2007)

[LANT07] R. Lantzsch, V. Galindo, I. Grants, C. Zhang, O. Pätzold, G. Gerbeth and M. Stelter, *"Experimental and numerical results on the fluid flow driven by a travelling magnetic field"*, Journal of Crystal Growth **305** (1), 249-256 (2007)

[LEGR98] B. A. Legrand, D. Chateigner, R. Perrier de la Bathie and R. Tournier , *"Orientation of samarium-cobalt compounds by solidification in a magnetic field"* Journal of Alloys and Compounds **275-277**, 660-664 (1998)

[LUDT04] G. M. Ludtka, R. A. Jaramillo, R. A. Kisner, D. M. Nicholson, J. B. Wilgen, G. Mackiewicz-Ludtka and P. N. Kalu, *"In situ evidence of enhanced transformation kinetics in a medium carbon steel due to a high magnetic field"* Scripta Materialia **51**, 171-174 (2004),

[MART81] H. O. Martikainen and V. K. Lindroos, *"Observation on the effect of magnetic field on the recrystallisation in ferrite"* Scandinavian Journal of Metallurgy **10**, 3-8 (1981)

[MARU02] K. Maruta and M. Shimotomai, *"Magnetic field-induced alignment of steel microstructures"*, Journal of Crystal Growth **237**, 1802-1805 (2002)

[MASSA90] T. B. Massalski, *"Binary Alloy Phase Diagrams"*, Second Edition , **2**, 1737 (1990)

[MEDI07] M. Medina, Y. Du Terrail, F. Durand and Y. Fautrelle, *"Channel segregation during solidification and the effects of an alternating travelling magnetic field"*, Metallurgical and Materials Transactions B **35** (4), 743-754 (2004)

[MOSH63] E. I. Moshkevich, A. N. Porada, and V. P. Akulov, *"Electromagnetic stirring in the melting of stainless steel in electric furnaces"*, Metallurgist **7** (4), 171-173 (1963)

[MOSS04] E. Mossang, F. Debray, H. Jongbloets, W. Joss, G. Martinez, P. Petmezakis, J. C. Picoche, P. Rub, P. Sala, C. Trophime, and P. Wyder, *"The Grenoble High Magnetic Field Laboratory as a user facility"*, Physica B: Condensed Matter **346-347**, 638-642 (2004)

[NAKA05]   S. Nakamichi and S. Tsurekawa, "*Diffusion of carbon and titanium in austenite in a magnetic field and a magnetic field gradient*", Journal of Materials Science **40**, 3191-3198 (2005)

[NICH04]   D.M.C. Nicholson, R.A. Kisner, G.M. Ludka, C.J. Sparks, L. Petit, R. Jaramillo, G. Mackiewicz-Ludtka, J.B. Wilgen, A.D. Sheikh-Ali, and P.N. Kalu, "*The effect of high magnetic field on phase stability in Fe-Ni*", Journal of Applied Physics **95** (2.11), 6580-6582 (2004)

[OHTS00a]   H. Ohtsuka, Y. Xu, and H. Wada, "*Alignment of Ferrite Grains during Austenite to Ferrite Transformation in a High Magnetic Field*", Materials Transactions **41** (8), 907-910 (2000)

[OHTS00b]   H. Ohtsuka, K. Ito, H. Wada, and Y. Xu, "*Effects of Strong Magnetic Field on Recrystallisation and Coarsening of Grains During Annealing in 3% Silicon Steel*", Journal of the Magnetics Society of Japan **24** (4-2), 651-654 (2000)

[OHTS01]   H. Ohtsuka, "*Effect of high magnetic field on diffusional transformation behaviours and structure*", National Institute for Materials Science, Tsukuba, 305-0003 (2001)

[OHTS06a]   H. Ohtsuka, "*Effects of a high magnetic field on bainitic transformation in Fe-based alloys*" Materials Science and Engineering: A **438-440**, 136-139 (2006)

[OHTS06b]   H. Ohtsuka and X. J. Hao, "*Effect of a High Magnetic field on Phase Transformation Behaviours and Structures*", ISIJ International, The 5th International Symposium on Electromagnetic Processing of Materials, 648-651 (2006)

[OHTS08]   H. Ohtsuka, "*Structural control of Fe-based alloys through diffusional solid/solid phase transformations in a high magnetic field*", Science and Technology of Advanced Materials **9**, 013004 (2008)

[OLIV04]   P. Olivas, A. Alemany, and F. H. Bark, "*Electromagnetic control of electroplating of a cylinder in forced convection*", Journal of Applied Electrochemistry **34** (1), 19-30 (2004)

[OTSU79]   K. Otsuka, H. Sakamoto, and K. Shimizu, "*Successive stress-induced martensitic transformations and associated transformation pseudo elasticity in Cu-Al-Ni alloys*", Acta Metallurgica **27** (4), 585-601 (1979)

[PALU08]   M. Palumbo, "*Thermodynamics of martensitic transformations in the framework of the CALPHAD approach*", Calphad **32** (4), 693-708 (2008)

[PATE53]   J. R. Patel and M. Cohen, *"Criterion for the action of applied stress in the martensitic transformation"*, Acta Metallurgica **1** (5), 531-538 (1953)

[PETE72]   C. T. Peters, P. Bolton, and A. P. Miodownik, *"The effect of magnetic fields on isothermal martensitic transformations"*, Acta Metallurgica **20** (7), 881-886 (1972)

[PETE73]   C. T. Peters and A. P. Miodownik, *"The effect of magnetic fields on phase equilibria in the iron-cobalt system"*, Scripta Metallurgica **7** (9), 955-958 (1973)

[PHIL98]   J. Philibert, A. Vignes, Y. J. M. Brechet, and P. Combrade, *"Métallurgie, du minerai au matériau"*, MASSON, (1998)

[PRIE06]   Janis Priede, Jacqueline Etay, and Yves Fautrelle, *"Edge pinch instability of liquid metal sheet in a transverse high-frequency ac magnetic field"*, Physical Review E (Statistical, Nonlinear, and Soft Matter Physics) **73** (6), 066303-066310 (2006)

[PURD84]   G.R. Purdy and M. Hillert, *"On the nature of the bainite transformation in steels"*, Acta Metallurgica **32** (6), 823-828 (1984)

[QIWA01]   J. Qi, N. I. Wakayama, and A. Yabe, *"Magnetic control of thermal convection in electrically non-conducting or low-conducting paramagnetic fluids"*, International Journal of Heat and Mass Transfer **44** (16), 3043-3052 (2001)

[QUID01]   D. Quidort and Y. J. M. Brechet, *"Isothermal growth kinetics of bainite in 0.5% C steels"*, Acta Materialia **49** (20), 4161-4170 (2001)

[QUID02]   D. Quidort and Y. Bréchet, *"The role of carbon on the kinetics of bainite transformation in steels"*, Scripta Materialia **47** (3), 151-156 (2002)

[REED92]   C. Reed and H. K. D. H. Bhadeshia, *"Kinetics of reconstructive austenite to ferrite transformation in low alloy steels"*, Materials Science and Engineering A **8**, 421-435 (1992)

[RIVO05]   S. Rivoirard, F. Gaucherand, E. Beaugnon, O. Bouaziz, and E. Pinto Da Costa, *"Effect of a high magnetic field on the ferritic transformation in a low carbon steel"*, Rev. Met. Paris (5), 393-397 (2005)

[RIVO06]   S. Rivoirard, F. Gaucherand, O. Bouaziz, E. Pinto Da Costa, and E. Beaugnon, *"Ferrite Transformation in High Magnetic Field Monitored by in-situ Magnetic Measurements"*, ISIJ International **46** (9), 1274-1276 (2006)

[RIVO09]   S. Rivoirard, T. Garcin, E. Beaugnon, and F. Gaucherand, *"High Temperature Dilatation Measurements By In Situ Laser Interferometry Under High Magnetic Field"*, Review of Scientific Instruments **80**, 103901 (2009)

[RUDN03] V. Rudnev, D. Loveless, R. Cook, and M. Black, *"Handbook of Induction Heating"* Manufacturing Engineering and Materials Processing, (2003)

[SATO89] M. Sato, *"Simple and approximate expressions of demagnetizing factors of uniformly magnetized rectangular rod and cylinder",* Journal of Applied Physics **66** (2), 983-985 (1989)

[SATY68] K. R. Satyanarayan, W. Eliasz, and A. P. Miodownik, *"The effect of a magnetic field on the martensite transformation in steels",* Acta Metallurgica **16** (6), 877-887 (1968)

[SCOT55] G. G. Scott, *"Gyromagnetic Ratio of Iron at Low Magnetic Intensities"*, Physical Review **99** (4), 1241 (1955)

[SERI91] R. W. Series and D. T. J. Hurle, *"The use of magnetic fields in semiconductor crystal growth",* Journal of crystal growth **113** (1-2), 305-328 (1991)

[SHIM00] M. Shimotomai and K. Maruta, *"Aligned two-phase structures in Fe-C alloys"* Scripta Materialia **42** (5), 499-503 (2000)

[SHIM03] M. Shimotomai, *"Influence of magnetic-field gradients on the pearlitic transformation in steels",* Materials Transactions **44** (12), 2524-2528 (2003)

[SHMA03] M. Shimotomai, K. Maruta, K. Mine, and M. Matsui, *"Formation of aligned two-phase microstructures by applying a magnetic field during the austenite to ferrite transformation in steels"*, Acta Materialia **51**, 2921-2932 (2003)

[SMOL49] R. Smoluchowski and R. W. Turner, *"Influence of Magnetic Field on Recristallization",* Journal of Applied Physics **20** (8), 745-746 (1949)

[SOMM66] A. Sommerfeld, *"Electrodynamics: Lectures on Theoretical Physics"*, New York: Academic Press, 372 (1966)

[SONG08] J.Y. Song, Y.D. Zhang, X. Zhao, and L. Zuo, *"Effects of high magnetic field strength and direction on pearlite formation in Fe–0.12%C steel",* Journal of Materials Science **43**, 6105-6108 (2008)

[TAKA89] K. Takahashi and H. K. D. H. Bhadeshia, *"The interpretation of dilatometric data for transformations in steels",* Journal of materials science letters **8** (4), 477-478 (1989)

[TANA97] T. Tanaka and K. Miyatani, *"Magneto static Critical-point phenomena of Fe",* Journal of Applied Physics **82** (11), 5658-5661 (1997)

[TZAV74] A. A. Tzavaras, *"A study of segregation phenomena in steel solidification structures grown under fluid flow",* Journal of Crystal Growth **24-25**, 471-476 (1974)

[VILL07] A. Villaume, D. Bourgault, L. Porcar, A. Girard, C.E. Bruzek, and P.F. Sibeud, *"Misalignment angles' reduction in Bi2212 multifilaments melted by dynamic heat treatment under a magnetic field",* IOP Superconductor Science and Technology **20**, 691-696 (2007)

[WAKA96] N. I. Wakayama, H. Ito, Y. Kuroda, O. Fujita, and K. Ito, *"Magnetic support of combustion in diffusion flames under microgravity",* Combustion and Flame **107** (1-2), 187-188 (1996)

[WANG02] L. B. Wang and Nobuko I. Wakayama, *"Control of natural convection in non- and low-conducting diamagnetic fluids in a cubical enclosure using inhomogeneous magnetic fields with different directions",* Chemical Engineering Science **57** (11), 1867-1876 (2002)

[WANG08] K. Wang, Q. Wang, C. Wang, E. Wang, C. Liu, and J. He, *"Formation of aligned two-phase microstructure in Fe-0.25 mass%C alloy under gradient high magnetic fields"* Materials Letters **62** (10-11), 1466-1468 (2008)

[WATA90] T. Watanabe, Y. Suzuki, S. Tanii, and H. Oikawa, *"The effects of magnetic annealing on recrystallisation and grain-boundary character distribution (GBCD) in iron-cobalt alloy polycrystals",* Philosophical Magazine Letters **62** (1), 9 - 17 (1990)

[WATS73] J. D. Watson and P. G. McDougall, *"The crystallography of Widmanstätten ferrite",* Acta Metallurgica **21** (7), 961-973 (1973)

[WITS00] J. J. Wits, T. A. Kop, Y. van Leeuwen, J. Seitsma, and S. van Der Zwaag, *"A study on the austenite-to-ferrite phase transformation in binary substitutional iron alloys" ,* Materials Science and Engineering A **283** (1-2), 234-241 (2000)

[WUHE07] Y. Wu, C.S. He, X. Zhao, L. Zuo, and T. Watanabe, *"Effect of High Magnetic Field an Field Direction on Recristallization and Recrystallisation Tecture in Cold-rolled IF Steel Sheet",* Materials Science Forum **558**, 401-406 (2007)

[XUOH99] Y. Xu, H. Ohtsuka, and H. Wada, *"Effect of high magnetic field on ferrite transformation in an Fe-based alloy",* International Symposium on New Magneto-Science, 211-217 (1999)

[YASU00] H. Yasuda, K. Tokieda, and I. Ohnaka, *"Effect of Magnetic Field on Periodic Structure Formation in Pb-Bi and Sn-Cd Peritectic Alloys",* Materials Transactions **41** (8), 1005-1012 (2000)

[ZHAN04] Y. Zhang, C. He, X. Zhao, L. Zuo, C. Esling, and C. He, *"New microstructural features occuring during transformation from austenite to ferrite under kinetics*

influence of magnetic field in a medium carbon steel", Journal of Magnetism and Magnetic Materials **284**, 287-293 (2004)

[ZHAN05] Y.D. Zhang, C. Esling, J. Muller, C.S. He, X. Zhao, and L. Zuo, *"Magnetic field induced grain elongation on a medium carbon steel during its austenite decomposition",* Applied Physics Letters **87**, 212504 (2005)

[ZAHE05] Y.D. Zhang, C.S. He, X. Zhao, Y.D. Wang, L. Zuo, and C. Esling, *"Calculation of Magnetisation and Phase Equilibrium in Fe-C Binary System under a Magnetic Field",* Solid State Phenomena **105**, 187-192 (2005)

[ZHAN06] Y.D. Zhang, C. Esling, M.L. Gong, G. Vincent, X. Zhao, and L. Zuo, *"Microstructural features induced by a high magnetic field in a hypereutectoid steel during austenitic decomposition",* Scripta Materialia **54** (11), 1897-1900 (2006)

[ZHAN07] Y.D. Zhang, C. Esling, M. Calcagnotto, M.L. Gong, X. Zhao, and L. Zuo, *"Shift of the eutectoid point in the Fe-C binary system by a high magnetic field",* J.Phys.D: Appl Phys **40**, 6501-6506 (2007)

[ZHUW06] L. Zhu, D.Wu, and X. Zhao, *"Effect of Silicon Content on Thermodynamics of Austenite Decomposition in C-Si-Mn TRIP Steels,"* Journal of Iron and Steel Research, International **13** (3), 57-73 (2006)

[ZHUW08] L. Zhu, D.Wu, and X. Zhao, *"Modelling of Austenite Decomposition in Low Si-Mn TRIP Steel During Cooling",* Journal of Iron and Steel Research, International **15** (6), 68-71 (2008)

Abstract

This work is devoted to the quantification of the magnetic field effect on phase transformations in iron based alloys and steels. Pure iron, Fe-xNi substitutional alloys, Fe-xC-Mn steels and Fe-C-Mn-xSi steels are used to explore a wide range of transformations and microstructures. A high temperature dilatometer and a magnetic balance for magnetic susceptibility measurements are used for the in situ characterisation of diffusional phase transformation in magnetic field up to 16T. A third device has been developed for the treatment of materials in magnetic field and includes, for the first time, a quenching step using water, oil or pulsed gas. Non-equilibrium transformation temperatures measured up to 16T in a large set of materials are found to be increased by the application of a magnetic field. In a similar approach as the model used to estimate the effect of hydrostatic pressure on the phase equilibrium, the shift induced by the magnetic field is calculated. Microstructure characterisation of rapidly cooled plain carbon steels has shown large structural modifications induced by the magnetic field. From a mixture of bainite and martensite in the sample treated without any magnetic field, the austenite transforms into allotriomorphic ferrite and Widmanstätten ferrite in a matrix of bainite and martensite in the presence of magnetic field. This work brings solid evidence that magnetic field can be used as a new degree of freedom in physical metallurgy. Combined with existing techniques, it could lead to the successful processing of improved materials.

Résumé

Ce travail est dédié à la quantification de l'effet du champ magnétique sur les transformations de phases dans les alliages à base de fer et en particulier dans les aciers. Le Fer pur, les alliages Fe-xNi, et les aciers au carbone faiblement alliés Fe-xC-Mn et Fe-C-Mn-xSi sont étudiés afin d'explorer une large gamme de transformations et de microstructures. Un dilatomètre haute-température et une balance magnétique pour la mesure de susceptibilité magnétique sont utilisés pour la caractérisation des transformations diffusive dans un champ magnétique allant jusqu'à 16T. Un troisième outil d'élaboration sous champ magnétique a été entièrement développé au cours de ce travail et permet pour la première fois une étape de trempe des matériaux à l'eau, à l'huile ou par gaz pulsé. Les températures de transformation hors-équilibre mesurées jusqu'à 16T dans une large gamme d'alliages sont augmentées par l'application d'un champ magnétique. Ces variations dans la température de transformation sont modélisées par un calcul thermodynamique basée sur une analogie avec l'effet d'une pression hydrostatique sur les équilibres de phases. Les microstructures d'aciers faiblement alliées obtenue par trempe sont largement modifiées par l'application du champ magnétique : d'une structure composée de martensite et de bainite sans l'application d'un champ magnétique, l'austénite se décompose en un mélange de ferrite allotriomorphe et de ferrite de Widmanstätten dans une matrice de bainite et de martensite en présence d'un champ magnétique. Ce travail apporte la preuve que le champ magnétique est devenu un paramètre prometteur en métallurgie physique. Associé aux techniques existantes, son utilisation peut conduire à l'obtention de matériaux aux propriétés innovantes.

Thèse préparée au Consortium de Recherche pour l'Emergence des Technologies Avancées
_ CNRS Grenoble _